Abstract

Autoregulation Mechanism of LIM Domain Kinases

Gabriela Casanova Sepúlveda

2023

LIM kinases 1 (LIMK1) and 2 (LIMK2) are major regulators of cytoskeletal dynamics in the cell. LIMK regulates actin dynamics by phosphorylating the actin-depolymerizing factor (ADF)/cofilin family of actin-binding proteins. Cofilin proteins bind preferentially and cooperatively to ADP-bound subunits in F-actin. This binding event changes the helical rotation of actin filaments, promoting actin filament severing. LIMKs promote actin filament stabilization by inactivating cofilin through phosphorylation of Ser3. Phosphorylation of cofilin at Ser3 deactivates cofilin severing activity by inhibition of cofilin binding to actin filaments. This cycling between actin depolymerization and polymerization impacts higher-order cellular processes, including motility, differentiation, and metastasis.

In the past 25 years, LIMK and cofilin have been heavily studied, but important questions remain regarding kinase regulation. Current literature proposes a model of regulation in which the N-terminus, which contains two LIM domains and one PDZ domain, acts as a negative regulator of the C-terminal kinase domain. These N-terminal domains, known to mediate protein-protein interactions, remain understudied in the context of LIMK autoregulation. Previous studies have mainly focused on immunoprecipitation and pull-down assays of

fragments of the N-terminal domains to the C-terminus kinase domain. However, no structure of the domains LIM and PDZ is published, nor details about the autoregulated complex is known. Thus, how these domains modulate the kinase activity of LIMK has yet to be revealed. The information in this dissertation aims to provide the molecular mechanism and structural details underlying the regulation of LIMK1 activity. **I hypothesize that the N-terminus of LIMK1 negatively regulates its kinase activity via a direct "head-to-tail" interaction.** I will test this hypothesis using biochemical, biophysical, cell-based, and structural biology techniques to understand molecular mechanisms underlying autoregulation.

I will accomplish the goals of this dissertation by setting two aims. **In Aim 1**, I study the N-terminal domains of LIMK. I use biochemical and structural techniques to gain a molecular-level understanding of the PDZ domains. Specifically, I obtain the crystal structure of the hLIMK2 PDZ domain and map the conservation of this domain using both LIMK1 and LIMK2 sequence alignments. I find a surface in this domain that is conserved from mammals to insects. I use homology- and structure-driven mutations to validate structure-defined and functional mechanisms of PDZ domain regulation. To test the effect of these mutations, I reconstructed the human LIMK pathway in *S. cerevisiae*. Expression of human LIMK1 phosphorylates and inactivates endogenous yeast cofilin; thus, I observe alterations in LIMK activity by measuring yeast growth. Using this assay, I screened for LIMK1 PDZ mutants that may be involved in kinase autoregulation. I have successfully used radiolabel assays to test the impact of these mutations

on kinase activity using cofilin as substrate *in vitro*. This combination of approaches allowed me to understand better the influence of the PDZ domain in kinase autoregulation.

In Aim 2, I used biochemical, biophysical, and activity-based assays to elucidate how the N-terminus domains of LIMK are responsible for autoregulatory interactions with the kinase domain and if LIMK is regulated in *cis or trans*. I began by directly addressing whether, in addition to the PDZ, other domains in the N-terminus of LIMK are responsible for kinase autoregulation. I found that the LIMK2 LIM2-PDZ domain fragment reduces the kinase activity of LIMK2 catalytic domain (CAT) *in vitro*. Furthermore, I used SEC-MALS to study the molecular arrangement of the LIM2-PDZ domains in solution.

Additionally, I explore the molecular arrangement of full-length LIMK. I purify human full-length LIMK2 protein and use negative staining electron microscopy to observe global conformational changes between the wild-type protein and kinase-inactive D451N mutant to differentiate between intra or intermolecular conformations. Negative staining electron microscopy suggests two different conformations where the full-length wild-type LIMK2 displays an elongated conformation, while the full-length catalytically inactive D451N mutant shows a more compact conformation. These discoveries lead me to propose that the N-terminal domains are responsible for the autoregulation of LIMKs and that the mode of regulation is intramolecular.

These findings provide a foundation for studying N-terminal autoregulation of LIMK kinase activity. Here, I present studies of autoregulatory interaction in LIMK in purified systems as well as in a eukaryotic system. This work provides the first crystal of the human LIMK2 PDZ domain and an in-depth study of its fold and conservation. Mutagenesis studies of the PDZ domain reported here provide strong evidence for how this domain undergoes autoregulation. Likewise, I provide insight into the molecular arrangement of LIMK N-terminus domains and full-length protein and provide a low-resolution understanding of its oligomeric state using SAXS and negative stain electron microscopy. Together, I propose that the LIM2-PDZ region of the N-terminus autoregulates LIMK activity.

Autoregulation Mechanism of LIM Domain Kinases

A Dissertation

Presented to the Faculty of the Graduate School

Of

Yale University

In Candidacy for the Degree of

Doctor of Philosophy

By

Gabriela Casanova Sepúlveda

Dissertation Director: Dr. Titus J. Boggon, Ph.D.

December 2023

Table of Contents

List of Figures

List of Tables

List of Abbreviations

Abl	Abelson kinase
ABLIM	actin binding LIM protein
Akt	Ak strain transforming
CAT	Catalytic kinase domain
CBP	Csk binding protein
Cdc42	Cell division cycle 42
Cdk	Cyclin-dependent kinase
CH	calponin homology
Chk	Checkpoint kinase
CRIB	Cdc42 and Rac interactive binding domain
CRP	Cysteine and glycine-rich protein
Csk	C-terminal Src kinase
Cx43	Connexin-43
DENSS	DENsity from Solution Scattering
EGFR	Epidermal growth factor receptor
EPLIM	epithelial protein lost in neoplasm (EPLIM)
F-actin	Filamentous actin
FA	Focal adhesion
FAK	Focal adhesion kinase
FHL	Four-and-a-half LIM protein
FL	Full-length protein

FoXS	Fast X-ray scattering
GluR2	Glutamate receptor subunit 2
GRIP	Glutamate receptor-interacting protein 1
ILK	Integrin-linked kinase
LASP	LIM and SH3 protein
LD	Leucine-aspartic acid motifs
LHX	LIM homeobox
LID	LIM binding domain
LIM	Lin11, Isl-1 & Mec-3
LIM-HD	LIM-Homeodomains
LIMK	LIM domain kinase
LMO	LIM domain only protein
MICAL	Microtubule-associated monooxygenase, calponin, and LIM domain-containing protein
MRCK	Myotonic dystrophy kinase-related Cdc42-binding kinases
PAK4	Serine/threonine p21-activated kinase
PBM	Protein binding motif
PDZ	**P**SD-95, **D**lg-1, and **Z**O-1
PET	N-terminal Prickle Espinas Testin
PH	Pleckstrin Homology domain
Phk	Phosphorylase kinase
PINCH	Particularly interesting new cysteine and histidine-rich protein

PKA	Protein kinase A
PKC	Protein kinase C
Rab	Ras-associated binding protein
Rac	Ras-related C3 botulinum toxin substrate 1
RBD	Ras binding domain
Rho	Ras homologous
RIL	Reverse induced LIM gene proteins
ROCK	Rho associated protein kinase
SAM	Sterile α-motif
SAXS	Small Angle X-ray Scattering
SCD	Ser-Gln/Thr-Gln (SQ/TQ) cluster domain
SH2	Src homology 2 domain
SH3	Src homology 3 domain
Src	proto-oncogene Sarcoma kinase
TES	Testin
TESK	testis expressed serine kinase
VHP	Villin headpiece domain
AURKA	Aurora kinase A
MK2	MAPK-activated protein kinase-2

Acknowledgments

To my family, thank your infinite love and unconditional support. I am here today because of all the sacrifices you have made for me. Thank you for believing in me, even when I sometimes did not. Thank you for supporting all my goals and being my place of happiness and safety.

Thank you to all the mentors who supported me through my scientific career. I am immensely proud of the scientist you have helped me become.

Max, thank you for your unconditional love.

Para ti madrina, Iris Y. Vega González. Sé que donde sea que estés me observas y acompañas con orgullo.

Chapter 1: Introduction and Background

1.1 LIM domain kinases history

Protein phosphorylation is the most common post-translational modification (PTM)[1-3]. The discovery of protein phosphorylation opened the door to a vital field in understanding cellular communication and pathway discovery. Protein phosphorylation reaction transfer of a γ-phosphate group from ATP to specific amino acid residues in proteins, most commonly Ser, Thr, and Tyr residues. This modification alters the protein substrate surface charge and conformation. Upon phosphorylation, proteins often become able to bind to other molecules, resulting in different protein complexes and signaling events. The protein enzymes catalyzing the covalent transfer of ATP γ-phosphate to a protein substrate are called protein kinases.

Since the 1950s, with the isolation of phosphorylase b, the study of protein phosphorylation expanded with the identification of protein kinases that could phosphorylate proteins on serine and threonine residues [4]. However, in the 1980s and 1990s, with the use of low-stringency screening, more protein kinases were identified[5,6]. These methods were used to identify novel classes of kinases that differed slightly in kinase domain sequence and substrate amino acid preference [7]. One kinase identified using these methods was LIMK. LIMK was identified as an overlapping clone in the human hepatoma HepG2 cells using the *c-sea* receptor tyrosine kinase cDNA as a probe [8-10]. The same year, while using the PCR technology and primers of a known tyrosine kinase, PTK, in mice olfactory

epithelium cells, a protein with a closely related catalytic domain was discovered and initially named Kiz-1 [11]

Kiz-1 was renamed to LIMK due to the identification of two LIM domains (**L**in11, **I**sl-1 & **M**ec-3) in its N-terminus and a kinase domain in its C-terminus. LIMK is a dual specificity kinase that belongs to the tyrosine kinase-like family of kinases and is involved in signaling downstream of RhoA [12,13] (**Figure 1.1**). Tyrosine-like kinase family members share high sequence similarity in the catalytic domain to tyrosine kinases but do not necessarily phosphorylate tyrosine residues. LIMK prefers to phosphorylate serine and tyrosine residues [14].

1.2 LIMK domain architecture

The LIM kinase family of proteins contains LIM kinase 1 and LIM kinase 2 (LIMK1, LIMK2), and lesser-known members, testis expressed serine kinase 1, and testis expressed serine kinase 2 (TESK1 and TESK2)[8-11,15,16]. The LIMK and TESK families share high similarity in their catalytic domain but differ in their overall domain architecture. LIMK1 and LIMK2 contain two sequential LIM domains and, a PDZ domain in their N-terminus and a C-terminal active kinase domain. TESK1 and TESK2, on the other hand, have N-terminal active kinase domains and proline-rich C-termini (**Figure 1.2).** All four members of this family of kinases are readily involved in regulating actin dynamics by the phosphorylation of cofilin proteins **(Figure 1.1).** My thesis focuses on the LIMK members of this family. References to LIMK imply both kinases and if a specific member of the LIMK kinases family is referred, the LIMK member (LIMK1, LIMK2) will be expressly stated.

Below, I will describe in depth the different components of the LIMK group, the LIM domains (sections 1.3 to 1.5), the PDZ domain (sections 1.6 to 1.9), and the catalytic kinase domain (sections 1.11). I will then describe precedents in the literature for autoregulation of catalytic activity in protein kinases by adjacent domains or protein partners (section 1.17).

1.3 LIMK contains two LIM domains

LIM domains are zinc finger domain structures characterized by their intricate involvement in various cellular processes, including cytoskeletal organization, cell lineage specification, gene transcription regulation, and organ development [17-19]**.** These protein domains are found in a wide variety of proteins, with 135 LIM domain coding sequences identified in 58 genes [20]. LIMK domains can be found in homeodomain transcription factors, kinases, and adaptor proteins. The LIM domain fold comprises dual zinc fingers, characterized by two zinc ion binding sites coordinated by cysteines and histidine. LIM domains most commonly contain the following sequence, $CX_2CX_{16-23}HX_2CX_2CX_2CX_{16-21}CX_2$(C/H/D), where X is any amino acid, C stands for cysteine and H for histidine, and "/" indicates alternative amino acid residue [20,21]. Studies of the zinc finger fold demonstrate that the classical zinc finger contains two β-sheets and one α-helix[22]. In LIM domains, the tandem zinc fingers follow this architecture; the first zinc finger includes β-hairpins 1 and 2, connected by rubredoxin-type zinc knuckles, and the second zinc finger includes β-hairpins 3 and 4, joined by tight turns [20,23,24]. LIM domains present conserved tetrahedral zinc coordination, which establishes the LIM domain's

secondary structure and tertiary fold, along with hydrophobic core residues. Sequence divergence among LIM domains allows unique surfaces for protein-protein interactions [25,26].

LIM domains are classified into four groups, termed groups 1, 2, 3, and 4 (**Figure 1.3**). This classification is based mainly on the arrangement of the LIM domain in the overall protein structure and the localization they portray. Most of these LIM groups, except for group 1, which is only nuclear, are found in the nucleus and the cytoplasm. In the following subsections, I will describe each group.

1.3.1 Group 1 LIM domains

Group 1 LIM domains are mainly found in LIM homeobox (LHX) protein and nuclear LMO 1-4 (LIM domain only 1-4) proteins, which have two tandem N-terminal LIM domains region [24]. This protein group is found in the nucleus and portrays distinct functions. Examples of members of this group are LIM homeodomains, transcription factors involved in the development of the nervous system. Other members, such as LMO proteins, are mainly known for their protein adaptor functions that contribute to developmental processes and oncogenesis [27].

1.3.2 Group 2 LIM domains

LIM domains that belong to group 2 consist of only LIM domains and can be found in both the nucleus and the cytoplasm of the cell [24]. This group comprises the following: the cysteine and glycine-rich protein (CRP), four-and-a-half LIM protein (FHL), and particularly interesting new cysteine and histidine-rich protein

(PINCH)[21,28,29]. CRP proteins are best known to be prominent regulators of muscle structure and myogenesis [25,30] and known protein binders of α-actinin [31].

1.3.3 Group 3 LIM domains

Members of LIM group 3 harbor one to five LIM domains and have other functional domains as part of their architecture. All LIM-containing proteins in this group have been associated with the actin cytoskeleton. Members of this group include the following families of proteins: paxillin, Zyzin, TES, PDZ-LIM proteins, actin binding LIM protein (ABLIM), epithelial protein lost in neoplasm (EPLIM), and LIM and SH3 (LASP) proteins. In this section, I will briefly describe each member mentioned above, along with a summary of the cytoskeletal functions of these proteins.

Paxillin and zyxin are markers for focal adhesions (FA) and act as protein adaptors to regulate cell shape and spreading via LIM-mediated protein interactions [21,28,32]. Paxillin mainly serves as an adaptor protein, mediated by its multiple protein-protein binding domains. Paxillin contains five LD motifs in the N-terminal region and four C-terminal LIM domains. The leucine-aspartic acid motifs (LD) serve as protein adaptor hubs and bind FA-associated proteins such as focal adhesion kinase (FAK), parvins, vinculin, talin, integrin-linked kinase (ILK), p21-activated kinase (PAK), and others [21,28,29,33]. When phosphorylated, the LIM domains of paxillin potentiate anchoring to the plasma membrane[33 34]. On the other hand, Zyxin is thought to be mechanosensory. Specifically, the LIM domains are responsible for localization force-bearing sites at the leading edge of the cell [35].

Testin, also called TES, localizes to FAs, stress fibers, and areas of cell-to-cell contact. It is believed to act as a tumor suppressor, as its expression in T47D breast cancer cells negatively regulates proliferation [36-39]. The LIM domains of TES have been associated with mechanically-strained F-actin [40]. Interestingly, the LIM domains are thought to mediate intramolecular and intermolecular interactions with the N-terminal PET domain in a "head-to-tail manner." However, no function has been attributed to these changes in conformation and oligomerization[41]. Transitions between the "open" and "closed" conformation of TES are believed to be regulated by the binding of protein partners or phosphorylation of the LIM domains[41].

PDZ-LIM proteins, also known as the ENIGMA family of proteins, are important for the migratory capacity of epithelial cells and muscle development. They are bound to the actin cytoskeleton via their association with α-actinin [36,42]. The LIM domain found in this family of proteins is known to bind protein kinases such as Ret and insulin receptors. In contrast, the PDZ domain directly interacts with actin filaments [43-45]. Intramolecular interactions of PDZ and LIM domains in this family of proteins have been observed, i.e., reverse-induced LIM genes (RIL) proteins, where the N-terminal PDZ domain interacts with the C-terminal LIM domain [46]. The specific sites mediating this interaction have yet to be identified as it is believed to be mediated independently of canonical PDZ binding [46]. The structural basis of this interaction has yet to be resolved.

Actin-binding LIM protein (ABLIM), like the rest of the members of LIM group 3, is associated with the actin cytoskeleton, showing strong binding to F-actin via its villin headpiece domain (VPH). At the same time, its LIM domains are involved in recruitment to cell-cell contacts[47]. EPLIN contains two actin-binding domains, N and C- terminal to the central LIM domain. More specifically, EPLIN has been associated with actin dynamics as it can function as an actin cross-linker [48]. Since it can bind more than one actin subunit, it lowers the dissociation rate constant at the pointed end of actin filaments, leading to actin filament stabilization [49]. Also, EPLIN is a protein binding partner of α-catenin, which links the cadherin-catenin complex to F-actin in adherent cell junctions, making it important for mechanical response [50]. Lastly, the LASP family of proteins, also actin-binding proteins, contain an N-terminal LIM domain, followed by two nebulin-like repeats, and an SH3 domain at the C-terminus [51]. The nebulin-like repeats are associated with actin filament binding, while the LIM domains are believed to mediate homodimerization. However, this has not been shown *in cells*. LASP LIM domain and the first nebulin repeat module are necessary for actin filament binding [52].

1.3.4 Group 4 LIM domains

The group 4 LIM domain proteins possess both an enzymatic domain and LIM domains. This family of proteins includes LIM domain kinases (LIMK1 and LIMK2) and microtubule-associated monooxygenase, calponin, and LIM domain-containing protein (MICAL).

LIMKs are involved in regulating actin dynamics by the phosphorylation of cofilin proteins. The LIM domains of LIMK bind to different protein partners and mediate autoregulation of the C-terminal kinase domain [16,53,54]. The various LIMK LIM domain binding partners are discussed in section 1.8. Although the LIM domains have been shown to increase LIMK kinase activity when mutated or deleted, the exact regulation mechanism remains elusive. I discuss this at length in Chapter 3, where I focus on the role of the LIM2-PDZ tandem domain in regulating LIMK catalytic activity.

The MICAL family of proteins contains a flavin monooxygenase domain in the N-terminus, followed by calponin homology (CH) and LIM domains, and a C-terminal Rab (Ras-associated binding) binding domain (RBD). The flavin monooxygenase domain binds and oxidizes F-actin to disassemble the actin cytoskeleton during repulsive axon guidance [55,56]. Interestingly, the MICAL N-terminal half (monooxygenase-CH-LIM) engages the C-terminal RBD domain intramolecularly [57]. This interaction is disrupted by the binding of Rab to the C-terminal RBD and is believed to regulate the activity of the monooxygenase domain [58].

LIM domain-containing proteins are heavily involved in actin cytoskeleton processes. They share diverse functions, are mainly believed to be protein-protein interaction domains, work to bring protein complexes together, and can also serve as autoregulatory activity agents when found in protein enzymes.

1.4 LIM domain binding modes

Although LIM domains are conserved in terms of their secondary structure, they recognize their targets in highly diverse modes **(Figure 1.4 A)**. Efforts to find binding sequences have yet to identify a consensus recognition motif in binding partners. However, when analyzing current structural information of LIM domain complexes, LIM domains usually bind partners in one of two opposing sides of the LIM domain. LIM domains bind via the front or zinc knuckle [59] **(Figure 1.4 B),** which is mediated by specific interaction in the zinc-containing face of the domain or the side opposite to the zinc knuckle, referred to as the beta zipper **(Figure 1.4 C).** The beta zipper face of the LIM domain interacts with binding partners often using its beta sheets [60]. In LIMK, LIM domains are believed to be involved in intramolecular or intermolecular interactions with the kinase domain. In Chapter 3, I describe my studies to assess the LIM domain's role in autoregulation.

1.5 LIM domain-general function

LIM domains can function in four ways - as adaptors, competitors, autoinhibitors, or localizers. Examples of each function will be given in the following subsections.

1.5.1 LIM domains as protein adaptors

LIM domains mediate protein-protein interactions. Therefore, LIM-containing proteins often function as scaffolds to support the assembly of multimeric protein complexes [25]. One example of LIM domain scaffolding function is observed between the Cysteine-rich protein (CRP) family of proteins and the regulation of muscle-expressed genes [61]. CRPs have two LIM domains linked by

two short glycine-rich repeats and are essential for cell differentiation, cytoskeletal remodeling, and transcriptional regulation. CRP protein members regulate transcription via the adaptor function of its LIM domains. CRP interacts with SRF (serum-response factor) when translocated to the nucleus via its N-terminal LIM domain and GATA-factors 4 and 5 via its C-terminal LIM domain. The recruitment of SRF and GATA-factors 4 and 5 by CRP LIM domains are important for the stimulation of expression of smooth muscle genes [61] (**Figure 1.5 A**).

1.5.2 LIM domains as protein competitors

Some LIM domains can regulate cellular activities by competing for LIM domain binding sites of common partners. LMO (LIM-only protein), LIM-HD (LIM-homeodomain), and Lbd1 (LIM domains-binding protein 1) are examples of the LIM domain's ability to regulate the transcription activity of developmental genes and cell fate. LIM-HD and LMO are regulated by Lbd1 [62,63].

Lbd1 contains an N-terminal dimerization region, central for its function, and a C-terminal LIM binding domain (LID) composed of 39 residues. Multimerization of Lbd1 enhances DNA binding by LIM-HDs. LMO regulates the transcription and downregulates LIM-HD activity by competing for binding to Lbd1 LID domain [64-66],

The structure of LMO LIM1-2 bound to the Lbd1 LID region reveals that the proteins form a rod-like structure, with the LID region bounded in an extended manner across the entire length of the two tandem LIM domains. This complex forms a tandem β-zipper mediated by a network of extensive hydrogen-bond and electrostatic integrations [65] (**Figure 1.4C**).

1.5.3 LIM domains in protein localization

LIM domains are essential for the proper distribution of proteins to specialized compartments. Zyxin, which contains three C-terminal LIM domains, has been shown to translocate testin (TES) to focal adhesions via its LIM1 domain. This recruitment is fundamental for the movement of TES to focal adhesions[36-39] (**Figure 1.4C**).

1.5.4. LIM domains as autoinhibition modules

Changes in conformation can regulate protein function. LIM domains serve an autoinhibition function in some LIM-containing proteins. Specifically, my thesis focuses on the autoregulation of LIMK via its N-terminal LIM and PDZ domains. As discussed in this thesis, the LIM domains of the LIMK family of proteins (LIMK1 and LIMK2), specifically the LIM2 domain, regulate the catalytic activity of LIMK [53,54]. This autoinhibition mechanism is crucial for adequately transducing signals in cofilin-dependent actin processes. (**Figure 1.4D**). In Chapter 3, I study how the LIM domains may work in concert with the PDZ to regulate the activity of LIMK.

1.6 LIMK contains a PDZ domain

Followed by two sequential LIM domains is a PDZ domain. PDZ domains, named after the **P**SD-95, **D**lg-1, and **Z**O-1 proteins where they were first discovered, are also protein-protein interaction modules involved in forming protein complexes [67, 68-72]. PDZ domains are among the most studied domains, with more than 268 domains in 151 unique human proteins [73-75]. PDZ domains contain a conserved structural fold consisting of 5 to 6 β-strands (βA-βF) and 2 to 3 α-helices (αA-αC)

[76-80]. In some cases, a C-terminal α-helix distal to the binding cleft is important for tight protein-protein interactions of target C-terminal partners [81-85]. (**Figure 1.6**).

In sections 1.6, 1.7, 1.8, and 1.9, I will discuss and describe PDZ domain function, classification, and regulation in depth. Specifically, in section 1.6, I describe the PDZ domain fold and canonical C-terminal binding. In section 1.7, I will discuss the classification of these domains and the sequence features they recognize. In section 1.8, I will discuss the main functions PDZ domains can portray, and lastly, in section 1.9, I will discuss the regulation of PDZ interactions. These sections will provide a framework for understanding the various roles of PDZ domains and why my discoveries addressed in Chapter 2 significantly advance the understanding of LIMKs and expand the understanding of the well-studied PDZ fold.

1.6.1 PDZ domains canonically contain a conserved x-Φ-G-Φ motif

PDZ domains often bind their biding partners via a conserved binding groove between the βB and αB containing a conserved sequence called the "GLGF" motif, or 'x-Φ-G-Φ' motif where x represents any amino acid, and Φ represents any hydrophobic amino acids [72, 86,87] (**Figure 1.7 A).** The second residue of this motif adopts an α-helix conformation, while the fourth adopts a β-sheet conformation. Notably, the carboxyl oxygen atom of the second residue forms H-bonds with a residue in the α-helix, stabilizing the short helix. The third Gly in this motif is completely conserved in PDZ domains and adopts the left-handed α-helical conformation, which is thought to be essential for the PDZ fold [87]. Notably, the

proper conformation of the residues in this loop permits amide groups to serve as the H-bonding donors [81,87-94]. In Chapter 2, I discuss the novelty of the LIMK PDZ domain, particularly its unusual features in the region of the x-Φ-G-Φ motif.

1.6.2 Canonical binding of peptide C-termini by PDZ domains

Canonical PDZ binding involves the C-terminus of a polypeptide chain interacting with the x-Φ-G-Φ, forming an extended antiparallel β-sheet that stacks against the βB helix through a network of H-bonds between the peptide and residues in the binding cleft [68] (**Figure 1.7 B**). The ligand binds to the PDZ domain as an anti-parallel extension of the β-sheet of the domain, and while ligands at positions -1 and -3 head toward the solvent, the positions 0 and -2 point toward the binding pocket [95]. Positions 0 and -2 are crucial for recognition by their corresponding PDZ domain partner [87]. The importance of this binding cleft region has been fundamental for the study of PDZ domains. Historically, the identity and mode of binding of a C-terminal sequence have been the basis for the PDZ classification.

1.7 PDZ classification

PDZ domains are mainly classified based on the C-terminus sequence these domains recognize, and three different classes have been characterized: Class I, Class II, and Class III [87,96-103]. Specificity in PDZ domains is driven mainly by the interaction of the first residue of helix αB (position αB1) and the side chain of the -2 residue of the C-terminal ligand [104]. The identity of other residues at the C-terminus of binding partners can contribute to specificity, such as the -3 position and position -8 [87]. Although this classification might be inaccurate in some instances, as PDZ

domains can bind some targets promiscuously, C-terminus binding sequence remains the primary classification mode for PDZ domains **(Table 1.1)**. In the following subsections, I describe each class and conclude by relating these classes to what is known about the LIMK PDZ domain categorization in Section 1.9.3.

1.7.1 Class I PDZ domains

Class I PDZ domains bind a consensus sequence X-T/S-X-ϕ-COOH, where a hydrophobic amino acid (ϕ) is at the C-terminus or position 0, followed by any amino acid (X) at -1, and then Ser or Thr at the -2 position [104,105]. Structurally, many of the PDZ members of this class contain a conserved His at the C-terminus of αB and mediate hydrogen bonding with the hydroxyl group of the S/T in the -2 position in the peptide binder[106 86,107,108].

1.7.2 Class II PDZ domains

Class II PDZs recognize ligand sequences with the ϕ-X-ϕ-COOH motif at the C-terminus. Unlike Class I PDZ domains, class II PDZ domain interactions are characterized by hydrophobic interactions. Instead of a His residue at the C-terminus of αB, Class II PDZ domains contain a hydrophobic residue [109-111].

1.7.3 Class III PDZ domains

Class III PDZ domains recognize D/E-X-Φ-COOH[71,105,112]. This specificity is determined by the coordination of a hydroxyl group of a Tyr residue in the C-terminus of αB with the side-chain of an Asp at position -4 in the C-terminal peptide [109,113].

To date, most PDZ domains are classified as Class I or Class II PDZ domains. However, only some PDZ domains in the human genome have been assigned a C-terminus binding sequence. Therefore, intersection of classes are believed to be the case for many PDZ domains. The LIMK PDZ domain has not been assigned to a PDZ class as no functional peptide C-terminal sequence identified binds specifically to it. A C-terminal Class III "DKV" motif in MT1-MMP was suggested to bind to the PDZ domain of LIMK1[14]. However, it is not clear if this interaction is direct. In section 1.15.1, I detail the interaction between LIMK1 and MT1-MMP protein.

1.8 PDZ domain functions

PDZ domains can exist as independently folded domains or in the presence of other domains as units within multi-domain proteins. Most PDZ-containing proteins lack intrinsic enzymatic activity and mainly function as scaffold proteins[71,87,109,114-118]. PDZ domains are fundamental for a wide range of cellular processes, including directed cell migration, establishment of cell polarity, embryonic development, trafficking and clustering of receptors, and targeting of signal complexes, and have been associated with different types of cancers [67,115,119-126].

In the following sections (1.8.1 – 1.8.7), I will discuss the various functions of PDZ domains and how these functions relate to the potential role of the PDZ domain of LIMKs.

1.8.1 PDZ mediated interactions and non-canonical PDZ binding of protein binding motifs (PBM)

In addition to C-terminal peptide binding, PDZ domains can mediate other non-canonical binding interactions. Non-canonical binding of PDZ domains involves binding internal loops and other non-terminal peptides such as ankyrin repeats, spectrin repeats, LIM domains, and phosphoinositide lipids[46,78,127-132]. In the following subsection, I provide an example of non-canonical PDZ domain binding.

1.8.2 Homotypic PDZ interactions

One prominent feature of PDZ domain proteins is that they commonly contain multiple PDZ domains. Often, in these various PDZ domains, the sequence between them is highly conserved and may play a role in the PDZ domain functionality. Frequently, PDZ domains in these proteins interact, forming homotypic PDZ interactions. One example of this is found in GRIP1.

Glutamate receptor-interacting protein 1 (GRIP1) is a PDZ domain only containing seven PDZ domains. GRIP1 PDZ4 and PDZ5 bind the C-terminal tail of the GluR2 subunit of the AMPA receptor [79]. The interactions occur specifically with PDZ5; however, PDZ5 cannot bind its target C-terminal peptide without PDZ4. A closer look at the published crystal structure reveals that the conserved linker between the two PDZ domains plays a critical role in integrating the function of the two PDZ domains by forming a β-strand antiparallel to βA of PDZ5 and by directly interacting with the N-terminal extension of PDZ4[133]. Interestingly, the PDZ5 on its own is unfolded and cannot bind the C-terminal peptide of GluR2, while the PDZ4

is stably folded. Therefore, the role of PDZ4 is to keep the PDZ in a stable fold, thus creating a PDZ supramodule apt for binding the C-terminus of GluR2[79] (**Figure 1.8.A).**

1.8.3 Heterotypic PDZ interactions

PDZ-containing proteins can also coexist with other protein-protein interaction domains or signaling modules. Observations of heterotypic PDZ supramodules have been observed and are considered fundamental for creating higher-order units that carry specific functions [73,123,134]. An example can be observed with the Harmonin and Sans complex.

Harmonin is a multi-PDZ-containing protein that, together with Sans (USH1G) and other protein members, forms the USH1 (Usher syndrome 1) protein complex [135]. Biochemical data have revealed that the Harmonin N-terminal domain, PDZ1, and a stretch of residues after PDZ1 are required to interact with the SAM (sterile α-motif) domain and C-terminal PDZ binding motif (PBM) of Sans [136]. This is explained by the N-terminal domain and PDZ1 being tethered by the C-terminal PDZ1 extension, creating a miniature domain composed of a β-hairpin followed by an α-helix. This supramodule can interact with Sans's C-terminal peptide and the SAM domain. The crystal structure of this complex revealed that the canonical Sans C-terminal sequence binds to the αB/βB groove of the PDZ1 of Harmonin, and the upstream four residues (-4 to -7 position of the C-terminal peptide of Sans) interact with the miniature domain extension that follows the PDZ1. PDZ1 is unstable when expressed independently and unable to bind to the

Sans C-terminal peptide. Therefore, the interaction between the N-terminal domain and PDZ1 of Harmonin is necessary to form a high-affinity complex with Sans's C-terminal PBM and SAM domain (**Figure 1.8.B).**

1.8.4 Internal Peptide Binding

PDZ domains primarily bind C-terminal peptides on their binding targets. This interaction is observed in the canonical binding cleft between the αB and βB structural features. Interestingly PDZ domains can interact with internal peptides in this cleft. One example is observed in Par-6 (partitioning defective)-6 PDZ domain and Pals1 PBM [128].

This complex structure revealed that the Pals1 internal PBM adopts an extended conformation compatible with binding to the αB and βB binding cleft. The aspartic acid side chain at position +1 in the internal peptide sequence simulates the carboxy group binding loop of the PDZ domain [128](**Figure 1.9 A).**

1.8.5 Distal interactions in canonical PDZ binding

In canonical PDZ binding, other PDZ-C-terminal interactions have been observed. In the case of Par-3 PDZ3 domain and the PTEN (phosphatase and tensin homolog deleted on chromosome 10) or VE-cadherin (vascular endothelial cadherin), two distinct binding sites have been observed. The first binding site is the canonical PDZ ligand binding cleft. The second binding site is distal to the binding cleft and mediates a charge interaction in the βB/βC loop [110,137]. The two distinct binding sites are thought to be necessary for interaction specificity [137]

(**Figure 1.9 B).** In Chapter 2, I discuss distal binding for the LIMK PDZ domain. My studies suggest this to be an important aspect of LIMK autoregulation.

1.8.6 Allosteric Regulation of PDZ binding activity

PDZ domains can also undertake allosteric regulation. Par-6 PDZ domain contains a semi-CRIB (cell division cycle 42/Rac-interactive binding) in its N-terminus known to bind covalently to the in its active GTP-bound form of Cdc42[138]. In its apo form, the Par-6 PDZ N-terminal CRIB extension is unstructured. However, upon Cdc42-GTP binding, it forms a β-strand extension antiparallel to both β2 of Cdc42 and βA of Par-6 PDZ. Also, Cdc42 interacts directly with the αA helix of Par-6. This new network of interactions mediated by the binding of Cdc42 allosterically affects the peptide binding groove of the Par-6 PDZ domain, enhancing its binding affinity to C-terminal peptide targets [139] (**Figure 1.10 A**). In Chapter 3, I also explore how a possible interaction between the LIM2 domain could allosterically affect PDZ binding to protein partners.

1.8.7 Domain swap dimerization of PDZ domains

PDZ domains can also recognize PDZ binding motifs using domain swap. Domain swaps happen when two or more identical protein monomers exchange structural elements and form dimers structurally similar to the original monomer[140]. This mechanism is observed in ZO-1 PDZ2 and Connexin43 (Cx43) [141]. The structure of this complex shows that the ZO-1 PDZ2 undergoes domain swap dimerization, induced by the lack of connecting residues between its βB and βC [141]. The domain swap dimerization is necessary to create a highly charged target-binding site at

the dimer interface, distal to the canonical C-terminal binding cleft. This new binding site increases the affinity and specificity of Cx43 in binding to ZO-1 PDZ2. Interestingly, two Ser residues at the -9 and -10 positions of the Cx43 C-terminal PBM are reported kinase substrates, and phosphorylation of these residues is thought to weaken the interaction with ZO-1 PDZ [142]. Dynamic modification of these residues is considered a regulatory switch (**Figure 1.10 B**). Clearly, in total, PDZ domain-mediated interactions can happen in distinct ways

LIMK PDZ domain might use one or more ways to target specific binding partners to LIMK. Also, its interaction with binding partners might be regulated by changes in the conformation of its binding cleft, or it may employ a novel recognition mechanism. In Chapter 2, I provide in-depth information on the PDZ domain of LIMK and how it may be involved in regulating catalytic activity.

1.9 Regulation of PDZ interactions

PDZ domain interactions are most often reversible. In the following subsections, I describe the functional regulation of PDZ interactions, including phosphorylation, autoinhibition, and allosteric regulation. I then discuss how the LIMK PDZ domain might utilize these functions to regulate kinase activity.

1.9.1 Phosphorylation in PDZ-mediated interactions

C-terminal PDZ binding motifs (PBM) contain Ser, Thr, and Tyr residues that participate in engagement with cognate PDZ binding partners [26,87,127,143-147]. Phosphorylation of these residues in PBMs is expected to weaken or completely disrupt their PDZ binding capabilities. An example of PBM phosphorylation is

observed in the subunit GluR2 tail of the AMPA receptors. As mentioned in a previous section, the GluR2 tail can bind the PDZ4 and PDZ5 of GRIP1. Also, it has been shown to bind to the PDZ domain of protein interacting with C kinase (PICK1). The GluR2 C-terminal sequence, IESVKI, is phosphorylated at position -3 (Ser) residue by Protein kinase C (PKC). This phosphorylation binding affinity to the GRIP1 PDZ4 and PDZ5 domains, but it retains a similar affinity towards the PICK1 PDZ domain. Structural studies were able to explain the reduction in affinity. The crystal structure of the GluR2 C-terminal tail bound to the PICK1 PDZ domain shows a Lys residue in the bottom of the αB1 position, possibly favorable for binding phosphorylated -3 Ser. On the other hand, GRIP1 contains a glutamic acid at this position. This charge would probably repel phosphorylated -3 Ser, making it an unfavorable interaction, which could explain the decrease in affinity (**Figure 1.11 A**). Therefore, phosphorylation of PBM is a regulatory mechanism that regulates PDZ binding interactions in the cell.

1.9.2 Autoinhibition of PDZ domains

Autoinhibition is a well-represented regulatory mechanism in protein signaling complexes. Some PDZ-containing proteins have a PBM at the C-terminus that can bind to their own PDZ and prevent binding from other ligands. One example of this is observed in X11α, a member of the X11/Mint family of multidomain scaffold proteins, comprising X11α/Mint1, X11β/Mint2, and X11γ/Mint. Each family member contains a conserved phosphotyrosine-binding domain (PTB) followed by two C-terminal PDZ domains. When isolated, the two PDZ domains exhibit

different binding properties than when expressed in tandem. Structural studies revealed that the two PDZ domains interact, forming a PDZ supramodule. The C-terminal tail of X11α folds back and inserts itself in the binding cleft of the first PDZ domain (PDZ1), creating a closed conformation of PDZ1[148].

Interestingly, this autoregulation is regulated by phosphorylation, as the C-terminal X11α tail contains a conserved Tyr at position -1 that is thought to act as a molecular switch. Mutation of -1Tyr to Glu releases the autoinhibitory tail of X11α from PDZ1, which then binds to the PDZ2 and mediates different signaling events [148]. This autoinhibition mechanism, coupled with phosphorylation observed in X11α, exemplifies how different regulatory mechanisms of PDZ-mediated interactions are important for X11α targeted interactions (**Figure 1.11 B**).

1.9.3 Allosteric conformation regulation

PDZ domains rely on allosteric conformational changes to regulate the propagation of signals[102,118,149]. Allostery in PDZ domains is a phenomenon where ligand-binding changes the conformation or dynamics of a distal region [102,118,127,149]. These changes in conformations not only affect local conformation but are also thought to change the thermodynamic landscape of the domain.

An example of allostery can be revisited from the Par-6 PDZ and CRIB domain complex. Specifically, changes in the αA helix induce allosteric changes in the PDZ domain. In the case of Par-6 PDZ and CRIB, binding of Cdc42 to the Par-6 PDZ αA-helix causes conformational changes that increase the binding affinity of C-terminal peptide ligands. However, internal peptide binding of Pals1 to the

Par-6 PDZ domain, independent of Cdc42, also induces conformational changes in the PDZ binding cleft that allow for peptide binding[128,138,139,150,151]. Pals1 relies on specific interactions beyond the residue at position 0 to take advantage of the carboxylate binding loop region conformation plasticity of the PDZ domain of Par-6[151]. Par-6 is an example of a two-way allosteric regulation, which is considered fundamental for regulating Par-6 binding partners. Allostery has been observed in other parts of the PDZ domain, such as the αA helix, the αB lower-loop, and the αC helix [73,103,116,149] (**Figure 1.10 A**). In my structural studies of the LIMK PDZ domain, I find unusual structural features in the canonical αA helix region, which may represent a potential inference of allosteric changes in LIMK PDZ.

1.9.3 LIMK PDZ domain peptide binders

In the case of LIMK, peptide binding screens such as phage display have failed to determine binding partners for LIMK PDZ [67,101,152,153]. Recently, a study found a consensus recognition sequence for LIMK PDZ domains [154]. This study used a PDZ-PBM interactome covering all 266 human PDZ domains to quantify dissociation constants of PDZ interactions with a 10-mer peptide library of viral and human PBM. Coupled with mass spectrometry and a threshold for identification between a K_d of 0.3 to 800 μM, this study found only nine peptides binding to LIMK1 PDZ and one binding to LIMK2 [154]. Based on their findings, a PBM consensus can be extracted from this study, ETXV/L-COOH, which would place LIMK as a Class I PDZ domain. However, LIMK does not contain a His residue C-terminal to the αB, a typical signature of Class I PDZ domains. One of the screen

hits corresponds to a C-terminal sequence from Lymphokine-activated killer T-cell-originated protein kinase (PKB). This C-terminal peptide binds LIMK1 PDZ with a K_d of 30 μM. However, more studies are needed to corroborate the *in vitro* binding of this PBM to LIMK1. A C-terminal Class III "DKV-COOH" motif in MT1-MMP has been reported to bind to the PDZ domain of LIMK1. However, no *in vitro* validation has been reported for this interaction. More studies are needed to validate whether the LIMK PDZ domain can bind a consensus Class I PDZ binding motif ETXV/L-COOH or a Class III PDZ binding motif sequence DKV-COOH or both.

The PDZ domain of LIMKs is an unusual PDZ domain. Many features of this domain do not follow canonical PDZ sequence or fold. In Chapter 2, I describe the unusual features found in this domain. However, as discussed in these sections, one might assume that the LIMK PDZ domain could regulate LIMK activity using an allosteric mechanism while interacting with the kinase domain in a non-canonical manner (LIMK does not contain a C-terminus PDZ binding motif). Protein binding partners could bind to this PDZ and interrupt PDZ-mediated regulation of LIMK. Regulation of these interactions could involve phosphorylation of binding regions and conformational changes upon binding that might affect the affinity of the PDZ domain to the kinase domain.

1.10 LIMK contains a Ser/Pro-rich region

Following the PDZ domain is a linker region rich in serine and proline residues (S/P rich region) (**Figure 1.2**). Although this region is less conserved than the LIMK

protein domains, it shows conservation in specific Ser residues (**Figure 1.12**). The Ser/Pro-rich region is considered flexible and important for activity regulation.

Conserved serine residues within the linker region are believed to be substrates for Aurora kinase [155], PKA [156], and MK2 [157] and could be significant in kinase regulation and pathway divergence. This topic will be described in a later section (Section 1.16).

In an intramolecular regulation model, this region's flexibility could be necessary for the N-terminus and C-terminal to come into proximity.

1.11 LIMK contains a kinase domain in the C-terminus

Protein phosphorylation is fundamental for regulating and coordinating different cellular processes, including gene expression, cell growth, differentiation, motility, and division [158-163]. Proper control of these processes is dependent, to some degree, on the activity and conformation of the kinase.

Over 500 protein kinases are recognized by sequence conservation, constituting the third most populous protein family, representing close to 2% of the expressed proteins of the human genome [162]. Most protein kinases phosphorylate serine or threonine residues, while a smaller number phosphorylate tyrosine [162,164]. The protein kinase fold is about 300 amino acids in length. The active site is "sandwiched" between an N-terminal lobe, mainly containing β-strands and one helix (termed the αC helix) and the C-lobe. The N-lobe includes the phosphate binding loop (P-loop), which is Gly-rich motif involved in the alignment of the phosphate groups for catalysis, an AxK sequence in the β3, where the Lys can

stabilize ATP binding in conformationally active kinases or form a salt bridge with an Asp in the αC in conformationally inactive kinases. The C-terminal lobe is connected by a linker, also known as the ”hinge region.” The C-lobe is bigger in size and includes the activation segment, composed of 20-35 residues located between a conserved DFG (Asp-Phe-Gly) motif and the APE (Asp-Pro-Glu) motif and an HRDXKXXN (His-Arg-Asp-X-Lys-X-X-Glu) sequence involved in the catalysis of the phosphotransfer reaction [165] (**Figure 1.13 A**). The conformation and phosphorylation state of the activation segment is often indicative of the “active” and “inactive” state of the kinase domain. This segment also includes the P+1 loop, which provides a docking site for the residue immediately after the target phosphorylation residue in the substrate [166-168]. The identity of the P+1 loop is usually correlated with the specificity of the kinase [166-168]. The P+1 loop is essential for the interaction of the peptide backbone of a bound substrate. It is crucial to control the distance of the peptide backbone from the active site, thus dictating the size of the phosphoacceptor that can be accommodated [169,170]. Moreover, docking interactions between short peptide motifs on the substrate and a groove on the catalytic domain outside the active site in the kinase/substrate can confer high specificity and, in some cases, allosteric regulation [171].

1.11.1 Protein kinase active conformation and inactive conformation

Protein kinase active conformation involves changes that allow for the proper positioning of the substrate and catalytic groups and the dissipation of any steric blocking to permit the substrate to access the catalytic site [165]. Phosphorylation of

the activation segment is known to change the kinase conformation to allow for substrate binding and catalysis. The activation segment can be phosphorylated by other kinases or the kinase itself. In some cases, it depends on the sequence around the phosphorylation residues and if this sequence agrees with the kinase specificity [165,172]. However, for some Ser/Thr kinases, the autophosphorylation site differs from the kinases' substrate specificity sequence [173].

In the inactive state, the activation loop is often structurally disordered. In contrast to the active kinase conformation, the inactive state is structurally highly diverse between protein kinases since there are no catalytic constraints on the fold. However, a common feature in inactive kinases includes the Phe from the DFG motif being turned toward the ATP binding site and changes in the orientation of the C-helix [162].

1.11.2 ATP engagement in the catalytic cleft

The kinase engagement with ATP is described as the C-helix packing the N-terminal lobe, with the Asp of the DFG motif chelating the Mg^{2+} ion to orient the ATP. The triphosphate group is oriented out of the ATP pocket to transfer the γ-phosphate to the peptide substrate. In the N-terminal lobe, a conserved Glu within the C-helix, a Lys on β3, a bound Mg^{2+} by the Asp in the DFG motif, and an Asn in the C-terminal lobe collectively help position the α and β phosphate groups within the ATP binding pocket. A second Mg^{2+} is often bound to an Asp and the β- and γ-phosphate groups, further stabilizing the ATP conformation. Other sidechain interactions are observed between the ATP β- and γ-phosphate groups, and the

glycine-rich loop located between β1 and β2 in the kinase N-lobe also stabilizes the ATP conformation (**Figure 1.13 B**).

Phosphorylation of the activation loop triggers the adoption of a catalytically competent conformation to recognize the peptide substrate. In the case of the Ser/Thr kinase PKA (PDB: 1ATP), phosphothreonine (pThr) is the center of a network of bonds with the residues His87 from the C-helix, Arg165 from the HRD motif, and Lys189 from the activation segment that helps "close" the two lobes for the correct change in conformation, compatible with substrate binding[174] (**Figure 1.12 C**). Not all kinases require activation loop phosphorylation to be catalytically active; other kinases can adopt the correct conformation through other interactions (e.g., phosphorylase kinase (PhK), epidermal growth factor (EGFR), and others). Other structural motifs have been related to active and inactive conformations, such as the position of the Asp in the DFG motif and the formation and the dynamic assembly of the "spine," composed of hydrophobic residues that help coordinate the active conformation[168,175].

1.11.3 Kinase reaction

The kinase reaction is thought to encompass three significant steps; first, the hydroxyl group of the side chains of Ser, Thr, or Tyr is positioned opposite to the leaving group (phosphate ester oxygen), leading to inversion of the configuration at the phosphorus, then nucleophilic attack by the substrate hydroxyl group, followed by general base catalysis from the catalytic Asp (HRD) and finally general acid catalysis for the transfer of the proton [162].

1.11.4 Ser/Thr kinases

Serine/Threonine kinases are involved in the phosphorylation of the hydroxyl group of Ser or Thr substrates and are the most populated group of the human kinome[12]. Structurally, the most studied group, the Serine/Threonine kinases, follow the canonical kinase fold and show conserved signature residues in the catalytic domain necessary for accommodating small aliphatic phosphoacceptor residues [169]. Some clues in their catalytic cleft provide information on their specificity. A Lys residue follows the catalytic Asp, two residues away, and contacts the γ-phosphate to stabilize the local negative charge during catalysis. The DFG motif also provides information about the substrate specificity of the kinase, as the DFG+1 residue dictates the preference for Ser or Thr in Ser/Thr kinases [176]. A β-branched residue in the DFG+1 position is most found in protein kinases that prefer Thr, while Phe dictates a preference for Ser[176]. LIMK contains a Leu in the DFG+1 position, which correlates with Ser specificity. However, this motif cannot explain its dual specificity activity.

1.11.5 Dual specificity kinases

Dual-specificity kinases can phosphorylate Ser/Thr and Tyr residues. Early research suggested that dual-specificity kinases could phosphorylate both Ser/Thr and have the capacity to autophosphorylate at Tyr residues. However, dual-specificity kinases have been shown to be true dual-specificity kinases with the ability to phosphorylate Ser/Thr and Tyr in exogenous substrates [177].

No consensus sequence has been found in the kinase domain that provides definite information about the dual specificity of a kinase. It is possible that one or more modifications in the amino acid sequence of a kinase domain can change the selectivity of a kinase by steric changes in the catalytic site that allow the accommodation of a larger residue. Moreover, dual-specificity kinases are thought to have a more flexible active site than the Ser/Thr kinases and Tyr kinases counterparts that permit positioning of either type of hydroxyl group. Also, the substrate is oriented in the active site, so the hydroxyl is directed toward the catalytic Asp (in the HRD motif). In Ser/Thr kinases, a Lys residue follows the catalytic Asp, two residues away, and contacts the γ-phosphate to stabilize the local negative charge during catalysis. An Arg residue, four residues away from the catalytic Asp, in tyrosine kinases, allows for the larger tyrosine residue [162]. Another key difference is the identity of the APE -5 residue (5 residues upstream of the APE motif at the end of the activation loop). In Ser/Thr kinases, a polar residue (usually Thr) always makes polar contact with the catalytic Asp. In Tyr kinases, it is always a Pro residue, which makes hydrophobic interaction with the Tyr aromatic ring form the substrate[178].

1.11.6 Tyrosine kinases

The tyrosine kinase family of proteins includes receptor tyrosine kinases and non-receptor tyrosine. These protein kinases are known to phosphorylate Tyr residues in different substrates and are the less populated group of the human kinome[12].

Receptor tyrosine kinases are cell-membrane receptors that carry catalytic activity. For most receptor tyrosine kinase binding of extracellular ligands, oligomerization, and transphosphorylation of the kinase domain activation loop lead to creating a catalytically competent kinase [170]. Below, I describe some of the regulation mechanisms for non-receptor tyrosine kinases. These mechanisms may provide insights into how the LIMKs are regulated as LIMK are dual specificity kinases.

Non-receptor Tyr kinases lack receptor-like features and are mainly localized in the cytoplasm and cell periphery due to lipid modifications and other types of interactions. Non-receptor Tyr kinases possess domains that mediate protein-protein interactions, such as the Src homology 2 (SH2) and 3 (SH3) domains, or domains required to localize to specific sites of the cell [170].

Tyr and Ser/Thr kinase domains share the same overall fold, resulting from the selective evolutionary pressure to retain catalytic activity. Differences are observed with insertions on surface loops and conservation in their catalytic domain that is thought to help accommodate the larger Tyr aromatic side chain [160,170]. The major difference between Ser/Thr kinases and Tyr kinases is observed in the activation loop, as the conformation of this loop depends on the phosphorylation state of the activation residue. In Ser/Thr kinases, a Lys residue follows the catalytic Asp, two residues away, and contacts the γ-phosphate to stabilize the local negative charge during catalysis. An Arg, four residues away from the catalytic Asp, in tyrosine kinases, allows for the larger tyrosine residue [162].

1.11.7 LIM domain kinases are dual-specificity kinases

The LIM domain kinases are dual specificity kinases and, together with the TESKs, are members of the tyrosine kinase-like group [12]. LIMK contains features in its kinase domain that resemble protein Tyr kinases but it phosphorylates both Ser/Thr and Tyr residues. LIMK kinase domain possesses all the conserved sequence motifs found in protein kinase domains, including a glycine-rich loop (G-loop/P-loop), a canonical lysine 355 (Lys355 in LIMK1 and Lys347 in LIMK2) involved in ATP binding, a DFG motif (involved in kinase activation by aiding the positioning of the magnesium), an APE motif, also involved in kinase activation and an HRD motif (residues 458-460) involved in substrate binding and kinase catalytic activity. LIMK is not reported to autophosphorylate and relies on upstream regulators for activation loop phosphorylation [179-181].

LIMK is believed to be a dual-specificity kinase, meaning it can phosphorylate serine, threonine, and tyrosine. LIMK has been shown to autophosphorylate itself and phosphorylate tyrosine *in vitro* by replacing Ser3 of cofilin with a Tyr [182-185]. However, in vitro experiments of Thr phosphorylation showed very low activity [13,185]. This could be explained by the identification of a Leu in the DFG+1 position that can likely create steric hindrance for the binding of the branched Thr [176].

The kinase fold and residues essential for catalysis are highly conserved. LIMK portrays a canonical kinase fold and contains all conserved residues critical for catalysis [186]. Different from other protein kinases is its dual specificity activity,

mainly for Ser and Tyr residues, rather than Thr. Also, only one characterized substrate has been extensively studied, cofilin, making it a highly monogamous kinase.

1.12 LIMK expression and localization

LIMK1 and LIMK2 are highly related members of the LIMK family with different expression and localization profiles. In its domain architecture, LIMK1 possesses a nuclear export signal (NES) in its PDZ domain and a nuclear localization signal (NLS) in its kinase domain [187]. On the other hand, LIMK2 contains an NLS in its kinase domain that, upon phosphorylation at this site by protein kinase C (PKC), partially inhibits nuclear import [188].

Human LIMK1 and LIMK2 are encoded by two different genes, located at 7q11.23 and 22q12.2, respectively [10]. Expression profiles differ, with LIMK1 having higher expression levels in the brain, kidney, lung, stomach, and testis, while LIMK2 has a broader expression profile observed in both adult and embryonic tissue. Interestingly, a testis-specific LIMK2, also named LIMK2t, lacks the N-terminal LIM domains and a portion of the PDZ domain. LIMK2t is expressed in testis tissues and is believed to be important for spermatogenesis [189,190]. Also, LIMK2-1 has been characterized as an isoform that contains a protein phosphatase 1 (PP1) inhibitory domain thought to regulate cofilin not by phosphorylation but by interacting with PP1 and inhibiting its dephosphorylation activity towards cofilin[191].

LIMK, phylogenetically, is present in vertebrates, *Drosophila*, and *Anopheles* but is absent in yeast, *C. elegans*, and *Dictyostelium.* Therefore, it has been proposed that LIMK and its role in cofilin phosphoregulation may have evolved to reorganize the actin cytoskeleton during complex multicellular processes in some higher organisms [192]. Primarily, LIMK has been associated with normal central system development, and deletion and misregulation of LIMK have been implicated in humans with developmental disorders including tumor-cell invasion, metastasis, and abnormal testis development, and others [17,193-201].

1.12.1 LIMK genetic deletions

Deletion of the region that encodes for the LIMK1 gene has been associated with abnormal nervous system development [17,202]. Specifically, LIMK1 gene deletions have been implicated in the development of the genetic condition Williams syndrome, characterized by impaired visuospatial cognition, neurological abnormalities, and cardiac disease [203-209]. In the case of LIMK2, deletion in mice has been shown to reduce spermatogenic ability [190]. Deletion of both LIMK1 and LIMK2 coding genes in mice impairs synaptic function [206]. Notably, the fact that the double knockouts of LIMK are not embryonic lethal may be related to the redundancy of functions with TESK1 and TESK2[210,211].

1.12.2 LIMK and disease

LIMK has been related to different diseases [17,197,200]. For example, LIMK1 has been linked to primary pulmonary hypertension (PPH), as it interacts with Bone Morphogenic Receptor II (BMPRII) tail [212]. Mutations and this tail region and

truncations have been observed in PPH patients. This interaction is briefly described in section 1.8.1, but the specific mechanism and effect of this interaction with LIMK1 activity remains to be elucidated. LIMK has also been readily shown to be involved in cancer metastasis.

LIMK, as a regulator of cell invasion, has been proposed to mediate cancer cell metastasis by controlling actin filament dynamics, as levels of phosphorylated and unphosphorylated cofilin play a crucial role in the metastatic potential of cancer cells[213-227]. LIMK overexpression coordinated with increased cofilin phosphorylation has been observed in a wide range of cancer cells, including melanoma cells, breast cancer cells, and prostate cancer tumors, and others [17,199,217,224,228-230].

1.13 LIMK signaling pathway

LIMK proteins are fundamental regulators of actin filament dynamics in the cell and act downstream of the Rho GTPases signaling cascade. In the following subsections, I describe the signaling steps that allow LIMK kinase to function downstream of RHO-mediated pathways and mediate cytoskeletal changes. In Chapter 2, I describe how I used LIMK monogamous substrate kinase pair relationship with cofilin to recapitulate the LIMK signaling pathway in yeast. Specifically, because of the changes in cofilin phosphorylation by exogenous expression of LIMK, I can test how autoregulation of LIMK by the N-terminus domains affects cofilin phosphorylation in yeast.

1.13.1 LIMK signaling is downstream of RHO GTPase pathways

Actin dynamics homeostasis is influenced by master regulators such as the small GTPases, precisely, members of the Rho GTPase family of proteins [231-233]. GTPases mediate the intrinsic exchange of Rac, Rho, and Cdc42 and have been associated with cell cytoskeleton changes by regulating LIMK1 and LIMK2 via activator protein kinases such as PAK, ROCK, and MRCK [179-181,234] (**Figure 1.4)**.

1.13.2 Rac, a member of the RHO GTPases, was the first upstream regulator to be identified

The first Rho GTPase to be associated with LIMK signaling was Rac. Rac (Ras-related C3 botulinum toxin substrate 1) is responsible for cytoskeletal changes that mainly include the generation of lamellipodia [231,235,236]. The Rac-LIMK connection came after a study identified β-actin as a LIMK binder in pulldown experiments [189]. To investigate how Rac-LIMK1 binding interactions impact the cytoskeleton, Yang et al. transfected HeLa cells with the cDNA of LIMK1 [189]. They observed the accumulation of polymerized actin in the cell periphery, showing that overexpression of LIMK1 significantly impacted actin dynamics. To identify the direct binding LIMK substrate that affects actin dynamics, LIMK1 immunoprecipitates were analyzed from COS7 cells transfected with LIMK cDNA. Immunoprecipitates were subjected to *in vitro* kinase reaction with radiolabeled ATP, which revealed cofilin as a phosphorylatable substrate. This observation was later supported by *in situ* experiments showing substantial cofilin phosphorylation,

not observed in the S3A cofilin mutant, corresponding to the physiological phosphorylation site [189].

Rac is known to regulate actin cytoskeletal organization, so the next step was to test if Rac is associated with LIMK-related cytoskeletal changes. For this, COS7 cells were transfected with Rac12V (active RAC mutant) and inactive LIMK1 D460A. Control cells with only transfected Rac12V showed enhanced lamellipodia formation compared to cells co-transfected with LIMK1 D460A and RacV12. Rac was also found to be an upstream regulator as transfection of dominant active RacV12 showed a two-fold increase in LIMK1 kinase activity in *in vitro* assays using cofilin as substrate [189]. These experiments first proved the connection between small GTPase proteins and upstream regulation of LIMKs [189]. Moreover, these studies also showed that co-transfection of LIMK1 and a construct lacking 21 amino acids in the kinase domain (kinase inactive) diminished the activity of endogenous LIMK1, signaling possible regulatory interactions between the catalytic domain and possibly other regions of LIMK [20,25,189].

1.13.3 PAK acts downstream of Rac to activate LIMK1 at Thr508

As Rac was found to be an indirect regulator of LIMK1, it was later discovered that p21-activated protein kinases (PAK), which are serine-threonine protein kinases directly downstream of Rac and Cdc42, was the bridging protein to LIMK [237]. Small GTPases regulate PAK kinases through a region called Cdc42/Rac1 binding domain (CRIB), also called the GTPase binding domain (GBD)[238,239]. This region is an autoinhibitory region that, upon binding Rac and Cdc42, relieves PAK1 of its

autoinhibition and allows autophosphorylation and activation. Radiolabeled kinase assays using LIMK treated with PAK1 and GTPγS-bound Cdc42 or Rac increased LIMK1 activity towards cofilin 11-fold [237]. Other members of the PAK family, such as PAK2, PAK3, and PAK4, are known to be activators of LIMK1 and LIMK2[181,229]. Interestingly, LIMK1 activation by PAK4 is markedly more efficient than PAK1[181]. PAK4-mediated activation of LIMK1 mainly is mediated through signaling by Cdc42 and, to a lesser extent, by Rac [181].

1.13.4 RHO is an upstream regulator of LIMK

Like the findings involving Rac regulation of LIMK upstream activation, Rho was discovered as an upstream regulator. In screens used to find Rho binding partners, cells treated with lysophosphatidic acid (LPA), which helps Rho-GDP transition to the active Rho-GTP form, identified Rho-associated serine-threonine protein kinase (ROCK) as a protein binder. After ROCK identification, N1E-115 neuroblastoma cells were treated with LPA, a ROCK activator, and Y-2763A, a ROCK inhibitor, to find ROCK substrates. Substrates were chosen if phosphorylation appeared upon the addition of LPA and disappeared upon Y-2763A addition [240]. At the time these results suggested that cofilin was a substrate of ROCK, however, it was later found that LIMK was the true substrate.

1.13.5 ROCK, downstream of Rho, activates LIMK at Thr508/505

Transfection of constitutively active ROCK showed an increase in ^{32}P incorporation into cofilin[240]. Furthermore, constitutively active Rho(V14) under Rac17N constitutively inactive expression (to rule out activation of Rac-mediated

phosphorylation of LIMK) increased cofilin phosphorylation in transfected cells. Rho-ROCK mediated activation of LIMK was further corroborated by morphological observations as LIMK1 overexpression in HeLa cells induces stress fiber formations, similar to the observations made by Rho and ROCK induction. Treatment of these cells with Y-2763A (ROCK inhibitor) resulted in reduced stress fiber formation. Later, the same group identified ROCK as a possible LIMK activator, and they were able to map the site of phosphorylation [179]. Using site-directed mutagenesis in the LIMK1 kinase domain, Thr508, within the activation loop, was identified as the activation loop phosphorylation site. This observation was supported by both *in viv*o and *in vitro* experiments. *In vitro* radiolabel kinase assays showed specific phosphorylation at Thr508 when LIMK was treated with ROCK, while T508A LIMK mutant was not.

Furthermore, LIMK treatment with ROCK enhanced LIMK activity towards cofilin. In *in vitro* experiments, immunoprecipitated LIMK from N1E-115 neuroblastoma cells treated with LPA (Rho activator) showed increased kinase activity towards cofilin. This effect was reversed when the cells were treated with Y-27632 (Rho inhibitor). Additionally, COS7 cells co-expressing ROCK and LIMK showed increased cofilin phosphorylation in contrast with cells co-expressing ROCK and LIMK T508A mutant [179]. While these experiments proved the RHO-ROCK-LIMK1 signaling transduction pathway, it was later found that a different GTPase is involved in the LIMK2 signaling events. Changes in the LIMK signaling pathway are often observed with changes in cofilin phosphorylation. This is

important in the context of autoregulation, as this will be later discussed in Chapter 2.

1.13.6 Cdc42, another member of the RHO GTPase family, is an upstream regulator of LIMK Thr508/505

Experiments using expressed LIMK1 or LIMK2 together with constitutively active RacV12, RhoV14, and Cdc42V12 or inactive RacN17, RhoN19, and Cdc42N17 showed LIMK1 to have a two-fold increased activity toward in contrast with cells expressing only LIMK1[241]. On the other hand, LIMK2 activity increased approximately two-fold in cells expressing either Cdc42V12 or RhoV14. Lastly, it was found that MRCK, a kinase downstream of Cdc42, was a LIMK activator [180].

1.13.7 MRCK, a kinase downstream of Cdc42 activates LIMK at Thr508/505

Myotonic dystrophy kinase-related Cdc42-binding kinases (MRCK) are serine-threonine protein kinases involved in the actin/myosin contractability in the cell [242,243]. These proteins are critical effectors of Cdc42 and are essential for Cdc42 actin-dependent reorganization. Cells co-transfected with MRCKα and either LIMK1 or LIMK2 showed a similar 1.9-to-2.3-fold increase in LIMK activity versus cells only transfected with LIMK1 or LIMK2. Like ROCKs and PAKs, LIMK1 and LIMK2 are phosphorylated at Thr508 and Thr505, respectively, by MRCK. *In vitro* kinase assays using cofilin as a substrate showed a 5 to 6-fold increase in immunoprecipitated LIMK2 protein from cells co-transfected with MRCK[180].

These studies revealed the distinct function of Rho GTPases preferecnes in LIMK activation. LIMK1 is mainly regulated by Rac, while LIMK2 is regulated by

Cdc42 and Rho [241]. Differences in RHO GTPase preference mediate different actin cytoskeletal changes in the cell. Signaling of LIMK through RHO-dependent pathways aims to remodel the actin cytoskeleton by tightly regulating cofilin proteins. As discussed in these sections, LIMK changes in autoregulation have also shown differences in signaling through cofilin phosphorylation.

In the next section, I describe the best characterized LIMK substrate, cofilin, how it relates LIMK to control actin dynamics, and how it has been used to study LIMK autoregulation.

1.14 Cofilin, LIMK's primary substrate, drives actin cytoskeleton dynamics

Cells remodel their cytoskeleton in response to external stimuli. Proper assembly of cytoskeletal building blocks, such as actin, must be spatially and temporally regulated. Actin regulation of assembly and disassembly of actin filaments is essential for cell migration, maintenance of cell polarity, cytokinesis, and differentiation [18]. One of the molecules associated with these events is cofilin [244], and LIMK mediates tight regulation of actin-driven events by its phosphorylation [18].

Cofilin, a member of the actin depolymerizing factors (ADF) family of actin-binding proteins, is ubiquitously expressed in every tissue and is essential for life in eukaryotes [245-249]. Cofilin proteins are widely known for severing actin-rich structures by preventing spontaneous nucleotide exchange of monomeric actin, preferentially binding ADP-actin over ATP-actin, and limiting incorporation of ADP-actin into filaments [250]. Additionally, cofilins promote actin filament assembly by

increasing the pool of actin monomers. These opposing functions are determined by the molar ratio of actin to cofilin in cells [246].

The discovery of cofilin as a substrate came four years after the discovery of LIMK. While it was known that phosphorylation inactivates cofilin at Ser-3, it was unknown which kinase was responsible for this phosphorylation. A clue that directed the field toward investigating actin-related pathways was that LIMK has 2 LIM domains in its N-terminus, which had been shown to interact with cytosolic proteins related to cytoskeletal changes. While observing phalloidin-stained actin filaments in cells, it became apparent that LIMK was involved in actin dynamics [189]. Cells expressing LIMK constructs lacking the N-terminal LIM domains showed dramatic actin accumulation into large clumps [251]. Around the same time, biochemical and cellular studies further elucidated the roles of LIMK in Rho-mediated pathways, as LIMKs interacted with Rac-mediated cytoskeletal actin reorganization [189]. COS-7 cells transfected with LIMK1 cDNA were used to perform *in vitro* kinase assays using γ-^{32}P ATP in immunoprecipitates [252]. These experiments showed two bands, around 70 and 20 kD, respectively. These bands were not observed in control experiments using inactive LIMK1 (D460A). The observation of a 20 kD molecular weight band served as the first proof of substrate identification, as cofilin has a molecular weight of 21 kD[189]. This hypothesis was later supported by *in vitro* kinase assays using wild-type cofilin and cofilin S3A phosphorylation-resistant mutants. These experiments showed efficient phosphorylation of WT cofilin, but not the cofilin S3A mutant, when treated with

active LIMK1. LIMK1 D460N mutant was used as a control, which could not phosphorylate either cofilin or cofilin mutants, affirming that cofilin is a substrate of LIMK1.

1.14.1 LIMK and cofilin are an unusual kinase/substrate pair

LIMKs are responsible for cytoskeletal remodeling by interacting with its most characterized substrate, cofilin. Cofilin phosphoregulation is an essential diver of actin filament dynamics. LIMK takes part in this fundamental process by phosphorylating cofilin at Ser3 and regulating the pool of soluble actin monomers and F-actin filaments for remodeling the cell [18,244]. LIMK-cofilin kinase substrate pair is interestingly unique as it involves a non-canonical mode of interaction [186].

Cofilin binding and specificity for LIMK do not follow the canonical linear motif as it does not interact with linear sequence elements residues around the phosphorylation site. Cofilin and LIMK are thought to be a monogamous pair. Cofilin/ADF proteins are processed to remove the N-terminal initiator methionine and are acetylated in its N-terminus, leaving only a single amino acid before the phosphorylation site Ser3 [253,254]. Cofilin proteins have a conserved fold, where α5 is situated perpendicular to the N-terminus, extending away from the main fold. A signature of LIMK interaction with cofilin involves α5 docking into a hydrophobic groove in the C-lobe of LIMK found between the C-terminal portion of the activation loop and the αFG loop. This interaction has been proposed to act as a "molecular drill jig" where the α5 helix of cofilin serves as the jig component that allows the Ser3 residue to be placed in the exact location for phosphotransfer to happen [186].

This kinase-substrate interaction observed in the LIMK family may explain the enhanced selectivity of LIMK towards the cofilin/ADF family of proteins **(Figure 1.14).**

To understand LIMK regulation, using cofilin as a substrate is fundamental to exploring changes in activity between different LIMK catalytically active constructs. In both Chapter 2 and Chapter 3, I use cofilin to test which LIMK N-terminal domains can regulate LIMK activity.

1.14.2 Slingshot phosphatase (SSH1) dephosphorylates LIMK at T508/T505

While phosphorylation is an essential post-translational signal, dephosphorylation events are also necessary for the homeostasis and proper propagation of signals in the cell. In the case of LIMK and cofilin, slingshot phosphatases are responsible for their dephosphorylation.

Regulation of cofilin activity is guided by phosphorylation and dephosphorylation at Ser3 [253]. This phosphorylation is an essential cue that guides cytoskeletal dynamics of actin filament assembly and disassembly while recuperating the actin monomer pool in the cell [255]. In the case of LIMK, phosphorylation on the activation loop is essential for the proper regulation and propagation of signals in actin in actin-driven events. The slingshot (SSH) family of phosphatases, SSH-1 (hSSH-1L), SSH-2, and SSH3, are involved in the dephosphorylation and reactivation of the ADF/cofilin family of proteins and the dephosphorylation of LIMK [256,257].

SSH proteins contain an A, B, and a phosphatase domain in the N-terminus and a serine-rich domain in the C-terminus [256,257]. While there are no reported functions for the A and B domains of SSH phosphatases, it has been shown that SSH1 phosphatase contains a PH-like domain close to the phosphatase catalytic domain, previously termed SSH-N, that encompasses the C-terminal part of the A-domain to the N-terminal region of the B-domain. This PH-domain is thought to play an essential role in F-actin binding and F-actin activation of the cofilin phosphatase activity of SSH1. While the first substrate for SSH phosphatase was cofilin, it has also been shown to dephosphorylate LIMK1 at Thr508[258].

In vitro kinase assays using auto-phosphorylated LIMK (pLIMK1) incubated with SSH1 showed increased free (^{32}P) levels when p-LIMK1 was incubated with active SSH. In contrast, in the presence of catalytically inactive SSH1 C393S (CS), there was no change in either p-LIMK1 or free (^{32}P) levels, suggesting that LIMK1 is a substrate for SSH1 phosphatase [258]. Immunoblotting experiments using phosphor-Thr508-specific antibodies were used to identify Thr508 in the activation loop of LIMK1 as the dephosphorylation site [258]. Dephosphorylated LIMK showed a 5-fold decrease in kinase activity towards cofilin. This study also revealed that SSH1 interacts with LIMK1 via the N-terminus of SSH1 and the C-terminal kinase domain of LIMK [258].

The interaction between the kinase domain and the N-terminus of SSH1 results in the dephosphorylation of LIMK and, therefore, the downregulation of

cofilin phosphorylation. This fine-tuning process is fundamental for the proper spatial regulation of the rapid turnover of actin filaments in the cell.

1.15 Other LIMK understudied substrates and binding partners

While cofilin has been extensively studied, other substrates for LIMK have been identified. However, the characterization of substrates in a cellular context and *in vitro* information on the mechanisms of these interactions need to be described to categorize these substrates as true LIMK substrates. One example of an uncharacterized LIMK substrate is the cyclic AMP response element binding protein (CREB). CREB has been reported to be phosphorylated by LIMK1 at Ser133. LIMK-CREB-dependent phosphorylation is believed to be essential for neurogenic factor-induced neuronal differentiation of CNS-derived hippocampal progenitor cells [259].

In contrast, another reported substrate, MT1-MMP, is a Tyr substrate that, in addition to being a substrate, has been shown to bind specifically with the PDZ domain of LIMK1. Section 1.15.1, I introduce MT1-MMP and provide an experimental summary of their discovery.

1.15.1 LIMK phosphorylates MT1-MMP at Tyr573 residue and interacts with LIMK PDZ domain

Membrane-type matrix metalloprotease 1 (MT1-MMP) is a type I transmembrane multidomain zinc-dependent endopeptidase. MT1-MMP protein is pivotal in remodeling the extracellular membrane matrix (ECM) as they are important in degrading extracellular matrix components. MT1-MMP protein is essential for

wound healing, bone growth, remodeling, pathological processes such as arthritis, and dissemination of carcinoma cells during cancer progression [260,261]. LIMK regulation of MT1-MMP1 happens through the phosphorylation of Tyr573, located in the cytoplasmatic tail on MT1-MMP. This substrate-kinase interaction is hypothesized to be mediated by the LIMK1 PDZ domain and a Class III C-terminus binding sequence, 'DKV-COOH' motif, found in the cytoplasmic tail of MT1-MMP [14]. However, no interaction analysis has been published, including dissociation constant experiments of the interaction between LIMK1 PDZ domain ante the 'DKV-COOH' motif.

This study also provides the first characterized Tyr substrate for LIMK. Phosphorylation at Tyr573 promotes tumor cell migration by controlling MT1-MMP function. This group showed that adding a LIMK-specific ATP competitive inhibitor or knocking down LIMK1 and LIMK2 in MDA-MB-231 cells abolishes Tyr573 phosphorylation by LIMK. Importantly, this study provides another possible function for the LIMK1 PDZ domain besides autoregulatory interaction towards the kinase domain. However, future biochemical and *in vitro* studies will be needed to confirm the interaction between the PDZ domain of LIMK1 and the 'DKV-COOH' motif of the MT1-MMP C-terminal tail. The study presented above also attributes LIMK Tyr phosphorylation to a novel substrate. However, the phosphorylation of MT1-MMP tail by LIMK1 needs further exploration, including phosphorylation analysis of a peptide carrying this sequence to determine kinetic and dissociation constants for this interaction.

1.15.2 LIMK binding partners impact LIMK regulation upon binding to the N-terminus

Various binding partners have been identified since the discovery of LIMK proteins. However, many of these interactors have yet to be fully characterized. Nonetheless, a prominent theme between these protein-binding partners is that they predominantly bind to the N-terminal region of LIMK. This binding interaction had been shown to impact LIMK kinase activity, further supporting the observation of autoregulation of LIMK activity by interactions with the N-terminus domain. Next, I discuss identified LIMK binding partners and describe the effects these binding interactions have on LIMK regulation.

1.15.3 BMPR-II interacts with the LIM1 and LIM2 domains of LIMK1

Over the years, the search for LIMK-interacting proteins has been performed using yeast two-hybrid experiments[212]. A hit from these experiments was a clone encompassing a cytoplasmatic region of Bone Morphogenic Receptor II (BMPR-II). Bone morphogenic proteins (BMP) are involved in cellular processes such as cell differentiation and migration and are fundamental for neuronal growth and morphological differentiation of dendrites [212]. BMPs conduct signaling events via Bone Morphogenic Receptors type I and type II (BMPR-I and BMPR-II), transmembrane receptor serine/threonine kinases that belong to the TGF beta receptor family. The binding of ligands to these receptors leads BMPR type II (BMPR-II) to phosphorylate and activate the type I receptors, BMPR-IA (also known as ALK3) and BMPR-IB (ALK6). BMPR-I then phosphorylates Smad

proteins, causing their activation and translocation to the nucleus, where they can regulate BMP-related genes [262].

LIMK1 and BMPR-II associate via the C-terminal tail domain of BMPR-II and the LIM domain region of LIMK1 [262,263]. Conflicting experimental data show different effects of this interaction on the activity of LIMK. One study reports inhibition of LIMK activity towards cofilin resulting from the interaction of the C-terminal tail of BMPRII[262]. In contrast, another study found enhanced LIMK activation in response to BMPR-II binding, and this activation was reverted by expression of a truncated form of BMPRII[262,263]. However, both studies agree on the relevance of the N-terminal LIM domains of LIMK in regulating activity towards cofilin [263]. This finding provides further evidence of regulatory interactions between the N-terminus domains, specifically the LIM domains, and kinase autoregulation, as binding of this region to the C-terminal tail of BMPR-II affects kinase activity. However, more studies are needed to differentiate the effect of LIMK interactions with BMPR-II and how these mediate different cytoskeletal changes.

1.15.4 LRAP25a interacts with the LIM domains of LIMK, bringing MRCK for activation loop phosphorylation.

Leucine repeat adaptor protein 35a (LRAP35a) is an adaptor protein involved in actomyosin retrograde flow and cell migration [243,264]. LRAP35 contains two leucine-rich repeats at its N-terminal region and a PDZ-binding motif at the extreme C-terminus [264]. In cultured cells, it has been shown to form a tripartite complex with MRCK [234] and a myosin protein, MYO18A, through the leucine-rich repeats and

the PDZ-binding motif, respectively [264,265]. Interestingly, LRAP25a, another adaptor protein related to LRAP35, has been shown to co-immunoprecipitate with MRCK[264]. In co-expression experiments using immunoprecipitated LRAP25a, wild-type LIMK1, and various deletion mutants of LIMK1, it was observed that LRAP25a interacts specifically with LIMK1 through the N-terminal LIM1 domain [234]. This interaction is believed to be involved in regulating LIMK1 activation loop phosphorylation as a LIMK1 mutant lacking the LIM1 domain had decreased levels of p-Thr508. Live cell imaging experiments revealed LRAP25a to act as an adaptor protein that brings together MRCK to promote LIMK1 activation in the lamellipodium, suggesting that LRAP25a targets MRCK to the lamellipodium for LIMK1 regulation [234]. MRCK, LIMK1, and LRAP25a are believed to form a stable tripartite complex involved in the efficient activation of LIMK1 [234]. These studies suggest that LIM1 is responsible for linking MRCK activation of LIMK proteins, providing further evidence of N-terminal regulatory interactions.

1.15.5 $p57^{kip2}$ interacts with the N-terminus of LIMK, increasing LIMK activity

$p57^{kip2}$ is a cyclin-dependent kinase inhibitor that belongs to the Cip/Kip family and is involved in embryogenesis, tissue differentiation, and neuronal development. Two studies have allocated different functions to the interaction of LIMK1 to $p57^{kip2}$. First, various studies showed that $p57^{kip2}$ binds to the N-terminus of LIMK1 and enables the translocation of LIMK from the cytoplasm to the nucleus [266,267]. This translocation is believed to be essential for reducing actin filament stabilization and stress fiber formation [267]. Later, another study found that in HeLa cells, instead of

mediating translocation of LIMK from the cytoplasm to the nucleus, $p57^{kip2}$ increased LIMK1 activity, independent of ROCK and Th508 activation loop phosphorylation status, by its interaction with the LIM domains of LIMK1[268]. Both studies suggest that the interaction of $p57^{kip2}$ with the LIM domain changes the activity of LIMK towards cofilin, further supporting the hypothesis that the N-terminus of LIMK autoregulates kinase activity. Further studies are needed to delineate the mechanisms by which $p57^{kip2}$ interacts with LIMK1.

The binding partners MT1-MMP, LRAP25a, and $p57^{kip2}$ have been shown to bind to the N-terminus domains and change the activity of LIMK. Binding of protein partners can disrupt interactions between the N-terminus and the C-terminal kinase domain, changing the activity of LIMK.

1.16 Extracatalytic phosphorylation regulates LIMK activity

LIMK binding partners have been shown to change LIMK regulation upon binding. However, LIMK regulation might involve interactions of domains outside the catalytic domain or phosphorylation at sites distinct from the activation loop residue Thr508/Thr505 to regulate kinase activity. Other kinases have been shown to phosphorylate LIMK at other sites besides the activation loop, specifically in the Ser/Pro-rich region. These phosphorylation events are proposed to be independent of the canonical Rho/Cdc42/Rac dependent pathways and are believed to change the activity of LIMK towards cofilin. These phosphorylation events are hypothesized to “open” or disrupt intramolecular interactions between the N-terminus and C-terminal kinase domains. This autoregulation disruption is

thought to “prime” LIMK into a conformation for the following activation steps involving the Rho GTPase effectors such as PAK, MRCK, and ROCK, allowing LIMK to reach its full activity levels. Here, I describe some of the kinases reported to phosphorylate LIMK outside the activation loop.

1.16.1 PKA and MK2 and AURKA phosphorylate LIMK in the S/P rich region

3',5'-cyclic adenosine monophosphate (cAMP)-dependent protein kinase (protein kinase A (PKA), is a master regulator of many different processes that include lipid metabolism, cardiac physiology, and neuronal function [269-271]. Prkar1a$^{-/-}$(cells lack the 1A regulatory subunit) mouse embryonic fibroblasts have shown increased levels of cofilin pSer3 and low levels of no GTP-loaded Rac and Rho. Later, it was shown that PKA phosphorylates LIMK1 at Ser596 (site not conserved in LIMK2), in the C-terminal kinase domain and Ser323 in the Ser/Pro-rich linker independently of the Rho/Rac/Cdc42 dependent pathways[156,272]. These phosphorylation events are thought to modulate LIMK activity by changing the conformation of the protein to make it more able to phosphorylate substrate. Therefore, PKA is thought to be important in cell morphology and migration through its ability to modulate the activity of LIMK directly.

Another example of extracatalytic phosphorylation is observed with Aurora kinase A (AURKA) and LIMK. Cooperativity between LIMK1 and AURKA is mediated by reciprocal phosphorylation. LIMK1 is recruited to centrosomes during early prophase, where it colocalizes with AURKA. The interaction of LIMK1 with AURKA induces indirect AURKA activation loop phosphorylation at Thr288, while

AURKA directly phosphorylates LIMK1 at Ser307. AURKA extracatalytic phosphorylation then causes an increase in activation loop phosphorylation at Thr508[155], increasing cofilin phosphorylation at Ser3.

Similarly, MAPK-activated protein kinase-2 (MK2) can phosphorylate LIMK1 at Ser323, a site outside the catalytic domain of LIMK1, in VEGF-stimulated endothelial cells [157]. This phosphorylation results in an increase in kinase activity towards cofilin independent of activation loop phosphorylation.

Phosphorylation events mediated by the Rho GTPase signaling cascade are necessary for LIMK activity. However, as mentioned before, extracatalytic phosphorylation events mediated by PKA, MK2, and AURKA have been shown to increase LIMK activation. Phosphorylation in the Ser/Pro-rich region (amino acids 261-328 in LIMK1 and 251-323 in LIMK2) is believed to induce conformational changes in LIMK that release the N-terminal region from autoinhibitory interaction with the C-terminus kinase domain. These studies suggest that phosphorylation of LIMK by Rho-GTPase-related kinases and other kinases outside this signaling cascade are necessary to achieve LIMK full activity. Therefore, autoregulation could involve distinct molecular steps, including binding of protein partners that release interaction between the N-terminus domains and the C-terminus kinase domain, and phosphorylation events in the Ser/Pro-rich region could help the further release of autoregulatory interactions. The complexity of these phosphorylation events results in different dynamics in the actin cytoskeleton.

1.17 Protein kinase autoregulation

Above, I have discussed the domains of the LIM domain kinases, their binding partners, the modes of interaction accessible and observed for the domains, broad mechanisms of regulation for protein kinase domains, and specific interactions of the LIM domain kinases. In this section, I discuss how protein kinases can be regulated and attempt to tie these modes of regulation to what we know about LIMK regulation.

Proper spatiotemporal control is essential for the normal transduction of cellular signals [165,167,273-277]. Phosphorylation of a kinase activation loop is often associated with increased enzymatic activity. While activation loop phosphorylation is essential, it is not the only means of regulation [165,166,278]. Many protein kinases contain multiple domains and employ inter- or intra-molecular interactions to alter catalytic rate [279-283]. The autoregulatory mechanism has not been revealed in the case of LIMK. However, autoregulatory mechanisms for other kinases have been reported. Next, I introduce examples of kinase autoregulatory mechanisms and how these may explain the autoregulation mechanism of LIMK.

1.17.1 Allosteric regulation

Protein kinase regulation can be achieved by phosphorylation of the activation loop or allosteric or pseudosubstrate regulation involving intra or intermolecular interactions. Allosteric regulation consists of the regulation of kinase activity by binding a regulator to a part of the protein distinct from the active site [273-276]. Often these binding events induce changes in the kinase domain conformation that

change the activity of the kinase. Examples of these regulatory interactions are observed in the non-receptor tyrosine kinases Abl and Src[282,284-287].

The Src family of kinases and its autoregulatory mechanism has been characterized and extensively studied [284,285,288]. Src domain architecture includes an Src homology 4 domain (SH4) domain, with an attached myristic acid moiety, a unique domain, followed by an Src homology 3 (SH3) domain which binds PxxP sequences in binding partners[289], an Src homology 2 (SH2) domain that binds phosphorylated tyrosine residues[290-292], and a C-terminal kinase domain, also known as an Src homology 1 (SH1) [285,293]. In this family of proteins, autoregulation is carried between the SH2 domain, the phosphorylated C-terminal tail, the SH3 domain, and the auto-phosphorylated SH2-kinase linker. Specifically, autoregulation is achieved indirectly via two ways: the SH2 domain binds to the phosphorylated Tyr530 at the C-terminus, "latching" the SH2 domain to the C-terminal lobe of the kinase domain [288]. Second, the SH3 domain interacts with the N-terminal lobe of the kinase domain and a conserved proline-containing linker (Pro249). This linker does not have a classical PxxP motif but forms a type II polyproline left-handed helix that allows for proper recognition by Src-SH3 domains[285,294-296]. These two interactions carried by the SH2 and SH3 domains in the "back" of the kinase lock it in an inactive state, as Glu313 in the αC is not found in the orientation compatible with an active conformation. Furthermore, hydrophobic interactions between Trp260 in the SH3 linker and Gln312 in the αC strengthens this autoregulatory conformation[286].

Src kinases are activated first by the release of the phosphorylated Y530 from the SH2 domain by Src SH2 binding partners. The now accessible pY530 can interact with protein phosphatase, unlocking Src from the inactive state. This allows for a more accessible kinase domain that can directly be phosphorylated by another Src molecule, giving rise to the active conformation. Src autoregulation occurs in trans, as exogenous substrates decrease autophosphorylation in the activation loop, and SH2 and SH3 Src binding partners disrupt the inactive conformation [286] **(Figure 1.15 A)**.

A similar autoregulatory mechanism is observed in Abl tyrosine protein kinases. Abl domain architecture includes a highly conserved N-terminal stretch, followed by an SH2 and an SH3 domain. Even though Abl kinase shares quite similar domain architecture, it lacks the autoregulatory Tyr found in Src kinase's C-terminus. In contrast to Src autoregulation, mutagenesis data suggest the autoregulation is directed by the Abl N-terminal region [297]. The model states that the first 81 amino acids in the N-terminal region contact the SH3 domain and the N-terminal kinase lobe, locking in an inactive state [298]. The inactive state displays interactions between the SH3 and its own SH2-kinase domain linker, which also adopts a polyproline type II helix compatible with SH3 binding partners. This interaction brings into proximity the N-terminal lobe of the kinase domain.

Moreover, unlike the Src SH2 domain, Abl SH2 cannot interact with a C-terminal phosphotyrosine residue. Abl's SH2 domain interacts with the C-terminal lobe of the kinase domain via an extensive network of hydrogen bonds that bends

the αI helix of the kinase domain, partially blocking the access of substrates to the active site [299]. The interaction is kept in place by the N-terminal myristate moiety that binds to the C-terminal lobe of the kinase domain. This model is further supported by the case of the BRC-ABL fusion gene resulting from the translocation of the ABL1 gene and the BRC gene, where the expression of an Abl kinase domain lacking the N-terminus domains shows constitutive activation [300].

Abl activation involves a change in binding between the SH2 domain and the kinase domain. Interestingly, the SH2 changes its interaction with the kinase domain, binding to the N-terminus lobe instead of the C-lobe, allosterically activating the kinase domain. SH2 change from an inhibiting agent to an activating agent is triggered by activation loop phosphorylation and kinase domain activation **(Figure 1.15 B)**[299,301].

1.17.2 Pseudosubstrate regulation

Intrasteric or pseudosubstrate regulation is often described as autoregulatory interactions where internal sequences within the protein kinase act as "pseudosubstrates," interacting directly in the active site [302]. Intrasteric regulatory interaction sequences (IRAseq) resemble the substrate's sequence or ligand and are responsible for the inhibition of the activity of the protein kinase. An example of this regulatory mechanism can be found in p21-activated kinase (PAK). Specifically, PAK4 kinases are regulated by an autoinhibitory pseudosubstrate sequence in its N-teminus [279]. This proline-rich sequence acts as a pseudosubstrate, rendering PAK4 inactive. Dissociation of this interaction is

hypothesized to be driven by the binding partner proteins in this proline-rich sequence [279]. This dissociation allows PAK4 to auto-phosphorylate itself and later phosphorylate its substrates (**Figure 1.16)**.

1.17.3 Activation by accessory domains

Protein kinases have a pliable fold, and regulation by association with different domains or separate subunits has been observed. Cyclin-dependent kinases (CDK) are examples of protein kinases relying on the association of a separate subunit, cyclin, for activity [303]. Cyclins are a group of proteins that control the progression of the cell cycle through its association and activation of CDKs. For example, in CDK2, a member of the CDK family of proteins, the cyclin subunit associates within the region of the C-helix and promotes a rotation that allows specific interactions with cyclin that relieve the blockade of the catalytic cleft. This movement now allows the activation loop Thr to become accessible for phosphorylation, completing the activation process for CDK2 [304] (**Figure 1.17)**.

1.17.4 Dimerization as a mechanism of kinase regulation

Within the Ser/Thr kinase family, dimerization-dependent phosphorylation in the activation segment in *trans* promotes kinase activation [162]. A specific example of dimerization-dependent activation occurs with checkpoint kinase 2 (Chk2)[305]. Human Chk2 consists of an N-terminal Ser-Gln/Thr-Gln (SQ/TQ) cluster domain (SCD), a central forkhead-associated (FHA) domain, and a C-terminal serine/threonine kinase domain [305]. Phosphorylation at a Thr residue in the SCD domain changes the conformation of the kinase, which now allows for dimerization

between the SCD domain of one molecule and the FHA domain of another. Dimerization of Chk2 allows for autophosphorylation in various sites, including the activation loop phosphorylation residue, allowing Chk2 to reach its full active conformation [306] (**Figure 1.18**).

The autoregulatory mechanisms described before are a limited list of examples of autoregulatory mechanisms. However, these models might help guide our understanding of LIMK autoregulation. Which autoregulation mechanism is present in LIMK remains unknown.

1.18 LIMK is autoregulated via its N-terminal domains.

Much research has been done to characterize one tier of LIMK regulation, phosphorylation in its activation loop by upstream activators. However, this is not the sole mechanism of LIMK regulation. LIMK regulation is believed to occur in two ways: 1) phosphorylation of the activation loop, and 2) autoregulatory interactions involving the N-terminal domains[54]. Upstream kinases phosphorylate the LIMK activation loop on residues Thr508 or Thr505 for LIMK1 or LIMK2, respectively, [179-181], but the LIMK autoregulatory mechanism remains unknown. Studies have pointed to the N-terminus domain of LIMK to be crucial for LIMK autoregulation. This was first shown in co-immunoprecipitation experiments using constructs for LIMK1 and LIMK2, where both proteins co-immunoprecipitated, pointing to possible self-association events [53]. This was further recapitulated with co-immunoprecipitation experiments with constructs that have N-terminal deletions [53]. Self-association was reiterated, involving heterotypic interactions between the N-

terminal half of the protein and the kinase domain. These experiments, using immunoprecipitated protein, were the first to point to an autoregulatory mechanism for the LIMK family of proteins.

Furthermore, adding the N-terminal domain to kinase assays using cofilin as substrates decreases kinase activity [54]. Limited proteolysis of immunoprecipitated LIMK1 using trypsin and lysyl endopeptidase produced two distinct fragments corresponding to the catalytic domain. Radiolabel kinase assays using these fragments showed, on average, a 5-fold increase in kinase activity. Furthermore, radiolabel kinase assays with immunoprecipitated N-terminal fragments that carry mutations in the LIM domains and PDZ domain recapitulate an increase in kinase activity [54].

In cells, mutations that perturb the hydrophobic core of the PDZ domain induce actin filament accumulation [307]. The same has been observed with mutations in the LIM2 domain, specifically in conserved cysteine residues involved in Zn^{2+} coordination. Actin filament accumulation is also observed in cells expressing only the LIMK1 kinase domain, further supporting the hypothesis that the N-terminus of LIMK inhibits kinase activity. Moreover, it has been reported that binding different protein partners to the N-terminus of LIMK results in changes in kinase activity (i.e., BMPR-II[262,263], LRAP25a[234], $p57^{kip2}$ [268]), further supporting the claim that LIMK is autoregulated by its N-terminal domains. However, the specific mode of this autoregulation remains to be discovered.

Two modes of autoregulatory mechanisms have been hypothesized, one where an intramolecular interaction occurs or two molecules of LIMK come together to regulate intermolecular activity [53,54]. Work by the Mizuno laboratory suggests that the LIM2 domain is important for autoregulation. Experimental data portrayed in this thesis supports an intramolecular model and provides evidence for the regulation of LIMK activity by its PDZ domain.

An intramolecular working model for describing this autoregulation is as follows. LIMK is believed to behave in a transient “open” conformation where the kinase domain is accessible for regulatory interactions either by activating kinases or deactivators such as SSH1 phosphatase and a closed “closed” conformation, mainly driven by autoregulatory interactions between the N-terminal domains and the C-terminal kinase domain. When the equilibrium is primarily in the “closed” conformation, phosphorylation in extracatalytic sites, accomplished by PKA, MAK2, and AURKA, in the S/P rich region, can shift this equilibrium by changing the conformation of LIMK kinase towards an “open” or extended conformation. This conformation change allows kinase activators to better access the activation loop. The appropriateness of this model is addressed through the work presented in this thesis. Another regulatory event could include binding protein partners to the N-terminus domains, stimulating the dissociation of the N-terminus domains from the kinase domain. Moreover, another autoregulation mechanism could consist of phosphorylation at sites outside the activation loop in the kinase domain that destabilize interactions between the N-terminus domains and the kinase domain.

1.19 Overview

The main goal of my thesis has been to address the central hypothesis that **the N-terminus of LIMK1 negatively regulates its activity by a direct "head-to-tail" interaction.** I report here the use of biochemical and biophysical techniques to determine which domains of the N-terminus of LIMK are responsible for autoregulation. Also, I present molecular-level information on the N-terminal PDZ domain. This work can be divided into two main aims: 1) structural studies of the N-terminal domains of LIMK and 2) identification of the specific N-terminal domains that interact and regulate the kinase activity of LIMK.

1.19.1 The N-terminal PDZ domain regulates the activity of LIMK

The N-terminus of LIMK regulates kinase activity towards cofilin. However, there are no published structures of the N-terminal domains, LIM and PDZ, responsible for autoregulation. Biochemical evidence supports that the complete elimination of the N-terminus or mutations in this region increases the kinase activity of LIMK. Yet, specific identification of the domains and binding regions responsible for interacting with the kinase domain remains to be solved. **Chapter 2** of this dissertation will present biophysical and structural studies of the LIM2 and PDZ domains. Expression, purification, and crystallization of the PDZ to a 2.04Å resolution will be shown, as well as conservation mapping to the solved structure.

Additionally, mutagenesis studies of this domain in highly conserved surfaces and expression and purification of FL LIMK1 PDZ mutants are used to validate the impact of PDZ mutations on kinase activity. These studies allow me to

map a possible regulatory surface of the PDZ domain. Also, I use SAXS-MALS to gain an overall fold representation of the LIM2-PDZ region.

1.19.2 Interaction between LIM2-PDZ region and the PDZ domain inhibits LIMK activity

In **Chapter 3** of this dissertation, I specifically look at the LIM2-PDZ region to study its impact on the kinase activity of LIMK2. I express and purify the LIM2-PDZ domains and express and purify FL and kinase domain constructs of LIMK from insect cells. I use radiolabel kinase assays to show that this region optimally inhibits kinase activity. I also use negative stain to observe overall conformational changes between LIMK2 full-length wild-type protein and a catalytically inactive LIMK2 D451N mutant. I observe distinct conformations between the LIMK2 full-length wild-type and D451N mutant.

1.20 Summation and impact

In summary, my work in this dissertation provides a deep structural and biochemical understanding of how LIMK N-terminus autoregulates LIMK and how this autoregulation affects kinase activity. Specifically, I provide the first crystal structure of the LIMK2 PDZ domain and use its conservation to help me hypothesize regions of autoregulation. I also recapitulate the human LIMK-cofilin pathway in yeast and use it to observe changes in kinase activity when I introduce mutations in the PDZ domain, as changes in kinase activity affect yeast survival. I further validate the importance of the PDZ domain in autoregulation by using cofilin radiolabeled kinase using PDZ mutants in the context of FL LIMK1 protein.

Furthermore, I test the titration of N-terminus constructs into cofilin radiolabeled kinase assays to find the minimum region in the N-terminus that optimally suppresses kinase activity. I use biophysical techniques such as SAXS and negative stain EM to study the overall conformation of the N-terminus LIM2-PDZ construct and full-length LIMK. The data presented here will answer questions relating to the importance of the N-terminus domains of LIMK, specifically the LIM2 and the PDZ, and how these impact LIMK autoregulation and activity towards cofilin.

1.21 Figures and tables

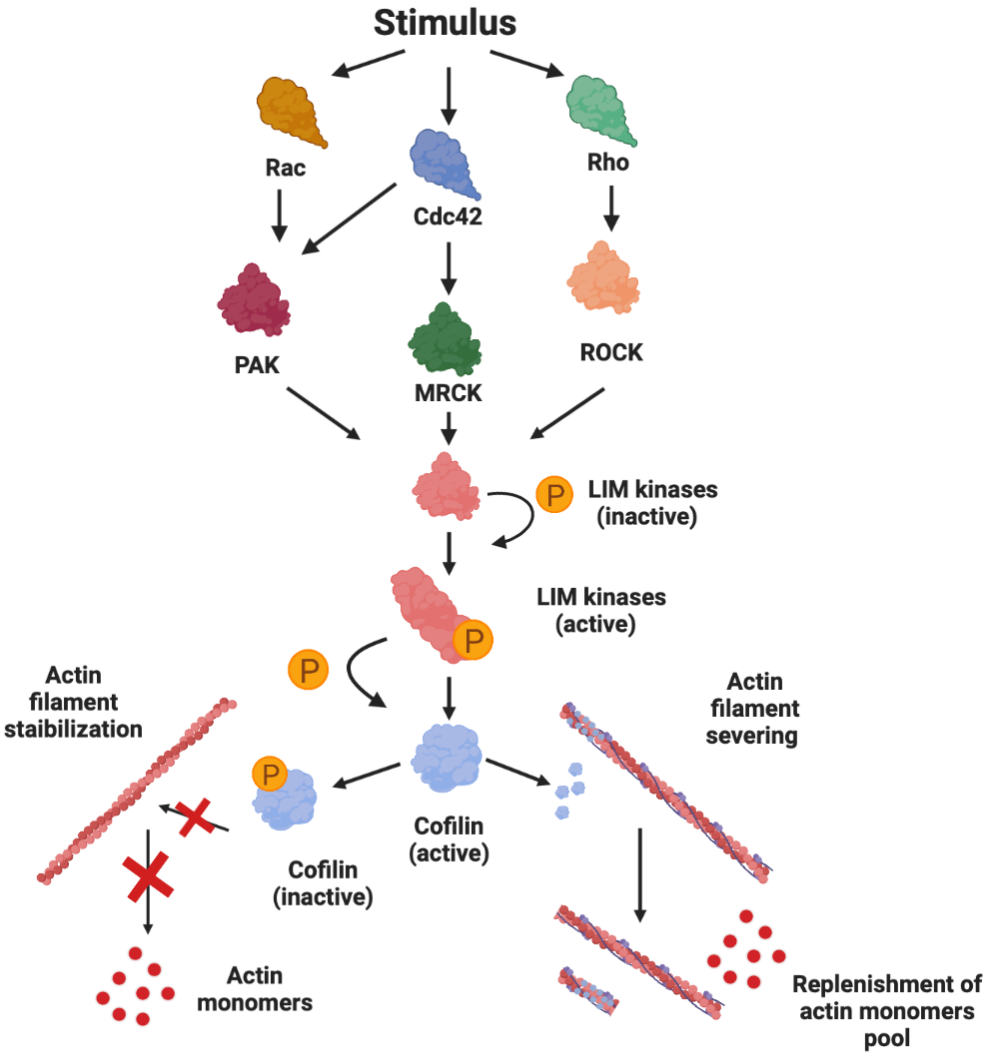

Figure 1.1 LIMK signaling pathway

LIMKacts downstream of Rho GTPase signaling pathways (Rac, Rho, and Cdc42). PAK, MRCK, and ROCK kinases activate LIMK1 and LIMK2 by phosphorylation at Thr508/Thr505, respectively. Active LIMK phosphorylates almost exclusively

members of the actin depolymerization family of proteins (ADF), also known as cofilin.

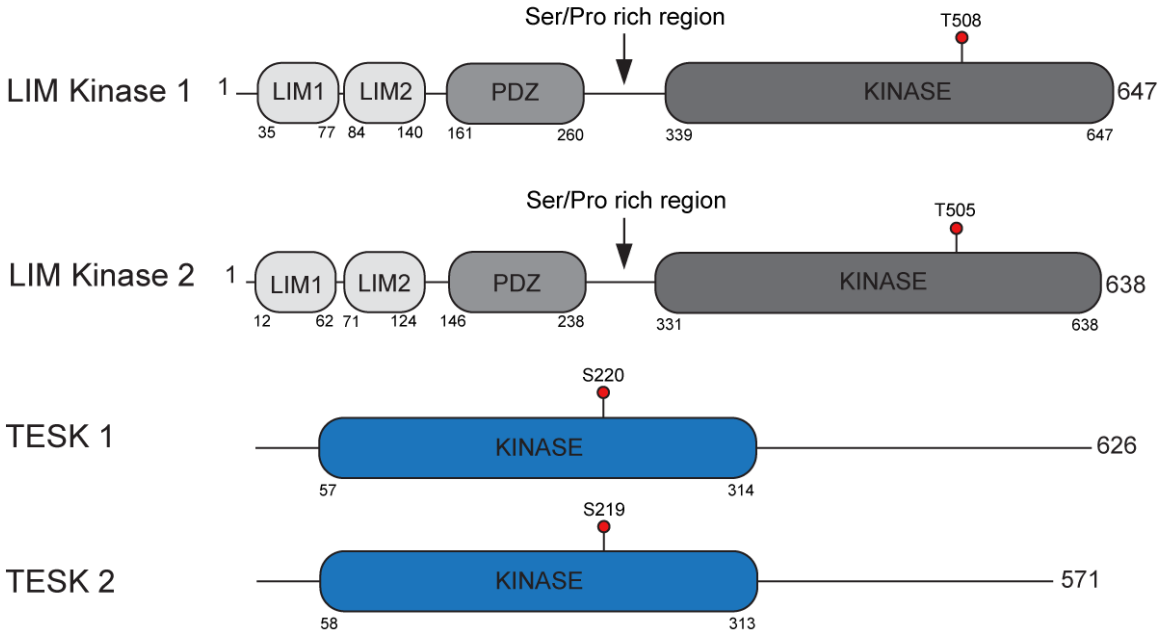

Figure 1.2. LIM domain kinase family of proteins domain architecture.

LIM domain kinase family architecture shows human LIMK1 (UniProt ID: P53667), human LIMK2 (UniProt ID: P53671), TESK1 (UniProt ID: Q15569), and TESK2 (UniProt ID: Q96S53). LIM1: first LIM domain, LIM2: second LIM domain, PDZ: PDZ domain, Kinase: kinase domain. Activation loop phosphorylation residues are indicated, T508/T505 for LIMK1 and LIMK2, and S220/S219 for TESK1 and TESK2, respectively.

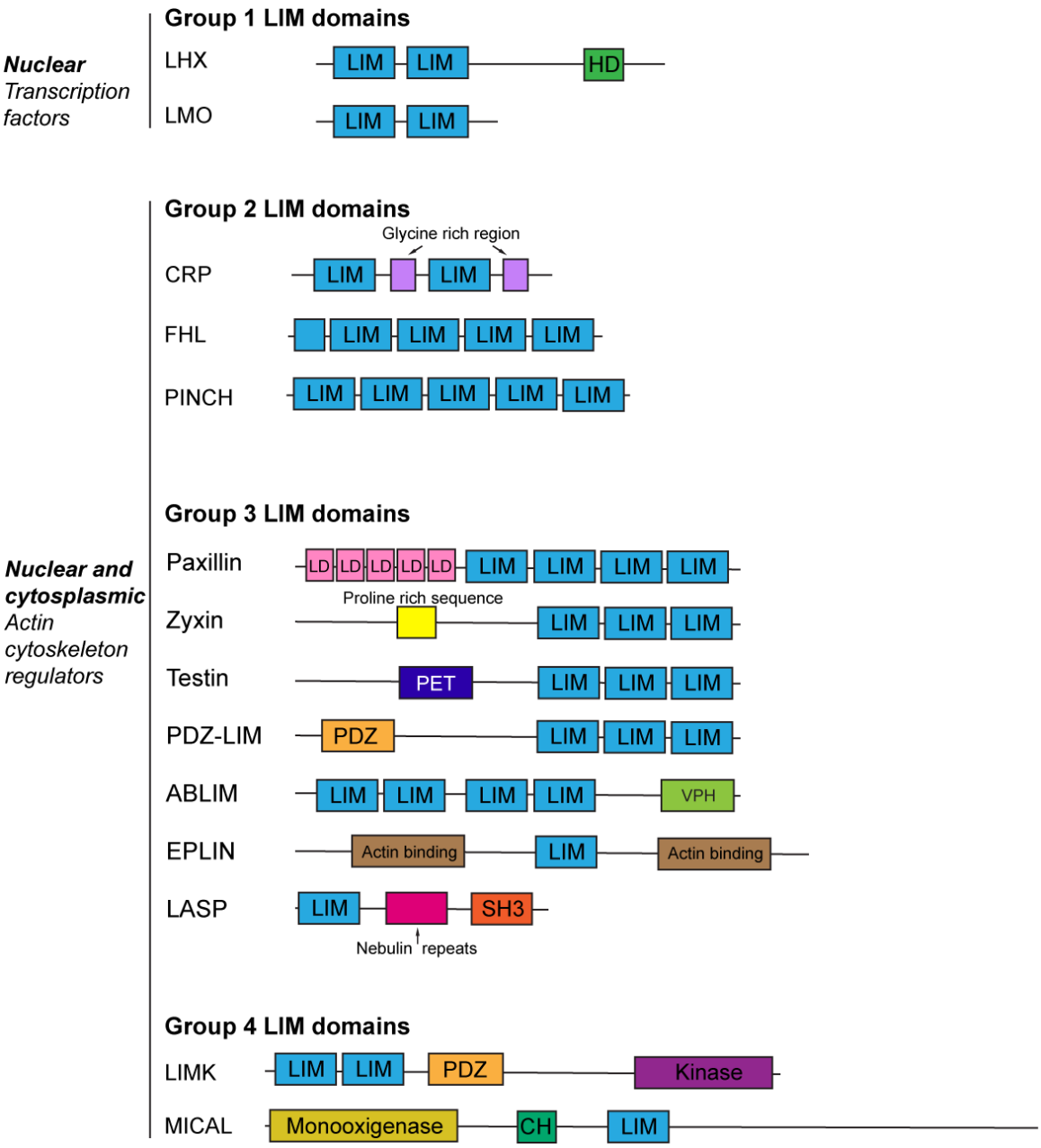

Figure 1.3. LIM domain groups.

LIM domain groups 1, 2, 3, and 4 and representative LIM protein members. Localization and general cellular function are also shown. Figure adapted from [308]

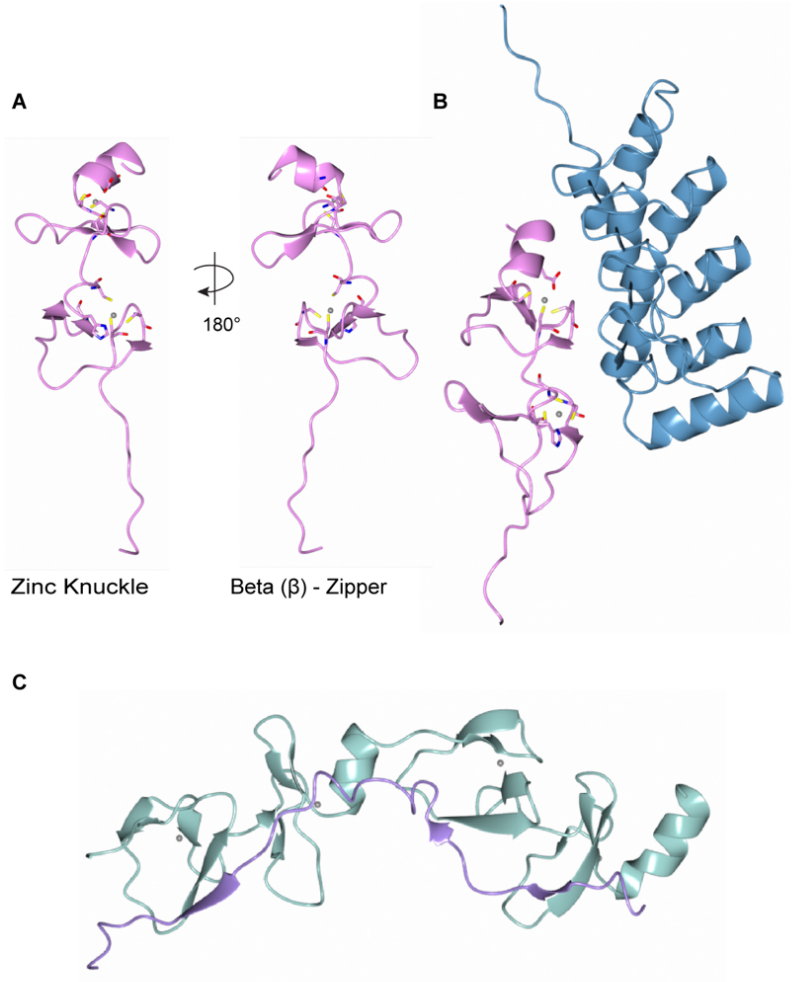

Figure 1.4. LIM domain structure and modes of binding.

A. LIM1 domain of PINCH2. Depicted on the left is the zinc knuckle side of LIM domains, and on the right is the LIM domains' β (beta) zipper side. **B.** Complex structure of PINCH2 LIM1 and ARD (ankyrin repeat domain) of ILK (integrin-linked kinase) This complex portrays the LIM domain binding using its zinc knuckle side (PDB: 3IXE). **C.** Complex of LMO4 (nuclear LIM-only) LIM domains 1 and 2 with the Ldb1 (LIM domain-binding protein-1) LID domain(LIM domain binding region).

This complex portrays the LIM domain of LMO4 binding Ldb1 using its beta zipper side (PDB:1RUT). Zinc atoms are shown as grey spheres.

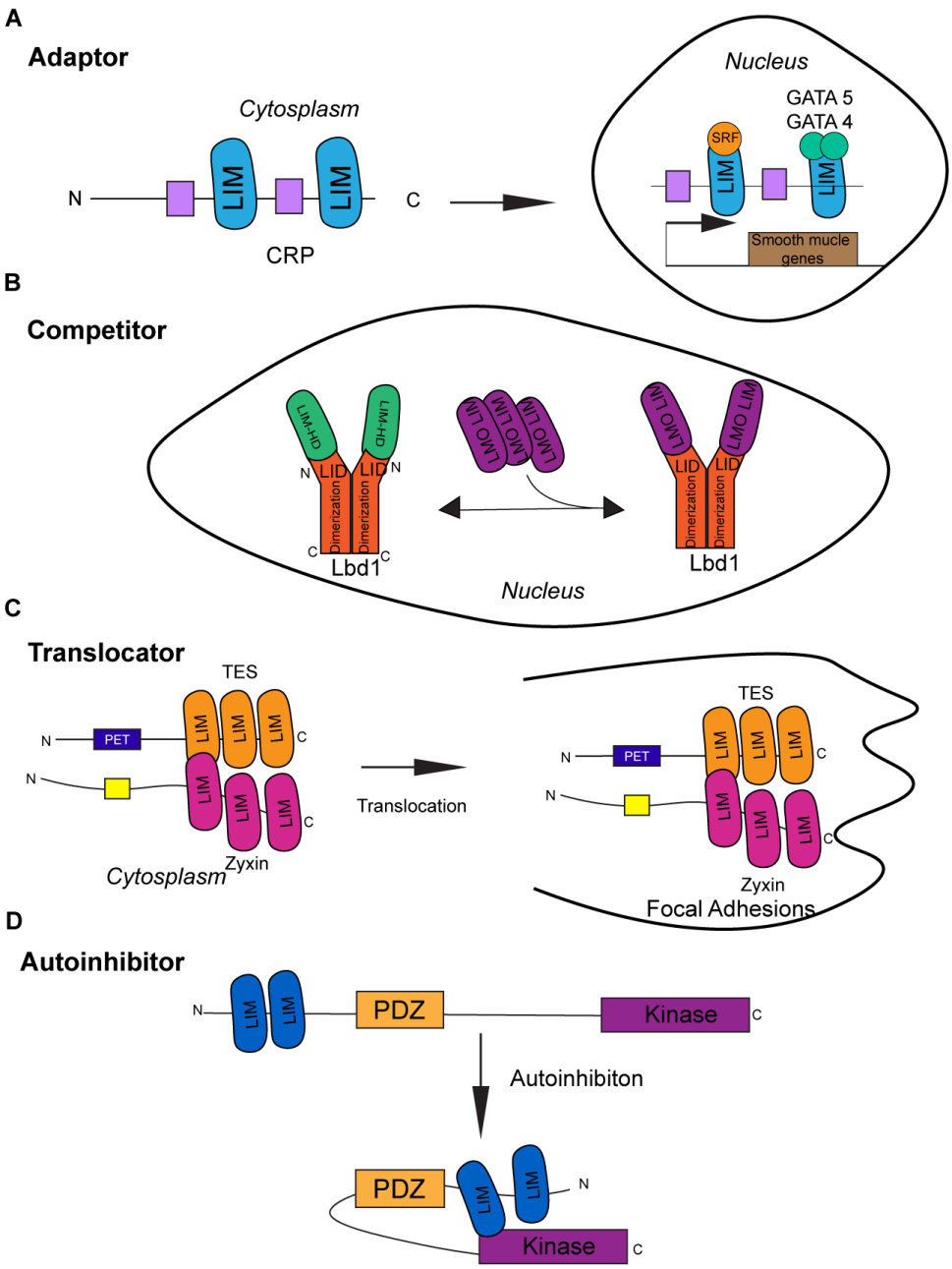

Figure 1.5. LIM domain functions.

A. LIM domains can act as adaptors. **B.** LIM domains can act as competitors. **C.** LIM domains can translocate proteins from one cell compartment to another. **D.** LIM domains can also serve as inhibitors and regulate the activity of proteins.

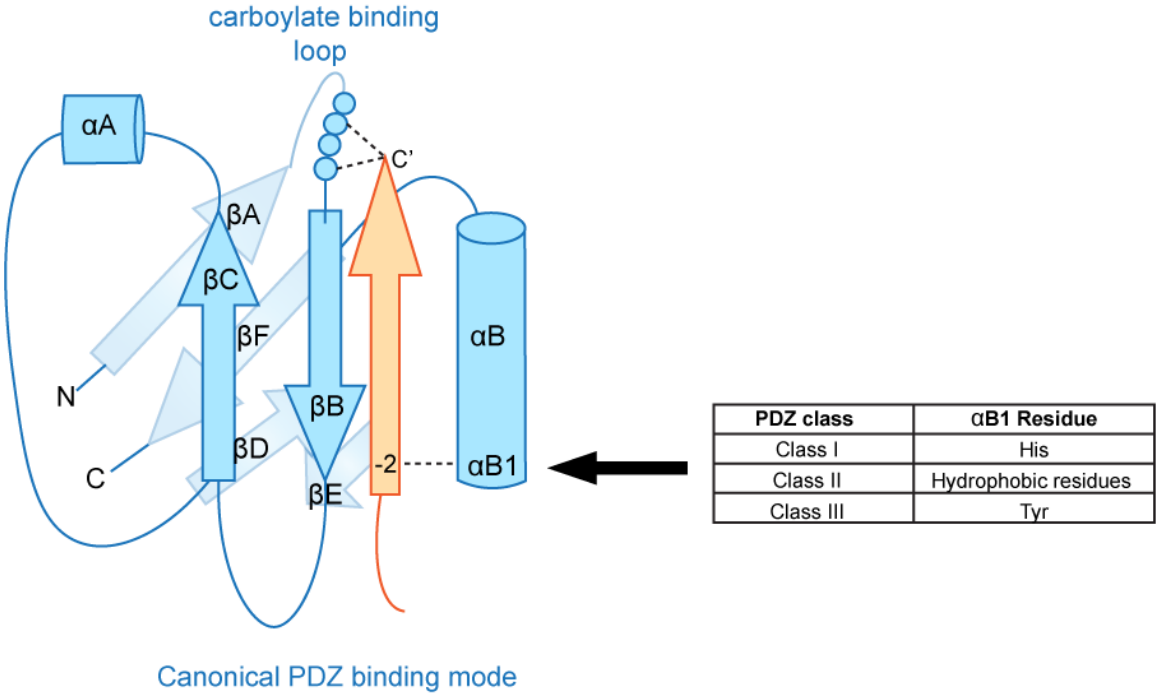

PDZ class	αB1 Residue
Class I	His
Class II	Hydrophobic residues
Class III	Tyr

Figure 1.6. General schematic of a PDZ domain fold bound to a C-terminal peptide

Shown are the secondary structural elements. Arrows point to important residues at the αB1 helix—figure adapted from [67].

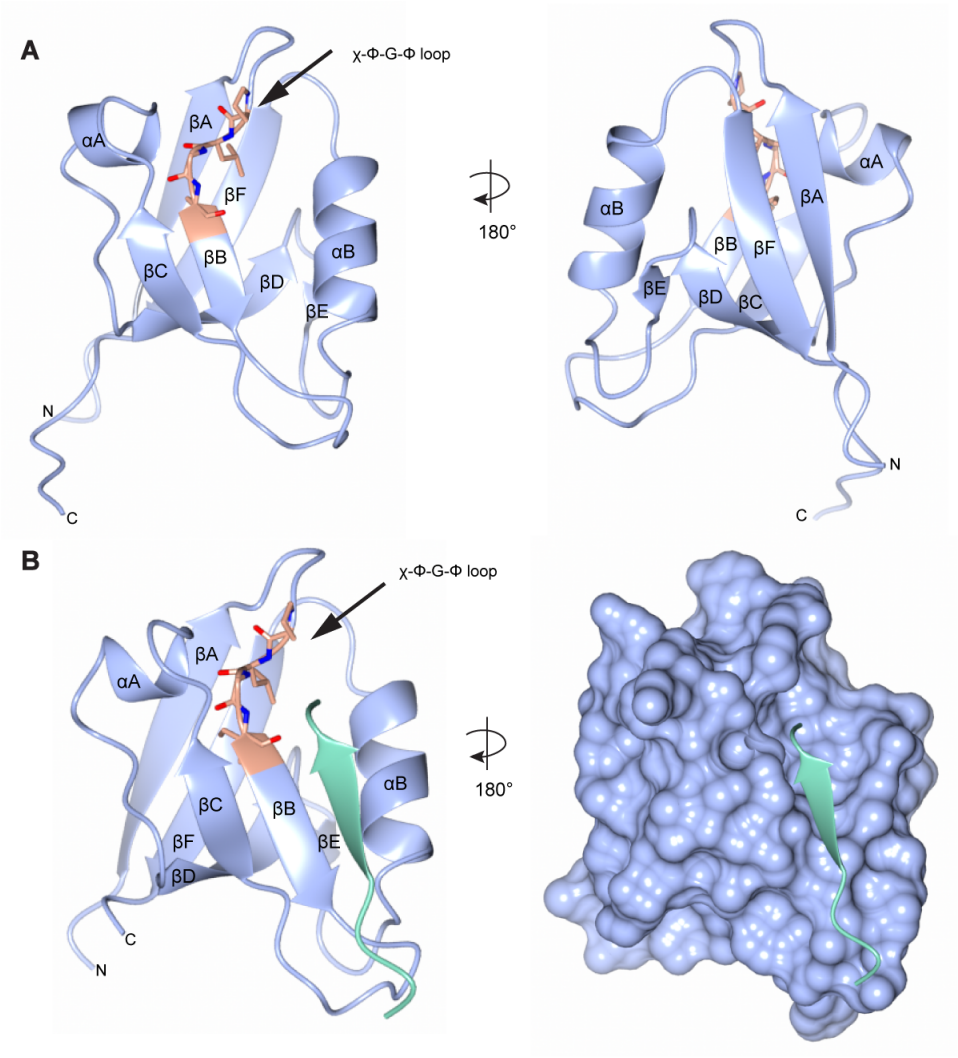

Figure 1.7. PDZ domain crystal structure in its apo and peptide-bound forms. GRIP1 PDZ6, a member of the Class II PDZ domain class (PDB: 1N7E). Secondary structure elements are shown. B. GRIP1 PDZ6 domain in complex with lipirin C-terminal peptide (PDB: 1N7F) (Uniprot: Q12959). Secondary structure elements are shown on the left, and surface representation of the PDZ binding cleft is on the right.

PDZ class	C-terminal binding motif	αB1 Residue
Class I	X-T/S-X-ϕ-COOH	His
Class II	ϕ -X- ϕ – COOH	Hydrophobic residues
Class III	D/E-X-Φ-COOH	Tyr

Table 1.1. PDZ domain classes.

PDZ domain classes, C-terminal binding motif they recognize, and identity at the bottom residue on the αB1.

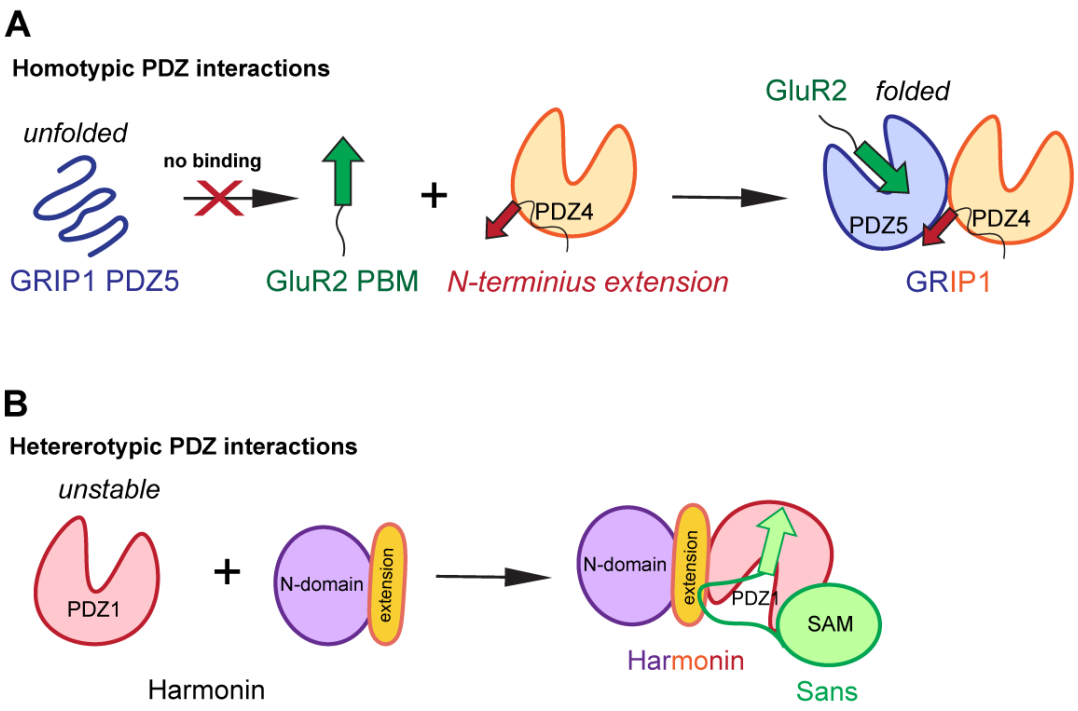

Figure 1.8. PDZ domain noncanonical interactions.

A. Homotypic PDZ interactions of GRIP protein PDZ5 and PDZ6 with GluR2 PDZ protein binding motif (PDB: 1P1D). **B.** Heterotypic PDZ Interaction between the N-terminal, extension, and PDZ domain of Harmonin with the SAM domain PDZ PBM of the SAM protein (PDB: 3K1R). Figure adapted from [67]

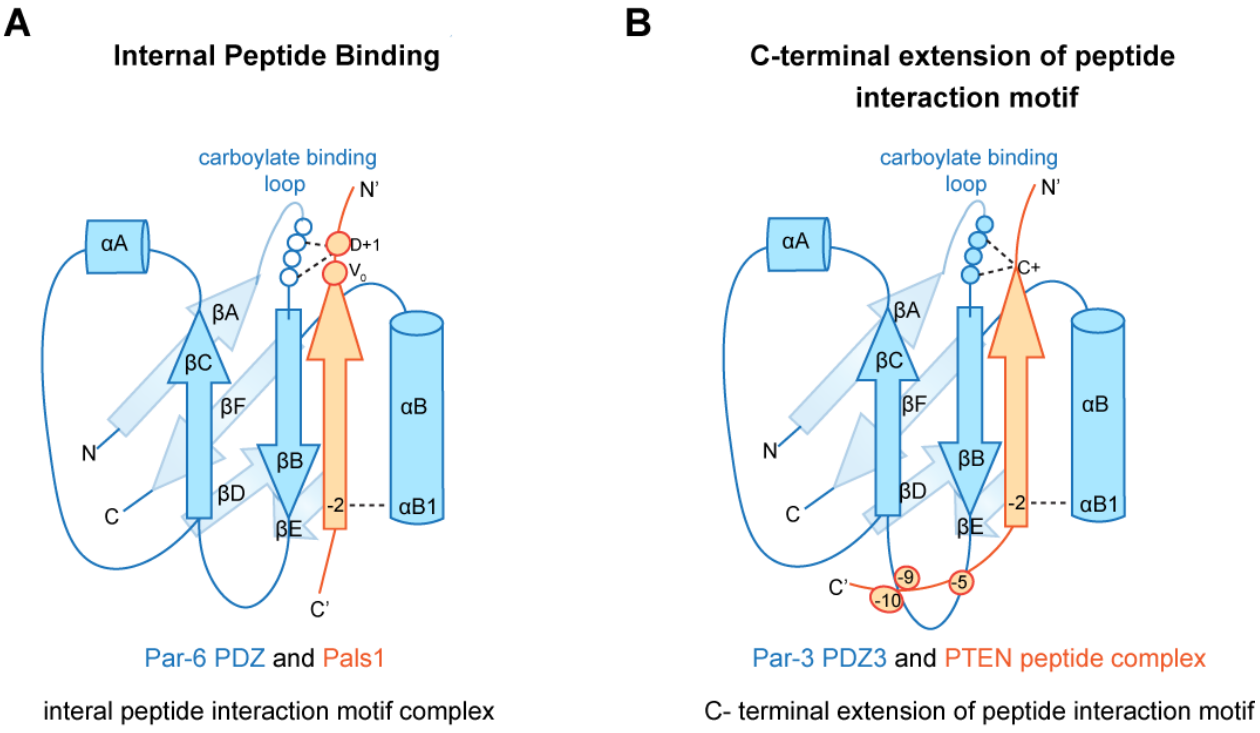

Figure 1.9. Noncanonical protein binding motif binding to PDZ domains.

A. Cartoon representation showing the Par-6 PDZ domain in complex with a Pals1 internal peptide (PDB code 1X8S). **B.** Cartoon representation showing Par-3 PDZ2 in complex with the PTEN peptide (PDB code 2K20). Figure adapted from [67]

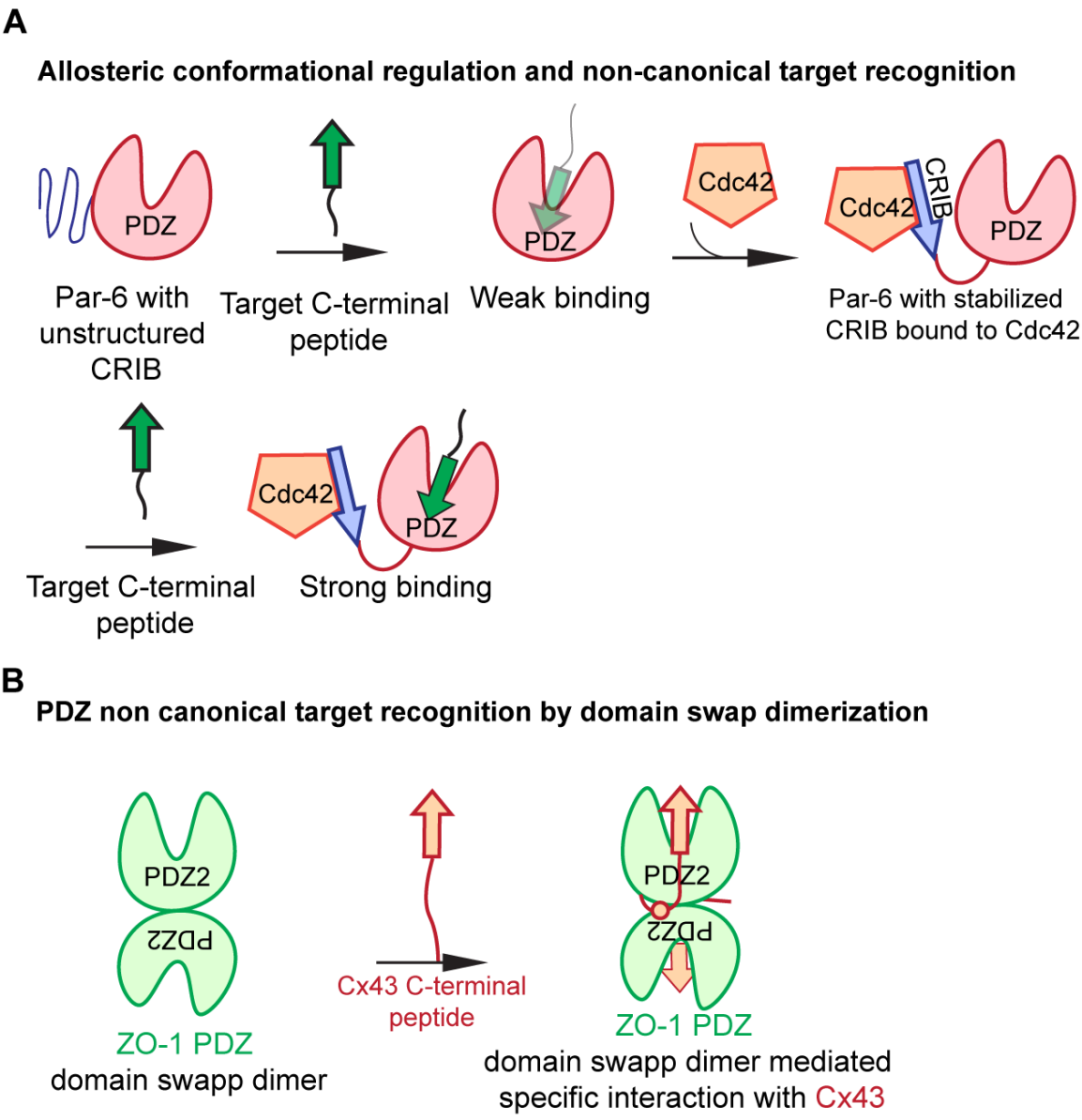

Figure 1.10. PDZ non-canonical target recognition and PDZ regulation mechanisms.

A. Allosteric conformational regulation is represented by the interaction in the Cdc42–Par-6 PDZ complex (PDB:1NF3). **B.** PDZ non-canonical target recognition mediated by domain swap dimerization of ZO-1 PDZ2 and binding pf Cx43 peptide (PDB: 3CYY). Figure adapted from [67]

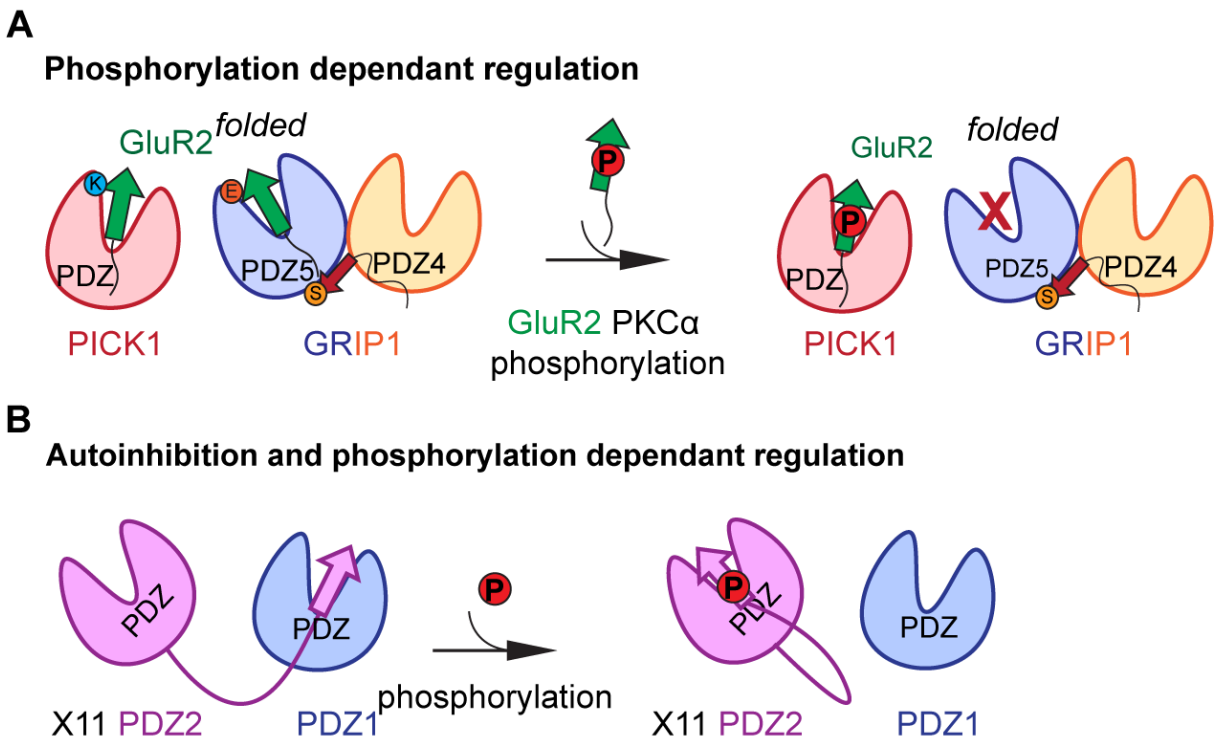

Figure 1.11. Regulation of PDZ-mediated interactions.

A. Regulation of PDZ interactions by phosphorylation. PKC phosphorylation of GluR2 differentially regulates its binding to GRIP1 PDZ45 and PICK1 PDZ. Lys83 at the αB1 position of PICK1 PDZ is highlighted (PDB: 2PKU). **B.** Autoinhibition and phosphorylation-dependent regulation. Schematic diagram showing the phosphorylation-mediated switch of the inhibition of the two X11α PDZ1 and PDZ1 domains by the C-terminal PBM (PDB:1U3B). Figure adapted from [67].

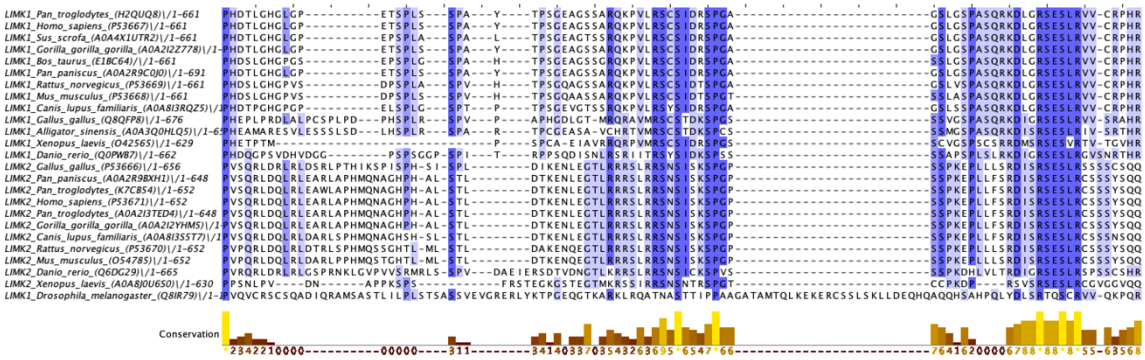

Figure 1.12. Conservation of the LIMK Ser/Pro domain.

Sequences were obtained from UniProt[309] and aligned in ClustalOmega[310]. Species and UniProt ID name each sequence. Conservation scores were calculated in Jalview[311]. Identical residues are highlighted in dark blue, and partially conserved residues are in light blue. Mutations used in kinase assays are shown under an arrow, and their LIMK1/LIMK2 residue numbers are shown.

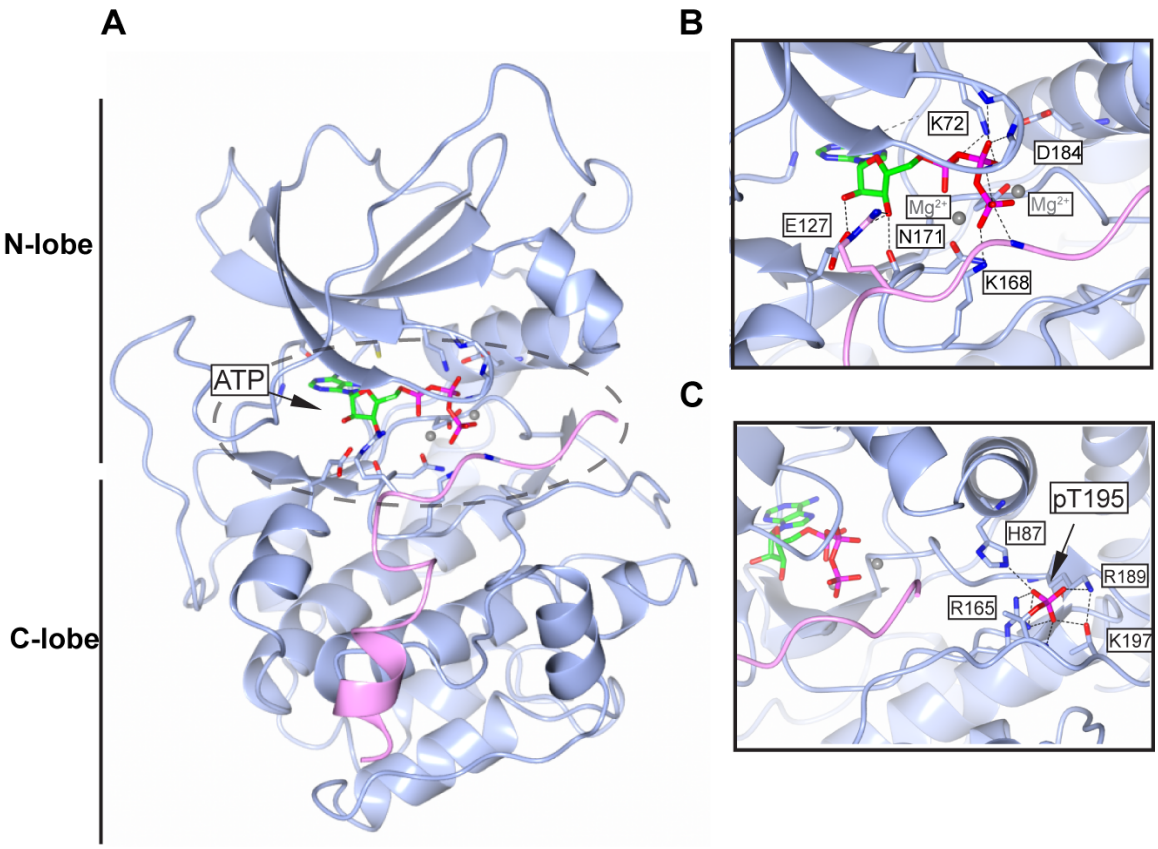

Figure 1.13. Ribbon representation PKA kinase domain bound to inhibitory peptide.

A. Ribbon representation of PKA kinase domain (PDB:1ATP). N-lobe and C-lobe are shown, the ATP molecule is pointed with an arrow, and the catalytic cleft is portrayed with a dashed grey oval. **B.** Panel focuses on the ATP engagement in the active site. Hydrogen bonds are also shown. **C.** Panel focus on the phosphorylated activation loop residues pThr195; hydrogen bonds involved in stabilizing the active conformation are also shown.

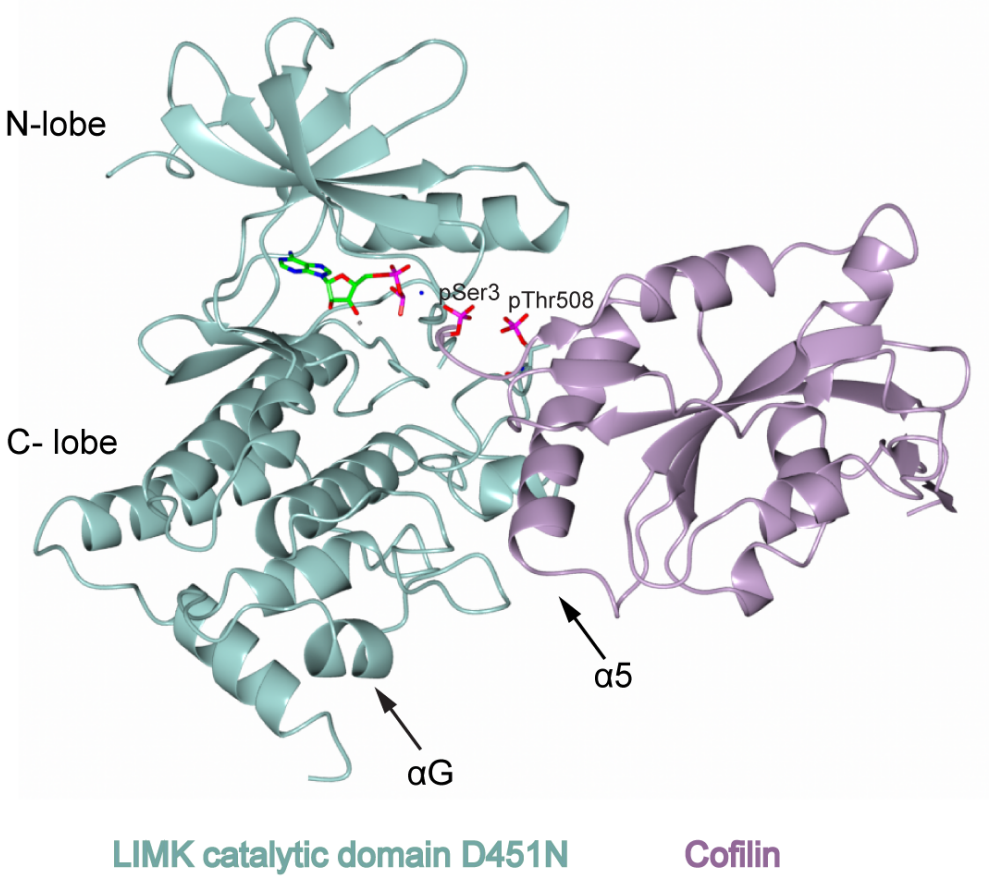

Figure 1.14. LIMK and cofilin complex.

LIMK1 D460N mutant (green) interaction with cofilin(purple) (PDB: 5HJV) is guided by monogamous interactions between αG in LIMK catalytic domain's C-lobe and the α5 in cofilin. The catalytic domain in LIMK shows interactions with AMP-PNP and phosphorylated Thr508. Cofilin shows N-terminus interaction with the catalytic cleft of LIMK, and pSer3 is also shown.

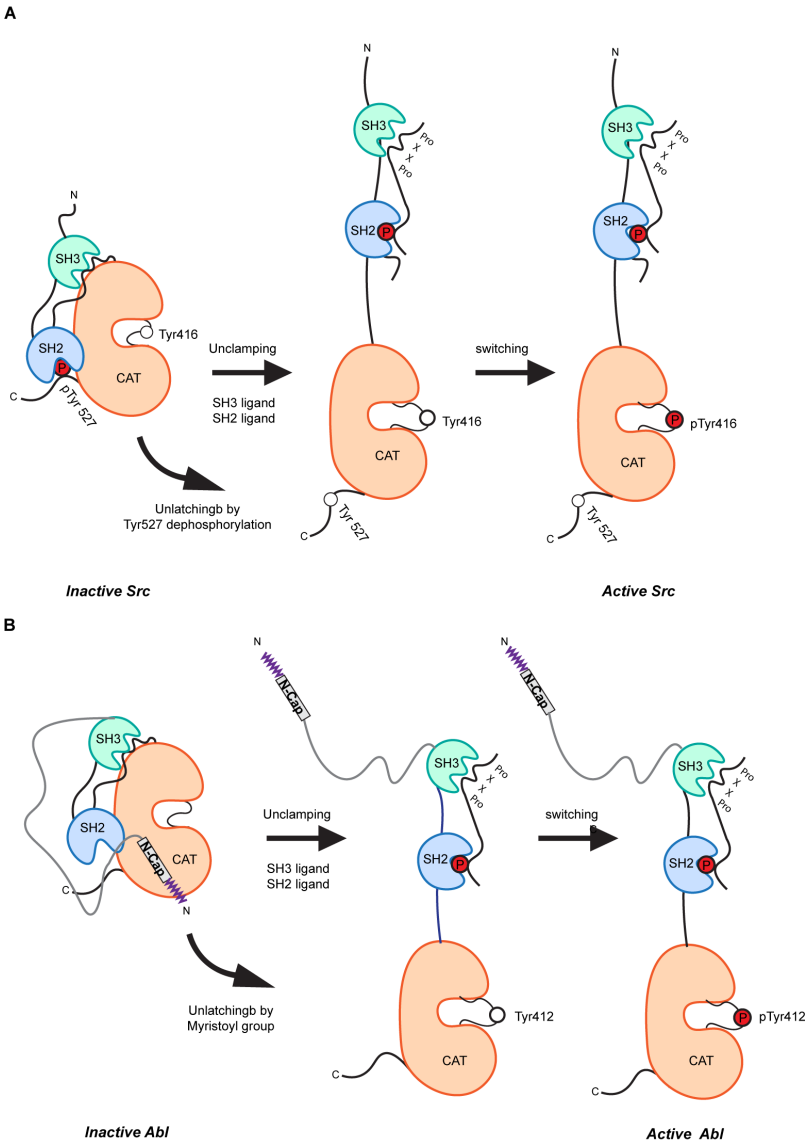

Figure 1.15. Src and Abl autoregulation mechanisms.

A. Autoregulation mechanism employed by Src kinase. On the top left is depicted the inactive conformation of Src, and on the top right is the active conformation. **B.** Autoregulation mechanism of Abl kinase. The inactive conformation of Src is shown on the bottom left, and on the bottom right is the active conformation. Both kinases share the same domain architecture: SH3 (Src Homology 3), SH2 (Src

Homology 2), and CAT (kinase domain), purple zip zag represents N-terminal myristoyl modification. Activation loop phosphorylation residue is also shown—figure adapted from [312].

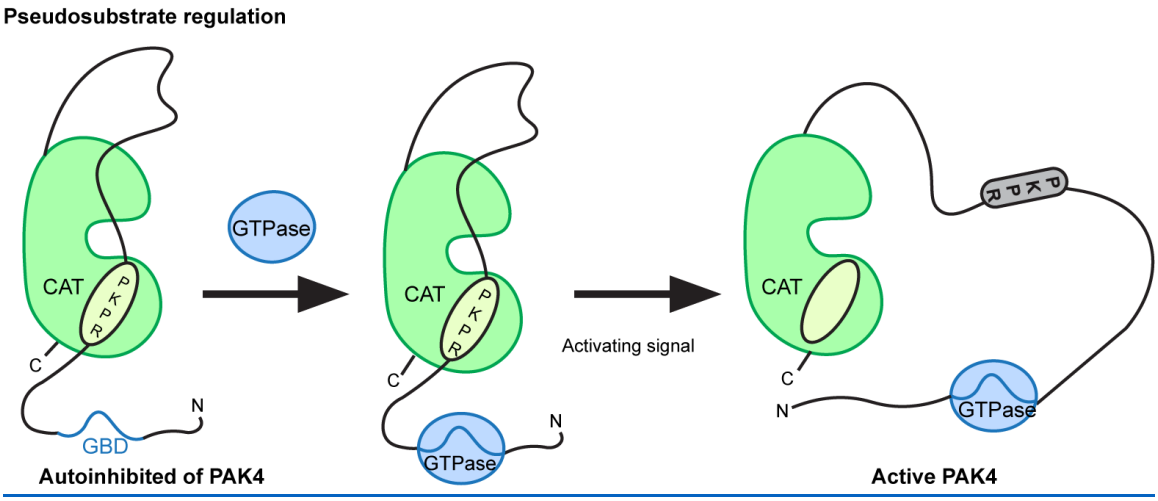

Figure 1.16. Kinase regulation by pseudosubstrate regulation.

Autoregulation mechanism employed by PAK4 kinase. Binding of GTPase to the GBD and subsequent SH3 binding of the pseudosubstrate region allows PAK4 to reach full activity. SH3 (Src Homology 3), GBD (GTPase binding domain), and CAT (kinase domain). Activation loop phosphorylation residue is also shown. Figure adapted from [279].

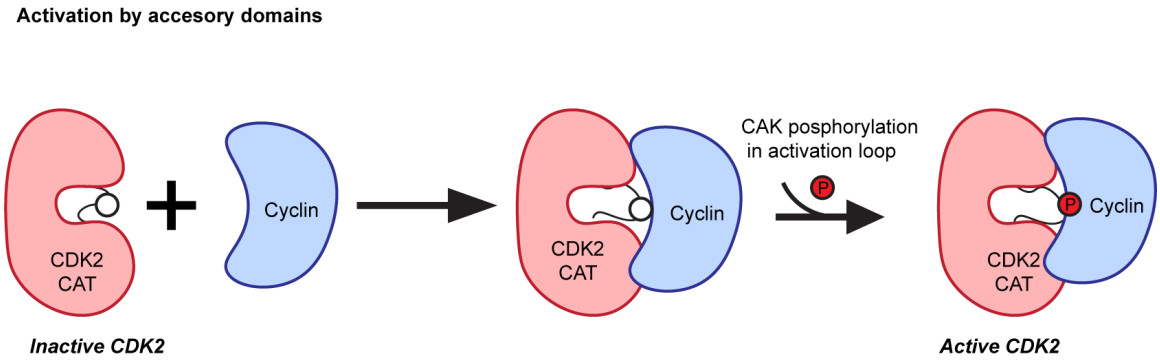

Figure 1.17. Kinase activation by accessory domains

Activation mechanisms employed by Cdk2 kinase. Cyclin binding to the kinase domain of Cdk2 relieves the blockade of the catalytic cleft. This movement now allows the activation loop Thr to become accessible for phosphorylation by CKA (CDK activating protein), completing the activation process for CDK2. CAT (kinase domain), cyclin, and activation loop phosphorylation residue are also shown.

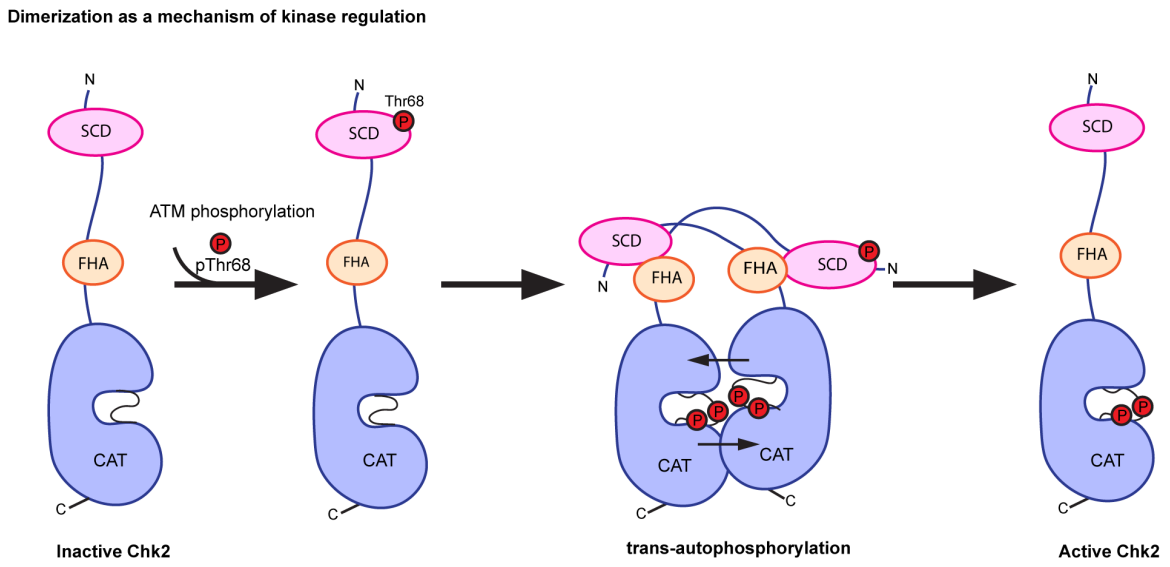

Figure 1.18. Kinase activation by phosphorylation outside the activation loop.

Chk2, upon DNA damage, goes through its activation mechanism. ATM kinase phosphorylates Chk2 at Thr68 at the SCD domain. Interaction of pThr68 of one molecule of Chk2 and the FHA domain of another drive the dimerization of Chk2. After dimerization, phosphorylation of the activation loop is possible via trans-autophosphorylation of two Thr residues in the activation segment. Dissociation of the dimer leaves a fully active cHK2. SQ/TQ cluster domain (SCD), CAT (kinase domain), and forkhead-associated (FHA) domain are shown along with the activation loop, and SCD phosphorylation residues are also shown.

Chapter 2: Autoregulation of LIM domain kinases by their PDZ domain

A portion of this research is under review as “Autoregulation of the LIM kinases by their PDZ domain” by Casanova-Sepúlveda, G., Sexton J., Turk B.E., Boggon, T.J.

2.1 Introduction

2.1.1 N-terminal PDZ domain is hypothesized to inhibit LIMK kinase activity

In humans, there are two LIMK genes, *LIMK1* and *LIMK2*. Their protein products, LIMK1 and LIMK2, are sequence (54% identical) and architecturally similar, with two N-terminal tandem-zinc finger LIM domains followed by a PDZ domain, a predicted unstructured region enriched in serine, proline, and glycine residues, and a C-terminal kinase domain (**Figure 1.2A**). They are highly conserved over evolution and are found across eukaryotes, mammals, fish, and insects. As mentioned above, and like many other kinases, activation of these conserved multi-domain enzymes is associated with phosphorylation of the kinase activation loop, at residues Thr508 in LIMK1 and Thr505 in LIMK2 [179,181,241,307]. LIMK activation loop phosphorylation is usually considered incompatible with its autoinhibited state, but the molecular basis for autoinhibition of the LIMKs remains unknown. As stated in Chapter 1, section 1.15, LIMK is suppressed by interactions with N-terminal domains [53,54,307]. Still, the molecular basis for this suppression of activity remains unclear.

2.1.2 LIMK contains an unusual PDZ domain

A closer analysis of the N-terminal region of the LIMKs has revealed the PDZ domain to be an unusual example of the PDZ fold [68-72,73,74]. As stated in Chapter 1, section 1.6, these non-catalytic domains are thought to mediate protein-protein interactions, most commonly by specific recognition of linear peptide motifs from protein binding partner carboxy-terminal tails [92,95,106,111,313,314]. However, this is not the case for the LIMK PDZ domain, which has not been found to interact with carboxy-terminal peptides with biological affinity values [75, 315]. The PDZ fold can also mediate protein interactions by using alternate binding modes, including by interactions of the canonical binding site with internal peptide motifs (i.e., non-terminal peptides) of partner proteins or by use of alternative binding surfaces as described extensively in Chapter 1, sections 1.6.8-1.6.10 [46,78,127-131]. LIMK PDZ domain might similarly use alternative binding surfaces for intermolecular protein-protein interactions; however, interactions with potential binding partners remain poorly understood [17,101,252,316,317]. However, the PDZ domain has yet to be extensively studied as a possible direct modulator of LIMK autoregulation. Despite the early studies, it remains unknown whether surfaces on the LIMK PDZ domain regulate LIMK catalytic activity or if it functions on catalytic activity by some other mechanism.

2.1.3 Significance and Project Aims

Biochemical studies of this domain point to an unusual example of a PDZ domain. However, studies have attributed autoregulatory effects to deletion or mutagenesis

of this domain. Therefore, I decided to study how the PDZ domain regulates the activity of the kinase domain of LIMK1 toward cofilin. To better study the LIMK2 PDZ domain fold, I obtained the crystal structure of human LIMK2 PDZ domain. I determined the 2.0 Å crystal structure of the LIMK2 PDZ domain and found a canonical PDZ fold with an unusually shallow peptide binding cleft and unique structural features. Upon mapping sequence conservation, I also found a highly conserved surface distal to the canonical peptide binding cleft, suggesting an unusual non-canonical role for LIMK PDZ. I next conducted targeted mutagenesis of the conserved surface and found suppression of proliferation in a yeast growth assay indicative of increased kinase activity. Likewise, in kinase activity assays, I found that mutations of the conserved surface of the LIMK1 PDZ domain result in increased catalytic activity, but that mutation of the canonical binding site does not. I conclude that the LIMKs contain an unusual PDZ domain that directly affects the autoinhibition of kinase activity via a previously unidentified conserved surface found. These findings shed new light on the regulation mechanism for both LIM domain kinases, LIMK1 and LIMK2. Taken together, this study suggests that this domain may allosterically inhibit kinase activity.

2.2 Methods

2.2.1 Protein Expression and Purification

The sequence encoding full-length human LIMK2 protein (UniProt ID: P53667) PDZ domain (131-25) was inserted using restriction enzymes BamHI and EcoRI into a modified *E. coli* expression vector pET28a containing an N-terminal FLAG

tag followed by a (His6) tag and a recognition sequence for tobacco etch virus (TEV) protease. A C173S point mutation was introduced using QuikChange Lightning site-directed mutagenesis kit (Agilent) to inhibit the disulfide bond formation and improve stability for crystallization experiments. Solubility testing of PDZ domain mutants was conducted on a C173S mutant background.

His-tagged LIMK2 PDZ was expressed in BL21(DE3) cells (Millipore Sigma) by induction with 0.5 mM isopropyl β-D-thiogalactopyranoside (IPTG) overnight at 16 °C. Cells were harvested by centrifugation at 2,000×g and lysed by suspension in nickel binding buffer (50 mM HEPES pH 7.5, 500 mM NaCl) including of 0.1 M phenylmethylsulfonyl fluoride (PMSF), Roche complete EDTA-Free protease inhibitor tablet) and lysozyme, followed by freeze/thaw cycles and sonication. Lysates were clarified by centrifugation at 5000×g for 1 hour. Supernatant was applied to nickel beads for affinity purification (Ni Sepharose 6 Fast Flow, GE Healthcare). Following elution of bound proteins by increasing concentrations of imidazole in nickel-binding buffer, the His-tag was removed from PDZ by incubation with TEV protease overnight during dialysis against buffer containing 50 mM HEPES pH 7.5, 500 mM NaCl. The cleavage reaction was then flowed over a nickel affinity column (HisTrap Fast Flow, GE Healthcare) to remove the liberated His6 tag, uncleaved His6-tagged protein, and the His6x-tagged TEV protease. The flow-through containing untagged PDZ protein was concentrated in a centrifugal filter (Amicon Ultra, Millipore Sigma), diluted to a salt concentration of 37 mM NaCl, and applied to a 5 ml anion exchange column (Mono Q GE Healthcare)

equilibrated in 20 mM Tris pH 7.5 buffer. Protein was eluted with a continuous gradient of NaCl, ranging from 0% to 40% 1 M NaCl, and 20 mM Tris pH 8, with the protein eluting at 12% 1 M NaCl. The eluted peak was concentrated and then purified by size exclusion chromatography on a Superdex 75 10/300 GL. PDZC173S eluted as a monodisperse peak.

2.2.2 Crystallization, data collection, and structure determination of LIMK2 PDZ domain.

Initial small cube-like clusters of PDZ crystals were obtained by sparse matrix screening using a TTP Labtech Mosquito by vapor diffusion in sitting drops at 4°C with a 2:1 (v/v) ratio of purified protein to reservoir solution containing 0.1 M HEPES pH 7.5, 10% 2-propanol and 20% PEG 4000. Optimization of crystals was carried by using sitting drop methodology. Crystals were harvested from the drop, quickly incubated in 15% glycerol as a cryoprotectant, and flash-cooled in liquid nitrogen. Four sets of diffraction data were collected from a single crystal at Northeastern Collaborative Access Team (NE-CAT) Beamline 24-ID-E at Argonne National Laboratory Advanced Photon Source, processed using XDS [318], and scaled using SCALA [319]. The data were processed in space group *P*21, with unit cell dimensions *a* = 80.94 Å, *b* = 83.03, *c* = 83.08 Å, α = 90°, β = 96.56°, γ = 90°. Matthew's probability calculation indicated 8 copies of the PDZ domain in the asymmetric unit. Phaser [320] confirmed the prediction using the predicted AlphaFold structure of LIMK2 PDZ as model (residues 131-250, LIMK2-AF-P53671-F1-model_v2.pdb). Model building was performed in Phenix Autobuild[321], and manual

autobuilding was performed in Coot [322]. Refinement was carried out in Phenix refine[323].

2.2.3 Conservation Analysis

LIMK1 and LIMK2 sequences were identified using NCBI BLAST [324]. A total of 421 sequences were aligned using the ClustalO[310] server and visualized using JalView [311]. PDZ sequences from other proteins were identified using NCBI BLAST [324]. For PDZ containing human proteins, a total of 967 sequences were filtered. Sequences were aligned using the ClustalO[310] server and visualized using JalView [311].

2.2.4 Yeast Growth Assays

The high copy vector for constitutive expression of N-terminally His_6-tagged human cofilin-1 in yeast (pRS423-GPD-cofilin-1) and the galactose-inducible expression vector for N-terminally FLAG epitope-tagged LIMK1 catalytic kinase domain (pRS415-GAL-LIMK1-CAT) was cloned into the BamHI and XhoI sites of pRS415-GAL were previously described [186]. All point mutants were prepared using QuikChange Lightning site-directed mutagenesis kit (Agilent) and verified by sequencing through the entire open reading frame. Yeast expressing human cofilin-1 was generated by plasmid shuffle starting with a *cof1Δ* strain supported by expression of yeast Cof1 from a *CEN URA3* plasmid (MHY8282, obtained from Mark Hochstrasser's laboratory [325]). This strain was transformed with pRS423-GPD-cofilin-1 (WT or S3A mutant), and then the yeast Cof1 plasmid was evicted by selection on solid media containing 5-FOA. This strain was then transformed

with the indicated LIMK1 expressing plasmids or the corresponding empty vectors. To assess the impact of LIMK1 expression on cell growth, yeast were grown overnight at 30 °C in synthetic complete media lacking histidine and leucine (SC-His-Leu) containing 2% glucose. The following day, cultures were diluted into SC-His-Leu containing 2% raffinose and grown overnight to mid-log phase. Serial 5-fold dilutions (starting OD = 0.2) were then spotted onto SC-His-Leu agar plates containing either 2% glucose or 2% raffinose/1% galactose, and plates were incubated at 30 ºC until colonies were visible at the highest dilution of the empty vector strain. Point mutations in pRS415-GAL-FLAG-LIMK1 were introduced by substituting residues Leu165, Asp221, Arg222, Glu225, and Gln251 with alanine and Lys175 with aspartate using QuickChange Lightning site-directed mutagenesis kit (Agilent). Primers used for mutagenesis are listed in **Table 2.2**.

2.2.5 Immunoblotting

Yeast cultures (500 ml) were grown to an OD_{600} of 1-2 in 2% raffinose at 30 °C, and then 1% galactose was added to induce LIMK1 expression. After 4 h, cells were harvested and lysed using a TCA extraction protocol adapted from [326] with the following modifications. Yeast cells were resuspended in a lysis buffer containing 10% TCA, 25 mM NH_4OAc, 10 mM Tris HCl, pH 8.0, and 1 mM DTT. Glass beads were added to the resuspended lysate and vortexed for 5 min at 4 °C. Lysed cells were centrifuged at 16900 x g in a 4 °C centrifuge for 10 min. Pellets were resuspended in 0.1M Tris pH 11 and 3% SDS. Pellets containing precipitated proteins were diluted 1:10 and then used for BCA assays. BCA assays

were used to normalize the amount of protein added. Equal amounts of lysate with 4X SDS-PAGE loading buffer (7 µg per lane) were fractionated by SDS-PAGE and transferred to polyvinyl difluoride (PVDF) (Sigma, IPFL85R) membrane. Membranes were blocked in Tris buffer saline (TBS) with 5% non-fat milk for 1 h and probed overnight at 4 °C with the indicated primary antibodies: mouse anti-FLAG antibody (Sigma, #F3165,1:5,000 dilution). Membranes were incubated for 30 min in fluorescently labeled secondary antibodies IRDye® 800CW goat anti-mouse IgG secondary Antibody (Licor, #D10603-05) and goat anti-rabbit IgG (H+L) Highly Cross-Adsorbed Secondary Antibody, Alexa Fluor 680 (Invitrogen, #A21109) in 1:10,000 dilution in TBS with 5% bovine serum albumin (BSA) and 0.1% Tween20. Membranes were scanned using a Li-Cor Odyssey Imaging system. 3.3 µg of FLAG-LIMK1 preparations purified from yeast were analyzed similarly for the assessment of activation loop phosphorylation. The following primary antibodies were used: mouse anti-FLAG antibody (Sigma, #F3165,1:5,000 dilution), rabbit anti-KSS1 (Santa Cruz Biotechnology, # sc-6775-R, 1:5,000 dilution), penta-His (Qiagen, # 34650, 1:5000), and p-Cofilin (Serine3) (Cell Signaling, #3311S, 1;1000), phospho-LIMK1/LIMK2 antibody (Thr508/Thr505) (Cell Signaling, #3841S 1;1000).

2.2.6 Yeast Protein Expression

The *cof1Δ* yeast strains co-transformed with pRS423 GPD-S3A His_6-hCofilin and FLAG-LIMK1 expression constructs were grown from an individual colony overnight at 30 °C in 5 mL of SC-His-Leu with 2% raffinose. The next day, the

culture was diluted into 500 ml SC-His-Leu with 2% raffinose to an OD_{600} of 0.1 and grown to an OD_{600} of ~2. Next, 225 ml of 3.5x yeast extract, peptone solution (YP), and 80.5 mL of 10% galactose were added to the flask to induce expression of LIMK1 for 8 h. Yeast were centrifuged at 2600 × g for 30min at 4°C. Cells were resuspended in 10 ml of sterile water, repelleted, snap-frozen in liquid nitrogen, and stored at -80°C.

FLAG- LIMK pellets were thawed on ice and resuspended in 5 ml of FLAG lysis buffer (50 mM HEPES, pH 7.4, 150 mM NaCl, 1 mM EDTA, 0.5% Triton X-100, 10% glycerol, 0.5 mM DTT, 1 mM PMSF, 2 µg/mL pepstatin A, 2.5 mM $NaPP_i$, 1 mM βGP, 1mM Na_3VO_4, and Roche complete EDTA-Free protease inhibitor tablet). Pellets were distributed into 10 microtubes with 150 µl of glass beads. Lysis was achieved by cell disruption caused by shaking the lysates with the beads using vortexing. Lysates were transferred to fresh tubes and centrifuged at 800 x g for 10 min at 4 °C. Thermo Scientific Pierce anti-DYKDDDDK M2 resin (300 µL) equilibrated in lysis buffer was added to the supernatant and incubated with rotation for 2 h at 4 °C. The resin was pelleted (197 x g, 2 min, 4 °C), resuspended in 1 ml lysis buffer, and washed twice with wash buffer (50 mM HEPES, pH 7.4, 100 mM NaCl, 1 mM DTT, 1 mM βGP, 100 µM Na_3VO_4, 0.01% NP-40, 10% glycerol). FLAG elution buffer (400 µl of 50 mM HEPES, pH 7.4, 100 mM NaCl, 1 mM DTT, 1 mM βGP, 100 µM Na_3VO_4, 0.01% NP-40, 10% glycerol and 0.5 mg/ml of FLAG peptide) was added, and the resin was incubated at 4 °C while rotating for 2 h. Resin was then centrifuged at 197x g for 2 min, and eluted protein was

collected, aliquoted, snap-frozen in liquid nitrogen, and stored at -80 °C. Purity and protein concentration were estimated against a BSA standard curve on SDS-PAGE (15% acrylamide) with Coomassie staining.

2.2.7 Mutagenesis and solubility test of His tagged LIMK2 PDZ mutants

Primers used are indicated in **Table 2.2**. All mutants were expressed in BL21 cells. Overnight cultures were inoculated into 1 L ml of Luria broth, and protein expression was induced with isopropyl 1-thio-β-d-galactopyranoside when OD_{600} = 0.6. Cells were grown overnight at 18 °C, harvested, and resuspended in 10 ml of 500 mM NaCl and 20 mm Tris, pH 8.0, supplemented with DTT, protease inhibitors, lysozyme, and DNase I. Resuspended cells were lysed by three freeze/thaw cycles in a dry ice/ethanol bath followed by sonication. Lysates (100 µl) were centrifuged at 20400 x g for 10 min. The supernatants were separated from the pellets. Pellets were resuspended in 100 µl of 6 M urea and diluted two-fold in lysis buffer. Samples were run on a 15% acrylamide SDS-PAGE and visualized by Coomassie staining.

2.7.8 Radiolabel kinase assays

Human cofilin was purified as previously described in [186]. Kinase reactions (25 µl) contained 5 nM purified LIMK1 and 6.7 µM cofilin in 50 mM HEPES, pH 7.5, 100 mM NaCl, 5 mM $MgCl_2$, 5 mM $MnCl_2$, 20 µM ATP, 1 mM DTT, 0.1 µCi/ml ^{32}P-ATP. Reactions were incubated 10 min at 30 °C, quenched by adding 1x SDS-loading buffer and resolved by SDS-PAGE on a 15% polyacrylamide gel. Dried gels were exposed to a phosphor screen, and the level of phosphorylated cofilin was

evaluated on a Bio-Rad Molecular Imager Fx system using Quantity One 1D Analysis software (Life Sciences Research). Data from 5 separate experiments were normalized to Flag-FL LIMK1 signal, and statistical analysis was carried out using a non-parametric unpaired Mann-Whitney test in GraphPad Prism.

2.3 Results

2.3.1 LIMK contains a divergent 'G-L-G-F' or 'χ-Φ-G-Φ' motif

To explore the role of the LIMK PDZ domain, I began by assessing the sequence of this domain between the LIMKs, across the LIMKs over evolution, and by comparison to other PDZ domains. I find that there is high conservation of the LIMK PDZ domain between human LIMK1 (residues 159-258) and human LIMK2 (residues 147-239), which are 47 % identical and 81% similar. This high conservation is maintained over evolution, and I find that LIMK PDZ domain sequence for human LIMK1 is 36% identical to that of drosophila LIMK1 and 56% identical to other insects. There is lower sequence similarity to canonical PDZ domains (21% identical to PSD95). Interestingly, I find that one of the defining features of canonical PDZ domains, a motif termed the 'G-L-G-F' or 'χ-Φ-G-Φ' motif [72,86,87], is divergent in the LIMKs over evolution and between LIMK1 and LIMK2 (**Figure 2.2 B, Figure 2.3**). For canonical PDZ domains, recognition of terminal carboxylate groups is 'conferred by a cradle of main chain amides' contributed by the 'χ-Φ-G-Φ' motif, where χ is any residue, and Φ is any hydrophobic residue [86]. Unusually, the LIMKs do not follow this consensus sequence. Instead, they harbor KRGL and RRGL sequences in LIMK1 and LIMK2,

respectively, replacing the first hydrophobic residue with a conserved arginine, Arg163 (**Figure 2.1 B**). The alignment of 241 human PDZ domains indicates that the LIMKs are the only PDZ domains harboring an arginine in the second position of the χ-Φ-G-Φ motif [87,127]. As stated in Chapter 1, section 1.5.1, this region usually contains hydrophobic residues, and its conformation is essential for allowing the amide groups to serve as H-bond donors and confer depth to the binding cleft. To investigate this in more detail, I determined the crystal structure of the LIMK2 PDZ domain.

2.3.2 Human LIMK2 PDZ crystal structure

I expressed and purified the human LIMK2 PDZ domain (residues 145-236) and determined its crystal structure to 2.0 Å resolution (**Figure 2.2 A, Table 2.1**). The crystal structure reveals a compact globular domain resembling a partially open barrel typical of the PDZ fold. I find the expected canonical six β-strands and the canonical αB helix. As stated in Chapter 1, section 1.6, canonical PDZ fold includes αA helix, but unusually, I found that helix αA is replaced by two 3_{10} helices, which I term αA' (residues R187-H189) and αA'' (residues P192-N194). Also, I found a third 3_{10} helix in the βD-αB loop, which I term the αB' helix (residues V212-T214) (secondary structure nomenclature as per [86]). Dali searches with the two orientations reveal that the LIMK2 PDZ domain is most similar to the PDZ domains of PP1α (RMSDs of 3.0 Å and 3.5 Å over 88 and 88 Cαs for the two LIMK orientations; PDB ID: 3EGG [327]), syntenin-1 (2.5 Å/2.5 Å over 78/80 Cαs; PDB ID: 5G1E [328]), disks large homolog 4 (2.8 Å/2.5 Å over 87/85 Cαs; PDB ID: 5HEY [329])

and harmonin (3.0 Å/2.8 Å over 85/84 Cαs; PDB ID: 3KLR [136]). The structure of the LIMK2 PDZ domain, therefore, reveals an overall canonical PDZ domain with unusual features, where the 'χ-Φ-G-Φ' motif includes two basic residues (KRGL, RRGL for LIMK1 and LIMK2, respectively) and a shallow binding cleft.

2.3.3 hLIMK2 PDZ domain R163 engages in extensive hydrogen bonding

Unusual features are observed when I look closely at the Arg163, which occupies the second hydrophobic position in the x-Φ-G-Φ motif. This residue is usually oriented towards the hydrophobic core of the domain, and similarly, but unexpectedly, for an arginine, I found that in my structure, Arg163 is pointed inwards towards the hydrophobic core. To balance the charge of the guanidino group, Arg163 engages in extensive hydrogen-bonding: it caps helix αB hydrogen bonding to the carboxyl oxygens of residues Ala223, Ile224, and Gln226, and hydrogen bonds to the carboxyl oxygen of Gln229 within the αB-βF loop (**Figure 2.2 B, C**). This seems to provide a rigid base for the C-terminus of the αB helix. A consequence of this inward-facing arginine residue, which is a member of the 'carboxylate-binding loop,' βA-βB, is that it helps create a somewhat shallow binding grove between the βB strand and αB helix (**Figure 2.2 D**). Canonical PDZ domains utilize the βB-αB groove to bind partner peptides and coordinate terminal carboxylate groups by backbone amide interactions of the central Φ-G residues of the 'x-Φ-G-Φ' motif. The inward orientation of Arg163 to cap helix αB seems to be key for orientations of the βA-βB and αB-βF loops, an inward orientation of helix αB and placement of Arg163's Cβ atom to encroach on the expected carboxylate

binding site, potentially providing a molecular explanation for why the LIMK PDZ domains have not been found to interact with carboxy-terminal peptides with measured affinities in a biological range [75,315]. Therefore, the LIMK2 PDZ domain shows unusual features that make it different from canonical PDZ domains; it contains a non-canonical 'χ-Φ-G-Φ' motif that does not contain the common hydrophobic residues at the first two positions of this motif. Instead, it contains two positively charged residues (KRGL, RRGL for LIMK1, and LIMK2, respectively). Also, the positively charged residues in the second position of the 'χ-Φ-G-Φ' motif are completely conserved and are important for the creation of a shallow binding grove between the βB strand and αB helix of the PDZ domain.

2.3.4 LIMK family conservation analysis

Considering the unusual nature of the completely conserved Arg163, I wanted to know whether a more detailed conservation analysis could shed light on the role of the LIMK PDZ domain. I, therefore, mapped conservation over 421 LIMK1 and LIMK2 sequences (**Figure 2.4A**) onto my crystal structure. Supporting my conjecture that the orientation and interactions of Arg163 may help preclude carboxy-terminal peptide interactions, I do not find complete conservation of the canonical βB-αB binding groove over all the LIMKs (**Figure 2.4 A**) or for segregated LIMK1 or LIMK2 (**Figure 2.5**). In contrast, I was surprised to discover almost complete conservation over evolution and across both LIMK family members of an extended surface distal to the βB-αB binding groove comprising parts of strands βA, βF, and βD (**Figure 2.4A**). Generation of electrostatic potential

indicates that this surface is predominantly hydrophobic (**Figure 2.4B**). This highly conserved hydrophobic βA-βF-βD surface suggested that it either plays a structural role in stabilizing the protein or indicates a conserved surface for inter- or intra-molecular interactions with the kinase domain or other protein partners. I, therefore, decided to study the role of this surface of LIMK in a living organism.

2.3.5 Reconstruction of the LIMK pathway in yeast

Building on work done by the Hochstrasser, de la Cruz, and Turk laboratories at Yale University, I reconstituted the mammalian LIMK1-cofilin pathway in budding yeast *Saccharomyces cerevisiae* to evaluate LIMK autoregulation in living cells. I modified the previously reported system in which the Boggon lab reconstituted the mammalian LIMK1-cofilin pathway in budding yeast [186]. The sole yeast cofilin ortholog (Cof1) is essential for viability, and expression of mammalian cofilin-1 can rescue the growth of a *cof1Δ* strain [330,331]. It was shown previously that expression of the LIMK1 catalytic domain suppresses the growth of yeast expressing human cofilin in a manner dependent on Ser3 phosphorylation [186]. I hypothesized that if full-length (FL) LIMK1 is autoinhibited by its N-terminal region, it would cause a less severe growth phenotype when expressed in yeast compared to the catalytic domain alone. Furthermore, I hypothesize that mutations in the PDZ domain that relieve autoinhibition will exacerbate growth suppression by FL LIMK1. I, therefore, used this *S. cerevisiae* system to assess the impact of mutations in the βA-βF-βD surface of the LIMK PDZ domain (**Figure 2.6**).

I transformed *cof1Δ* yeast with two plasmids, one constitutively expressing human cofilin-1 and the other expressing WT LIMK1 or various mutants in a galactose-inducible manner. I then examined cell growth under conditions that either induce (galactose) or do not induce (glucose) LIMK expression. In contrast to the induction of LIMK1 kinase domain expression, which resulted in complete growth suppression, the expression of FL LIMK1 reduced but did not eliminate growth. These observations suggest decreased cofilin phosphorylation by the presumably lower kinase activity of FL LIMK1 (**Figure 2.7A**)[186]. I found no reduction in growth for cofilin-S3A expressing yeast upon induction of either kinase domain or FL LIMK1, confirming that growth suppression depends on cofilin Ser3 phosphorylation and is not due to non-specific toxicity (**Figure 2.7A**).

2.3.6 Mutation in PDZ conserved patch increases growth inhibition

I then analyzed my crystal structure of the LIMK2 PDZ domain and assessed the conservation and solvent exposure of residues within the conserved βA-βF-βD surface. Based on the high sequence similarity of LIMK1 and LIMK2 in the PDZ domain (47% identical, 81% similar) (**Figure 2.7 B**), I introduced point mutations to interrupt either the electrostatics (E225A, D221A, R222A, Q251A; LIMK1 numbering) or to alter the hydrophobic surface (L165A) of the conserved βA-βF-βD patch. I first assessed the mutants' expression in yeast and found that all constructs expressed to the same levels as WT LIMK1 (**Figure 2.8**). I then evaluated the impact of these mutations on yeast growth. All five-point mutations suppress growth compared to full-length LIMK1, and E225A (equivalent to LIMK2

E206) results in a complete loss of yeast growth, suggesting LIMK activity comparable to the uninhibited kinase domain (**Figure 2.7A**).

To assess whether these alterations in yeast growth are due to alterations in LIMK catalytic activity, I conducted in vitro kinase activity assays. I purified full-length LIMK1 from yeast cultures and similarly purified E225A, L165A, D221A, R222A, K175D, and Q251A mutated full-length LIMK1 and catalytic domain control. Using these purified LIMK1s, I assessed the phosphorylation of purified human cofilin. I found that while the K175D and controls show no difference in cofilin phosphorylation compared to the wild-type full-length LIMK1, all mutants show an increase in kinase activity of at least approximately 4-fold with E225A demonstrating a 7.5-fold increase in kinase activity (**Figure 2.9**). I, therefore, conclude that the conserved βA-βF-βD surface of the PDZ domains of LIM domain kinases represents an intramolecular regulatory surface essential for normal modulation of LIMK kinase activity. Solubility analysis for the PDZ domain alone suggests that D221A and R222A are destabilizing but that Q251A and E225A remain soluble, potentially indicating divergent mechanisms for changes in LIMK activity (**Figure 2.10**). Overall, I infer that the conserved βA-βF-βD surface of the PDZ domains of LIM domain kinases represents an intramolecular regulatory surface that can autoinhibit LIMK kinase activity.

2.3.7 Mutations in conserved PDZ surface increase activation loop phosphorylation

I finally assessed the role of the PDZ domain in regulating LIMK activation loop phosphorylation. The regulation steps for these kinases still need to be solved, and it is still being determined how autoregulation and activation loop phosphorylation coordinate to regulate activity. Therefore, could introducing these point mutations impact the phosphorylation of the LIMK activation loop? In keeping with coordinated autophosphorylation and intramolecular interactions, activation loop phosphorylation was consistently elevated for point mutations that increased kinase activity. I observed higher activation loop phosphorylation in both my yeast growth assays (**Figure 2.11**) and the purified protein used for my kinase assays (**Figure 2.12**).

2.4 Discussion

The LIM domain kinases are critical regulators of cytoskeletal dynamics in the cell. They recognize and phosphorylate ADF/cofilin proteins by an unusual mechanism. The uniqueness of this near-monogamous kinase-substrate relationship makes the LIMKs fundamental for regulating actin filament stabilization. Nonetheless, the regulation mechanisms by which the LIMKs are themselves controlled still need to be described. In this chapter, I provide new insights into the molecular basis of LIMK autoregulation by using a structure-directed approach to understand the role of the LIMK PDZ domain. I determined the 2.0 Å crystal structure of the LIMK2

PDZ domain and found key differences between this domain and the rest of the members of the PDZ family.

My structure-based conservation mapping onto the LIMK2 PDZ domain revealed a previously undescribed highly conserved surface patch and led us to investigate the role of this region in autoregulation. As discussed in Chapter 1, section 1.6, PDZ domains most often bind protein partners via a cleft in the PDZ fold. However, based on my structure and conservation analysis, I find this surface to be non-optimal for canonical PDZ C-terminal binding. Therefore, I decided to introduce point mutations in a conserved surface distal to the canonical binding groove that shows high conservation. I found that the disruption of this conserved surface results in a complete loss of growth in a yeast assay, suggesting increased LIMK catalytic activity. *In vitro* kinase assays using full-length protein harboring mutations in the conserved surface also demonstrate increased kinase activity compared to wild-type proteins. My work, therefore, provides new insights into the PDZ and how this domain might regulate the activity of the kinase domain. Likewise, it highlights a conserved surface on the unusual PDZ domain as a critical component of the regulatory mechanisms for the LIM domain kinases.

My crystal structure of the LIMK2 PDZ domain reveals an unusual addition to this common fold. My analysis of the LIMK2 PDZ domain and comparison to the over 250 mammalian PDZ domains [74,87,332] reveals three unusual features suggestive of functional relevance. Next, I describe how the PDZ domain of LIMK diverges from the canonical features described in Chapter 1, sections 1.6 to 1.6.3.

First, I observe that the canonical peptide binding cleft between the βB strand and αB helix is particularly shallow and that the orientation of the αB-βF loop encroaches on the binding grove. As discussed in section 1.6.2, the depth and composition of residues in this cleft are important to fit the C-terminal carboxy binding site to the cleft. While it is not necessarily unusual to observe a shallow cleft in PDZ domains (for example, PDZ7 of GRIP[333]), this feature provides a rationale for why the LIM domain kinase PDZ domains have not so far been found to interact with C-terminal peptides in PDZ interaction screening studies [75,315]. Second, I find that the second position of the 'χ-Φ-G-Φ' motif is unique among the PDZ fold as hydrophobic core-facing arginine (Arg163 in LIMK2 and Arg176 in LIMK1). The hydrogen-bonding of this completely conserved arginine caps the αB helix, coordinates the αB-βF loop, and seems to provide a rigid base for the C-terminus of the αB helix. Third, I find that the αA helix is replaced by two 3_{10} helices. This combination of unusual features for the LIMK PDZ domain makes it difficult to place into the previously assigned PDZ classes (class I, class II and class III) [67,100,103,118,127]. These features do, however, tempt conjecture that this PDZ domain may be able to engage in bi-directional allostery. An example of allosteric regulation of PDZ interactions is discussed in Chapter 1, section 1.6.13, with Par-6 and Cdc42, where interactions with helix αA can increase carboxylate peptide binding affinity and vice versa [149,150]. It is interesting to speculate that the LIMK PDZ domain may be primed for carboxylate peptide binding but require allosteric-

induced conformational movements to reveal the high-affinity binding site. Further studies are required to probe this more fully.

My structure also provides an interesting insight into the current state of macromolecular structure prediction. Comparison of my crystal structure with the unpublished NMR structure of the LIMK2 PDZ domain (Riken Structural Genomics Proteomics Initiative; PDB ID: 2YUB) reveals that some of the unique features of the LIMK PDZ domain are not found by NMR, including the 3_{10} helices, αA' and αA'', and that the buried 'χ-Φ-G-Φ' arginine, Arg163, is surface exposed in the majority of the 20 models (17/20). In contrast, Alphafold (model AF-P53671-F1-model_v2.pdb [334]) predicts the 3_{10} helices, αA' and αA'', and the buried Arg163 (**Figure 2.13)**. My molecular replacement solution of the crystal structure was more accurate using the AlphaFold model than the NMR structure (TFZ score of 28 versus 7, respectively), and the final structure displays RMSDs of 0.76 Å over 91 Cαs and 1.42 Å over 89 Cαs when compared to the AlphaFold and NMR models, respectively. RMSD differences between the AlphaFold model and the crystal structure of the hLIMK2PDZ domain between members A and B of the asymmetrical unit are 0.76 Å and 0.70 Å between 91 and 83 equivalent Cα positions, respectively. These analyses suggest that AlphaFold can provide near-experimental accuracy for molecular models even with unique structural features. As discussed in Chapter 1, section 1.8, it is common among protein kinases that release from autoregulation is associated with activation loop phosphorylation [179,241,307,335]. Still, the details of how the LIMKs are autoregulated remain unclear.

Early studies suggested a ‘head-tail’ interaction between the N-terminal LIM and PDZ domains and the C-terminal kinase domain [53,54,307], and the activity of the catalytic domain alone is qualitatively about 100-fold higher than the full-length protein [186]. This Chapter begins to provide some molecular-level details on this regulation mechanism. Unexpectedly, on mapping evolutionary conservation, I found a lack of conserved residues in the canonical βB-αB cleft but extremely high conservation on the βA-βF-βD surface. The importance of this βA-βF-βD surface in LIMK regulation has not been established. Introduction of point mutations increases the full-length protein's catalytic activity, consistent with the interruption of an autoinhibited conformation. My studies strongly imply that the βA-βF-βD surface, particularly the conserved glutamic acid, Glu206 (LIMK2) / E225 (LIMK1), is critical for autoregulation. Importantly, surface mutations outside this region and in the βB-αB cleft do not impact activity. Conversely, mutation of PDZ domain hydrophobic core residues increased catalytic activity (not shown). Mutation of these residues caused the isolated PDZ domain to be insoluble when expressed in bacteria suggesting that proper folding of the PDZ domain is required for autoregulation. My studies demonstrate that a previously unidentified and completely conserved surface on the properly folded PDZ domain is necessary for normal autoregulation of the LIMKs. This work provides a first molecular-level insight into the molecular surfaces important for autoregulation of LIMK. Based on the superposition of over 40 Alphafold models of LIMK1 and LIMK2 in different species (for further discussion, refer to Chapter 3), I find that the βA-βF-βD surface

is almost completely surface exposed, with a small portion of the surface (residue L152 and residues of βA which makes an anti-parallel β-sheet interaction with LIM2) consistently found to interact with the adjacent LIM2 domain. In these models, residue Glu206 (LIMK2) / Glu225 (LIMK1) is always surface exposed, further supporting my finding that the βA-βF-βD surface has the potential to regulate the kinase directly. I believe the disruption of the surface that mediates autoregulatory interactions between the PDZ domain with the kinase domain allows LIMK to reach a more “open” conformation. This “open” conformation allows for activation loop phosphorylation by upstream activators or a worse substrate for LIMK phosphatases. This model is supported by increased kinase activity and activation loop phosphorylation in PDZ mutants. Overall, the data presented in this chapter clearly demonstrate that a previously unidentified surface on the PDZ domain plays a pivotal role in the autoregulation of the LIM domain kinases.

2.5 Figures and Tables

Table 2.1 Data collection and refinement statistics.

Statistics for the highest-resolution shell are shown in parentheses. RMSD: root-mean-square deviation.

Data Collection	**LIMK2 PDZ**
PDB accession code	8GI4
Wavelength (Å)	0.97918
Resolution range (Å)	80.42 - 2.06 (2.13 - 2.04)
Space group	*P* 2_1
Cell dimensions a, b, c (Å)	80.9 83.0 83.1
α, β, γ (°)	90, 96.6, 90
Unique reflections	67631 (6631)
Multiplicity	20.2 (14.1)
Completeness (%)	99.8 (98.3)
Mean *I*/σ*I*	23.9 (2.0)
Wilson B factor (Å^2)	45.76
R_{pim}	4.491 (40.21)
CC½	99.5 (0.3)
CC*	99.9 (0.68)
Refinement	
Resolution range (Å)	80.42 - 2.06 (2.13 - 2.06)
Reflections used in refinement	67544 (6630)
Reflections used for R_{free}	3197 (271)
% Reflections used for R_{free}	4.7 (4.1)
R_{work} (%)	21.0 (36.2)
R_{free} (%)	23.3 (36.6)
No. of non-hydrogen atoms	
Protein	6091
RMSD	
Bond lengths (Å)	0.002
Bond angles (°)	0.45
Ramachandran plot	
Favored, allowed, outliers (%)	98.1, 2.0, 0.0
Rotamer outliers (%)	0
MolProbity clashscore	1.5 (100th percentile)

Average *B* factor (Å^2)	59.8

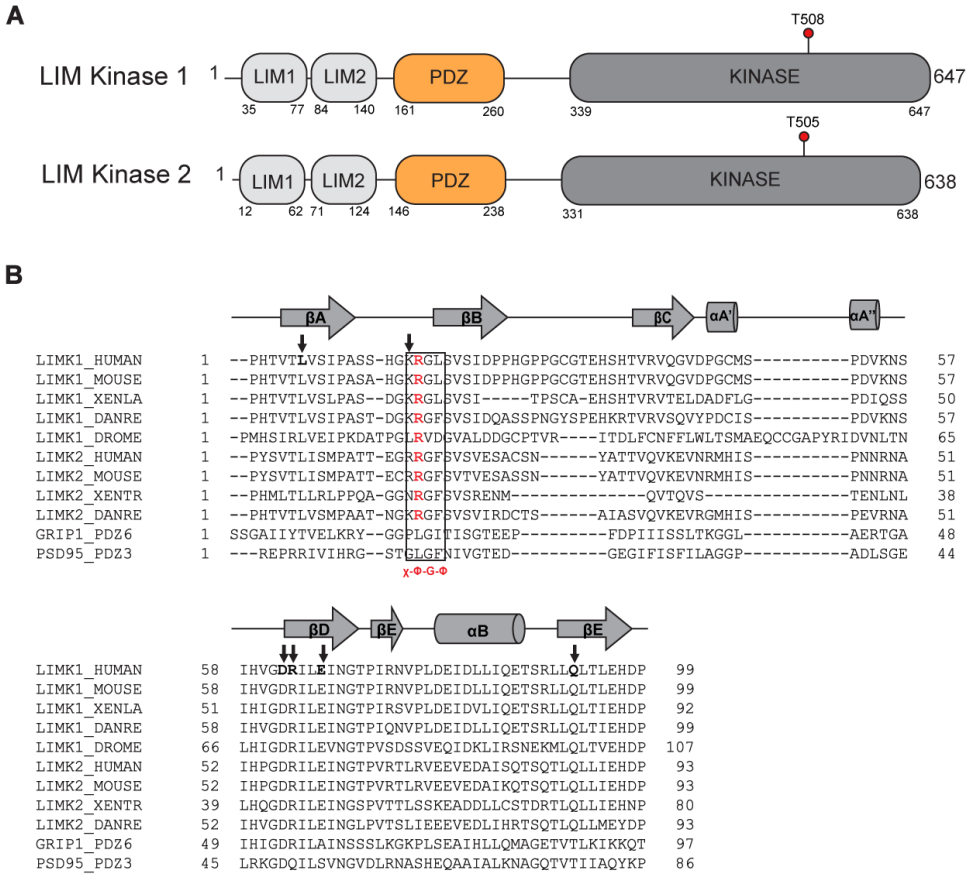

Figure 2.1. LIMK domain architecture.

A. LIM domain kinase family architecture showing human LIMK1 (UniProt ID: P53667) and human LIMK2 (UniProt ID: P53671). LIM1: first LIM domain, LIM2: second LIM domain, PDZ: PDZ domain, Kinase: kinase domain. Activation loop phosphorylation residues indicated, Thr508/Thr505 for LIMK1 and LIMK2, respectively. Residue numbers are shown. **B.** Sequence alignment of PDZ domains. Alignment was created using PROMALS[336]. Uniprot ID for LIMK1_HUMAN, P53667; LIMK1_MOUSE, P53668; LIMK1_XENLA, O42565;

LIMK1_DANRE, B3DIV5; LIMK1_DROME, Q8IR79; LIMK2_HUMAN, P53671; LIMK2_MOUSE, O54785; LIMK2_XENTR, F7AFJ1; LIMK2_DANRE, Q6DG29; GRIP1_PDZ6_HUMAN_, P97879; PSD95_ PDZ3 RAT, P31016. GRIP1_PDZ6 is a Class I PDZ domain, and PSD95_PDZ3 is a Class II PDZ domain. 'χ-Φ-G-Φ' sequence is inside a black-lined box. The conserved arginine residue equivalent to Arg163 in human LIMK1 is colored red. Conserved amino acid residues targeted in mutagenesis studies are in bold and under a black arrow.

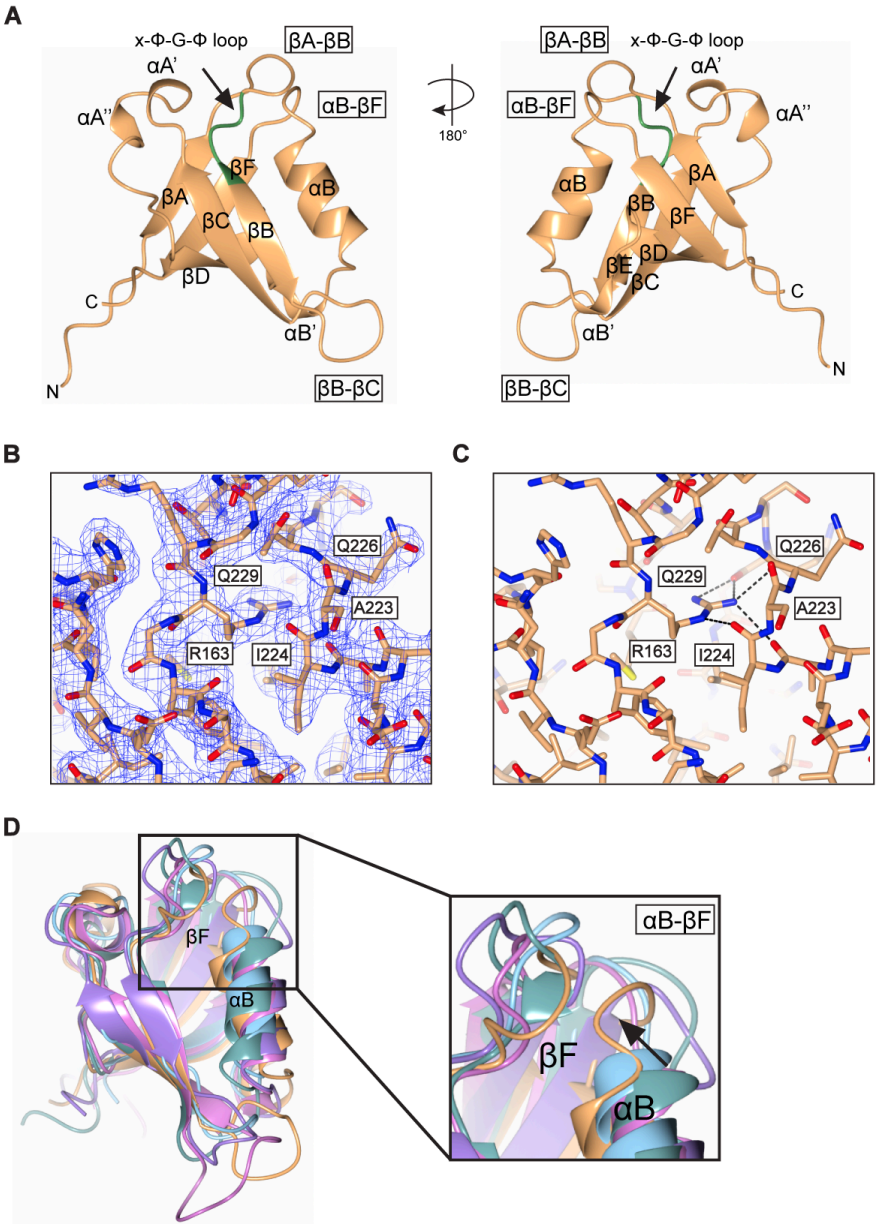

Figure 2.2. Structure of LIMK2 PDZ domain.

A. Human LIMK2 PDZ domain determined to 2.0 Å resolution shown in cartoon format. Secondary structure named. The 'x-Φ-G-Φ' loop, βA-βB loop, αB-βF loop, and βB-βC loop are indicated, and the x-Φ-G-Φ' loop is colored green. **B.** Electron

density map of Arg163. $2F_{obs}$ - F_{calc} electron density map contoured at 1σ (blue). F_{obs} - F_{calc} electron density map contoured at +3σ (green) and -3σ (red). **C.** Hydrogen bonds of Arg163. **D.** Inward orientation of the αA-βF loop. Comparison of the αA-βF loop orientation of LIMK2 PDZ crystal structure (orange) and the most similar PDZ domains structures from Dali[337]; spinophilin, PDB ID: 3EGG[327] (pink), disks large homolog 4, PDB ID: 5HEY[329] (light blue), harmonin, PDB ID: 3K1R[136] (purple), and syntenin-1, PDB ID: 5G1E[328] (teal). The inward orientation of helix αB helps create a somewhat shallow binding grove between the βB strand and αB helix compared to these most similar PDZ domains. Images generated using CCP4mg[338].

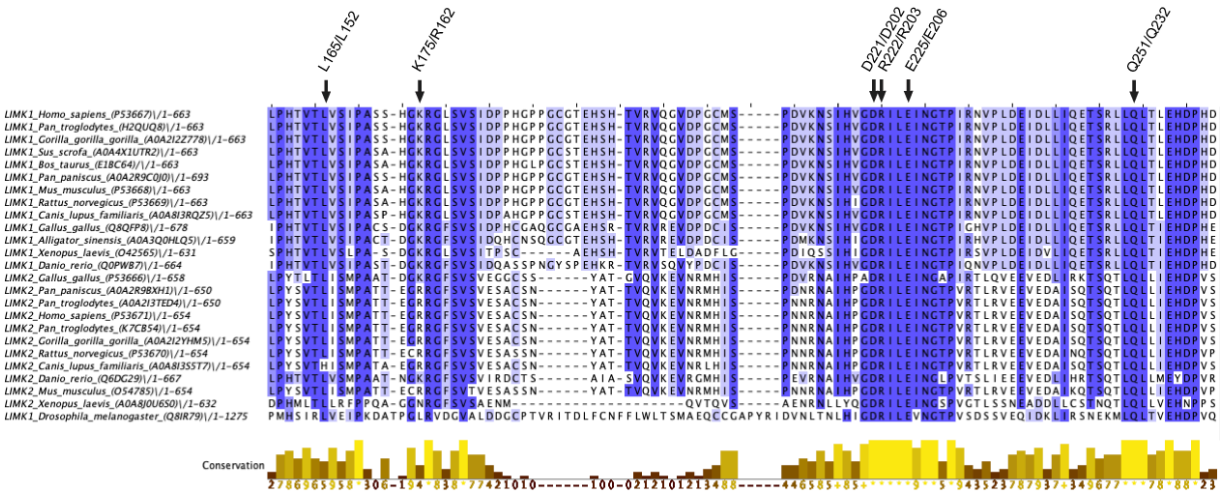

Figure 2.3. Conservation of the LIMK PDZ domain.

Sequences were obtained from UniProt[309] and aligned in ClustalOmega[310]. Each sequence is named by species and UniProt ID. Conservation scores were calculated in Jalview[311]. Identical residues are highlighted in dark blue, and partially conserved residues in light blue. Mutations used in kinase assays are shown under an arrow, and their LIMK1/LIMK2 residue numbers shown.

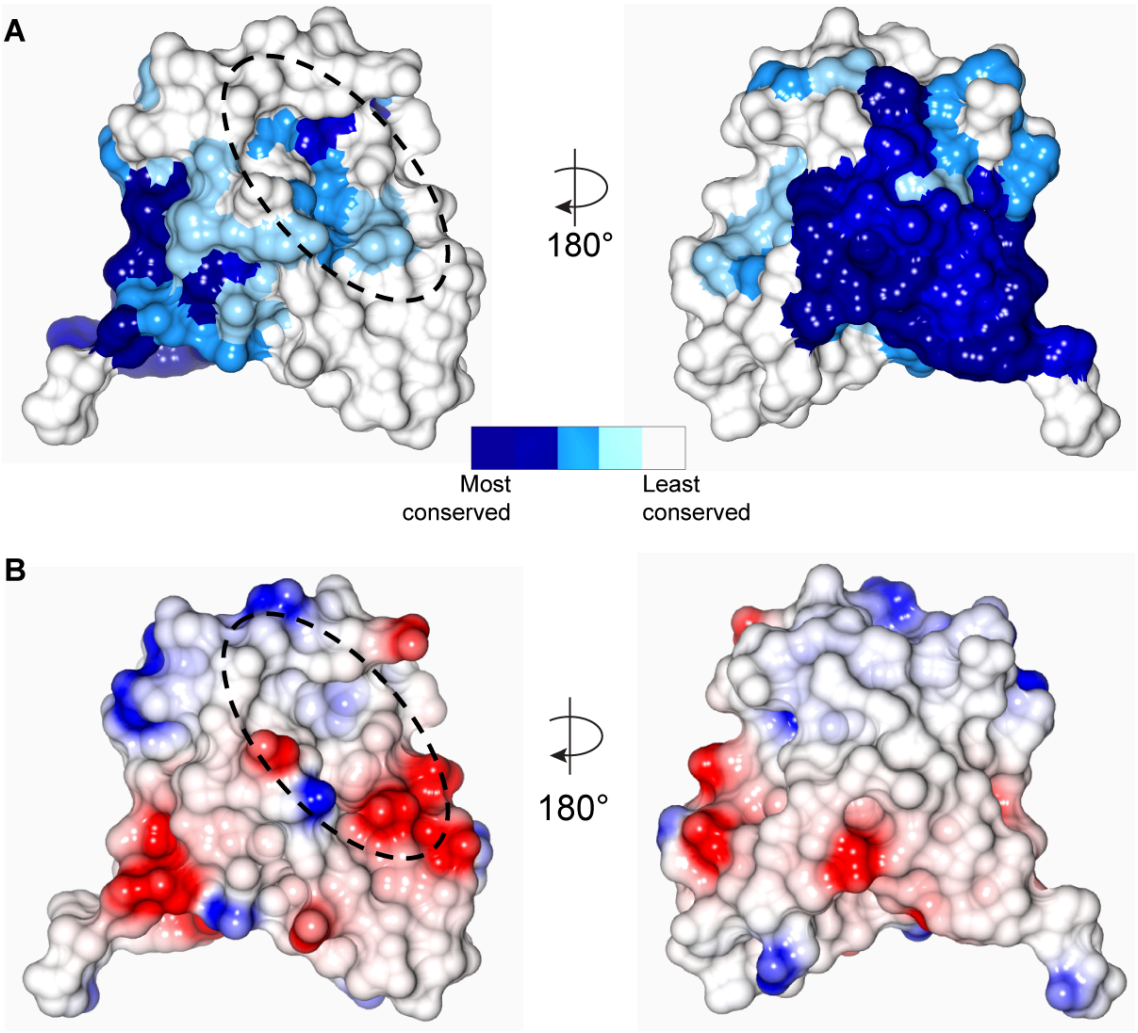

Figure 2.4. Surface analysis of LIMK2 PDZ domain.

A. Conservation of the LIMK2 PDZ domain. PDZ domain conservation mapped onto the structure of LIMK2 PDZ for 421 aligned LIMK sequences from mammals, birds, fish, and insects. Dashed oval indicates the canonical PDZ binding cleft. **B.** Surface electrostatics of the LIMK2 PDZ domain calculated by CCP4mg[338]. Red indicates negatively charged surfaces, blue indicates positively charged surfaces,

and white surfaces indicate neutrally charged surfaces. Dashed oval indicates the canonical PDZ binding cleft.

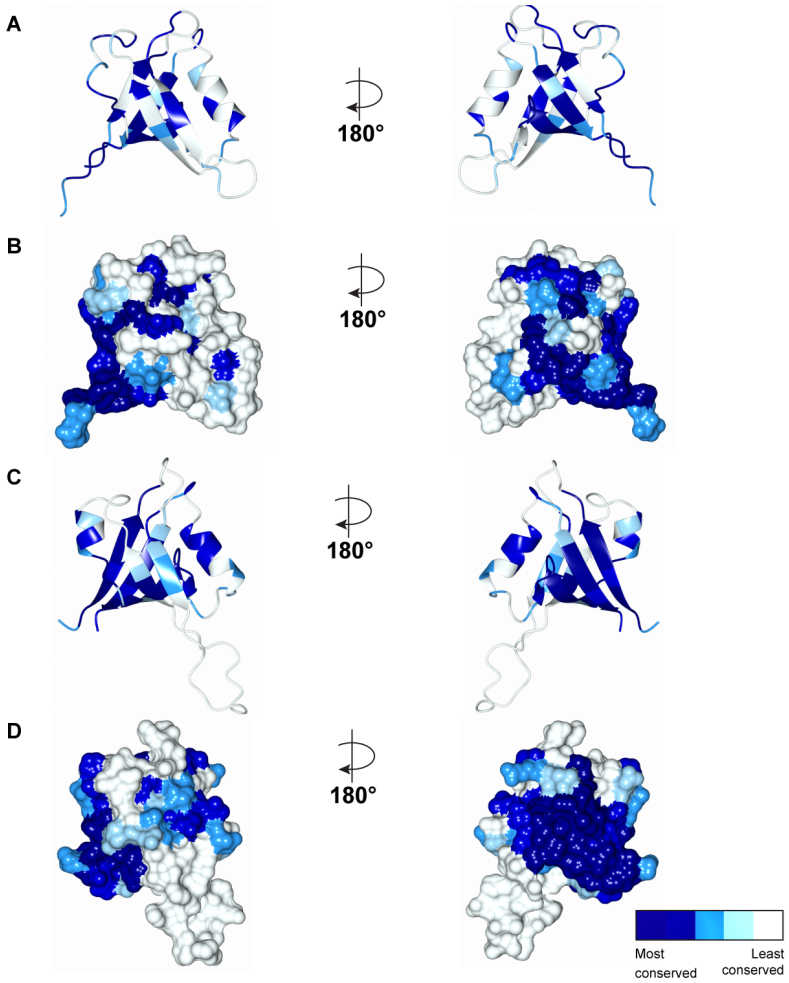

Figure 2.5. Conservation of the PDZ domain within LIMK2 and LIMK1 sequences.

A, B. Cartoon and surface representations showing the LIMK2 PDZ domain conservation across LIMK2 sequences mapped to my crystal structure. Sequence alignment of 209 sequences of LIMK2 was made using ClustalO[310]. Species in this alignment include mammals, birds, fish, and insects. **C, D.** Cartoon and surface representations showing the LIMK1 PDZ domain conservation across LIMK1 sequences mapped to residues 160 to 260 of the AlphaFold model (AF-P53667-

F1-model_v2). Sequence alignment of 212 sequences of LIMK1 was made using ClustalO[310]. Completely conserved residues are colored dark blue, less strongly conserved residues are colored lighter shades of blue, and non-conserved residues are white. Image generated using CCP4mg [338].

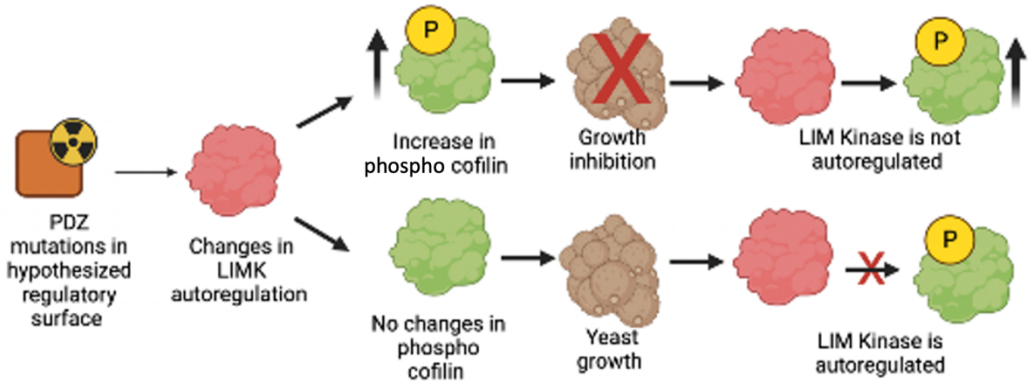

Figure 2.6. Reconstitution of the LIM-cofilin pathway in yeast.

Mutations in hypothesized regulatory surface change LIMK autoregulation. Autoregulation disruption induces growth inhibition.

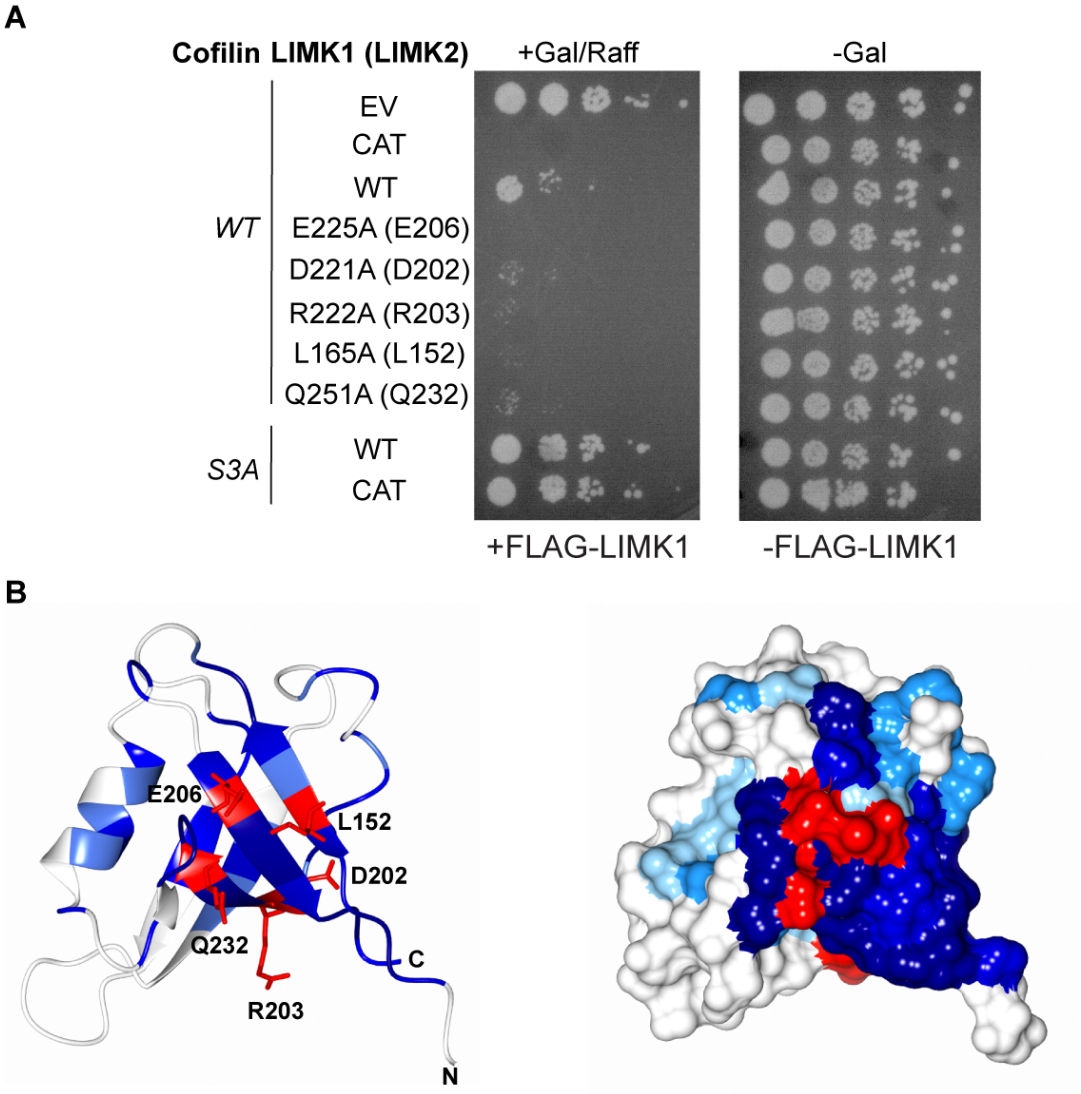

Figure 2.7. PDZ domain mutants suppress yeast growth.

A. Serial dilutions of *cof1Δ* yeast expressing human cofilin and the indicated human LIMK1 mutants. Controls of human LIMK1 constructs, full-length (FL), kinase domain (CAT), unphosphorylatable cofilin S3A (S3A) and empty vector (EV). Mutants of full-length LIMK1: E225A, D221A, R222A, L165A, Q251A. Corresponding LIMK2 residue is shown in parentheses. Five-fold dilutions of yeast cultures were plated on solid media in the presence of glucose (-Gal) or galactose

and raffinose (+Gal/Raff) to induce LIMK1 expression. Plates were grown at 30°C for 2 days (glucose plate) or 4 days (galactose plate). Representative of 3 independent experiments. **B.** Mutants assessed are shown on the cartoon and surface representations of the conservation map of the LIMK2 PDZ domain. Residues shown and equivalent human LIMK1 residue numbers: L152 (L165 in LIMK1), Q232 (Q251 in LIMK1), D202 (D221 in LIMK1), R203 (R222 in LIMK1) and E206 (E225 in LIMK1).

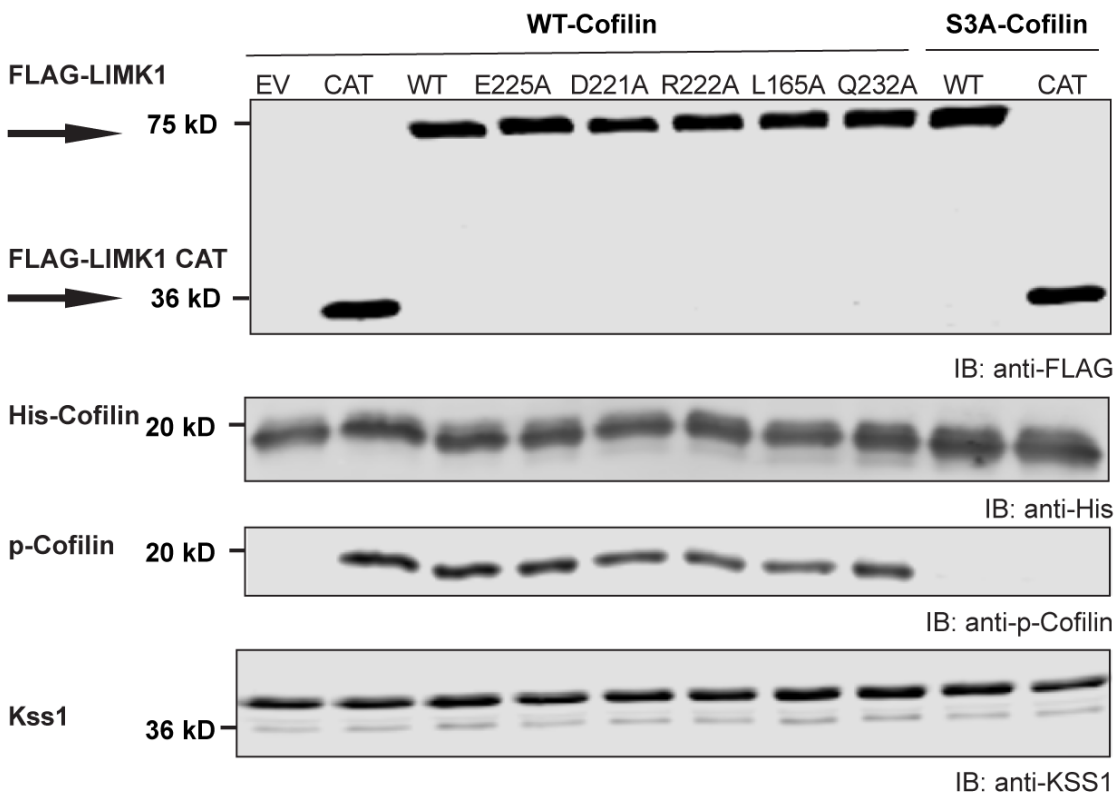

Figure 2.8. LIMK1 protein expression in yeast and kinase activity assessment

Immunoblot analysis of FLAG-LIMK1 and PDZ mutants expressed in yeast Kss1 loading control, His-cofilin, and cofilin phosphor-Ser3. WT indicates full-length LIMK1, and CAT indicates catalytic domain.

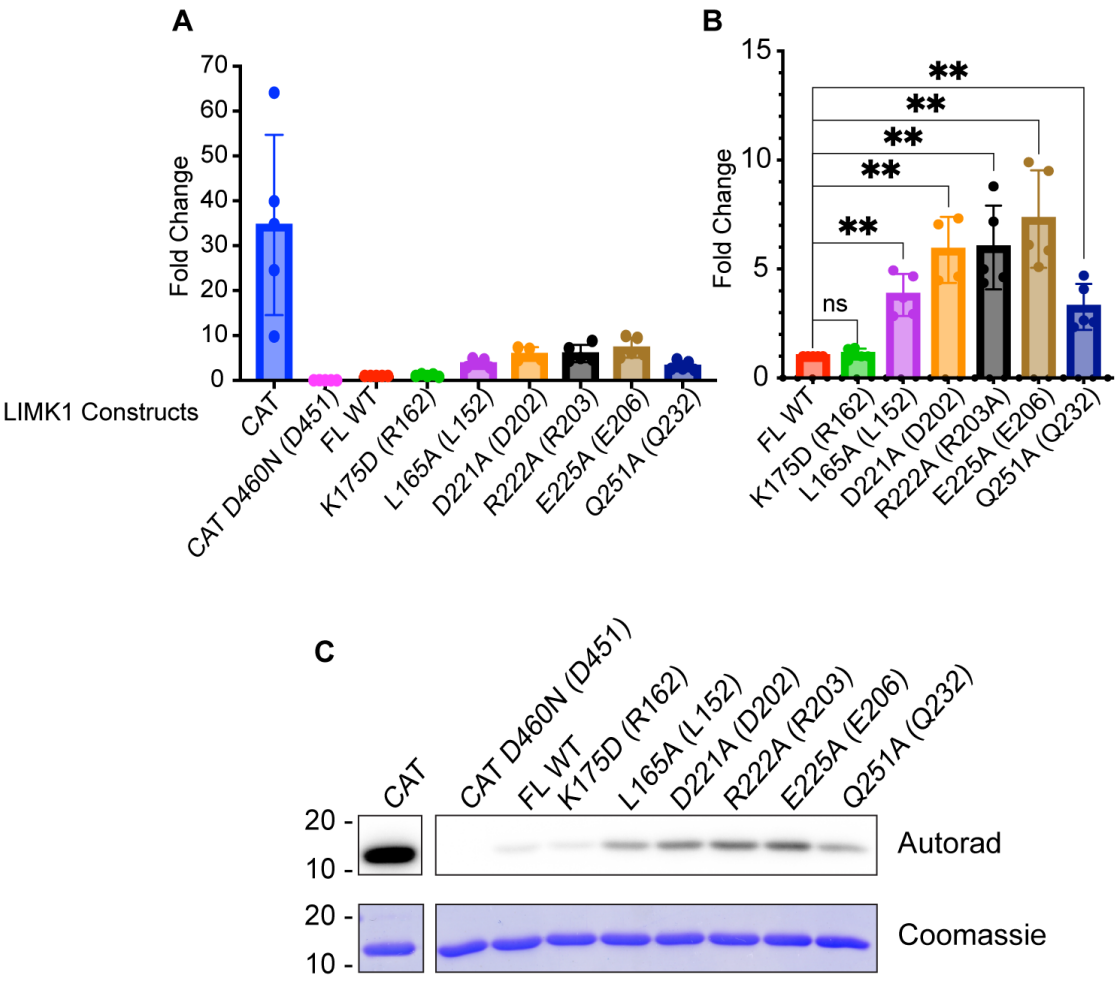

Figure 2.9. Increased *in vitro* kinase activity for LIMK1 PDZ mutants.

Quantified autoradiography from radiolabel cofilin kinase activity of FLAG-LIMK1 constructs purified from yeast. **A.** Full-length wild type (WT), kinase domain alone (CAT), and catalytically inactive kinase domain (CAT D460N) were used as positive and negative controls, respectively. PDZ domain mutants of conserved residues in FL LIMK1 are shown (equivalent residue in LIMK2 shown in parentheses). **B.** Graph focused on full-length mutant constructs compared to WT. **C.** Lower panel shows representative autoradiography reading of cofilin

phosphorylation for kinase assays with corresponding Coomassie staining. Statistical analysis was carried out using a non-parametric unpaired Mann-Whitney test. Two stars (**) indicate $p < 0.0079$. A total of 5 replicates were analyzed using GraphPad Prism.

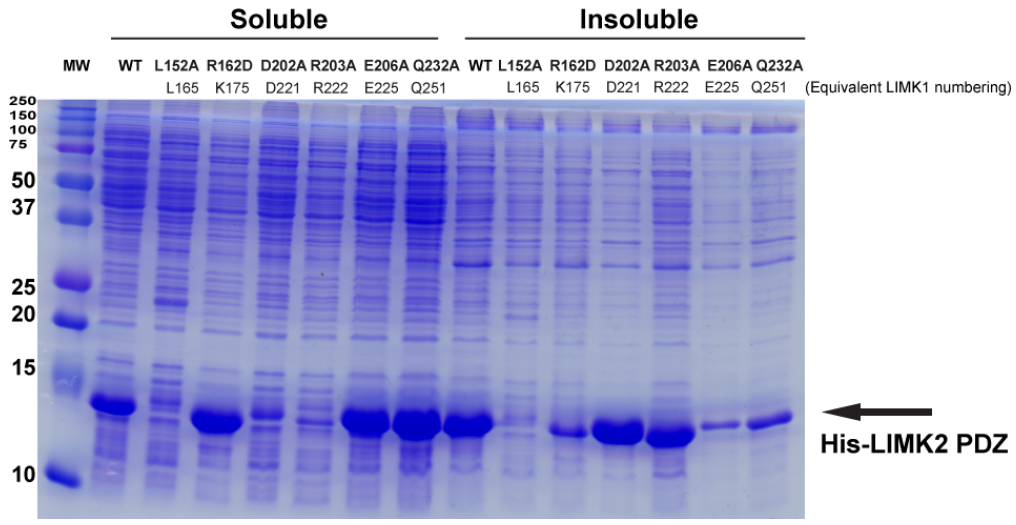

Figure 2.10. Bacterial expression and solubility tests for LIMK2 PDZ domain mutants.

*E. co*li lysate fractionation of the crystallized his-tagged LIMK2 PDZ domain construct and comparison with PDZ mutants in this construct. Residue number for mutations corresponding to LIMK1 (top) and equivalent LIMK2 residue (bottom) are shown in the gel.

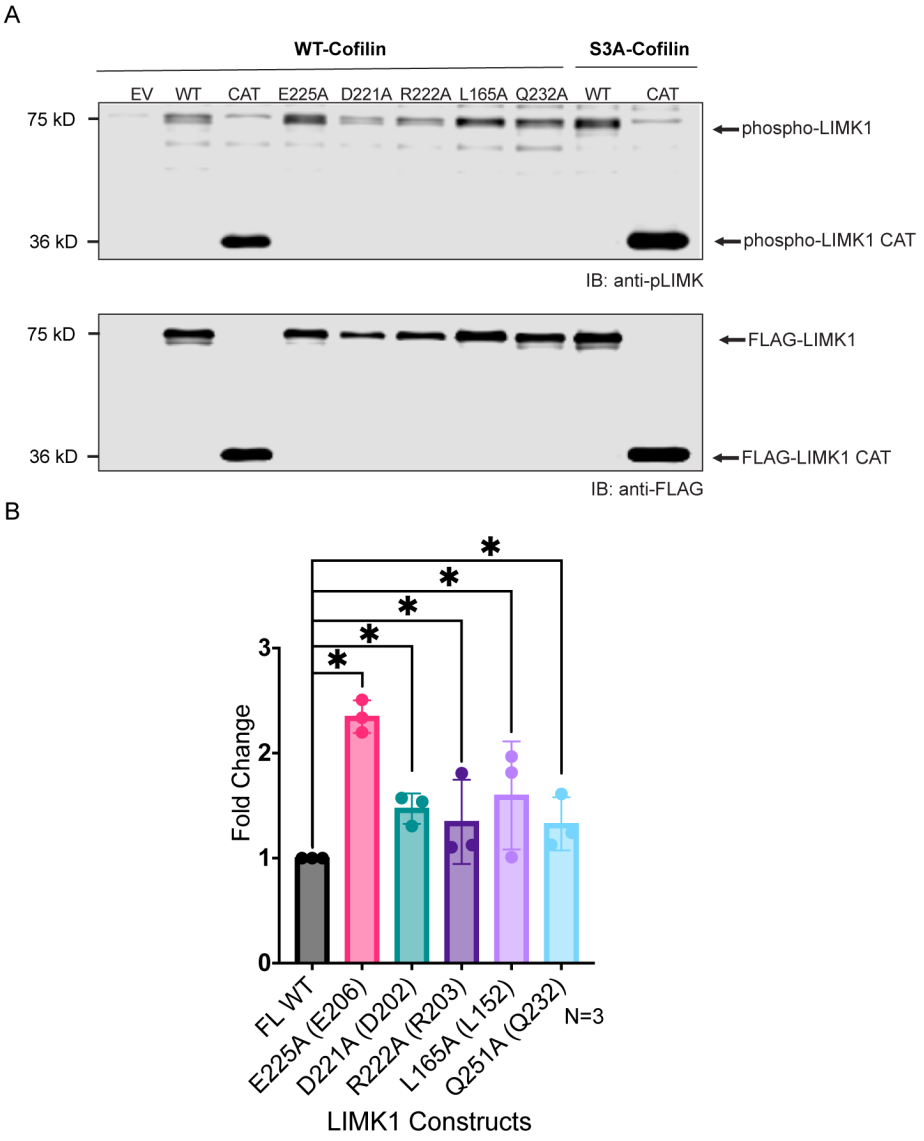

Figure 2.11. Assessment of LIMK activation loop phosphorylation in yeast.

A. Immunoblot assessing activation loop phosphorylation in LIMK1 constructs from my yeast growth assays. The top panel shows yeast lysates blotted with anti-pLIMK1 antibody. The second panel purified yeast protein blotted with anti-FLAG. **B.** Quantification of immunoblot signal. Signal was first normalized to FLAG signal of each construct and then to the signal from full-length WT LIMK1. Graph focused

on full-length mutant constructs compared to WT LIMK1. Statistical analysis was carried out using a non-parametric unpaired Mann-Whitney test. One star (*) indicates $p = 0.05$. A total of 3 replicates were analyzed using GraphPad Prism.

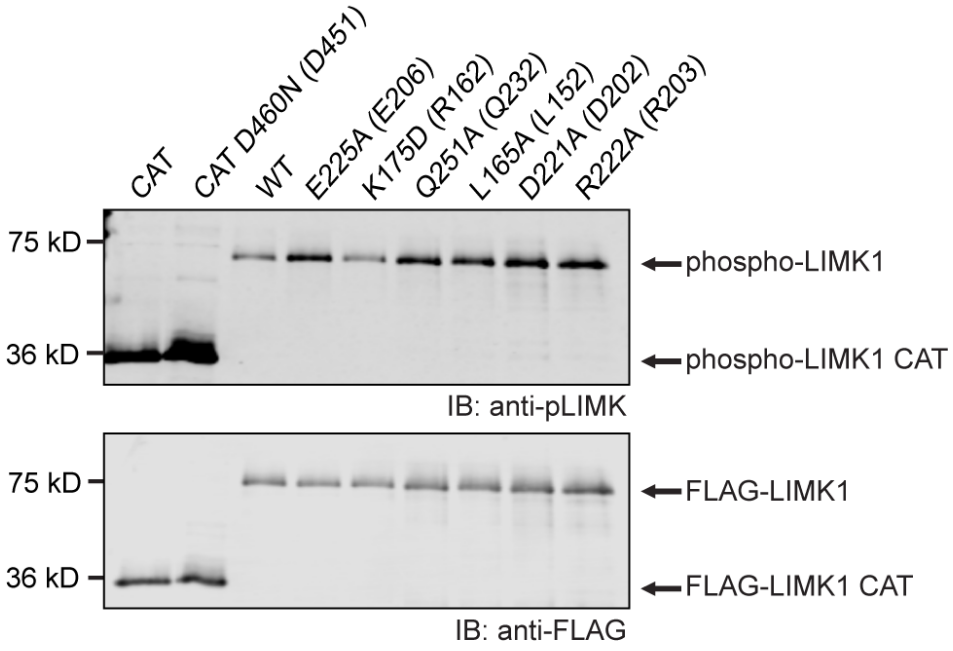

Figure 2.12. Assessment of LIMK activation loop phosphorylation.

Blot assessing activation loop phosphorylation in LIMK1 constructs purified from yeast. Top panel yeast lysates blotted with anti-FLAG antibody for FLAG-LIMK1 as loading control. Second panel purified yeast protein blotted with anti-phospho LIMK1. Parentheses indicate equivalent LIMK2 residue.

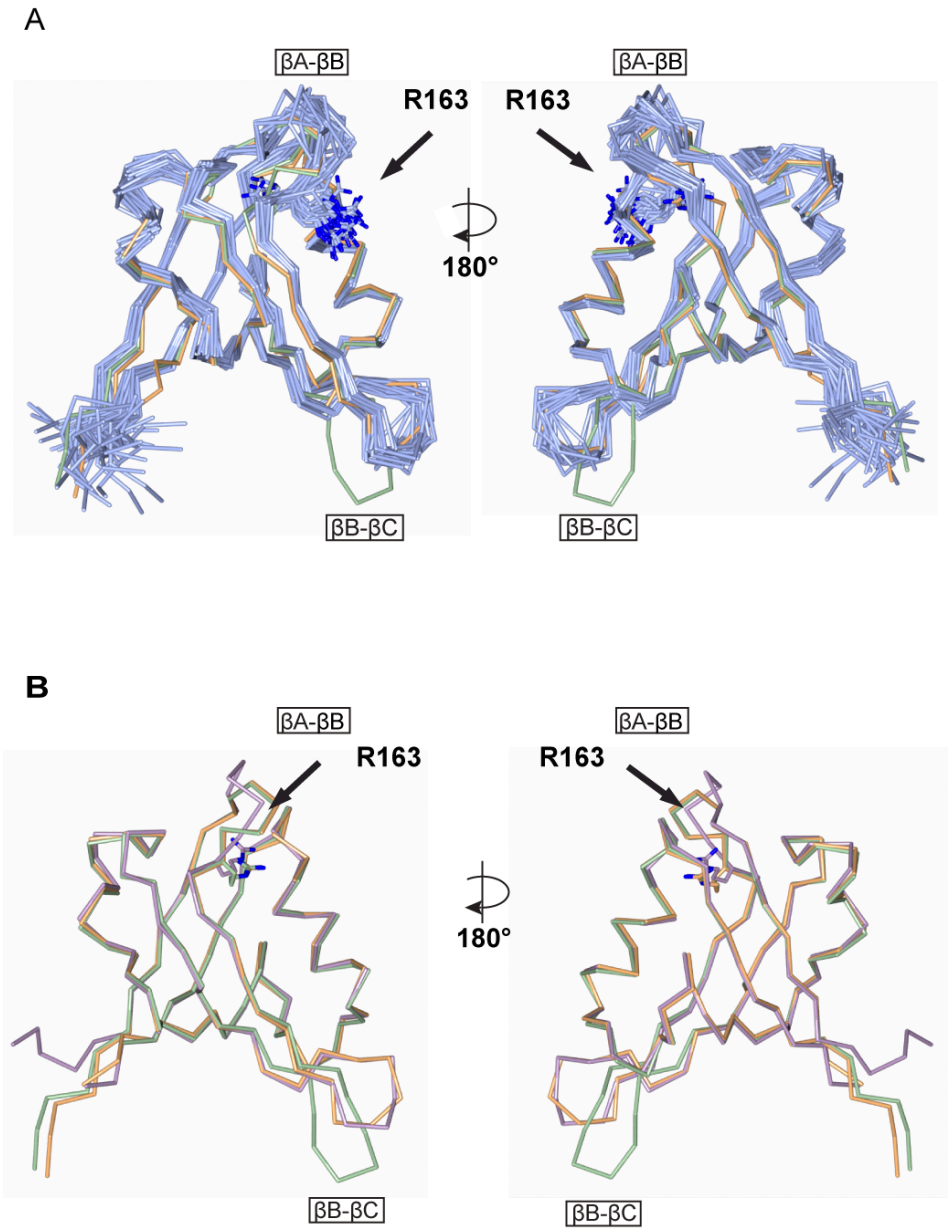

Figure 2.13. Comparison of LIMK PDZ structures.

Superposition of both conformations of the LIMK2 PDZ crystal structure (orange and green) with the 20 deposited NMR states of mouse LIMK2 PDZ domain (PDB: 2YUB; unpublished) (blue). Arg163 is indicated for the NMR structures, 17 copies are surface exposed, and 3 copies point towards the core. **B.** Superposition of both

conformations of the LIMK2 PDZ crystal structure (orange and green) with AlphaFold model of LIMK2 PDZ (pink) (LIMK2-AF-P53671-F1-model_v2.pdb).

Table 2.2. Primers used for mutagenesis.

Protein Construct	Mutation	Forward primer sequence	Reverse primer sequence
pRS415-GAL-FLAG-LIMK1	**L165A**	5'-CGCACACCGTTACGGCGGTCAGCATTCCGG-3'	3'-CCGGAATGCTGACCGCCGTAACGGTGTGCG-5'
	D221A	5'-TCCATTCACGTTGGTGCTCGCATTCTGGAAATC-3'	3'-GATTTCCAGAATGCGAGCACCAACGTGAATGGA
	R222A	5'-ATTCACGTTGGTGATGCCATTCTGGAAATCAACGGC-3'	3'-GCCGTTGATTTCCAGAATGGCATCACCAACGTGAAT-5
	E225A	5'-GTGATCGCATTCTGGCAATCAACGGCACCCC-3'	3'-GGGGTGCCGTTGATTGCCAGAATGCGATCAC-5'
	Q251A	5'-ATGTTCCAGCGTCAGTGCCAGCAGACGGCTG-3'	3'-CAGCCGTCTGCTGGCACTGACGCTGGAACAT-5'
	K175D	5'-GCCAGCTCTCACGGTGATCGCGGCCTGTCCGTT-3'	3'-AACGGACAGGCCGCGATCACCGTGAGAGCTGGC-5'
pET HIS-hLIMK2 PDZ C173S	**C173S**	5'-GTGGAGAGTGCCTCCTCCAACTACG- 3'	3'-CGTAGTTGGAGGAGGCACTCTCCAC- 5'
	L152A	5'-CCCTACTCTGTCACGGCCATCTCCATGCCGGCC-3'	3'-GGCCGGCATGGAGATGGCCGTGACAGAGTAGGG-5'
	D202A	5'-GCCATCCACCCTGGGGCTCGCATCCTGG-3'	3'-CCAGGATGCGAGCCCCAGGGTGGATGGC-5';
	R203A	5'-CACCCTGGGGACGCCATCCTGGAGATCAAT-3'	3'-ATTGATCTCCAGGATGGCGTCCCCAGGGTG-5'
	E206A	5'-GACCGCATCCTGGCGATCAATGGGACCCCCGTC-3'	3'-GACGGGGGTCCCATTGATCGCCAGGATGCGGTC-5'
	Q232A	5'-CGAGCCAGACACTTGCGCTGTTGATTGAAC-3'	3'-GTTCAATCAACAGCGCAAGTGTCTGGCTCG-5'
	R162D	5'-GGCCACCACTGAAGGCGATCGGGGCTTCTCCGTG-3	3'-CACGGAGAAGCCCCGATCGCCTTCAGTGGTGGCC-5'

Chapter 3: Insight into the global conformation and autoinhibition of LIM domain kinases by its N-terminus

3.1 Introduction

3.1.1 LIMK is an important player in the regulation of actin dynamics

As discussed in Chapter 1, sections 1.9 to 1.10, the LIMK family of proteins are important downstream effectors of RHO GTPase actin cytoskeleton-dependent pathways. LIMK is an important cue that guides cytoskeletal dynamics in the cell, as it is an important regulator of cofilin proteins [255]. Thus, LIMKs are critical nodes that direct cells to many actin-dependent processes, such as directed smooth muscle contraction, cell polarity, maintenance of neuronal projection, and ring contractibility during mitosis [18,19,155,339].

3.1.2 Protein kinases are often regulated at multiple levels

As Chapter 1, section 1.12 states, protein kinases are often regulated at multiple levels. Different levels of regulation are essential for the fidelity and timely regulation of cellular signals mediated by protein kinases [165,167,273-277]. These distinct levels of regulation can be observed in intrinsically inactive protein kinases. Intrinsically inactive kinases often require activation by protein regulators to catalyze the phosphotransfer reaction, frequently needing the kinase domain to be in the correct conformation for activation. In other cases, kinases can be intrinsically active and require regulation mechanisms such as intramolecular domain interactions to limit catalytic activity. Many protein kinases employ a variety of mechanisms to regulate the activation and inactivation of the catalytic

activity. To better understand how LIMK may be regulated, let us discuss some well-studied examples of protein kinase regulation in more depth. The reader is referred to sections 1.13.1-1.13.5 for further discussion on kinase regulation.

Phosphorylation of a kinase activation loop is often associated with increased enzymatic activity. While activation loop phosphorylation is important, it is usually not the only means of regulation [165,166,278]; many protein kinases contain multiple domains and employ inter- or intra-molecular interactions to alter catalytic rate [279-283]. Allosteric regulation, as well as pseudosubstrate regulation, are autoregulation mechanisms that have been observed in protein kinases.

Allosteric regulation is described as the intramolecular transmission of signals in one part of a protein that affects its structure and dynamics in regions elsewhere in the protein [171,329]. Examples of this type of regulation include binding of ligands to receptors or intramolecular regulation between domains inside the same or different polypeptide chain that, upon binding to catalytic regions, changes the activity and conformation of the enzyme. In protein kinases, allosteric regulation can enhance or diminish the catalytic activity of a kinase. For example, two members of the non-receptor tyrosine kinase of families Csk (C-terminal Src kinase) and Src (proto-oncogene Sarcoma) have two different autoregulation mechanisms. Csk is thought to exhibit intramolecular interactions that favor the active conformation [340]. Csk domain architecture includes, like Src, an SH3 domain and an SH2 domain [341]. Activation is thought to be mediated by Cask binding protein (CBP) binding to the SH2 domain via a phosphorylated tyrosine in CBP.

This complex can then bind to the N-lobe of the kinase domain and promote an active conformation compatible with catalysis[342,343]. In contrast, the Src kinase domain is thought to exist in an inactive state via intramolecular interactions in resting cells.

The Src family of kinases contains N-terminal SH3 and SH2 domains and a C-terminal kinase domain [289-292]. As mentioned in section 1.13.1, autoregulation is achieved by two protein interactions: binding of the N-terminal SH2 domains to a pTyr in the C-terminus and binding of the SH3 domain to the kinase lobe via a conserved Pro in the linker region [284,285,288,294-296]. Src protein kinase is thought to be basally autoinhibited in a “closed, globular” conformation through these different interactions, which keep the kinase domain in a conformation incompatible with catalysis. Activation is achieved by dephosphorylation of the C-terminal tail, binding of Src SH2 and SH3 ligands, and activation loop phosphorylation. These events create significant conformational changes, liberating conformational restraints in the kinase domain. As domain interactions allosterically keep protein kinases in the active or inactive state, other interactions, such as pseudosubstrate interactions, have been shown to regulate protein kinases' catalytic activity.

Pseudosubstrate regulation is described as binding a regulatory subunit in the same or different polypeptide chain to the enzyme's active site [302,344]. Separate from allosteric regulation, pseudosubstrate regulators mimic the substrate, denying true substrate binding. As discussed in Chapter 1, section 1.13.2, protein kinases such as the p21-activated kinases of the type II subgroup (PAKs) are well-

characterized Ser/Thr kinases that portrays pseudosubstrate regulation. In the case of PAK4, the domain architecture includes a GBD (GTPase binding domain, also known as Cdc42/Rac1 interactive domain, CRIB) and a protein kinase in the C-terminus. Pseudosubstrate autoregulation is mediated by the binding of a Pro motif in the linker region between the GBD and the kinase domain to the activated PAK4 kinase domain [345]. Localization of PAK4 by binding of Cdc42 to the GBD and subsequent binding of a binding partner to the Pro-motif releases the pseudosubstrate motif and allows PAK4 to have catalytic activity [279]. As mentioned above, autoregulatory modules can exist in the same polypeptide chain in pseudosubstrate and allosteric regulation [278]. LIMK autoregulation is also thought to be mediated by interactions with its N-terminus domains.

3.1.3 LIMKs are autoregulated by their N-terminus

In the case of the LIMK family of proteins, activation loop phosphorylation by upstream regulators and interactions mediated by the N-terminus and the C-terminal kinase domain is thought to regulate LIMK activity. The N-terminal of LIMK contains protein-protein interaction domains hypothesized to autoregulate the activity of LIMK.

LIMKs are multi-domain proteins containing two N-terminal zinc finger LIM (**L**in11, **I**sl1, **M**ec-3) domains, a PDZ (**P**SD95, **D**lg1, **Z**o-1) domain, and a C-terminal catalytic domain [16] (**Figure 3.1A**). As described in Chapter 1, LIM domains are composed of tandem zinc fingers and are found in kinases, adaptor proteins, and transcription factors [20] (**Figure 3.1B**). They usually mediate protein-protein

interactions, but no binding sequence preference has been found across the family [20]. LIM domains can recognize various protein partners in variable manners [28,59,60,346]. In contrast, PDZ domains have a well-characterized binding sequence preference. These domains recognize specific C-terminal and internal motifs in partner proteins, mostly found in the cytoplasmic tails of transmembrane receptors and channels [67,76-80,316,317]. Interestingly, PDZ domains are thought to be promiscuous binders and non-canonical binding of PDZ domains to protein partners has also been reported [67,71,87,109,116].

Multiple lines of evidence suggest the LIMK N-terminus acts as a negative regulator for catalytic activity, including mutations and deletions in the N-terminus, which increased activity and accumulation of actin filaments in cultured cells [53,251,307], *in vitro* kinase activity assays which showed increased phosphorylation by truncated LIMK compared to the full-length protein, and titration of LIMK1 N-terminal constructs which diminished the catalytic activity when added to the isolated kinase domain [53,251,307].

The binding partners of the LIMK LIM and PDZ domains need to be better understood [101,316,317]. However, a common theme observed in these studies relates to changes in activity upon binding protein partners to N-terminal domains [234,262,263,268]. As mentioned in Chapter 1, section 1.11.2, BMPR-II[262,263], LRAP25a[234], and $p57^{kip2}$ [268] are N-terminal protein partners that are known to change the activity of LIMK. These observations further support an autoregulation mechanism in which the N-terminus autoregulates LIMK activity. The next step

would have been obtaining the N-terminal domains' crystal structure. I expressed and purified the LIM2-PDZ domain of LIMK at high concentrations; however, this construct's crystallization trials were unsuccessful.

To surmount this problem, I used AlphaFold predictions to hypothesize how autoregulatory interactions can mediate LIMK autoregulation conformation. Interestingly, AlphaFold predictions show the LIM2-PDZ portion of LIMK to interact with one another. This observation can be realistic, as LIM and PDZ interactions have been reported. Cases of intramolecular interactions of PDZ and LIM domains in this family of proteins have been observed, i.e., reverse-induced LIM genes (RIL) proteins, where the N-terminal PDZ domain interacts with the C-terminal LIM domain [46]. However, the crystal suture of a LIM-PDZ complex has yet to be solved experimentally. The mechanism of LIM-mediated regulation of enzymatic activity for LIMK remains unresolved [53,54]. However, there is a precedent of LIM-mediated activity regulation in the MICAL family of proteins [57,58,347].

As described in Chapter 1, the MICAL (microtubule-associated monooxygenase, calponin, and LIM domain-containing protein) family of proteins contains a monooxygenase domain in the N-terminus, followed by a calponin domain (CH) and a LIM domain, and a C-terminal Rab (Ras-associated binding) binding domain (RBD) [55,56]. Indirect regulation of this protein is mediated by the N-terminal half of MICAL (monooxygenase-CH-LIM), which directly interacts with the C-terminal RBD domain in an intramolecular fashion[57]. This interaction is disrupted

by the binding of Rab to the C-terminal RBD and is believed to regulate the activity of the monooxygenase domain [58].

PDZ domains, as shown in Chapter 2, are involved in regulating LIMK catalytic activity. The PDZ domain's most common function is to act as a protein scaffold. However, it has been shown to indirectly regulate the activity of protein enzymes by binding regulatory units. This is observed with the iNOS PDZ, where its C-terminal PDZ binding motif bins to its own PDZ domain to regulate NO synthesis [348].

3.1.4 Significance and Project Aims

The inactive state of LIMK is thought to involve multi-domain interactions between the N-terminal LIM and PDZ domains and the C-terminal kinase domain. In this chapter, I shed light on the global features that describe the autoregulation mechanism of LIM domain kinases. I use biochemical, biophysical, and computational techniques to understand better the N-terminus domains and how LIMK may be autoregulated. I use conservation and AlphaFold prediction analysis [334,349] to hypothesize that the LIM2-PDZ region may behave as a multidomain in solution using SAXS. I perform *in vitro* kinase assays with purified LIMK2 active kinase domain and titrate purified LIM2-PDZ to obtain IC50 values for this inhibition. I also use negative stain electron microscopy and observe large conformational changes between the full-length (FL) WT active protein and the kinase-inactive D451N mutant. I found that the WT LIMK FL protein shows an elongated conformation compared to the kinase-inactive mutant, suggesting the

kinase is regulated in cis and keeps a “closed, globular” conformation. I also provide novel data suggesting that the LIMK2 kinase domain does not phosphorylate mutant cofilin where the phosphorylation residue Ser3 is mutated to Thr (S3T) *in vitro.*

3.2 Methods

3.2.1 Conservation study of LIMK1 and LIMK2

To explore the role of the LIMK LIM2-PDZ domain, I used my already created sequence conservation analysis of all LIMK family members to observe the conservation of these two domains between the LIMKs, across the LIMKs over evolution. LIMK1 and LIMK2 sequences were identified using NCBI BLAST [324]. A total of 800 downloaded sequences were filtered for correct LIMK sequences and full-length isoforms. Sequences were aligned using the ClustalO [310] server and visualized using JalView [311]. PDZ sequences were identified using NCBI BLAST [324]. A total of 967 sequences downloaded were filtered for only human-containing PDZ proteins. Sequences were aligned using the ClustalO [310] server and visualized using JalView [311].

3.2.2 LIM2-PDZ protein expression and purification

The complementary DNA (cDNA) encoding human LIMK2 (UniP ID: P53667) LIM2-PDZ domain (61-250) was inserted into pGEX-6p1 using enzymes BamHI and EcoRI (GE Healthcare) for expression as a GST-fusion protein in *Escherichia coli*. A point mutation was introduced in residue Cys173 to Ser using QuikChange Lightning site-directed mutagenesis kit (Agilent). Cys173 in the PDZ domain was

mutated to Ser to inhibit the formation of disulfide bonds and to improve stability for biophysical experiments. Forward primer 5'-GTGGAGAGTGCCTCCTCCAACTACG- 3' and reverse primer 5'-CGTAGTTGGAGGAGGCACTCTCCAC- 3'.

GST-tagged hLIMK2 LIM2-PDZ was expressed in BL21 (DE3) cells (Millipore Sigma) by induction with 0.5 mM isopropyl β-D-thiogalactopyranoside (IPTG) overnight at 16 °C. Cells were harvested by centrifugation at 2,000×g and lysed in nickel binding buffer (20 mM Tris pH 7.5, 150 mM NaCl, 1 mM DTT) by addition of 0.1 M phenylmethylsulfonyl fluoride (PMSF), Roche complete EDTA-Free protease inhibitor tablet and lysozyme, followed by freeze/thaw cycles and sonication. Lysates were clarified by centrifugation at 5000×g for 1 hour. Supernatant was applied to glutathione-Sepharose 4B beads (GE Healthcare) to capture GST-fusion proteins. The GST tag was removed by enzymatic cleavage with Prescission protease on-bead. The cleavage reaction was then flowed over a GST affinity column (gluthatione-Sepharose, GE Healthcare) to remove the GST tags, uncleaved GST-tagged protein, and the GST- tagged PreScission protease. The flow-through containing untagged LIM2-PDZ protein was concentrated in a centrifugal filter (Amicon Ultra, Millipore Sigma), diluted to a salt concentration of 37mM NaCl and applied to a 5ml Anion Exchange column (Mono Q GE Healthcare) equilibrated in 20 mM Tris pH 7.5 buffer. LIM2-PDZ was eluted with increasing concentrations of NaCl. The eluted peak was concentrated and then

purified by Size exclusion chromatography on a Superdex 75 10/300 GL column. PDZ^{C173S} eluted as a monodisperse peak.

3.2.4 LIMK2 kinase domain protein expression and purification

A sequence encoding human LIM kinase 2 (LIMK2) residues 322-638 of the kinase domain (CAT) was subcloned into a GST tagged transfer vector derived from pFastBac Htb (Invitrogen) using SalI and XhoI restriction enzyme sites. Recombinant baculovirus was generated using the Bac-to-Bac baculovirus expression system (Invitrogen), and the kinase domain was expressed as a glutathione S-transferase (GST) fusion protein with a tobacco etch virus protease (TEV) site located between GST and LIMK2 CAT. *Spodoptera frugiperda* Sf9 cells (Gibco) infected with the recombinant baculovirus were grown in shaker flasks and ESF921 media (Expression Systems) and harvested 48 hours after infection. Cells were harvested and resuspended in 10 ml lysis buffer (50 mM Tris, pH 7.5, 150 mM NaCl, 1 mM DTT, 1% Triton X-100, protease inhibitor cocktail (Roche), and 0.1 mM PMSF) and lysed by incubation at 4°C, rotating for 30min. Following cell lysis, lysates were clarified by centrifugation at 5000×g for 1 hour. Clarified supernatant is applied to 1 ml glutathione Sepharose 4B resin (GE Healthcare) and incubated for 2 hrs at 4°C. Bound protein to beads was washed with 50 ml of GST wash buffer containing 50 mM Tris, pH 7.5, 150 mM NaCl, 1 mM dithiothreitol [DTT]. Overnight treatment with GST-TEV protease at 4°C cleaved GST and LIMK2 CAT, and the eluate (containing LIMK2 CAT) was stored supplemented with 5% glycerol. Aliquots of protein were stored at -80°C.

3.2.5 LIMK2 LIM2-PDZ size exclusion chromatography – small angle X-ray scattering (SEC-SAXS) studies

Purified LIMK2 LIM2-PDZ C173S was concentrated to approximately 11 mg/mL. Protein samples and SEC buffer (150 mM NaCl, 20 mM Tris, pH 8) were flash-frozen in liquid nitrogen and later defrosted for SEC-MALS-SAXS experiments at Brookhaven National Laboratory. The samples were thawed and centrifuged to pellet any precipitates on the day of data collection. The samples were injected at room temperature onto an SEC column (Cytiva Superdex 200 Increase 5/150 GL) in 1X SEC buffer at a flow rate of 0.35 mL/min using a 1260 Infinity II HPLC (Agilent). The sample elution was first detected by UV (Agilent UV monitor). The sample flowed to the SAXS sample chamber where X-ray scattering data were collected at room temperature by a Pilatus900k detector at a wavelength of 0.819 Å, camera length of 3.686 m, and an exposure time of 0.5 s. Detector configuration yielded an accessible scattering angle of $0.006 < q < 3.0$ Å^{-1}, where q is the momentum transfer, defined as $q = 4\pi \sin(\theta)/\lambda$ (λ is the wavelength and 2θ is the scattering angle). Data were normalized using an active beamstop containing a silicon PIN diode. All data were collected at BNL, NSLS-II, LiX, and Beamline16-ID using synchrotron radiation.

3.2.6 LIMK2 LIM2-PDZ SEC SAXS data analysis

Image files were reduced using BioXTAS RAW (v 2.0.3)[350], and the total intensity per frame was calculated to produce a scattergram. From this scattergram, buffer subtraction was performed by binning and averaging approximately 100 frames of

the eluate before the elution of the protein from the column, also in BioXTAS RAW. Frames were chosen from the sample peak and averaged based on initial R_g calculations. The averaged frames were saved as a single intensity profile and used for further data analysis. Using BioXTAS RAW as a GUI interface [350], Guinier analysis was performed on each intensity profile to determine data quality. Molecular weight estimations were performed in RAW[351,352]. Pair Distribution functions were determined by using GNOM in RAW using default parameters. DENSS models were created using default parameters in RAW, which generated 20 initial models, which were then aligned, averaged, and refined[353].

3.2.7 AlphaFold prediction analysis

AlphaFold models of LIMK2 LIM2-PDZ were downloaded from https://alphafold.ebi.ac. In 11 AlphaFold models, from human LIMK1 and LIMK2 to fish LIMK1, LIMK2 was structurally aligned using CCP4mg[338].

Table 3.1. AlphaFold PDB codes used for the analysis of LIMK full-length protein prediction

Protein	Species	AlphaFold code
LIMK1	*Homo sapiens*	F-P53667-F1-model_v4 human.pdb
	Mus musculus	AF-P53668-F1-model_v4.pdb
	Gallus gallus	AF-Q8QFP8-F1-model_v4.pdb
	Danio rerio	AF-B3DIV5-F1-model_v4.pdb
	Xenpus laevis	AF-O42565-F1-model_v4.pdb
	Drosophila melanogaster	AF-Q8IR79-F1-model_v4.pdb
	Homo sapiens	AF-P53671-F1-model_v4.pdb

LIMK2	*Mus musculus*	AF-O54785-F1-model_v4.pdb
	Gallus gallus	AF-P53666-F1-model_v4.pdb
	Danio rerio	AF-Q6DG29-F1-model_v4.pdb
	Xenpus tropicalis	AF-F7AFJ1-F1-model_v4.pdb

3.2.8 LIMK2 FL WT and FL D451N sample preparation

The complementary DNA (cDNA) encoding full-length Homo sapiens (human) LIM kinase 2 (LIMK2) protein (UniProt ID: P53667) containing residues (1-638) of the full-length and the kinase-inactive D451N (FL D451N) was subcloned into a GST tagged transfer vector derived from pFastBac Htb (Invitrogen) using KasI and EcoRI restriction enzyme sites. Recombinant baculovirus was generated using the Bac-to-Bac Baculovirus expression system (Invitrogen), and the full-length was expressed as a Glutathione S- transferase (GST) fusion protein with a Tobacco Etch Virus protease (TEV) site located between GST and FL LIMK2 WT and FL LIMK2 D451N. *Spodoptera frugiperda* (Sf9) cells (Gibco) infected with the recombinant baculovirus were grown in shaker flasks and ESF921 media (Expression Systems) and harvested 48 hours after infection. Cells were harvested and resuspended in 10 ml lysis buffer (50 mM Tris, pH 7.5, 150 mM NaCl, 1 mM dithiothreitol [DTT], 1% Triton X-100, protease inhibitor cocktail (Roche), and 0.1mM PMSF) and lysed by incubation at 4°C, rotating for 30min. Following cell lysis, lysates were clarified by centrifugation at 5000×g for 1 hour. Clarified supernatant is applied to 1 ml Glutathione Sepharose 4B resin (GE Healthcare)

and incubated for 2hrs at 4°C. Bound protein to beads was washed with 50mls of GST wash buffer containing 50 mM Tris, pH 7.5, 150 mM NaCl, and 1 mM dithiothreitol [DTT]. Overnight treatment with GST-TEV protease at 4°C cleaved GST and FL LIMK2, and the eluate (containing FL LIMK2) was then concentrated to 500μl in a centrifugal filter (Amicon Ultra, Millipore Sigma). Concentrated protein was then purified by size exclusion chromatography on a Superdex 200 10/300 Increase. FL LIMK2 and FL LIMK2 D451N were eluted as monodisperse peaks. Protein was then concentrated again to a final concentration of 0.6μl for negative stain electron microscopy experiments.

3.2.9 LIMK2 FL WT and FL D451N protein negative stain electron microscopy

Negative stain electron microscopy grids were prepared by applying 1 μL of protein solution (~0.6 μM) onto a carbon-coated copper grid previously irradiated under a UV lamp for 40 min. The grid was then stained with 1% uranyl acetate. Grids were imaged using a Tecnai T12 microscope fitted with a Tungsten filament operating at 120 kV. 100 micrographs were recorded at a nominal magnification of 6700× on a 4 k × 4 K Gatan CCD camera resulting in an Å/pixel value of 4.0. Automated particle picking was performed using RELION 3.1. Three rounds of reference-free 2D classification were carried out in Relion 3.1, resulting in 20 classes for both FL LIMK2 WT and FL LIMK2 D451N.

3.2.10 LIM2-PDZ inhibition of LIMK2 CAT kinase activity

Human cofilin was purified as described in [186]. CAT WT LIMK2 purified from insect cells at a 2nM concentration was mixed with cofilin at a final concentration of 6.7

μM and increasing concentrations (4-120 μM of LIMK2 LIM2-PDZ) in a final volume of 20 μl. The incubation mixture contained 20 mM Tris, pH 7.5, 150 mM NaCl, 5 mM MgCl2, 5 mM MnCl2, 20 μM ATP, 1 mM DTT, 0.1 μCi/ml ^{32}P-ATP and reactions was carried out at 30 °C for 10 minutes. Reactions were quenched by adding 1x SDS-loading buffer and resolved by SDS-PAGE on a 15% polyacrylamide gel. Dried gels were are subjected to autoradiography, and the level of phosphorylated cofilin was evaluated on a Bio-Rad Molecular Imager Fx system using Quantity One 1D Analysis software (Life Sciences Research). A total of 3 replicates were analyzed using GraphPad Prism. Data were normalized to a sample containing only the kinase domain signal. Statistical analysis was carried out using non-linear regression, dose-response for inhibition.

3.3 Results

3.2.1 LIMK N-terminus conservation shows high conservation for the LIM2-PDZ domains

Conservation analysis is a powerful tool for studying proteins, as selective pressures over evolution usually retain functionally essential regions. LIMK contains three N-terminal protein-protein binding domains, two LIM, and a PDZ domain (**Figure 3.1A**). As mentioned in Chapter 2, the PDZ domain has a functionally conserved region involved in autoregulating the kinase activity in LIMK proteins. Further analysis of the N-terminus, especially the remaining LIM1 and LIM2 domains, also can provide some information on other regions that could also be involved in autoregulation (**Figure 3.1B**). Preliminary data from my lab suggests

that the LIM2 domain is also involved in autoregulation. A closer look at these domain sequences shows that LIM1 and LIM2 domains of LIMK1 and LIMK2 share 54% identity and 65% similarity. Individually, LIM1 is 47% identical and 63% similar between LIMK1 and LIMK2, while LIM2 is 60% identical and 67% similar. Conservation analysis on the N-terminal LIM1 and LIM2 domains shows high conservation, especially in the LIM2 region (**Figure 3.2**). Mapping this conservation to the 3D structure of this domain would have been the next step, but unfortunately, crystallization of the LIM2-PDZ region was unsuccessful. However, using the prediction tool, AlphaFold[354], I mapped the conservation of 421 aligned sequences of LIMK1 and LIMK2 to the predicted model of human LIMK1 and LIMK2 LIM2-PDZ domain [334,349].

3.3.2 The LIMK LIM2-PDZ domains are predicted to interact with each other

The mapped conservation of the N-terminus shows a more conserved LIM2 domain in comparison to the LIM1 domain (**Figure 3.3 A, B, Figure 3.4**). As stated in Chapter 1, section 1.3, LIM domain architecture comprises the following: the first zinc finger contains β-hairpins 1 and 2, and the second zinc finger includes β-hairpins 3 and 4, finishing with a short α-helix. Rubredoxin-type zinc knuckles connect the short strands of β-hairpins 1 and 3, and the longer strands of β-hairpins 2 and 4 are connected by tight turns. The PDZ domain, as reported in Chapter 2, is a partially open β-barrel.

Interestingly, 10 models of both LIMK1 and LIMK2 of species ranging from human to insect consistently predict a beta-strand addition interaction between the

PDZ domain and the LIM2 domain (**Figure 3.3 C**). This beta strand addition is predicted to occur between the third beta-strand of the LIM2 domain second zinc finger and the βA of the PDZ domain, forming a multidomain module. βA contains highly conserved amino acids, and one of the mutations used in my mutagenesis analysis of the PDZ domain mentioned in Chapter 2 is in this area. It is important to note that this interaction is predicted to occur near the highly conserved surface of the PDZ domain. However, none of the residues used in my mutagenesis are predicted to interact via side-chain interactions (**Figure 3.5**). I used Small Angle X-ray scattering (SAXS) to obtain low-resolution information on these domains.

3.3.3 SAXS data shows a globular monomeric molecule

SAXS is a biophysical technique that provides low-resolution information on the shape, conformational flexibility, and assembly of protein complexes in solution. When coupled with size exclusion chromatography (SEC), it can also provide a quality assessment of individual populations in the sample. This technique can also help me find the oligomeric state and molecular weight of the domains and help me understand if the LIM2-PDZ of LIMK behaves like a globular module or two independent domains, like “two beads on a string.” I, therefore, expressed and purified human LIMK2 LIM2-PDZ protein fragments and investigated the conformational state of the LIM2-PDZ region of the N-terminus using SEC-SAXS (**Figure 3.6**). I find that LIMK LIM2-PDZ behaves as a monodisperse species and has a molecular weight consistent with a monomer (21 kD as a monomer in solution) **(Table 3.2 and 3.3).** Likewise, the scattering intensity and the radius of

gyration across the SEC elution peak are consistent with a homogeneous protein sample (**Figure 3.7A**). Guinier analysis and the plotted residuals between the data and fit show no systematic deviations from linearization for the sample, indicating high-quality data. (**Figure 3.7B**). The Kratky analysis does not decay to zero, and the Porod-Debye does not plateau, indicating a flexible molecule (**Figure 3.7C, D**). The overall shape of the pair distribution function suggests that the sample exists as a globular protein (**Figure 3.7E**). Using DENSS (DENsity from Solution Scattering[354]), I calculated a three-dimensional particle electron density map for the experimental solution scattering. I observed that it does not fit appropriately when superposed to the AlphaFold predicted model (**Figure 3.8B**). Using two different servers, FoXS and CRYSOL, which compute a theoretical scattering profile of a structure and fit it to an experimental profile, I tested if the predicted model theoretical scattering fits my experimental SAXS data [355,356,357]. The χ^2 values obtained were 36 and 6, respectively, indicating that the model does not fit the experimental SAXS profile. (**Figure 3.8B**). However, as this is a predicted model, it is not unlikely that it fails to accurately represent the molecule in solution. Taken together, my SAXS analysis provides new insights into the molecular level conformation of the LIM2-PDZ region of the LIMK and reveals a globular protein with some degree of flexibility.

3.3.4 The LIM2-PDZ region of the N-terminus inhibits kinase activity in radiolabel kinase assays.

To probe the ability of the LIM2-PDZ module to inhibit the kinase activity of LIMK2, I assessed its inhibitory activity using radiolabel kinase assays. I titrated the N-terminal LIM2-PDZ domains into radiolabel kinase reactions using active LIMK2 kinase domain (CAT) and cofilin as substrate to test their respective inhibitory activities. I observe that the LIM2-PDZ domains inhibit the kinase activity of LIMK. Initial IC_{50} values of 26 μM are obtained. (**Figure 3.9 A, B**). Moreover, there seems to be activation when adding the lowest amount of LIM2-PDZ into the reaction. This could be explained by a crowding effect, where an increase in total protein enhances kinase activity.

3.3.4 S3T cofilin is not phosphorylated by LIMK2 catalytic domain

A question yet to be answered in the field is whether LIMK2 can phosphorylate S3T cofilin *in vitro*. In kinase assays using WT cofilin and S3T cofilin (kindly provided by Dr. Joel Sexton from the Turk laboratory), where a Thr replaces the biological phosphorylation site Ser, I observe no phosphorylation. *(***Figure 3.9 C***)*.

3.3.5 Assessment of LIMK2 full-length conformation using negative stain electron microscopy

Since the SEC-SAXS experiment of LIMK2 full-length protein will require a substantial amount of protein, I decided to pursue negative stain electron microscopy to observe large conformational changes between full-length LIMK2 wilt-type and catalytically inactive. I chose to use catalytically inactive full-length

protein as it has the potential of showing a different conformation because of its inability to autophosphorylate other protein regions. These experiments were in collaboration with the Mi laboratory, specifically with Dr. Yunxiang Zang. Negative stain electron microscopy experiments were performed on a TF12 with a magnification of 6700x. A 2D class average of around 100 classes was obtained for both samples (**Figure 3.10 A, B**). The particles in LIMK2 full-length wild-type protein display an elongated conformation (**Figure 3.10 C**), while the D451N mutant displays a more compact conformation, resembling a triangle (**Figure 3.10 D**). Both samples have similar dimensions of around 8-10 nm. Therefore, these experiments tentatively show different conformational flexibility between the two constructs, suggesting that conformational flexibility is associated with the phosphorylation state of the protein with a more flexible conformation for wild-type LIMK2 compared to the kinase-inactive D451N compact conformation. Further studies are required to build on these preliminary results.

3.4 Discussion

LIMK proteins are autoregulated via two modes: one, by activation loop phosphorylation, and two, by autoregulatory interactions with the kinase domain. This chapter explored larger conformational changes or arrangements in LIMK that can help me better understand how LIMK can be autoregulated. Since experimental structure determination can be challenging for multidomain complexes, let alone full-length proteins with flexible regions, the development of AlphaFold has become a useful and accessible tool to explore how proteins fold

with the help of artificial intelligence and multiple sequence alignment. I, consequently, decided to use this tool to examine LIMK full-length protein predictions. Stinkingly, as mentioned in Chapter 2, the PDZ AlphaFold prediction served as a better molecular replacement model for the deposited NMR structure for the experimental structure determination of the human LIMK2 PDZ domain. A closer look at other N-terminus of LIMK shows an interesting interaction. The LIM2-PDZ region interacts via beta strand addition between the βA of the PDZ domain and the LIM2 β-hairpin 3. Both surfaces are highly conserved based on my conservation analyses. Furthermore, this interaction is recapitulated in about 20 models inspected from LIMK1 and LIMK2 from different organisms. Even though proteins containing both LIM and PDZ domains exist, no experimental structure of these two domains in complex has been published. I, therefore, decided to test if these two domains can form a multidomain module and behave as a globular entity or if they behave as “two beads on a string” using SEC-SAXS.

Indeed, I observe a flexible globular module, pointing at a possible multidomain interaction between the LIM2 and the PDZ domain of LIMK. More experimental data is needed to test if this interaction is relevant to the autoregulatory mechanism of LIMK. Nevertheless, I was able to test if this region of the N-terminus can inhibit kinase activity in radiolabeled kinase assays. In these experiments, I can observe inhibitory action as I increase the concentration of the LIM2-PDZ region titrated in the kinase assay. Initial analysis suggests an IC_{50} of 26 μM, a value appropriate for an autoregulatory interaction. Another question that

remains is if the PDZ region alone can inhibit the activity of LIMK. Preliminary experiments show that the PDZ can regulate the activity of LIMK, but higher concentrations are needed to reach similar inhibition as the one observed with the LIM2-PDZ region. Interestingly, to answer some questions regarding LIMK2 dual-specificity, the catalytic domain does not phosphorylate S3T cofilin *in vitro*. This suggests that a Thr residue is a poor substrate for LIMK2.

Further support of an autoregulatory interaction between the N-terminus and the C-terminus of LIMK is suggested in my preliminary negative stain electron microscopy experiments of full-length LIMK in the wild-type form and kinase-inactive D451N. These show two very distinct states. A more elongated shape is observed for the wild-type protein, while a compact, triangular shape is observed for the kinase-inactive. This conformationAal flexibility may be associated with the phosphorylation state of the protein. These data suggest that the phosphorylation state of the protein pushes the equilibrium from the more stable autoinhibited conformation to the more flexible active state. The inability of the kinase-inactive full-length LIMK to autophosphorylate in other regions of the protein outside the activation loop could impact the overall conformation of LIMK. These initial negative stain electron microscopy data may also suggest a predominantly *cis* autoregulation mechanism where the N-terminus folds into the kinase domain to execute its autoinhibition. Further studies are needed to delineate the phosphorylation state between the two conformations to better understand global changes in conformation in LIMK. The experiments presented in this study reveal

the conformational state of the autoregulatory unit LIM2-PDZ in the N-terminus and demonstrate its autoregulatory action towards the kinase domain. Also, it provides preliminary evidence on large conformational changes in full-length LIMK2 between wild-type and kinase-inactive D451N, where autoregulation is thought to happen in *cis* with an autoregulated protein in a triangular-like conformation and a more elongated conformation when active.

3.5 Tables and figures

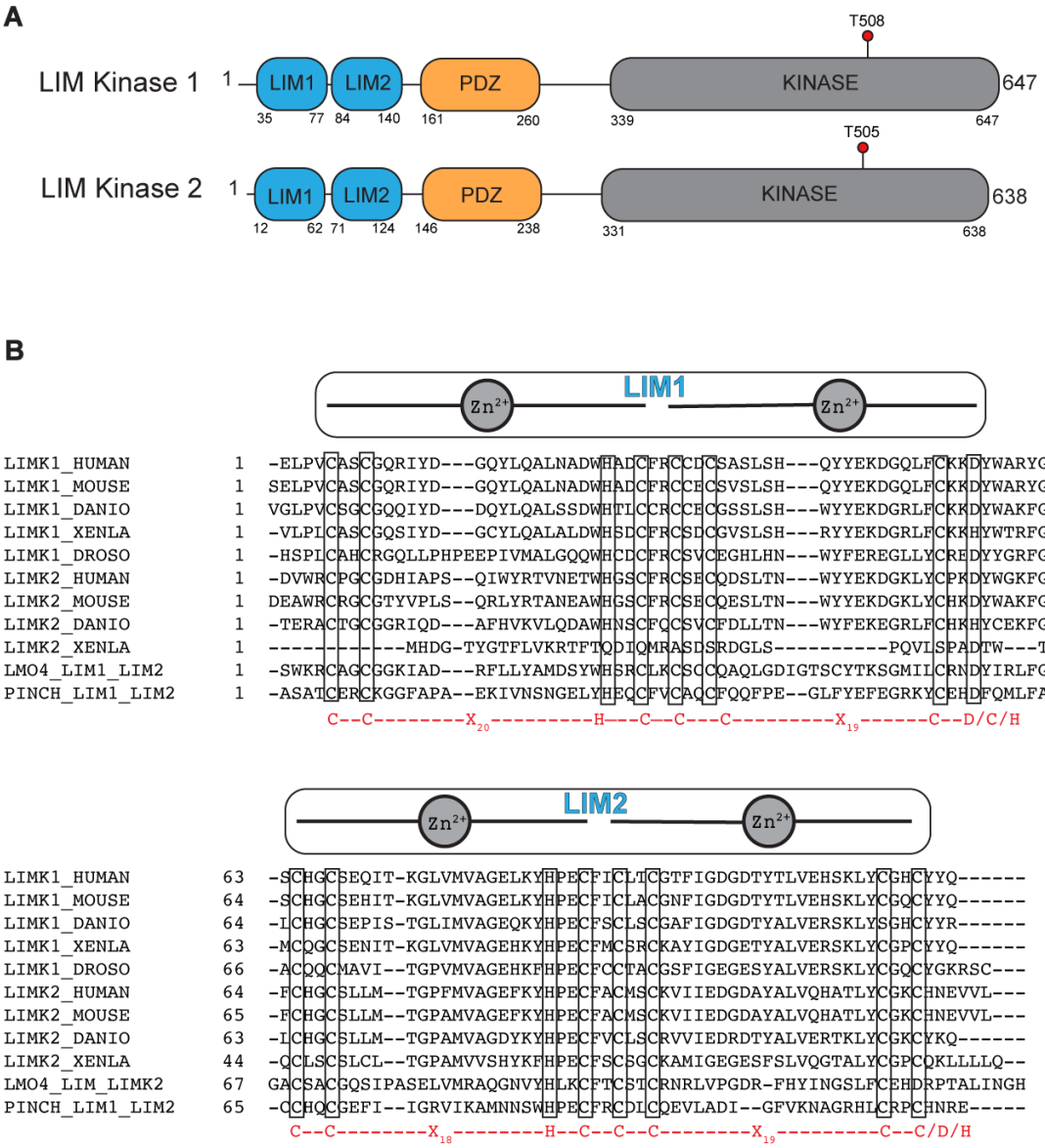

Figure 3.1. Sequence alignment of the N-terminal LIM1 and LIM2 domains of LIMK.

A. LIM domain kinase family architecture showing human LIMK1 (UniProt ID: P53667) and human LIMK2 (UniProt ID: P53671). LIM1: first LIM domain, LIM2: second LIM domain, PDZ: PDZ domain, Kinase: kinase domain. Activation loop

phosphorylation residues indicated, Thr508/Thr505 for LIMK1 and LIMK2, respectively. Residue numbers are shown. **B.** Sequence alignment of PDZ domains. Alignment was created using PROMALS[336]. Uniprot ID for LIMK1_HUMAN, P53667; LIMK1_MOUSE, P53668; LIMK1_XENLA, O42565; LIMK1_DANRE, B3DIV5; LIMK1_DROME, Q8IR79; LIMK2_HUMAN, P53671; LIMK2_MOUSE, O54785; LIMK2_XENTR, F7AFJ1; LIMK2_DANRE, Q6DG29; LMO4_LIM1&2_MOUSE_, P61969; PINCH_ LIM1&2 HUMAN, P48059. Red letters at the bottom of the alignment show the double zinc finger sequence motif. Top panel denotes the sequence for the LIM1 domains and the bottom panel denotes the sequence of the second LIM2 domain.

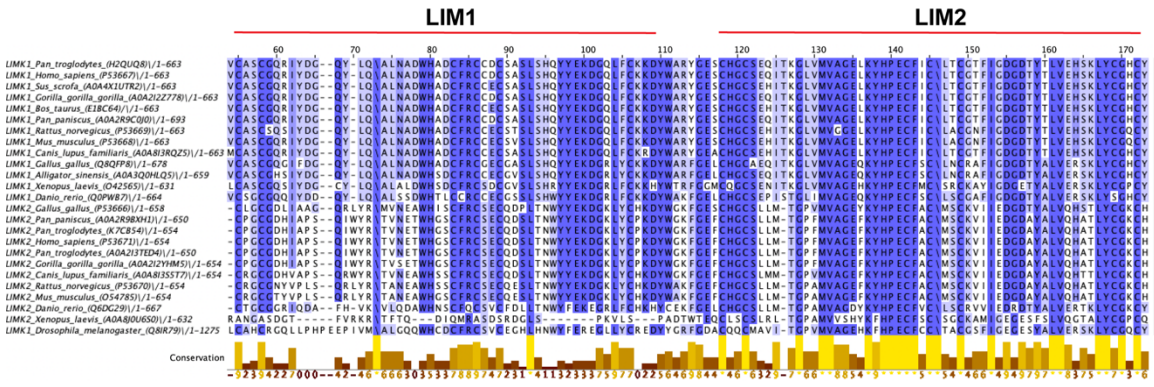

Figure 3.2. Sequence alignment of LIMK1 and LIMK2 shows high conservation for the LIM2 domain.

Sequences were obtained from UniProt[309] and aligned in ClustalOmega[310]. Each sequence is named by species and UniProt ID. Conservation scores were calculated in Jalview[311]. Identical residues are highlighted in dark blue, and partially conserved residues are in light blue.

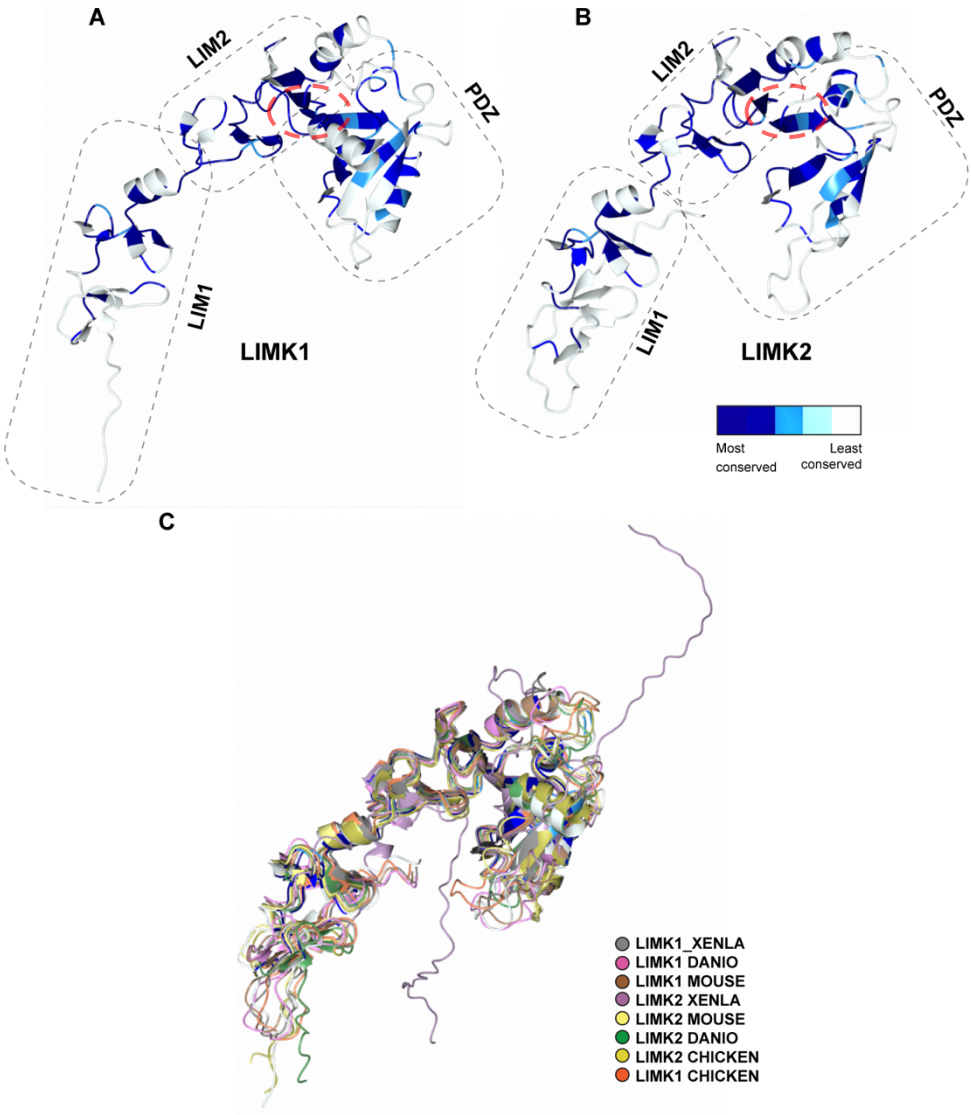

Figure 3.3. AlphaFold models with mapped conservation show, consistently, an interaction between the LIM2 and the PDZ domain.

Conservation LIMK LIM1, LIM2, and PDZ domains mapped onto the predicted structure of LIMK1 and LIMK2 N-terminus models. 421 aligned LIMK sequences from mammals, birds, fish, and insects were used for the conservation analysis. Dashed red circle indicates the β-strand addition between the LIM2 domain and βF in the PDZ domain.

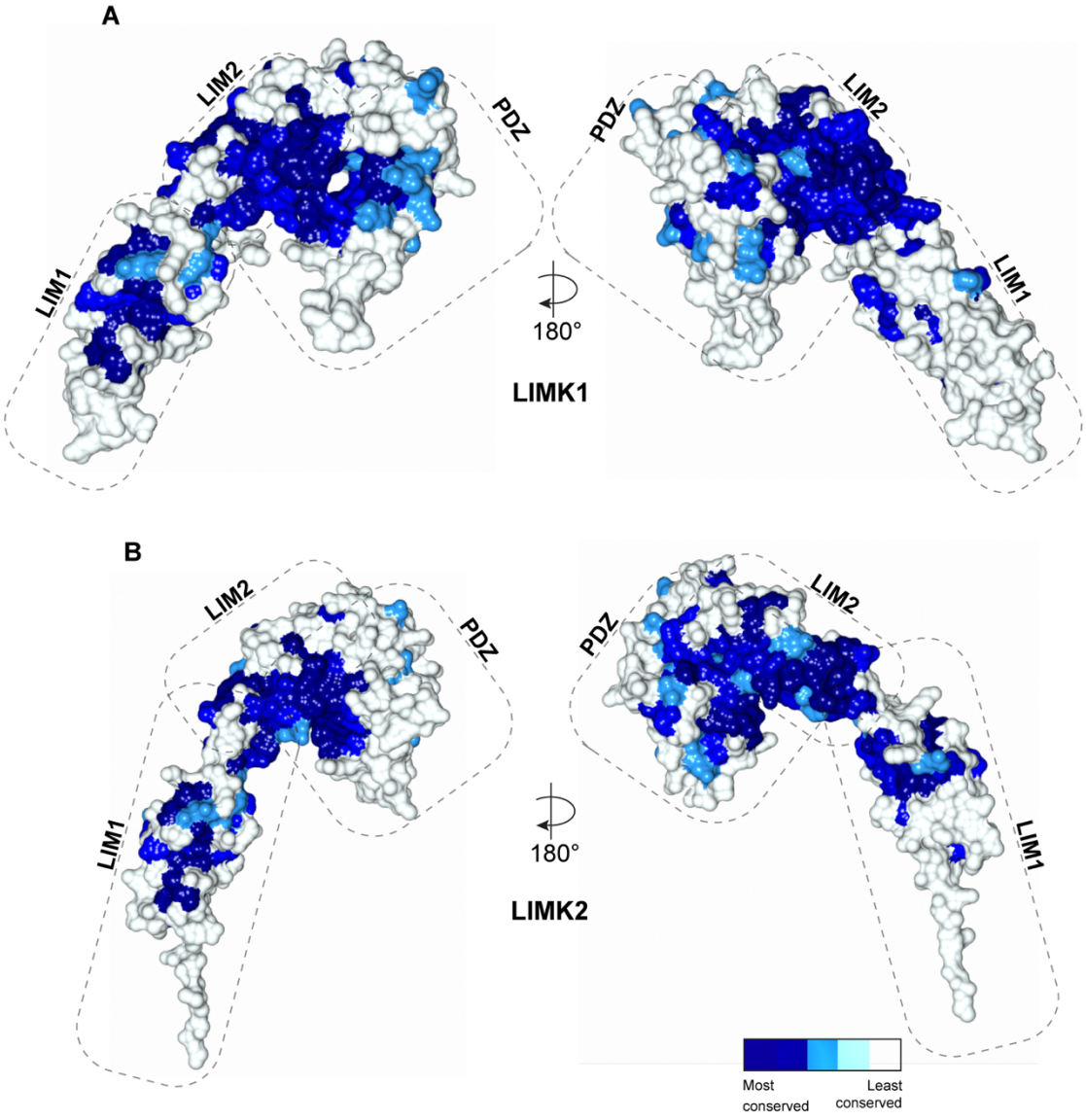

Figure 3.4. Conservation mapped to the Alphafold predicted model of human LIMK1 and LIMK2 LIM2-PDZ domain.

LIM1, LIM2 and PDZ domain conservation mapped onto the Alphafold model of LIMK1 and 2 N-terminus for 421 aligned LIMK sequences from mammals, birds,

fish, and insects. Dashed rectangles indicate the N-terminal binding domains LIM1, LIM2, and PDZ.

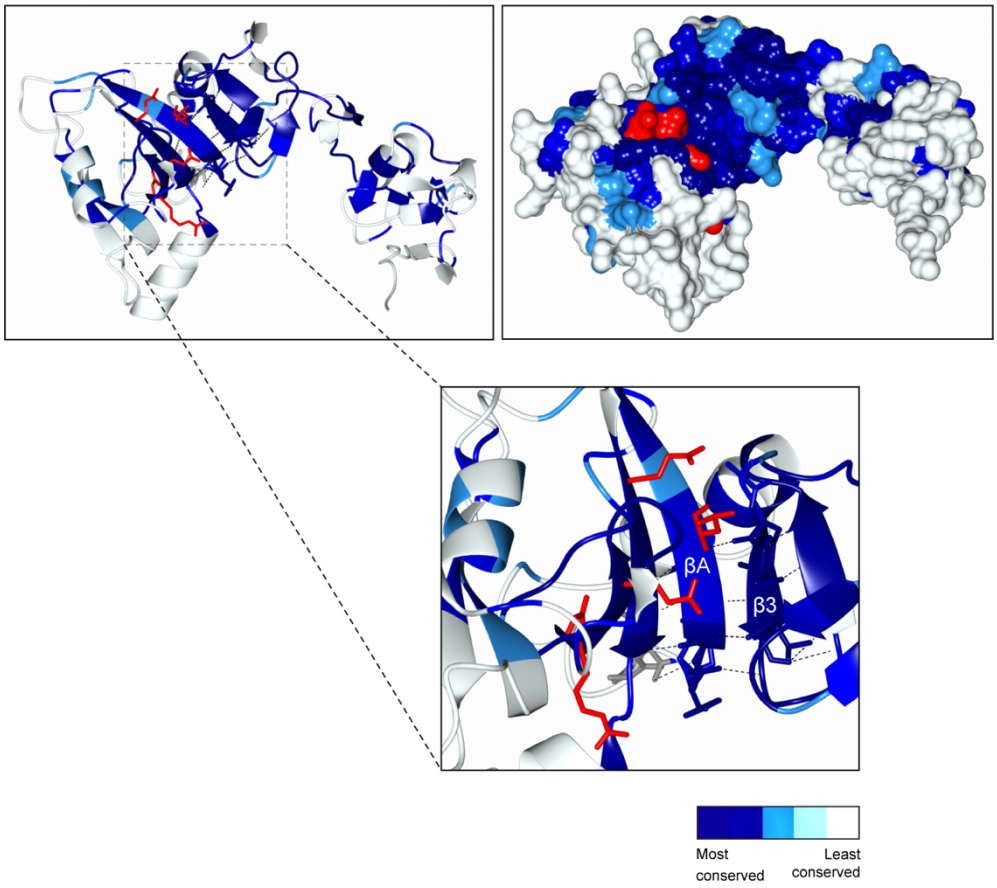

Figure 3. 5. LIM2-PDZ interaction models.

Models predict interaction mediated by the β hairpin 3 of the LIM2 domain and the βA strand of the PDZ domain. However, the models do not predict the interaction between the side chains of the amino acids used for the mutation analysis of the PDZ domain. In red, amino acids used for mutagenesis analysis in Chapter 2, E225, D221, R222, Q251, L165A (LIMK1 numbering). Top right panel shows

surface conservation, red surface shows mutated residues. Bottom panel shows predicted hydrogen bond interactions between the LIM2 and PDZ domains.

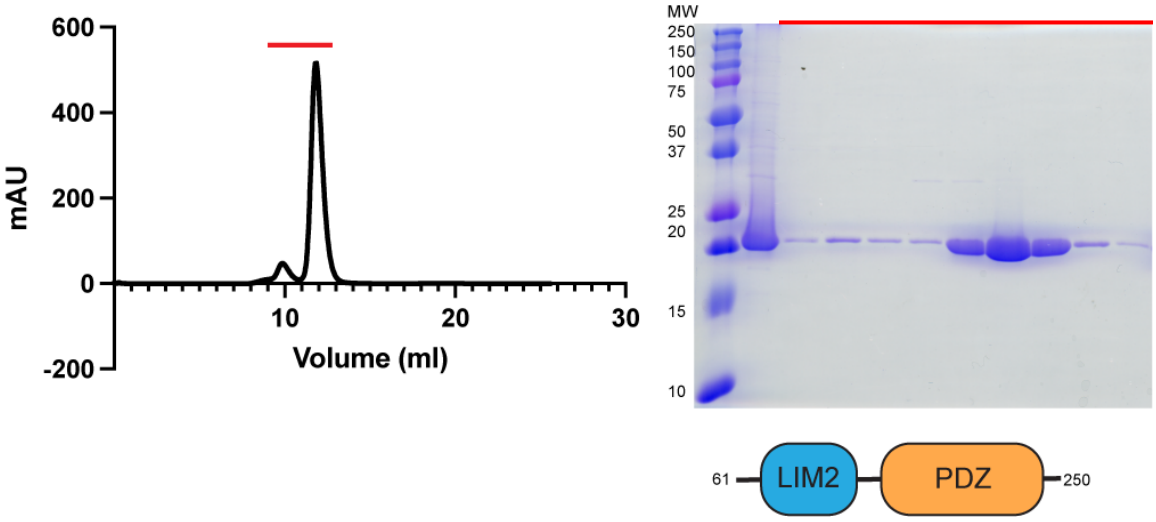

Figure 3. 6. Purification of human LIMK2 LIM2-PDZ fragment.

On the left, size exclusion chromatography (SEC) chromatogram from the human LIMK2 LIM2-PDZ fragment purification. Top right, SDS-page of SEC run, bottom right cartoon representation of construct boundaries.

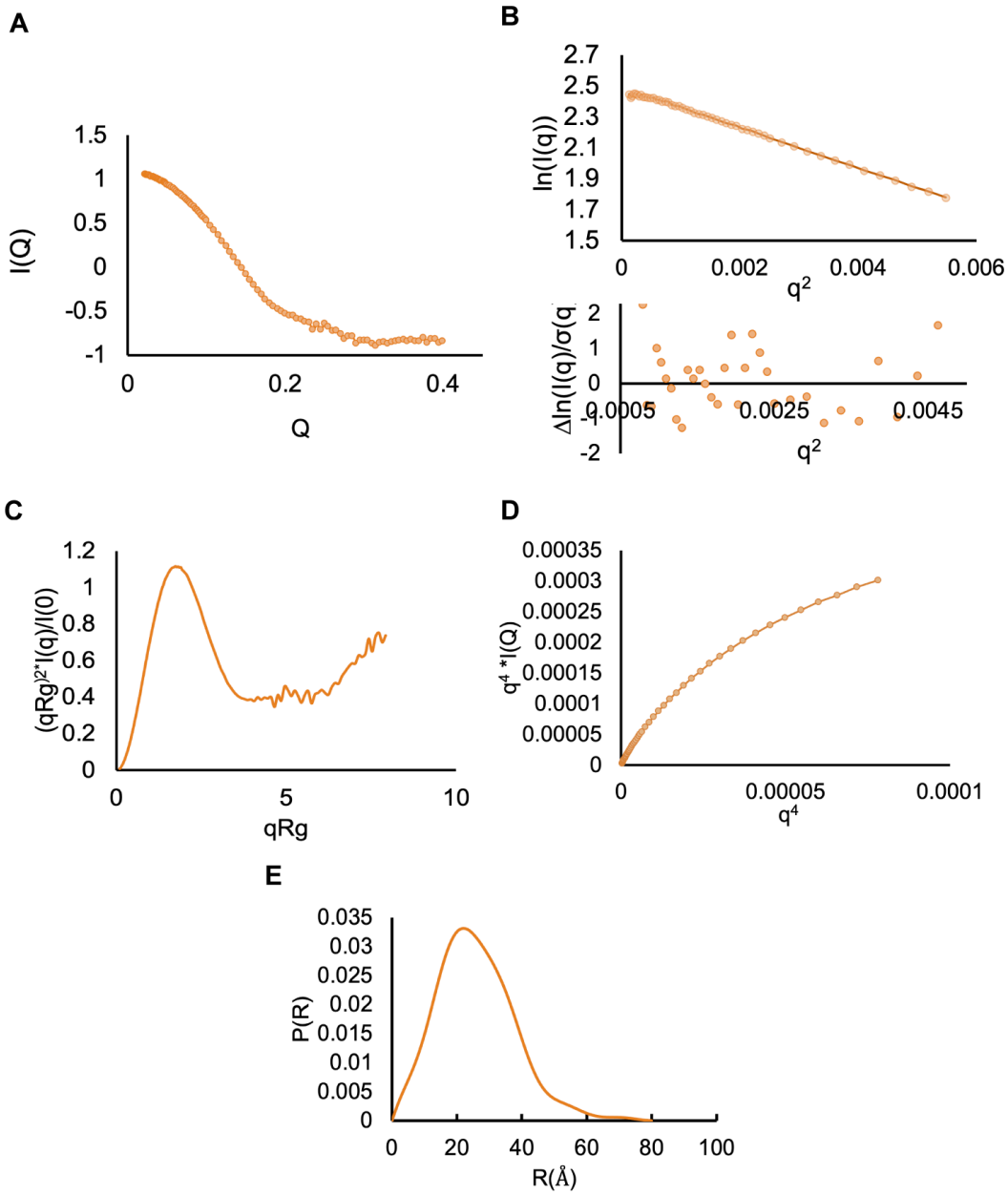

Figure 3.7. The LIM2-PDZ displays a globular fold in solution.

A. SAXS scattering profile averaged across the protein elution peak. **B.** Guinier analysis (top) and the plotted residuals between the data and fit (bottom) are shown. There are no systematic deviations from linearization for either sample, indicating high-quality data. **C.** Kratky analysis. **D.** Porod-Debye analysis, flexibility

is suggested as the curve fails to plateau. **E.** Pair distribution functions. Curve suggests protein is globular.

Rg (Å) (from Guinier analysis)	19.82 ± 0.13
Dmax (Å) (from P(R))	80
Volume of Correlation (Vc) MW (kDa)	20.6
Theoretical MW (kDa)	21.4

Table 3.2. SAXS measurements of LIMK2 LIM2-PDZ regions of the N-terminus. Full SAXS parameters are shown in Table 3.3.

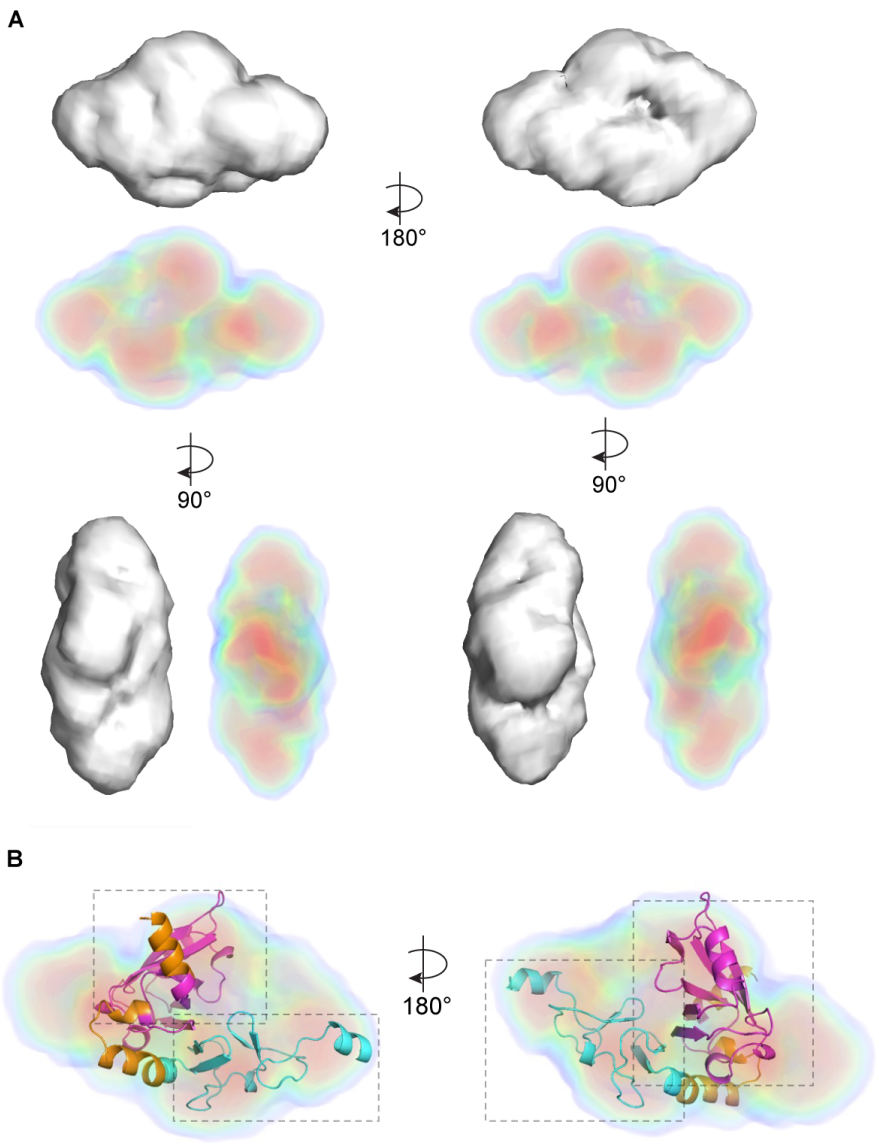

Figure 3.8. 3D particle electron density reconstruction of LIMK2 LIM2-PDZ domain. DENSS.

A. Grey particles represent the particle envelope, while the colored particles inform of the concentration of electron density within the particle envelope. **B.** LIMK2 LIM2-PDZ region model superposed onto the DENSS colored envelope. LIM2

domain cartoon is colored cyan, PDZ is colored magenta, and linker regions are orange. Model includes all residues included in the experimental protein construct.

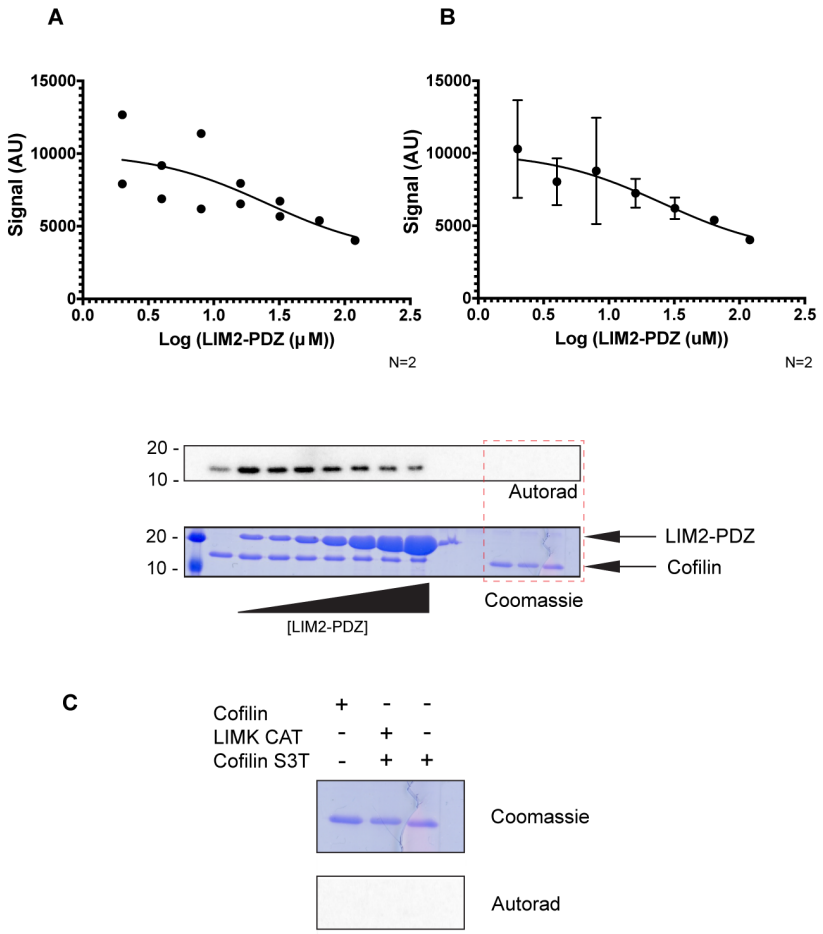

Figure 3.9. The LIM2-PDZ domain inhibits the kinase activity of LIMK2 C-terminus kinase domain.

A. Left, quantified autoradiography from radiolabel cofilin kinase activity of LIMK2 catalytic domains with increasing concentrations of LIM2-PDZ domains, all data points shown (dots, $n = 2$). **B.** Data are shown as mean values (line) +/− SD (error bars). Cofilin alone, kinase domain alone, and LIM2-PDZ domain alone were used as negative controls. Lower panel shows representative autoradiography readings of cofilin phosphorylation for kinase assays with corresponding Coomassie staining. Statistical analysis was carried out using non-linear regression, dose-

response for inhibition. Mean and error are portrayed, along with the standard deviation. A total of 2 replicates were analyzed using GraphPad Prism. **C.** Representative autoradiography readings of S3T cofilin phosphorylation for kinase assays with corresponding Coomassie staining.

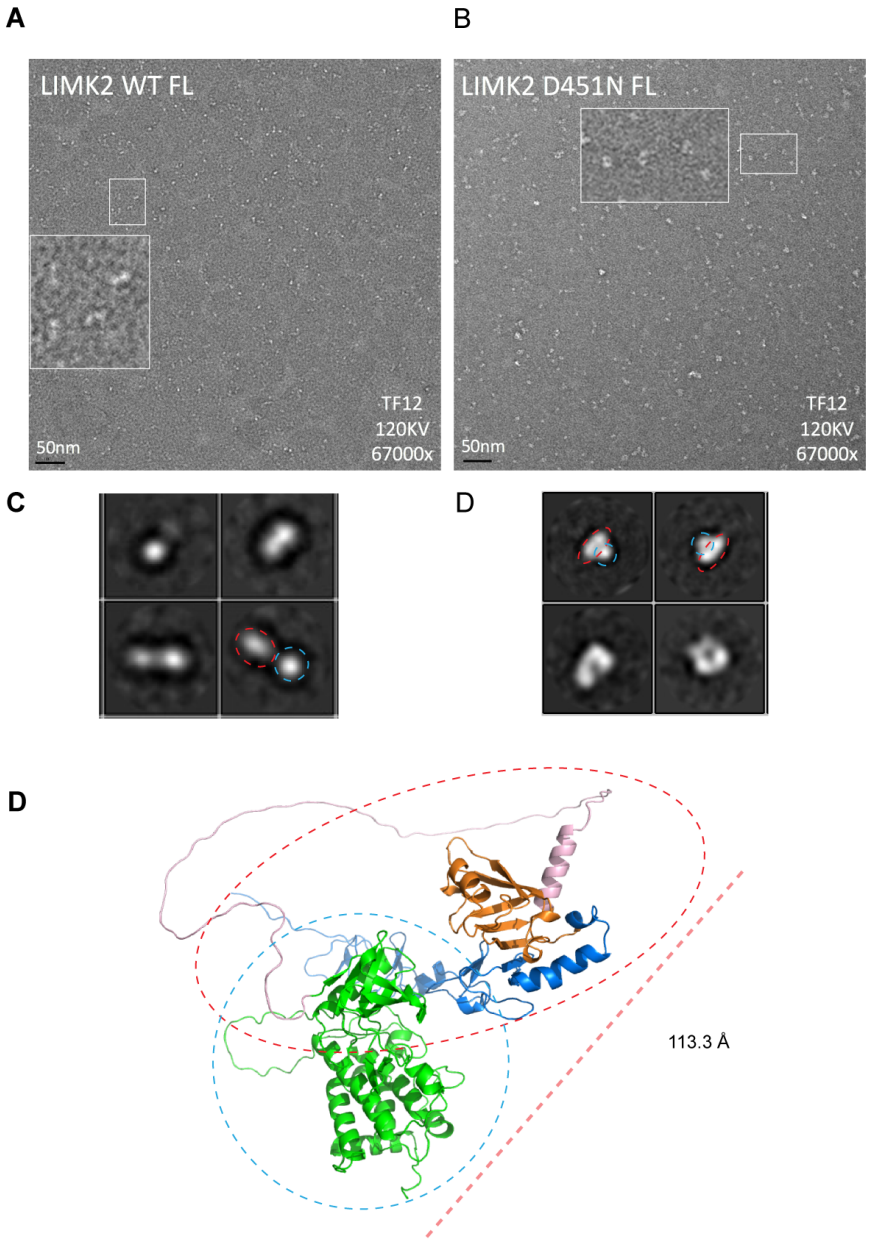

Figure 3.10. LIMK2 FL negative strain studies reveal two different conformations between WT and kinase-inactive D451N.

A. Representative micrograph of LIMK2 FL wild-type sample. Particle size is around 100 Å**. B.** Representative micrograph of LIMK2 FL kinase inactive D451N. Particle size is around 80 Å **. C.** Class averages of LIMK2 FL wild-type sample. **D.**

Class averages of LIMK2 FL kinase inactive D451N. **D.** AlphaFold model of LIMK2 FL wild type proposes a length of around 113 Å for LIMK. Dashed red circle indicates the N-terminus domains, blue dashed oval indicates the kinase domain.

Table 3.3. SAXS sample, data collection, and data analysis, related to Figure 3.7

Organism	Human
Source	*E. coli*
Sequence of construct	GSPKDYWGKFGEFCHGCSLLMTGPFMVAGEF KYHPECFACMSCKVIIEDGDAYALVQHATLYCG KCHNEVVLAPMFERLSTESVQEQLPYSVTLISM PATTEGRRGFSVSVESASSNYATTVQVKEVNR MHISPNNRNAIHPGDRILEINGTPVRTLRVEEVE DAISQTSQTLQLLIEHDPVSQRLDQLRLE
Extinction coefficient ε (M^{-1} cm^{-1})	14440
MW (kDa)	21.4
Loading concentration (mg mL^{-1})	11
Injection volume (µL)	60
Flow Rate (ml min^{-1})	0.35
Solvent composition	150mM NaCl, 20mM Tris pH 8, 1mM DTT
SAXS Data Collection Parameters	
Instrument	BNL, NSLS-II, LiX Beamline, sector 16-ID
Wavelength (Å)	0.819
Camera length (m)	3.686
Beam size	150 (h) x 25 (v) focused at the detector
q-measurment range (Å-1)	0.006 < q < 3.0 Å−1
Absoute scaling method	Glassy Carbon, NIST SRM 3600
Basis for normalization to constant counts	To transmitted intensity by beam-stop counter
Method for monitoring radiation damage	Automated frame-by-frame comparison of relevant regions using CORMAP[358] implemented in BioXTAS RAW

Sample configuration	SEC-MALS-DLS-RI-SAXS. Size separation used a Superdex 200 Increase 5/150 GL column (Wyatt Technology) and a 1260 Infinity II HPLC (Agilent Technologies). UV data was measured in the Agilent
Exposure time (s)	0.5
Exposure period (s)	2
Sample temperature (˚C)	22
Software employed for SAXS data reduction	
SAXS data reduction	Radial averaging; frame comparison, averaging, and subtraction done using BioXTAS RAW 2.0.3[350]
Basic analysis: Guinier, M.W., P(R)	Guinier fit and M.W. using BioXTAS RAW, P(r) function using GNOM [359]. RAW uses MoW and Vc M.W. methods[50,352]
e from sequence	ProtParam Tool - ExPASy
Electron density	Performed in RAW v2.1.3 according to[353]
Molecular graphics	CCP4mg
Structural parameters	
Guinier Analysis	
I(0) (cm^{-1})	0.08269
R_g (Å)	19.822
q-range ($Å^{-1}$)	0.022 to 0.068
P(R) Analysis	
R_g (Å)	20.25
D_{max} (Å)	80
q-range ($Å^{-1}$)	0.005 - 0.04
Porod Volume (Vp) MW (kDa)	18.82

Volume of Correlation (Vc) MW (kDa)	20.6
DENSS Reconstructions	
Chi squared value	1.54996
Model R_g (Å)	19.38
Model resolution (Å)	24.35 +/- 4.55

Chapter 4: Overall discussion and concluding remarks

4.1 Introduction

The LIMK domain family of proteins are enzymes fundamental for cytoskeletal dynamics [237,240,307,360,361]. The LIMKs phosphorylate cofilin, an essential actin depolymerizing factor, and mediate signal-driven changes in the depolymerization rate of actin filaments in the cell [189,251,307]. In the past 25 years, LIMK and cofilin have been heavily studied since LIMK1 was discovered, but important questions still need to be answered regarding kinase regulation. Current literature proposes a model of regulation in which the N-terminus, which contains two LIM domains and one PDZ domain, acts as a negative regulator of the kinase domain at the C-terminus. These domains, known to mediate protein-protein interactions, remain understudied in the context of LIMK autoregulation. Thus, the proposed mechanisms of how these domains modulate the kinase activity of LIMK have yet to be revealed. I hypothesize that the N-terminus of LIMK negatively regulates its activity via a direct "head-to-tail" interaction. The work presented in this thesis improves the molecular understanding of LIMK autoregulation mechanism using structure and conservation-directed approaches and biochemical and biophysical techniques.

To better understand the autoregulation mechanism of LIMK, I designed two aims. For aim 1, I proposed to reveal the molecular basis for the autoinhibition of LIMK, and for aim 2, I proposed to understand LIMK autoregulation using enzymatic assays. In **Chapter 2**, I use biochemical and structural techniques to

gain a molecular-level understanding of the PDZ domain of LIMK. Specifically, I obtained the crystal structure of the human LIMK2 PDZ domain and mapped a conserved surface that, when mutated, increases the catalytic activity of LIMK1. These findings suggest that the PDZ domain contains a functionally important surface involved in autoregulation. In **Chapter 3**, I explore the conformation of another domain of the N-terminus, LIM2, and use AlphaFold prediction models of full-length LIMK to explore interactions between the LIM2 and PDZ domain that might be important for autoregulation. I use biophysical techniques to examine the conformation of these two domains and the overall fold of LIMK. I find that the LIM-PDZ domain portrays a globular conformation, with a distinction of it showing a certain degree of flexibility in solution using SAXS. I also explore the effect of these domains on the activity of LIMK using *in vitro* kinase assays. I also find that negative stain electron microscopy studies of full-length LIMK in the wild type and kinase-inactive D451N mutant suggest 2 distinct conformations. LIMK2 FL wild-type proteins show an extended conformation, unlike the kinase-inactive D451N mutant, which shows a compact “triangular” like conformation.

The data described within this dissertation contributes towards a more complete understanding of LIMK autoregulation, as it describes biochemically the effect of the N-terminus domains in autoregulation and low-resolution information of the conformation of the full-length LIMK. The body of work presented, therefore, significantly advances our understanding of the LIMK autoregulation mechanism and the first report of PDZ-mediated regulatory interactions in a protein kinase.

Further studies are needed to delineate, at an atomic level, the direct interactions that the PDZ domain has on regulating LIMK.

4.2 Discovery of a PDZ domain conserved surface involved in LIMK regulation of LIMK

4.2.1 Summary of findings

I first decided to study the PDZ domain of LIMK. I used biochemical and structural techniques to gain a molecular-level understanding of the PDZ domains. Specifically, I obtained the crystal structure of the human LIMK2 PDZ domain and mapped the conservation of this domain using both LIMK1 and LIMK2 sequence alignments. My conservation analysis allowed me to find a surface in this domain that is conserved from mammals to insects. I use homology- and structure-driven mutations to validate structure-defined and functional mechanisms of PDZ domain regulation.

To test the effect of these mutations, I reconstructed the LIMK pathway in *S. cerevisiae*, as yeast does not express a LIMK homolog. Expression of human LIMK1 phosphorylates and inactivates endogenous cofilin; thus, I observed alterations in LIMK activity by measuring yeast viability. Using this assay, I screened for LIMK1 PDZ mutants that may be involved in kinase autoregulation. I successfully expressed and purified LIMK1 PDZ mutants of interest and used *in vitro* radiolabeled kinase assays to test the impact of functionally important mutations on kinase activity using cofilin as a substrate. This combination of approaches allowed me to find a highly conserved surface in the PDZ that

mediates regulatory interactions with the kinase domain that, when mutated, affects the activity of LIMK1. This study also suggests that disruption of the surface that mediates autoregulatory interactions between the PDZ domain and the kinase domain allows LIMK activators to phosphorylate LIMK in its activation loop better than the wild-type counterpart as phosphorylation levels in LIMK1 full-length PDZ mutants are higher than in the wild-type protein. This more suitable conformation could allow for better activation loop access by upstream activators or be a worse substrate for LIMK phosphatases.

4.2.2. Implications for further research

This work presented in this thesis provides biochemical evidence of conserved surfaces involved in autoregulation; however, the mode in which this domain exerts autoregulation on the kinase domain has yet to be known. Understanding the molecular interaction between the PDZ and kinase domains at an atomic level would greatly benefit this study. Obtaining the crystal structure of this complex would show, specifically, what kind of interaction is mediated between these two domains. The PDZ domain could bind directly to the kinase domain and promote an incompatible confirmation for activation by upstream regulators. The PDZ domain could do this by binding, possibly in a non-canonical manner, the catalytic domain. I hypothesize that this autoregulatory interaction could happen in the N-terminal lobe of the kinase domain. Conservation analysis of the LIMK kinase domain shows high conservation in the N-lobe, in contrast to the C-lobe (**Figure 4.1**). Moreover, autoregulatory interactions in protein kinases have been observed

more often in the N-lobe than the C-lobe [298,362,363]. For example, members of the AGC kinase family, the Src kinases, Crk kinases, the Abl family, and others show changes in activity with the binding of interactors to the N-lobe of the kinase domain.

Another beneficial experiment would be to test the phosphorylation of the catalytic domain by a protein kinase activator, such as PAK4, in the presence of PDZ and other N-terminal domains. These experiments will allow me to observe if the binding of the PDZ and other N-terminal domains to the kinase domain of LIMK prevents or lowers LIMK activation loop phosphorylation. If a decrease in the activation by PAK4 phosphorylation is observed when adding LIM2-PDZ domains, it would imply that the autoregulation of the N-terminus to the kinase domain is hindering the activation by upstream regulators, possibly potentiating an inactive conformation. If kinase activity does not change, it would suggest a different autoregulation mechanism than allosteric regulation.

4.3 The LIM2-PDZ domains are thought to behave as a module and regulate the activity of LIMK

4.3.1 Summary of findings

In Chapter 3, I use biochemical, biophysical, and activity-based assays to elucidate how the N-terminus domains of LIMK are responsible for autoregulatory interactions towards the kinase domain. I begin by directly addressing whether, in addition to the PDZ, other domains in the N-terminus of LIMK are responsible for kinase autoregulation. I titrated the N-terminus LIM2-PDZ domains into

radiolabeled kinase assays using active LIMK2 kinase domain to test their respective inhibitory activities. I discovered that a LIMK fragment that includes the LIM2-PDZ domains decreases the kinase activity of LIMK. Additionally, I look more closely into the LIM2-PDZ domain and use SEC-SAXS to study its arrangement in solution. SEC-SAXS data suggest these two domains form a multi-domain module by interacting with each other. This multidomain module might be necessary for LIMK autoregulation.

4.3.2. Implications for further research

A finding we did not expect was the possible interaction between the LIM2- PDZ domains. However, SEC-SAXS data can only provide low-resolution information on the conformational states of these domains. Therefore, the next step would be to obtain the crystal structure of these two domains in complex. This would benefit the understanding of LIM autoregulation and offer novel information on the possible non-canonical binding of a PDZ domain to a LIM domain. Also, studying, *in vitro*, the effect of the PDZ domain in autoregulation would allow me to differentiate if the effect observed in my *in vitro* kinase assays using the LIM2-PDZ constructs is an effect of the PDZ domain exerting inhibition on the kinase domain or if the LIM2 contributes to inhibition. Moreover, the structure of the complex between the LIM2-PDZ region with the kinase domain in the inactive state (D451N) would help improve the understanding of LIMK autoregulation.

4.4 Negative stain experiments suggest LIMK is regulated in cis

4.4.1 Summary of findings

This work also explores the arrangement of full-length LIMK. I purified human full-length LIMK2 protein and used negative staining electron microscopy to observe global conformational changes between full-length wild-type protein (FL WT) vs. kinase dead D451N mutant. This technique allowed me to differentiate between intra or intermolecular conformations in full-length LIMK. Negative stain electron microscopy experiments suggest two different conformations, where the FL WT displays an elongated conformation, while the FL D451N mutant displays a more compact conformation. These discoveries suggest that the N-terminus domains are responsible for the autoregulation of LIMKs and that the mode of regulation is intramolecular.

4.4.2. Implications for further research

As crystallization experiments can be quite challenging regarding the quantity of protein needed and the accomplishment of protein crystallization, the full-length LIMK can be done through single-particle electron cryo-microscopy (cryo-EM). Even though LIMK has an approximate molecular weight of 72 kD, preliminary Cryo-EM conditions can be investigated. If processing cannot be accomplished due to a lack of recognizable shape features that facilitate initial image alignment at low resolution, adding stable tags could help achieve a bigger particle volume. Tags that can increase the size of the particles can be nanobodies, binding partners, or stable protein tags.

4.5 Concluding remarks

These findings provide a foundation for studying the effect of the N-terminus LIM and PDZ domains in the autoregulation of LIMK. I conducted kinase studies to test autoregulatory interactions in LIMK in purified systems as well as in a eukaryotic system. This work delivers the first crystal of the human LIMK2 PDZ domain and an in-depth study of its fold and conservation. Mutagenesis studies of the PDZ domain reported here provide strong evidence for how this domain undergoes autoregulation. Moreover, I provide insight into the molecular arrangement of LIMK and provide a low-resolution understanding of its oligomeric state using SAXS. This work also includes low-resolution information on the conformational arrangement of LIMK in terms of full-length protein using negative stain electron microscopy. Together, these data propose the following autoregulation model: LIMK kinase exists in an equilibrium between “open” and “closed” conformation. The “open conformation” is characterized by an accessible kinase domain and an extended N-terminus. The “closed” conformation is portrayed by *cis* interactions between the N-terminal PDZ or LIM2-PDZ conserved surfaces and the kinase domain N-lobe. Changes in conformation equilibrium could be mediated by phosphorylation events in the Ser/Pro-rich region or the binding of protein partners to the N-terminus domains. When equilibrium is pushed towards a more “open” conformation, upstream activators can access the activation loop and phosphorylate Thr508/Thr505 in LIMK1 and LIMK2, respectively. LIMK, then, in the active state, is in the extended conformation. This mechanism could portray

the characteristics of autoregulation of kinase such as Abl and Akt, where binding domains or motifs in the same polypeptide chain keep the kinase domain in a conformation unsuitable for activation (**Figure 4.2**). PDZ and LIM domains mediate this autoregulation, unlike other kinase autoregulation mechanisms. The mode in which this autoregulation is mediated, specifically how and where these N-terminal domains bind the kinase domain, remains to be elucidated.

4.1.Figures

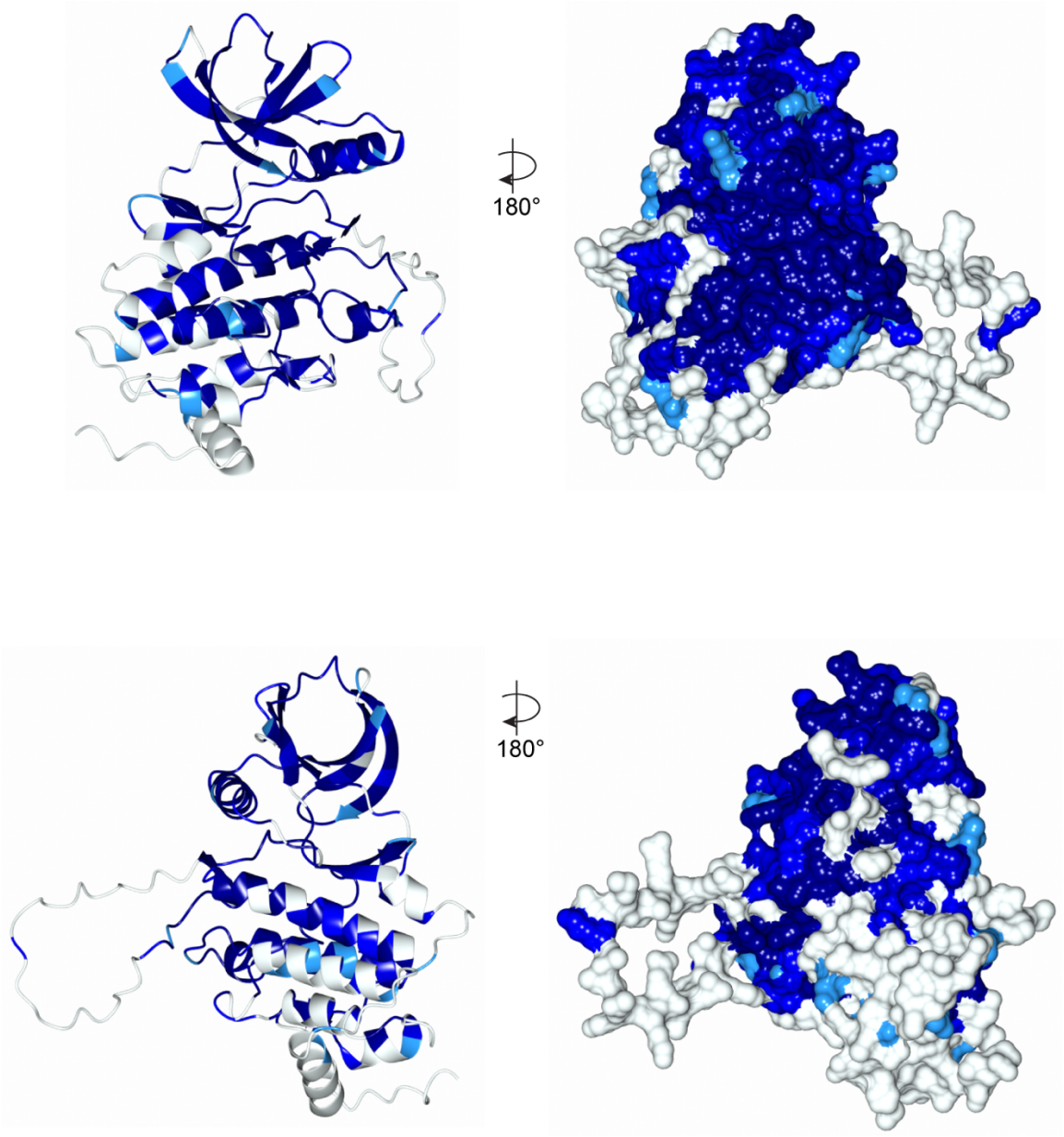

Figure 4. 1. Human LIMK2 mapped conservation of the kinase domain.

Kinase domain conservation mapped onto the AlphaFold kinase domain predicted structure using 421 aligned LIMK sequences from mammals, birds, fish, and insects.

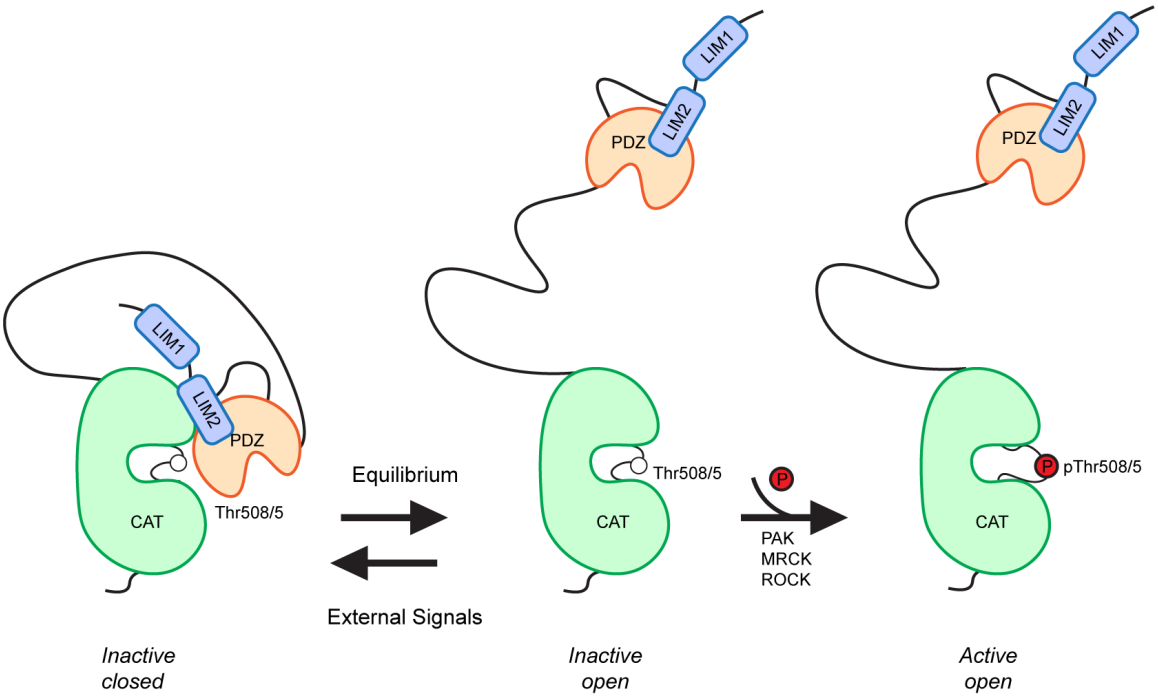

Figure 4.2. LIMK autoregulation model.

LIMK kinase exists in an equilibrium between “open” and “closed” conformation. The “open conformation” is characterized by an accessible kinase domain and an extended N-terminus. The “closed” conformation is characterized by *cis* interactions between the N-terminal LIM2-PDZ domains with the kinase domains. Changes. In conformation, equilibrium could be mediated by phosphorylation events in the Ser/Pro-rich region or binding of protein partners to the N-terminus domains. When equilibrium is pushed towards a more “open” conformation, upstream activators can access the activation loop and phosphorylate Thr508/Thr505 in LIMK1 and LIMK2, respectively. LIMK is in the extended conformation in its active state.

References

1. Sacco, F., Perfetto, L., Castagnoli, L. & Cesareni, G. The human phosphatase interactome: An intricate family portrait. *FEBS Lett* **586**, 2732-9 (2012). PMC3437441

2. Li, X., Wilmanns, M., Thornton, J. & Kohn, M. Elucidating human phosphatase-substrate networks. *Sci Signal* **6**, rs10 (2013).

3. Hunter, T. Why nature chose phosphate to modify proteins. *Philos Trans R Soc Lond B Biol Sci* **367**, 2513-6 (2012). PMC3415839

4. Fischer, E.H. & Krebs, E.G. Conversion of phosphorylase b to phosphorylase a in muscle extracts. *J Biol Chem* **216**, 121-32 (1955).

5. Wilks, A.F. Two putative protein-tyrosine kinases identified by application of the polymerase chain reaction. *Proc Natl Acad Sci U S A* **86**, 1603-7 (1989). PMC286746

6. Partanen, J., Makela, T.P., Alitalo, R., Lehvaslaiho, H. & Alitalo, K. Putative tyrosine kinases expressed in K-562 human leukemia cells. *Proc Natl Acad Sci U S A* **87**, 8913-7 (1990). PMC55070

7. Cartwright, C.A., Kaplan, P.L., Cooper, J.A., Hunter, T. & Eckhart, W. Altered sites of tyrosine phosphorylation in pp60c-src associated with polyomavirus middle tumor antigen. *Mol Cell Biol* **6**, 1562-70 (1986). PMC367682

8. Mizuno, K., Okano, I., Ohashi, K., Nunoue, K., Kuma, K., Miyata, T. & Nakamura, T. Identification of a human cDNA encoding a novel protein kinase with two repeats of the LIM/double zinc finger motif. *Oncogene* **9**, 1605-12 (1994).

9. Ohashi, K., Toshima, J., Tajinda, K., Nakamura, T. & Mizuno, K. Molecular cloning of a chicken lung cDNA encoding a novel protein kinase with N-terminal two LIM/double zinc finger motifs. *J Biochem* **116**, 636-42 (1994).

10. Okano, I., Hiraoka, J., Otera, H., Nunoue, K., Ohashi, K., Iwashita, S., Hirai, M. & Mizuno, K. Identification and characterization of a novel family of serine/threonine kinases containing two N-terminal LIM motifs. *J Biol Chem* **270**, 31321-30 (1995).

11. Bernard, O., Ganiatsas, S., Kannourakis, G. & Dringen, R. Kiz-1, a protein with LIM zinc finger and kinase domains, is expressed mainly in neurons. *Cell Growth Differ* **5**, 1159-71 (1994).

12. Manning, G., Whyte, D.B., Martinez, R., Hunter, T. & Sudarsanam, S. The protein kinase complement of the human genome. *Science* **298**, 1912-34 (2002).

13. Proschel, C., Blouin, M.J., Gutowski, N.J., Ludwig, R. & Noble, M. Limk1 is predominantly expressed in neural tissues and phosphorylates serine, threonine and tyrosine residues in vitro. *Oncogene* **11**, 1271-81 (1995).

14. Lagoutte, E., Villeneuve, C., Lafanechère, L., Wells, C.M., Jones, G.E., Chavrier, P. & Rossé, C. LIMK Regulates Tumor-Cell Invasion and Matrix Degradation Through Tyrosine Phosphorylation of MT1-MMP. **6**, 24925 (2016).

15. Toshima, J., Ohashi, K., Okano, I., Nunoue, K., Kishioka, M., Kuma, K., Miyata, T., Hirai, M., Baba, T. & Mizuno, K. Identification and characterization of a novel protein kinase, TESK1, specifically expressed in testicular germ cells. *J Biol Chem* **270**, 31331-7 (1995).

16. Nunoue, K., Ohashi, K., Okano, I. & Mizuno, K. LIMK-1 and LIMK-2, two members of a LIM motif-containing protein kinase family. *Oncogene* **11**, 701-10 (1995).

17. Scott, R.W. & Olson, M.F. LIM kinases: function, regulation and association with human disease. *J Mol Med (Berl)* **85**, 555-68 (2007).

18. Amano, T., Kaji, N., Ohashi, K. & Mizuno, K. Mitosis-specific activation of LIM motif-containing protein kinase and roles of cofilin phosphorylation and dephosphorylation in mitosis. *J Biol Chem* **277**, 22093-102 (2002).

19. Kaji, N., Muramoto, A. & Mizuno, K. LIM kinase-mediated cofilin phosphorylation during mitosis is required for precise spindle positioning. *J Biol Chem* **283**, 4983-92 (2008).

20. Kadrmas, J.L. & Beckerle, M.C. The LIM domain: from the cytoskeleton to the nucleus. *Nat Rev Mol Cell Biol* **5**, 920-31 (2004).

21. Chiswell, B.P., Zhang, R., Murphy, J.W., Boggon, T.J. & Calderwood, D.A. The structural basis of integrin-linked kinase–PINCH interactions. *Proceedings of the National Academy of Sciences* **105**, 20677-20682 (2008).

22. Gibson, T.J., Postma, J.P., Brown, R.S. & Argos, P. A model for the tertiary structure of the 28 residue DNA-binding motif ('zinc finger') common to many eukaryotic transcriptional regulatory proteins. *Protein Eng* **2**, 209-18 (1988).

23. Mizuno, K. & Higuchi, O. [LIM domains: double zinc finger motifs involved in protein-protein interactions]. *Tanpakushitsu Kakusan Koso* **42**, 2061-71 (1997).

24. Zheng, Q. & Zhao, Y. The diverse biofunctions of LIM domain proteins: determined by subcellular localization and protein-protein interaction. *Biol Cell* **99**, 489-502 (2007).

25. Khurana, T., Khurana, B. & Noegel, A.A. LIM proteins: association with the actin cytoskeleton. *Protoplasma* **219**, 1-12 (2002).

26. Jelen, F., Oleksy, A., Smietana, K. & Otlewski, J. PDZ domains - common players in the cell signaling. *Acta Biochim Pol* **50**, 985-1017 (2003).

27. Rabbitts, T.H. LMO T-cell translocation oncogenes typify genes activated by chromosomal translocations that alter transcription and developmental processes. *Genes Dev* **12**, 2651-7 (1998).

28. Chiswell, B.P., Stiegler, A.L., Razinia, Z., Nalibotski, E., Boggon, T.J. & Calderwood, D.A. Structural basis of competition between PINCH1 and PINCH2 for binding to the ankyrin repeat domain of integrin-linked kinase. *J Struct Biol* **170**, 157-63 (2010). PMC2841223

29. Stiegler, A.L., Grant, T.D., Luft, J.R., Calderwood, D.A., Snell, E.H. & Boggon, T.J. Purification and SAXS analysis of the integrin linked kinase, PINCH, parvin (IPP) heterotrimeric complex. *PLoS One* **8**, e55591 (2013). PMC3561323

30. Arber, S., Halder, G. & Caroni, P. Muscle LIM protein, a novel essential regulator of myogenesis, promotes myogenic differentiation. *Cell* **79**, 221-31 (1994).

31. Sadler, I., Crawford, A.W., Michelsen, J.W. & Beckerle, M.C. Zyxin and cCRP: two interactive LIM domain proteins associated with the cytoskeleton. *J Cell Biol* **119**, 1573-87 (1992). PMC2289750

32. Wu, C. & Dedhar, S. Integrin-linked kinase (ILK) and its interactors: a new paradigm for the coupling of extracellular matrix to actin cytoskeleton and signaling complexes. *J Cell Biol* **155**, 505-10 (2001). PMC2198863

33. Schaller, M.D. Paxillin: a focal adhesion-associated adaptor protein. *Oncogene* **20**, 6459-72 (2001).

34. Brown, M.C., Perrotta, J.A. & Turner, C.E. Identification of LIM3 as the principal determinant of paxillin focal adhesion localization and characterization of a novel

motif on paxillin directing vinculin and focal adhesion kinase binding. *J Cell Biol* **135**, 1109-23 (1996). PMC2133378

35. Uemura, A., Nguyen, T.N., Steele, A.N. & Yamada, S. The LIM domain of zyxin is sufficient for force-induced accumulation of zyxin during cell migration. *Biophys J* **101**, 1069-75 (2011). PMC3164133

36. Vallenius, T., Scharm, B., Vesikansa, A., Luukko, K., Schafer, R. & Makela, T.P. The PDZ-LIM protein RIL modulates actin stress fiber turnover and enhances the association of alpha-actinin with F-actin. *Exp Cell Res* **293**, 117-28 (2004).

37. Coutts, A.S., MacKenzie, E., Griffith, E. & Black, D.M. TES is a novel focal adhesion protein with a role in cell spreading. *J Cell Sci* **116**, 897-906 (2003).

38. Garvalov, B.K., Higgins, T.E., Sutherland, J.D., Zettl, M., Scaplehorn, N., Kocher, T., Piddini, E., Griffiths, G. & Way, M. The conformational state of Tes regulates its zyxin-dependent recruitment to focal adhesions. *J Cell Biol* **161**, 33-9 (2003). PMC2172870

39. Tobias, E.S., Hurlstone, A.F., MacKenzie, E., McFarlane, R. & Black, D.M. The TES gene at 7q31.1 is methylated in tumours and encodes a novel growth-suppressing LIM domain protein. *Oncogene* **20**, 2844-53 (2001).

40. Sala, S. & Oakes, P.W. Stress fiber strain recognition by the LIM protein testin is cryptic and mediated by RhoA. *Mol Biol Cell* **32**, 1758-1771 (2021). PMC8684727

41. Sala, S., Catillon, M., Hadzic, E., Schaffner-Reckinger, E., Van Troys, M. & Ampe, C. The PET and LIM1-2 domains of testin contribute to intramolecular and homodimeric interactions. *PLoS One* **12**, e0177879 (2017). PMC5436826

42. Loughran, G., Healy, N.C., Kiely, P.A., Huigsloot, M., Kedersha, N.L. & O'Connor, R. Mystique is a new insulin-like growth factor-I-regulated PDZ-LIM domain protein that promotes cell attachment and migration and suppresses Anchorage-independent growth. *Mol Biol Cell* **16**, 1811-22 (2005). PMC1073663

43. Wu, R., Durick, K., Songyang, Z., Cantley, L.C., Taylor, S.S. & Gill, G.N. Specificity of LIM domain interactions with receptor tyrosine kinases. *J Biol Chem* **271**, 15934-41 (1996).

44. Durick, K., Gill, G.N. & Taylor, S.S. Shc and Enigma are both required for mitogenic signaling by Ret/ptc2. *Mol Cell Biol* **18**, 2298-308 (1998). PMC121481

45. Guy, P.M., Kenny, D.A. & Gill, G.N. The PDZ domain of the LIM protein enigma binds to beta-tropomyosin. *Mol Biol Cell* **10**, 1973-84 (1999). PMC25398

46. Cuppen, E., Gerrits, H., Pepers, B., Wieringa, B. & Hendriks, W. PDZ motifs in PTP-BL and RIL bind to internal protein segments in the LIM domain protein RIL. *Mol Biol Cell* **9**, 671-83 (1998). PMC25295

47. Matsuda, M., Yamashita, J.K., Tsukita, S. & Furuse, M. abLIM3 is a novel component of adherens junctions with actin-binding activity. *Eur J Cell Biol* **89**, 807-16 (2010).

48. Song, Y., Maul, R.S., Gerbin, C.S. & Chang, D.D. Inhibition of anchorage-independent growth of transformed NIH3T3 cells by epithelial protein lost in neoplasm (EPLIN) requires localization of EPLIN to actin cytoskeleton. *Mol Biol Cell* **13**, 1408-16 (2002). PMC102278

49. Maul, R.S., Song, Y., Amann, K.J., Gerbin, S.C., Pollard, T.D. & Chang, D.D. EPLIN regulates actin dynamics by cross-linking and stabilizing filaments. *J Cell Biol* **160**, 399-407 (2003). PMC2172667

50. Abe, K. & Takeichi, M. EPLIN mediates linkage of the cadherin catenin complex to F-actin and stabilizes the circumferential actin belt. *Proc Natl Acad Sci U S A* **105**, 13-9 (2008). PMC2224173

51. Tomasetto, C., Moog-Lutz, C., Regnier, C.H., Schreiber, V., Basset, P. & Rio, M.C. Lasp-1 (MLN 50) defines a new LIM protein subfamily characterized by the association of LIM and SH3 domains. *FEBS Lett* **373**, 245-9 (1995).

52. Nakagawa, H., Suzuki, H., Machida, S., Suzuki, J., Ohashi, K., Jin, M., Miyamoto, S. & Terasaki, A.G. Contribution of the LIM domain and nebulin-repeats to the interaction of Lasp-2 with actin filaments and focal adhesions. *PLoS One* **4**, e7530 (2009). PMC2761545

53. Hiraoka, J., Okano, I., Higuchi, O., Yang, N. & Mizuno, K. Self-association of LIM-kinase 1 mediated by the interaction between an N-terminal LIM domain and a C-terminal kinase domain. *FEBS Lett* **399**, 117-21 (1996).

54. Nagata, K., Ohashi, K., Yang, N. & Mizuno, K. The N-terminal LIM domain negatively regulates the kinase activity of LIM-kinase 1. *Biochem J* **343 Pt 1**, 99-105 (1999). PMC1220529

55. Hung, R.J., Yazdani, U., Yoon, J., Wu, H., Yang, T., Gupta, N., Huang, Z., van Berkel, W.J. & Terman, J.R. Mical links semaphorins to F-actin disassembly. *Nature* **463**, 823-7 (2010). PMC3215588

56. Hung, R.J., Pak, C.W. & Terman, J.R. Direct redox regulation of F-actin assembly and disassembly by Mical. *Science* **334**, 1710-3 (2011). PMC3612955

57. Fremont, S., Romet-Lemonne, G., Houdusse, A. & Echard, A. Emerging roles of MICAL family proteins - from actin oxidation to membrane trafficking during cytokinesis. *J Cell Sci* **130**, 1509-1517 (2017).

58. Terman, J.R., Mao, T., Pasterkamp, R.J., Yu, H.H. & Kolodkin, A.L. MICALs, a family of conserved flavoprotein oxidoreductases, function in plexin-mediated axonal repulsion. *Cell* **109**, 887-900 (2002).

59. Boëda, B., Briggs, D.C., Higgins, T., Garvalov, B.K., Fadden, A.J., McDonald, N.Q. & Way, M. Tes, a Specific Mena Interacting Partner, Breaks the Rules for EVH1 Binding. *Molecular Cell* **28**, 1071-1082 (2007).

60. Deane, J.E., Ryan, D.P., Sunde, M., Maher, M.J., Guss, J.M., Visvader, J.E. & Matthews, J.M. Tandem LIM domains provide synergistic binding in the LMO4:Ldb1 complex. *EMBO J* **23**, 3589-98 (2004). PMC517615

61. Chang, D.F., Belaguli, N.S., Iyer, D., Roberts, W.B., Wu, S.P., Dong, X.R., Marx, J.G., Moore, M.S., Beckerle, M.C., Majesky, M.W. & Schwartz, R.J. Cysteine-rich LIM-only proteins CRP1 and CRP2 are potent smooth muscle differentiation cofactors. *Dev Cell* **4**, 107-18 (2003).

62. Burglin, T.R. & Affolter, M. Homeodomain proteins: an update. *Chromosoma* **125**, 497-521 (2016). PMC4901127

63. Mukhopadhyay, M., Teufel, A., Yamashita, T., Agulnick, A.D., Chen, L., Downs, K.M., Schindler, A., Grinberg, A., Huang, S.P., Dorward, D. & Westphal, H. Functional ablation of the mouse Ldb1 gene results in severe patterning defects during gastrulation. *Development* **130**, 495-505 (2003).

64. Matthews, J.M. & Visvader, J.E. LIM-domain-binding protein 1: a multifunctional cofactor that interacts with diverse proteins. *EMBO Rep* **4**, 1132-7 (2003). PMC1326422

65. Deane, J.E., Mackay, J.P., Kwan, A.H., Sum, E.Y., Visvader, J.E. & Matthews, J.M. Structural basis for the recognition of ldb1 by the N-terminal LIM domains of LMO2 and LMO4. *EMBO J* **22**, 2224-33 (2003). PMC156068

66. Hobert, O. & Westphal, H. Functions of LIM-homeobox genes. *Trends Genet* **16**, 75-83 (2000).

67. Ye, F. & Zhang, M. Structures and target recognition modes of PDZ domains: recurring themes and emerging pictures. *Biochem J* **455**, 1-14 (2013).

68. Cho, K.O., Hunt, C.A. & Kennedy, M.B. The rat brain postsynaptic density fraction contains a homolog of the Drosophila discs-large tumor suppressor protein. *Neuron* **9**, 929-42 (1992).

69. Itoh, M., Nagafuchi, A., Yonemura, S., Kitani-Yasuda, T., Tsukita, S. & Tsukita, S. The 220-kD protein colocalizing with cadherins in non-epithelial cells is identical to ZO-1, a tight junction-associated protein in epithelial cells: cDNA cloning and immunoelectron microscopy. *J Cell Biol* **121**, 491-502 (1993). PMC2119563

70. Woods, D.F. & Bryant, P.J. The discs-large tumor suppressor gene of Drosophila encodes a guanylate kinase homolog localized at septate junctions. *Cell* **66**, 451-64 (1991).

71. Nourry, C., Grant, S.G. & Borg, J.P. PDZ domain proteins: plug and play! *Sci STKE* **2003**, RE7 (2003).

72. Kennedy, M.B. Origin of PDZ (DHR, GLGF) domains. *Trends Biochem Sci* **20**, 350 (1995).

73. Christensen, N.R., Calyseva, J., Fernandes, E.F.A., Luchow, S., Clemmensen, L.S., Haugaard-Kedstrom, L.M. & Stromgaard, K. PDZ Domains as Drug Targets. *Adv Ther (Weinh)* **2**, 1800143 (2019). PMC7161847

74. Morais Cabral, J.H., Petosa, C., Sutcliffe, M.J., Raza, S., Byron, O., Poy, F., Marfatia, S.M., Chishti, A.H. & Liddington, R.C. Crystal structure of a PDZ domain. *Nature* **382**, 649-52 (1996).

75. Tonikian, R., Zhang, Y., Sazinsky, S.L., Currell, B., Yeh, J.-H., Reva, B., Held, H.A., Appleton, B.A., Evangelista, M., Wu, Y., Xin, X., Chan, A.C., Seshagiri, S., Lasky, L.A., Sander, C., Boone, C., Bader, G.D. & Sidhu, S.S. A Specificity Map for the PDZ Domain Family. **6**, e239 (2008).

76. Kornau, H.C., Schenker, L.T., Kennedy, M.B. & Seeburg, P.H. Domain interaction between NMDA receptor subunits and the postsynaptic density protein PSD-95. *Science* **269**, 1737-40 (1995).

77. Niethammer, M., Kim, E. & Sheng, M. Interaction between the C terminus of NMDA receptor subunits and multiple members of the PSD-95 family of membrane-associated guanylate kinases. *J Neurosci* **16**, 2157-63 (1996).

78. Hillier, B.J., Christopherson, K.S., Prehoda, K.E., Bredt, D.S. & Lim, W.A. Unexpected modes of PDZ domain scaffolding revealed by structure of nNOS-syntrophin complex. *Science* **284**, 812-5 (1999).

79. Zhang, Q., Fan, J.S. & Zhang, M. Interdomain chaperoning between PSD-95, Dlg, and Zo-1 (PDZ) domains of glutamate receptor-interacting proteins. *J Biol Chem* **276**, 43216-20 (2001).

80. Wong, H.C., Bourdelas, A., Krauss, A., Lee, H.J., Shao, Y., Wu, D., Mlodzik, M., Shi, D.L. & Zheng, J. Direct binding of the PDZ domain of Dishevelled to a conserved internal sequence in the C-terminal region of Frizzled. *Mol Cell* **12**, 1251-60 (2003). PMC4381837

81. Bhattacharya, S., Ju, J.H., Orlova, N., Khajeh, J.A., Cowburn, D. & Bu, Z. Ligand-induced dynamic changes in extended PDZ domains from NHERF1. *J Mol Biol* **425**, 2509-28 (2013). PMC4058784

82. Chi, C.N., Haq, S.R., Rinaldo, S., Dogan, J., Cutruzzola, F., Engstrom, A., Gianni, S., Lundstrom, P. & Jemth, P. Interactions outside the boundaries of the canonical binding groove of a PDZ domain influence ligand binding. *Biochemistry* **51**, 8971-9 (2012).

83. Doyle, D.A., Lee, A., Lewis, J., Kim, E., Sheng, M. & MacKinnon, R. Crystal Structures of a Complexed and Peptide-Free Membrane Protein–Binding Domain: Molecular Basis of Peptide Recognition by PDZ. *Cell* **85**, 1067-1076 (1996).

84. Mostarda, S., Gfeller, D. & Rao, F. Beyond the binding site: the role of the beta(2)-beta(3) loop and extra-domain structures in PDZ domains. *PLoS Comput Biol* **8**, e1002429 (2012). PMC3297566

85. Zhang, J., Petit, C.M., King, D.S. & Lee, A.L. Phosphorylation of a PDZ domain extension modulates binding affinity and interdomain interactions in postsynaptic density-95 (PSD-95) protein, a membrane-associated guanylate kinase (MAGUK). *J Biol Chem* **286**, 41776-85 (2011). PMC3308886

86. Doyle, D.A., Lee, A., Lewis, J., Kim, E., Sheng, M. & MacKinnon, R. Crystal structures of a complexed and peptide-free membrane protein-binding domain: molecular basis of peptide recognition by PDZ. *Cell* **85**, 1067-76 (1996).

87. Lee, H.J. & Zheng, J.J. PDZ domains and their binding partners: structure, specificity, and modification. *Cell Commun Signal* **8**, 8 (2010). PMC2891790

88. Kozlov, G., Gehring, K. & Ekiel, I. Solution structure of the PDZ2 domain from human phosphatase hPTP1E and its interactions with C-terminal peptides from the Fas receptor. *Biochemistry* **39**, 2572-80 (2000).

89. Tochio, H., Hung, F., Li, M., Bredt, D.S. & Zhang, M. Solution structure and backbone dynamics of the second PDZ domain of postsynaptic density-95. *J Mol Biol* **295**, 225-37 (2000).

90. Au, Y., Atkinson, R.A., Guerrini, R., Kelly, G., Joseph, C., Martin, S.R., Muskett, F.W., Pallavicini, A., Faulkner, G. & Pastore, A. Solution structure of ZASP PDZ domain; implications for sarcomere ultrastructure and enigma family redundancy. *Structure* **12**, 611-22 (2004).

91. De Los Rios, P., Cecconi, F., Pretre, A., Dietler, G., Michielin, O., Piazza, F. & Juanico, B. Functional dynamics of PDZ binding domains: a normal-mode analysis. *Biophys J* **89**, 14-21 (2005). PMC1366512

92. Grembecka, J., Cierpicki, T., Devedjiev, Y., Derewenda, U., Kang, B.S., Bushweller, J.H. & Derewenda, Z.S. The binding of the PDZ tandem of syntenin to target proteins. *Biochemistry* **45**, 3674-83 (2006).

93. Cierpicki, T., Bielnicki, J., Zheng, M., Gruszczyk, J., Kasterka, M., Petoukhov, M., Zhang, A., Fernandez, E.J., Svergun, D.I., Derewenda, U., Bushweller, J.H. & Derewenda, Z.S. The solution structure and dynamics of the DH-PH module of PDZRhoGEF in isolation and in complex with nucleotide-free RhoA. *Protein Sci* **18**, 2067-79 (2009). PMC2786971

94. Lee, I., Choi, S., Yun, J.H., Seo, S.H., Choi, S., Choi, K.Y. & Lee, W. Crystal structure of the PDZ domain of mouse Dishevelled 1 and its interaction with CXXC5. *Biochem Biophys Res Commun* **485**, 584-590 (2017).

95. Daniels, D.L., Cohen, A.R., Anderson, J.M. & Brunger, A.T. Crystal structure of the hCASK PDZ domain reveals the structural basis of class II PDZ domain target recognition. *Nat Struct Biol* **5**, 317-25 (1998).

96. Kalyoncu, S., Keskin, O. & Gursoy, A. Interaction prediction and classification of PDZ domains. *BMC Bioinformatics* **11**, 357 (2010). PMC2909223

97. van Ham, M. & Hendriks, W. PDZ domains-glue and guide. *Mol Biol Rep* **30**, 69-82 (2003).

98. Nourry, C., Grant, S.G.N. & Borg, J.-P. PDZ Domain Proteins: Plug and Play! *Science's STKE* **2003**, re7-re7 (2003).

99. Kay, B.K. & Kehoe, J.W. PDZ domains and their ligands. *Chem Biol* **11**, 423-5 (2004).

100. Jemth, P. & Gianni, S. PDZ domains: folding and binding. *Biochemistry* **46**, 8701-8 (2007).

101. Teyra, J., Sidhu, S.S. & Kim, P.M. Elucidation of the binding preferences of peptide recognition modules: SH3 and PDZ domains. *FEBS Lett* **586**, 2631-7 (2012).

102. Ivarsson, Y. Plasticity of PDZ domains in ligand recognition and signaling. *FEBS Lett* **586**, 2638-47 (2012).

103. Chi, C.N., Bach, A., Stromgaard, K., Gianni, S. & Jemth, P. Ligand binding by PDZ domains. *Biofactors* **38**, 338-48 (2012).

104. Songyang, Z., Fanning, A.S., Fu, C., Xu, J., Marfatia, S.M., Chishti, A.H., Crompton, A., Chan, A.C., Anderson, J.M. & Cantley, L.C. Recognition of unique carboxyl-terminal motifs by distinct PDZ domains. *Science* **275**, 73-7 (1997).

105. Stricker, N.L., Christopherson, K.S., Yi, B.A., Schatz, P.J., Raab, R.W., Dawes, G., Bassett, D.E., Jr., Bredt, D.S. & Li, M. PDZ domain of neuronal nitric oxide synthase recognizes novel C-terminal peptide sequences. *Nat Biotechnol* **15**, 336-42 (1997).

106. Elkins, J.M., Papagrigoriou, E., Berridge, G., Yang, X., Phillips, C., Gileadi, C., Savitsky, P. & Doyle, D.A. Structure of PICK1 and other PDZ domains obtained with the help of self-binding C-terminal extensions. *Protein Sci* **16**, 683-94 (2007). PMC2203335

107. Harris, B.Z., Hillier, B.J. & Lim, W.A. Energetic determinants of internal motif recognition by PDZ domains. *Biochemistry* **40**, 5921-30 (2001).

108. Karthikeyan, S., Leung, T., Birrane, G., Webster, G. & Ladias, J.A. Crystal structure of the PDZ1 domain of human Na(+)/H(+) exchanger regulatory factor provides insights into the mechanism of carboxyl-terminal leucine recognition by class I PDZ domains. *J Mol Biol* **308**, 963-73 (2001).

109. Hung, A.Y. & Sheng, M. PDZ domains: structural modules for protein complex assembly. *J Biol Chem* **277**, 5699-702 (2002).

110. Tyler, R.C., Peterson, F.C. & Volkman, B.F. Distal interactions within the par3-VE-cadherin complex. *Biochemistry* **49**, 951-7 (2010). PMC2819025

111. Kang, B.S., Cooper, D.R., Devedjiev, Y., Derewenda, U. & Derewenda, Z.S. Molecular roots of degenerate specificity in syntenin's PDZ2 domain: reassessment of the PDZ recognition paradigm. *Structure* **11**, 845-53 (2003).

112. Kock, G., Dicks, M., Yip, K.T., Kohl, B., Putz, S., Heumann, R., Erdmann, K.S. & Stoll, R. Molecular Basis of Class III Ligand Recognition by PDZ3 in Murine Protein Tyrosine Phosphatase PTPN13. *J Mol Biol* **430**, 4275-4292 (2018).

113. Ma, S., Song, E., Gao, S., Tian, R. & Gao, Y. Rapid characterization of the binding property of HtrA2/Omi PDZ domain by validation screening of PDZ ligand library. *Sci China C Life Sci* **50**, 412-22 (2007).

114. Fanning, A.S. & Anderson, J.M. Protein-protein interactions: PDZ domain networks. *Curr Biol* **6**, 1385-8 (1996).

115. Ponting, C.P., Phillips, C., Davies, K.E. & Blake, D.J. PDZ domains: targeting signalling molecules to sub-membranous sites. *Bioessays* **19**, 469-79 (1997).

116. Bezprozvanny, I. & Maximov, A. PDZ domains: More than just a glue. *Proc Natl Acad Sci U S A* **98**, 787-9 (2001). PMC33366

117. Harris, B.Z. & Lim, W.A. Mechanism and role of PDZ domains in signaling complex assembly. *J Cell Sci* **114**, 3219-31 (2001).

118. Gautier, C., Laursen, L., Jemth, P. & Gianni, S. Seeking allosteric networks in PDZ domains. *Protein Eng Des Sel* **31**, 367-373 (2018). PMC6508479

119. Levchenko, I., Smith, C.K., Walsh, N.P., Sauer, R.T. & Baker, T.A. PDZ-like domains mediate binding specificity in the Clp/Hsp100 family of chaperones and protease regulatory subunits. *Cell* **91**, 939-47 (1997).

120. Saras, J., Engstrom, U., Gonez, L.J. & Heldin, C.H. Characterization of the interactions between PDZ domains of the protein-tyrosine phosphatase PTPL1 and the carboxyl-terminal tail of Fas. *J Biol Chem* **272**, 20979-81 (1997).

121. Kim, E., DeMarco, S.J., Marfatia, S.M., Chishti, A.H., Sheng, M. & Strehler, E.E. Plasma membrane Ca2+ ATPase isoform 4b binds to membrane-associated

guanylate kinase (MAGUK) proteins via their PDZ (PSD-95/Dlg/ZO-1) domains. *J Biol Chem* **273**, 1591-5 (1998).

122. Fanning, A.S. & Anderson, J.M. PDZ domains and the formation of protein networks at the plasma membrane. *Curr Top Microbiol Immunol* **228**, 209-33 (1998).

123. Fanning, A.S. & Anderson, J.M. PDZ domains: fundamental building blocks in the organization of protein complexes at the plasma membrane. *J Clin Invest* **103**, 767-72 (1999). PMC408156

124. Kang, S., Xu, H., Duan, X., Liu, J.J., He, Z., Yu, F., Zhou, S., Meng, X.Q., Cao, M. & Kennedy, G.C. PCD1, a novel gene containing PDZ and LIM domains, is overexpressed in several human cancers. *Cancer Res* **60**, 5296-302 (2000).

125. Nakagawa, N., Hoshijima, M., Oyasu, M., Saito, N., Tanizawa, K. & Kuroda, S. ENH, containing PDZ and LIM domains, heart/skeletal muscle-specific protein, associates with cytoskeletal proteins through the PDZ domain. *Biochem Biophys Res Commun* **272**, 505-12 (2000).

126. Meerschaert, K., Bruyneel, E., De Wever, O., Vanloo, B., Boucherie, C., Bracke, M., Vandekerckhove, J. & Gettemans, J. The tandem PDZ domains of syntenin promote cell invasion. *Exp Cell Res* **313**, 1790-804 (2007).

127. Liu, X. & Fuentes, E.J. Chapter Five - Emerging Themes in PDZ Domain Signaling: Structure, Function, and Inhibition. in *International Review of Cell and Molecular Biology*, Vol. 343 (ed. Galluzzi, L.) 129-218 (Academic Press, 2019).

128. Penkert, R.R., Divittorio, H.M. & Prehoda, K.E. Internal recognition through PDZ domain plasticity in the Par-6–Pals1 complex. **11**, 1122-1127 (2004).

129. Mack, N.A., Porter, A.P., Whalley, H.J., Schwarz, J.P., Jones, R.C., Khaja, A.S.S., Bjartell, A., Anderson, K.I. & Malliri, A. β2-syntrophin and Par-3 promote an apicobasal Rac activity gradient at cell–cell junctions by differentially regulating Tiam1 activity. *Nature Cell Biology* **14**, 1169-1180 (2012).

130. Xia, H., Winokur, S.T., Kuo, W.L., Altherr, M.R. & Bredt, D.S. Actinin-associated LIM protein: identification of a domain interaction between PDZ and spectrin-like repeat motifs. *J Cell Biol* **139**, 507-15 (1997). PMC2139795

131. Maekawa, K., Imagawa, N., Naito, A., Harada, S., Yoshie, O. & Takagi, S. Association of protein-tyrosine phosphatase PTP-BAS with the transcription-

factor-inhibitory protein IkappaBalpha through interaction between the PDZ1 domain and ankyrin repeats. *Biochem J* **337 (Pt 2)**, 179-84 (1999). PMC1219950

132. Wu, H., Feng, W., Chen, J., Chan, L.N., Huang, S. & Zhang, M. PDZ domains of Par-3 as potential phosphoinositide signaling integrators. *Mol Cell* **28**, 886-98 (2007).

133. Feng, W., Shi, Y., Li, M. & Zhang, M. Tandem PDZ repeats in glutamate receptor-interacting proteins have a novel mode of PDZ domain-mediated target binding. *Nat Struct Biol* **10**, 972-8 (2003).

134. Cousido-Siah, A., Carneiro, L., Kostmann, C., Ecsedi, P., Nyitray, L., Trave, G. & Gogl, G. A scalable strategy to solve structures of PDZ domains and their complexes. *Acta Crystallogr D Struct Biol* **78**, 509-516 (2022).

135. El-Amraoui, A. & Petit, C. Usher I syndrome: unravelling the mechanisms that underlie the cohesion of the growing hair bundle in inner ear sensory cells. *J Cell Sci* **118**, 4593-603 (2005).

136. Yan, J., Pan, L., Chen, X., Wu, L. & Zhang, M. The structure of the harmonin/sans complex reveals an unexpected interaction mode of the two Usher syndrome proteins. *Proc Natl Acad Sci U S A* **107**, 4040-5 (2010). PMC2840103

137. Feng, W., Wu, H., Chan, L.N. & Zhang, M. Par-3-mediated junctional localization of the lipid phosphatase PTEN is required for cell polarity establishment. *J Biol Chem* **283**, 23440-9 (2008).

138. Whitney, D.S., Peterson, F.C., Kittell, A.W., Egner, J.M., Prehoda, K.E. & Volkman, B.F. Binding of Crumbs to the Par-6 CRIB-PDZ Module Is Regulated by Cdc42. *Biochemistry* **55**, 1455-61 (2016). PMC5433836

139. Whitney, D.S., Peterson, F.C. & Volkman, B.F. A conformational switch in the CRIB-PDZ module of Par-6. *Structure* **19**, 1711-22 (2011). PMC3217198

140. Baiesi, M., Orlandini, E., Trovato, A. & Seno, F. Linking in domain-swapped protein dimers. *Sci Rep* **6**, 33872 (2016). PMC5034241

141. Chen, J., Pan, L., Wei, Z., Zhao, Y. & Zhang, M. Domain-swapped dimerization of ZO-1 PDZ2 generates specific and regulatory connexin43-binding sites. *EMBO J* **27**, 2113-23 (2008). PMC2516886

142. Solan, J.L. & Lampe, P.D. Connexin phosphorylation as a regulatory event linked to gap junction channel assembly. *Biochim Biophys Acta* **1711**, 154-63 (2005).

143. Chung, H.J., Xia, J., Scannevin, R.H., Zhang, X. & Huganir, R.L. Phosphorylation of the AMPA receptor subunit GluR2 differentially regulates its interaction with PDZ domain-containing proteins. *J Neurosci* **20**, 7258-67 (2000). PMC6772789

144. Koo, B.K., Jung, Y.S., Shin, J., Han, I., Mortier, E., Zimmermann, P., Whiteford, J.R., Couchman, J.R., Oh, E.S. & Lee, W. Structural basis of syndecan-4 phosphorylation as a molecular switch to regulate signaling. *J Mol Biol* **355**, 651-63 (2006).

145. Lau, A.G. & Hall, R.A. Oligomerization of NHERF-1 and NHERF-2 PDZ domains: differential regulation by association with receptor carboxyl-termini and by phosphorylation. *Biochemistry* **40**, 8572-80 (2001).

146. Lin, D.T. & Huganir, R.L. PICK1 and phosphorylation of the glutamate receptor 2 (GluR2) AMPA receptor subunit regulates GluR2 recycling after NMDA receptor-induced internalization. *J Neurosci* **27**, 13903-8 (2007). PMC6673624

147. Sulka, B., Lortat-Jacob, H., Terreux, R., Letourneur, F. & Rousselle, P. Tyrosine dephosphorylation of the syndecan-1 PDZ binding domain regulates syntenin-1 recruitment. *J Biol Chem* **284**, 10659-71 (2009). PMC2667753

148. Long, J.F., Feng, W., Wang, R., Chan, L.N., Ip, F.C., Xia, J., Ip, N.Y. & Zhang, M. Autoinhibition of X11/Mint scaffold proteins revealed by the closed conformation of the PDZ tandem. *Nat Struct Mol Biol* **12**, 722-8 (2005).

149. Stevens, A.O. & He, Y. Allosterism in the PDZ Family. *Int J Mol Sci* **23**(2022). PMC8836106

150. Peterson, F.C., Penkert, R.R., Volkman, B.F. & Prehoda, K.E. Cdc42 regulates the Par-6 PDZ domain through an allosteric CRIB-PDZ transition. *Mol Cell* **13**, 665-76 (2004).

151. Penkert, R.R., DiVittorio, H.M. & Prehoda, K.E. Internal recognition through PDZ domain plasticity in the Par-6-Pals1 complex. *Nat Struct Mol Biol* **11**, 1122-7 (2004). PMC2140275

152. Stiffler, M.A., Chen, J.R., Grantcharova, V.P., Lei, Y., Fuchs, D., Allen, J.E., Zaslavskaia, L.A. & Macbeath, G. PDZ Domain Binding Selectivity Is Optimized Across the Mouse Proteome. **317**, 364-369 (2007).

153. Ivarsson, Y., Arnold, R., McLaughlin, M., Nim, S., Joshi, R., Ray, D., Liu, B., Teyra, J., Pawson, T., Moffat, J., Li, S.S.C., Sidhu, S.S. & Kim, P.M. Large-scale

interaction profiling of PDZ domains through proteomic peptide-phage display using human and viral phage peptidomes. **111**, 2542-2547 (2014).

154. Gogl, G., Zambo, B., Kostmann, C., Cousido-Siah, A., Morlet, B., Durbesson, F., Negroni, L., Eberling, P., Jane, P., Nomine, Y., Zeke, A., Ostergaard, S., Monsellier, E., Vincentelli, R. & Trave, G. Quantitative fragmentomics allow affinity mapping of interactomes. *Nat Commun* **13**, 5472 (2022). PMC9482650

155. Ritchey, L., Ottman, R., Roumanos, M. & Chakrabarti, R. A functional cooperativity between Aurora A kinase and LIM kinase1: implication in the mitotic process. *Cell Cycle* **11**, 296-309 (2012). PMC3293380

156. Nadella, K.S., Saji, M., Jacob, N.K., Pavel, E., Ringel, M.D. & Kirschner, L.S. Regulation of actin function by protein kinase A-mediated phosphorylation of Limk1. *EMBO Rep* **10**, 599-605 (2009). PMC2711837

157. Kobayashi, M., Nishita, M., Mishima, T., Ohashi, K. & Mizuno, K. MAPKAPK-2-mediated LIM-kinase activation is critical for VEGF-induced actin remodeling and cell migration. *EMBO J* **25**, 713-26 (2006). PMC1383554

158. (!!! INVALID CITATION !!! {}).

159. Hunter, T. A thousand and one protein kinases. *Cell* **50**, 823-9 (1987).

160. Hunter, T. Protein kinase classification. *Methods Enzymol* **200**, 3-37 (1991).

161. Hunter, T. Protein kinases and phosphatases: the yin and yang of protein phosphorylation and signaling. *Cell* **80**, 225-36 (1995).

162. Endicott, J.A., Noble, M.E. & Johnson, L.N. The structural basis for control of eukaryotic protein kinases. *Annu Rev Biochem* **81**, 587-613 (2012).

163. Giese, K.P. & Mizuno, K. The roles of protein kinases in learning and memory. *Learn Mem* **20**, 540-52 (2013).

164. Bhullar, K.S., Lagaron, N.O., McGowan, E.M., Parmar, I., Jha, A., Hubbard, B.P. & Rupasinghe, H.P.V. Kinase-targeted cancer therapies: progress, challenges and future directions. *Mol Cancer* **17**, 48 (2018). PMC5817855

165. Johnson, L.N., Noble, M.E.M. & Owen, D.J. Active and Inactive Protein Kinases: Structural Basis for Regulation. *Cell* **85**, 149-158 (1996).

166. Taylor, S.S. & Radzio-Andzelm, E. Three protein kinase structures define a common motif. **2**, 345-355 (1994).

167. Nolen, B., Taylor, S. & Ghosh, G. Regulation of Protein Kinases: Controlling Activity through Activation Segment Conformation. *Molecular Cell* **15**, 661-675 (2004).

168. Kornev, A.P., Haste, N.M., Taylor, S.S. & Eyck, L.F. Surface comparison of active and inactive protein kinases identifies a conserved activation mechanism. *Proc Natl Acad Sci U S A* **103**, 17783-8 (2006). PMC1693824

169. Taylor, S.S., Radzio-Andzelm, E. & Hunter, T. How do protein kinases discriminate between serine/threonine and tyrosine? Structural insights from the insulin receptor protein-tyrosine kinase. *FASEB J* **9**, 1255-66 (1995).

170. Hubbard, S.R. & Till, J.H. Protein tyrosine kinase structure and function. *Annu Rev Biochem* **69**, 373-98 (2000).

171. Remenyi, A., Good, M.C. & Lim, W.A. Docking interactions in protein kinase and phosphatase networks. *Curr Opin Struct Biol* **16**, 676-85 (2006).

172. Johnson, S.A. & Hunter, T. Kinomics: methods for deciphering the kinome. *Nat Methods* **2**, 17-25 (2005).

173. Pike, A.C., Rellos, P., Niesen, F.H., Turnbull, A., Oliver, A.W., Parker, S.A., Turk, B.E., Pearl, L.H. & Knapp, S. Activation segment dimerization: a mechanism for kinase autophosphorylation of non-consensus sites. *EMBO J* **27**, 704-14 (2008). PMC2239268

174. Zheng, J., Trafny, E.A., Knighton, D.R., Xuong, N.H., Taylor, S.S., Ten Eyck, L.F. & Sowadski, J.M. 2.2 A refined crystal structure of the catalytic subunit of cAMP-dependent protein kinase complexed with MnATP and a peptide inhibitor. *Acta Crystallogr D Biol Crystallogr* **49**, 362-5 (1993).

175. Kornev, A.P., Taylor, S.S. & Ten Eyck, L.F. A helix scaffold for the assembly of active protein kinases. *Proc Natl Acad Sci U S A* **105**, 14377-82 (2008). PMC2533684

176. Chen, C., Ha, B.H., Thevenin, A.F., Lou, H.J., Zhang, R., Yip, K.Y., Peterson, J.R., Gerstein, M., Kim, P.M., Filippakopoulos, P., Knapp, S., Boggon, T.J. & Turk, B.E. Identification of a major determinant for serine-threonine kinase phosphoacceptor specificity. *Mol Cell* **53**, 140-7 (2014). PMC3898841

177. Lindberg, R.A., Quinn, A.M. & Hunter, T. Dual-specificity protein kinases: will any hydroxyl do? *Trends Biochem Sci* **17**, 114-9 (1992).

178. Kannan, N. & Neuwald, A.F. Evolutionary constraints associated with functional specificity of the CMGC protein kinases MAPK, CDK, GSK, SRPK, DYRK, and CK2alpha. *Protein Sci* **13**, 2059-77 (2004). PMC2279817

179. Ohashi, K., Nagata, K., Maekawa, M., Ishizaki, T., Narumiya, S. & Mizuno, K. Rho-associated kinase ROCK activates LIM-kinase 1 by phosphorylation at threonine 508 within the activation loop. *J Biol Chem* **275**, 3577-82 (2000).

180. Sumi, T., Matsumoto, K., Shibuya, A. & Nakamura, T. Activation of LIM kinases by myotonic dystrophy kinase-related Cdc42-binding kinase alpha. *J Biol Chem* **276**, 23092-6 (2001).

181. Dan, C., Kelly, A., Bernard, O. & Minden, A. Cytoskeletal changes regulated by the PAK4 serine/threonine kinase are mediated by LIM kinase 1 and cofilin. *J Biol Chem* **276**, 32115-21 (2001).

182. Endo, M., Ohashi, K., Sasaki, Y., Goshima, Y., Niwa, R., Uemura, T. & Mizuno, K. Control of growth cone motility and morphology by LIM kinase and Slingshot via phosphorylation and dephosphorylation of cofilin. *J Neurosci* **23**, 2527-37 (2003).

183. Ohashi, K., Sampei, K., Nakagawa, M., Uchiumi, N., Amanuma, T., Aiba, S., Oikawa, M. & Mizuno, K. Damnacanthal, an effective inhibitor of LIM-kinase, inhibits cell migration and invasion. *Mol Biol Cell* **25**, 828-40 (2014). PMC3952852

184. Raymond, K., Bergeret, E., Avet-Rochex, A., Griffin-Shea, R. & Fauvarque, M.O. A screen for modifiers of RacGAP(84C) gain-of-function in the Drosophila eye revealed the LIM kinase Cdi/TESK1 as a downstream effector of Rac1 during spermatogenesis. *J Cell Sci* **117**, 2777-89 (2004).

185. Salah, E., Chatterjee, D., Beltrami, A., Tumber, A., Preuss, F., Canning, P., Chaikuad, A., Knaus, P., Knapp, S., Bullock, A.N. & Mathea, S. Lessons from LIMK1 enzymology and their impact on inhibitor design. *Biochem J* **476**, 3197-3209 (2019). PMC6835155

186. Hamill, S., Lou, H.J., Turk, B.E. & Boggon, T.J. Structural Basis for Noncanonical Substrate Recognition of Cofilin/ADF Proteins by LIM Kinases. *Mol Cell* **62**, 397-408 (2016). PMC4860616

187. Yang, N., Higuchi, O. & Mizuno, K. Cytoplasmic localization of LIM-kinase 1 is directed by a short sequence within the PDZ domain. *Exp Cell Res* **241**, 242-52 (1998).

188. Goyal, P., Pandey, D. & Siess, W. Phosphorylation-dependent regulation of unique nuclear and nucleolar localization signals of LIM kinase 2 in endothelial cells. *J Biol Chem* **281**, 25223-30 (2006).

189. Yang, N., Higuchi, O., Ohashi, K., Nagata, K., Wada, A., Kangawa, K., Nishida, E. & Mizuno, K. Cofilin phosphorylation by LIM-kinase 1 and its role in Rac-mediated actin reorganization. *Nature* **393**, 809-12 (1998).

190. Takahashi, H., Koshimizu, U. & Nakamura, T. A novel transcript encoding truncated LIM kinase 2 is specifically expressed in male germ cells undergoing meiosis. *Biochem Biophys Res Commun* **249**, 138-45 (1998).

191. Vallee, B., Cuberos, H., Doudeau, M., Godin, F., Gosset, D., Vourc'h, P., Andres, C.R. & Benedetti, H. LIMK2-1, a new isoform of human LIMK2, regulates actin cytoskeleton remodeling via a different signaling pathway than that of its two homologs, LIMK2a and LIMK2b. *Biochem J* **475**, 3745-3761 (2018).

192. Ohashi, K. Roles of cofilin in development and its mechanisms of regulation. *Dev Growth Differ* **57**, 275-90 (2015).

193. Wang, W., Yang, C., Nie, H., Qiu, X., Zhang, L., Xiao, Y., Zhou, W., Zeng, Q., Zhang, X., Wu, Y., Liu, J. & Ying, M. LIMK2 acts as an oncogene in bladder cancer and its functional SNP in the microRNA-135a binding site affects bladder cancer risk. *Int J Cancer* **144**, 1345-1355 (2019). PMC6587996

194. McConnell, B.V., Koto, K. & Gutierrez-Hartmann, A. Nuclear and cytoplasmic LIMK1 enhances human breast cancer progression. *Mol Cancer* **10**, 75 (2011). PMC3131252

195. Li, R., Doherty, J., Antonipillai, J., Chen, S., Devlin, M., Visser, K., Baell, J., Street, I., Anderson, R.L. & Bernard, O. LIM kinase inhibition reduces breast cancer growth and invasiveness but systemic inhibition does not reduce metastasis in mice. *Clin Exp Metastasis* **30**, 483-95 (2013).

196. Heredia, L., Helguera, P., de Olmos, S., Kedikian, G., Sola Vigo, F., LaFerla, F., Staufenbiel, M., de Olmos, J., Busciglio, J., Caceres, A. & Lorenzo, A. Phosphorylation of actin-depolymerizing factor/cofilin by LIM-kinase mediates amyloid beta-induced degeneration: a potential mechanism of neuronal dystrophy in Alzheimer's disease. *J Neurosci* **26**, 6533-42 (2006). PMC6674046

197. Cuberos, H., Vallee, B., Vourc'h, P., Tastet, J., Andres, C.R. & Benedetti, H. Roles of LIM kinases in central nervous system function and dysfunction. *FEBS Lett* **589**, 3795-806 (2015).

198. Chen, Q., Gimple, R.C., Li, G., Chen, J., Wu, H., Li, R., Xie, J. & Xu, B. LIM kinase 1 acts as a profibrotic mediator in permanent atrial fibrillation patients with valvular heart disease. *J Biosci* **44**(2019).

199. Chen, J., Ananthanarayanan, B., Springer, K.S., Wolf, K.J., Sheyman, S.M., Tran, V.D. & Kumar, S. Suppression of LIM Kinase 1 and LIM Kinase 2 Limits Glioblastoma Invasion. *Cancer Res* **80**, 69-78 (2020). PMC6942638

200. Ben Zablah, Y., Zhang, H., Gugustea, R. & Jia, Z. LIM-Kinases in Synaptic Plasticity, Memory, and Brain Diseases. *Cells* **10**(2021). PMC8391678

201. Aggelou, H., Chadla, P., Nikou, S., Karteri, S., Maroulis, I., Kalofonos, H.P., Papadaki, H. & Bravou, V. LIMK/cofilin pathway and Slingshot are implicated in human colorectal cancer progression and chemoresistance. *Virchows Arch* **472**, 727-737 (2018).

202. Zhang, R.Y., Ding, Y.M. & Zhang, L.H. [LIM kinases and their roles in the nervous system]. *Zhejiang Da Xue Xue Bao Yi Xue Ban* **43**, 119-25 (2014).

203. Tassabehji, M., Metcalfe, K., Fergusson, W.D., Carette, M.J., Dore, J.K., Donnai, D., Read, A.P., Proschel, C., Gutowski, N.J., Mao, X. & Sheer, D. LIM-kinase deleted in Williams syndrome. *Nat Genet* **13**, 272-3 (1996).

204. Osborne, L.R., Martindale, D., Scherer, S.W., Shi, X.M., Huizenga, J., Heng, H.H., Costa, T., Pober, B., Lew, L., Brinkman, J., Rommens, J., Koop, B. & Tsui, L.C. Identification of genes from a 500-kb region at 7q11.23 that is commonly deleted in Williams syndrome patients. *Genomics* **36**, 328-36 (1996).

205. Monaco, A.P. Human genetics: dissecting Williams syndrome. *Curr Biol* **6**, 1396-8 (1996).

206. Meng, Y., Zhang, Y., Tregoubov, V., Janus, C., Cruz, L., Jackson, M., Lu, W.Y., MacDonald, J.F., Wang, J.Y., Falls, D.L. & Jia, Z. Abnormal spine morphology and enhanced LTP in LIMK-1 knockout mice. *Neuron* **35**, 121-33 (2002).

207. Hoogenraad, C.C., Akhmanova, A., Galjart, N. & De Zeeuw, C.I. LIMK1 and CLIP-115: linking cytoskeletal defects to Williams syndrome. *Bioessays* **26**, 141-50 (2004).

208. Gregory, M.D., Mervis, C.B., Elliott, M.L., Kippenhan, J.S., Nash, T., J, B.C., Prabhakaran, R., Roe, K., Eisenberg, D.P., Kohn, P.D. & Berman, K.F. Williams syndrome hemideletion and LIMK1 variation both affect dorsal stream functional connectivity. *Brain* **142**, 3963-3974 (2019). PMC6906590

209. Frangiskakis, J.M., Ewart, A.K., Morris, C.A., Mervis, C.B., Bertrand, J., Robinson, B.F., Klein, B.P., Ensing, G.J., Everett, L.A., Green, E.D., Proschel, C., Gutowski, N.J., Noble, M., Atkinson, D.L., Odelberg, S.J. & Keating, M.T. LIM-kinase1 hemizygosity implicated in impaired visuospatial constructive cognition. *Cell* **86**, 59-69 (1996).

210. Takahashi, H., Funakoshi, H. & Nakamura, T. LIM-kinase as a regulator of actin dynamics in spermatogenesis. *Cytogenet Genome Res* **103**, 290-8 (2003).

211. Acevedo, K., Moussi, N., Li, R., Soo, P. & Bernard, O. LIM kinase 2 is widely expressed in all tissues. *J Histochem Cytochem* **54**, 487-501 (2006).

212. Lee-Hoeflich, S.T., Causing, C.G., Podkowa, M., Zhao, X., Wrana, J.L. & Attisano, L. Activation of LIMK1 by binding to the BMP receptor, BMPRII, regulates BMP-dependent dendritogenesis. *The EMBO Journal* **23**, 4792-4801 (2004).

213. Mukhopadhyay, S., Chatterjee, A., Kogan, D., Patel, D. & Foster, D.A. 5-Aminoimidazole-4-carboxamide-1-beta-4-ribofuranoside (AICAR) enhances the efficacy of rapamycin in human cancer cells. *Cell Cycle* **14**, 3331-9 (2015). PMC4825547

214. Wang, W., Mouneimne, G., Sidani, M., Wyckoff, J., Chen, X., Makris, A., Goswami, S., Bresnick, A.R. & Condeelis, J.S. The activity status of cofilin is directly related to invasion, intravasation, and metastasis of mammary tumors. *J Cell Biol* **173**, 395-404 (2006). PMC2063840

215. Mardilovich, K., Gabrielsen, M., McGarry, L., Orange, C., Patel, R., Shanks, E., Edwards, J. & Olson, M.F. Elevated LIM kinase 1 in nonmetastatic prostate cancer reflects its role in facilitating androgen receptor nuclear translocation. *Mol Cancer Ther* **14**, 246-58 (2015). PMC4297197

216. Tapia, T., Ottman, R. & Chakrabarti, R. LIM kinase1 modulates function of membrane type matrix metalloproteinase 1: implication in invasion of prostate cancer cells. *Mol Cancer* **10**, 6 (2011). PMC3027192

217. Bagheri-Yarmand, R., Mazumdar, A., Sahin, A.A. & Kumar, R. LIM kinase 1 increases tumor metastasis of human breast cancer cells via regulation of the urokinase-type plasminogen activator system. *Int J Cancer* **118**, 2703-10 (2006).

218. Davila, M., Frost, A.R., Grizzle, W.E. & Chakrabarti, R. LIM kinase 1 is essential for the invasive growth of prostate epithelial cells: implications in prostate cancer. *J Biol Chem* **278**, 36868-75 (2003).

219. Yang, J.Z., Huang, L.H., Chen, R., Meng, L.J., Gao, Y.Y., Ji, Q.Y. & Wang, Y. LIM kinase 1 serves an important role in the multidrug resistance of osteosarcoma cells. *Oncol Lett* **15**, 250-256 (2018). PMC5768095

220. Finn, R. LIM kinase appears critical in metastasis, but how? *J Natl Cancer Inst* **93**, 88-9 (2001).

221. Prunier, C., Josserand, V., Vollaire, J., Beerling, E., Petropoulos, C., Destaing, O., Montemagno, C., Hurbin, A., Prudent, R., de Koning, L., Kapur, R., Cohen, P.A., Albiges-Rizo, C., Coll, J.L., van Rheenen, J., Billaud, M. & Lafanechere, L. LIM Kinase Inhibitor Pyr1 Reduces the Growth and Metastatic Load of Breast Cancers. *Cancer Res* **76**, 3541-52 (2016).

222. Mardilovich, K., Baugh, M., Crighton, D., Kowalczyk, D., Gabrielsen, M., Munro, J., Croft, D.R., Lourenco, F., James, D., Kalna, G., McGarry, L., Rath, O., Shanks, E., Garnett, M.J., McDermott, U., Brookfield, J., Charles, M., Hammonds, T. & Olson, M.F. LIM kinase inhibitors disrupt mitotic microtubule organization and impair tumor cell proliferation. *Oncotarget* **6**, 38469-86 (2015). PMC4770715

223. Manetti, F. LIM kinases are attractive targets with many macromolecular partners and only a few small molecule regulators. *Med Res Rev* **32**, 968-98 (2012).

224. Scott, R.W., Hooper, S., Crighton, D., Li, A., Konig, I., Munro, J., Trivier, E., Wickman, G., Morin, P., Croft, D.R., Dawson, J., Machesky, L., Anderson, K.I., Sahai, E.A. & Olson, M.F. LIM kinases are required for invasive path generation by tumor and tumor-associated stromal cells. *J Cell Biol* **191**, 169-85 (2010). PMC2953444

225. Vlecken, D.H. & Bagowski, C.P. LIMK1 and LIMK2 are important for metastatic behavior and tumor cell-induced angiogenesis of pancreatic cancer cells. *Zebrafish* **6**, 433-9 (2009).

226. Johnson, E.O., Chang, K.-H., Ghosh, S., Venkatesh, C., Giger, K., Low, P.S. & Shah, K. LIMK2 is a crucial regulator and effector of Aurora-A-kinase-mediated malignancy. *Journal of Cell Science* **125**, 1204-1216 (2012).

227. Jang, I., Jeon, B.T., Jeong, E.A., Kim, E.J., Kang, D., Lee, J.S., Jeong, B.G., Kim, J.H., Choi, B.H., Lee, J.E., Kim, J.W., Choi, J.Y. & Roh, G.S. Pak1/LIMK1/Cofilin Pathway Contributes to Tumor Migration and Invasion in Human Non-Small Cell Lung Carcinomas and Cell Lines. *Korean J Physiol Pharmacol* **16**, 159-65 (2012). PMC3394917

228. Su, Y., Xu, B., Shen, Q., Lei, Z., Zhang, W. & Hu, T. LIMK2 Is a Novel Prognostic Biomarker and Correlates With Tumor Immune Cell Infiltration in Lung Squamous Cell Carcinoma. *Front Immunol* **13**, 788375 (2022). PMC8902256

229. Misra, U.K., Deedwania, R. & Pizzo, S.V. Binding of activated alpha2-macroglobulin to its cell surface receptor GRP78 in 1-LN prostate cancer cells regulates PAK-2-dependent activation of LIMK. *J Biol Chem* **280**, 26278-86 (2005). PMC1201553

230. Liao, Q., Li, R., Zhou, R., Pan, Z., Xu, L., Ding, Y. & Zhao, L. LIM kinase 1 interacts with myosin-9 and alpha-actinin-4 and promotes colorectal cancer progression. *Br J Cancer* **117**, 563-571 (2017). PMC5558682

231. Sadok, A. & Marshall, C.J. Rho GTPases: masters of cell migration. *Small GTPases* **5**, e29710 (2014). PMC4107589

232. Etienne-Manneville, S. & Hall, A. Rho GTPases in cell biology. *Nature* **420**, 629-35 (2002).

233. Sit, S.-T. & Manser, E. Rho GTPases and their role in organizing the actin cytoskeleton. *Journal of Cell Science* **124**, 679-683 (2011).

234. Lee, I.C., Leung, T. & Tan, I. Adaptor protein LRAP25 mediates myotonic dystrophy kinase-related Cdc42-binding kinase (MRCK) regulation of LIMK1 protein in lamellipodial F-actin dynamics. *J Biol Chem* **289**, 26989-7003 (2014). PMC4175338

235. Nobes, C.D. & Hall, A. Rho, rac, and cdc42 GTPases regulate the assembly of multimolecular focal complexes associated with actin stress fibers, lamellipodia, and filopodia. *Cell* **81**, 53-62 (1995).

236. Tapon, N. & Hall, A. Rho, Rac and Cdc42 GTPases regulate the organization of the actin cytoskeleton. *Curr Opin Cell Biol* **9**, 86-92 (1997).

237. Edwards, D.C., Sanders, L.C., Bokoch, G.M. & Gill, G.N. Activation of LIM-kinase by Pak1 couples Rac/Cdc42 GTPase signalling to actin cytoskeletal dynamics. *Nat Cell Biol* **1**, 253-9 (1999).

238. Manser, E., Leung, T., Salihuddin, H., Zhao, Z.S. & Lim, L. A brain serine/threonine protein kinase activated by Cdc42 and Rac1. *Nature* **367**, 40-6 (1994).

239. Knaus, U.G., Morris, S., Dong, H.J., Chernoff, J. & Bokoch, G.M. Regulation of human leukocyte p21-activated kinases through G protein--coupled receptors. *Science* **269**, 221-3 (1995).

240. Maekawa, M. Signaling from Rho to the Actin Cytoskeleton Through Protein Kinases ROCK and LIM-kinase. *Science* **285**, 895-898 (1999).

241. Sumi, T., Matsumoto, K., Takai, Y. & Nakamura, T. Cofilin phosphorylation and actin cytoskeletal dynamics regulated by rho- and Cdc42-activated LIM-kinase 2. *J Cell Biol* **147**, 1519-32 (1999). PMC2174243

242. Leung, T., Chen, X.Q., Tan, I., Manser, E. & Lim, L. Myotonic dystrophy kinase-related Cdc42-binding kinase acts as a Cdc42 effector in promoting cytoskeletal reorganization. *Mol Cell Biol* **18**, 130-40 (1998). PMC121465

243. Zhao, Z. & Manser, E. Myotonic dystrophy kinase-related Cdc42-binding kinases (MRCK), the ROCK-like effectors of Cdc42 and Rac1. *Small GTPases* **6**, 81-8 (2015). PMC4601156

244. Theriot, J.A. Accelerating on a treadmill: ADF/cofilin promotes rapid actin filament turnover in the dynamic cytoskeleton. *J Cell Biol* **136**, 1165-8 (1997). PMC2132515

245. McGough, A., Pope, B. & Weeds, A. The ADF/cofilin family: accelerators of actin reorganization. *Results Probl Cell Differ* **32**, 135-54 (2001).

246. Andrianantoandro, E. & Pollard, T.D. Mechanism of actin filament turnover by severing and nucleation at different concentrations of ADF/cofilin. *Mol Cell* **24**, 13-23 (2006).

247. De La Cruz, E.M. How cofilin severs an actin filament. *Biophys Rev* **1**, 51-59 (2009). PMC2917815

248. Elam, W.A., Kang, H. & De la Cruz, E.M. Biophysics of actin filament severing by cofilin. *FEBS Lett* **587**, 1215-9 (2013). PMC4079045

249. Bamburg, J.R., McGough, A. & Ono, S. Putting a new twist on actin: ADF/cofilins modulate actin dynamics. *Trends Cell Biol* **9**, 364-70 (1999).

250. Pollard, T.D. Actin and Actin-Binding Proteins. *Cold Spring Harb Perspect Biol* **8**(2016). PMC4968159

251. Arber, S., Barbayannis, F.A., Hanser, H., Schneider, C., Stanyon, C.A., Bernard, O. & Caroni, P. Regulation of actin dynamics through phosphorylation of cofilin by LIM-kinase. *Nature* **393**, 805-9 (1998).

252. Prunier, C., Prudent, R., Kapur, R., Sadoul, K. & Lafanechere, L. LIM kinases: cofilin and beyond. *Oncotarget* **8**, 41749-41763 (2017). PMC5522193

253. Agnew, B.J., Minamide, L.S. & Bamburg, J.R. Reactivation of phosphorylated actin depolymerizing factor and identification of the regulatory site. *Journal of Biological Chemistry* **270**, 17582-17587 (1995).

254. Kanamori, T., Suzuki, M. & Titani, K. Complete amino acid sequences and phosphorylation sites, determined by Edman degradation and mass spectrometry, of rat parotid destrin- and cofilin-like proteins. *Arch Oral Biol* **43**, 955-67 (1998).

255. Bamburg, J.R. Proteins of the ADF/cofilin family: Essential regulators of actin dynamics. in *Annual Review of Cell and Developmental Biology* Vol. 15 185-230 (1999).

256. Niwa, R., Nagata-Ohashi, K., Takeichi, M., Mizuno, K. & Uemura, T. Control of actin reorganization by Slingshot, a family of phosphatases that dephosphorylate ADF/cofilin. *Cell* **108**, 233-46 (2002).

257. Ohta, Y., Kousaka, K., Nagata-Ohashi, K., Ohashi, K., Muramoto, A., Shima, Y., Niwa, R., Uemura, T. & Mizuno, K. Differential activities, subcellular distribution and tissue expression patterns of three members of Slingshot family phosphatases that dephosphorylate cofilin. *Genes Cells* **8**, 811-24 (2003).

258. Soosairajah, J., Maiti, S., Wiggan, O., Sarmiere, P., Moussi, N., Sarcevic, B., Sampath, R., Bamburg, J.R. & Bernard, O. Interplay between components of a novel LIM kinase-slingshot phosphatase complex regulates cofilin. *EMBO J* **24**, 473-86 (2005). PMC548651

259. Yang, E.J., Yoon, J.H., Min, D.S. & Chung, K.C. LIM kinase 1 activates cAMP-responsive element-binding protein during the neuronal differentiation of immortalized hippocampal progenitor cells. *J Biol Chem* **279**, 8903-10 (2004).

260. Remacle, A. Membrane type I-matrix metalloproteinase (MT1-MMP) is internalised by two different pathways and is recycled to the cell surface. *Journal of Cell Science* **116**, 3905-3916 (2003).

261. Knapinska, A.M. & Fields, G.B. The Expanding Role of MT1-MMP in Cancer Progression. *Pharmaceuticals (Basel)* **12**(2019). PMC6630478

262. Foletta, V.C., Lim, M.A., Soosairajah, J., Kelly, A.P., Stanley, E.G., Shannon, M., He, W., Das, S., Massagué, J. & Bernard, O. Direct signaling by the BMP type II receptor via the cytoskeletal regulator LIMK1. **162**, 1089-1098 (2003).

263. Aihara, S., Fujimoto, S., Sakaguchi, R. & Imai, T. BMPR-2 gates activity-dependent stabilization of primary dendrites during mitral cell remodeling. *Cell Rep* **35**, 109276 (2021).

264. Tan, I., Yong, J., Dong, J.M., Lim, L. & Leung, T. A Tripartite Complex Containing MRCK Modulates Lamellar Actomyosin Retrograde Flow. **135**, 123-136 (2008).

265. Cao, J.-M., Cheng, X.-N., Li, S.-Q., Heller, S., Xu, Z.-G. & Shi, D.-L. Identification of novel MYO18A interaction partners required for myoblast adhesion and muscle integrity. **6**, 36768 (2016).

266. Kremer, D., Heinen, A., Jadasz, J., Gottle, P., Zimmermann, K., Zickler, P., Jander, S., Hartung, H.P. & Kury, P. p57kip2 is dynamically regulated in experimental autoimmune encephalomyelitis and interferes with oligodendroglial maturation. *Proc Natl Acad Sci U S A* **106**, 9087-92 (2009). PMC2690052

267. Yokoo, T., Toyoshima, H., Miura, M., Wang, Y., Iida, K.T., Suzuki, H., Sone, H., Shimano, H., Gotoda, T., Nishimori, S., Tanaka, K. & Yamada, N. p57Kip2 regulates actin dynamics by binding and translocating LIM-kinase 1 to the nucleus. *J Biol Chem* **278**, 52919-23 (2003).

268. Vlachos, P. & Joseph, B. The Cdk inhibitor p57(Kip2) controls LIM-kinase 1 activity and regulates actin cytoskeleton dynamics. *Oncogene* **28**, 4175-88 (2009).

269. Sethi, J.K. & Vidal-Puig, A.J. Thematic review series: adipocyte biology. Adipose tissue function and plasticity orchestrate nutritional adaptation. *J Lipid Res* **48**, 1253-62 (2007). PMC4303760

270. Park, H. & Poo, M.M. Neurotrophin regulation of neural circuit development and function. *Nat Rev Neurosci* **14**, 7-23 (2013).

271. Perera, R.K. & Nikolaev, V.O. Compartmentation of cAMP signalling in cardiomyocytes in health and disease. *Acta Physiol (Oxf)* **207**, 650-62 (2013).

272. Romarowski, A., Battistone, M.A., La Spina, F.A., Puga Molina Ldel, C., Luque, G.M., Vitale, A.M., Cuasnicu, P.S., Visconti, P.E., Krapf, D. & Buffone, M.G. PKA-dependent phosphorylation of LIMK1 and Cofilin is essential for mouse sperm acrosomal exocytosis. *Dev Biol* **405**, 237-49 (2015). PMC4546557

273. Pearson, R., Wettenhall, R., Means, A., Hartshorne, D. & Kemp, B. Autoregulation of enzymes by pseudosubstrate prototopes: myosin light chain kinase. **241**, 970-973 (1988).

274. Kobe, B., Heierhorst, J., Feil, S.C., Parker, M.W., Benian, G.M., Weiss, K.R. & Kemp, B.E. Giant protein kinases: domain interactions and structural basis of autoregulation. *The EMBO Journal* **15**, 6810-6821 (1996).

275. Cutler, R.E., Stephens, R.M., Saracino, M.R. & Morrison, D.K. Autoregulation of the Raf-1 serine/threonine kinase. **95**, 9214-9219 (1998).

276. Diskar, M., Zenn, H.-M., Kaupisch, A., Prinz, A. & Herberg, F.W. Molecular basis for isoform-specific autoregulation of protein kinase A. **19**, 2024-2034 (2007).

277. Ha, B.H., Davis, M.J., Chen, C., Lou, H.J., Gao, J., Zhang, R., Krauthammer, M., Halaban, R., Schlessinger, J., Turk, B.E. & Boggon, T.J. Type II p21-activated kinases (PAKs) are regulated by an autoinhibitory pseudosubstrate. **109**, 16107-16112 (2012).

278. Nolen, B., Taylor, S. & Ghosh, G. Regulation of Protein Kinases. *Molecular Cell* **15**, 661-675 (2004).

279. Ha, B.H., Davis, M.J., Chen, C., Lou, H.J., Gao, J., Zhang, R., Krauthammer, M., Halaban, R., Schlessinger, J., Turk, B.E. & Boggon, T.J. Type II p21-activated kinases (PAKs) are regulated by an autoinhibitory pseudosubstrate. *Proceedings of the National Academy of Sciences* **109**, 16107-16112 (2012).

280. Tan, I., Seow, K.T., Lim, L. & Leung, T. Intermolecular and intramolecular interactions regulate catalytic activity of myotonic dystrophy kinase-related Cdc42-binding kinase alpha. *Mol Cell Biol* **21**, 2767-78 (2001). PMC86907

281. Jebelli, J.D., Dihanich, S., Civiero, L., Manzoni, C., Greggio, E. & Lewis, P.A. GTP binding and intramolecular regulation by the ROC domain of Death Associated Protein Kinase 1. *Sci Rep* **2**, 695 (2012). PMC3458246

282. Nam, H.-J., Haser, W.G., Roberts, T.M. & Frederick, C.A. Intramolecular interactions of the regulatory domains of the Bcr–Abl kinase reveal a novel control mechanism. *Structure* **4**, 1105-1114 (1996).

283. Gonfloni, S., Frischknecht, F., Way, M. & Superti-Furga, G. Leucine 255 of Src couples intramolecular interactions to inhibition of catalysis. *Nature Structural Biology* **6**, 760-764 (1999).

284. Cooper, J.A., Gould, K.L., Cartwright, C.A. & Hunter, T. Tyr527 is phosphorylated in pp60c-src: implications for regulation. *Science* **231**, 1431-4 (1986).

285. Brown, M.T. & Cooper, J.A. Regulation, substrates and functions of src. *Biochim Biophys Acta* **1287**, 121-49 (1996).

286. Roskoski, R., Jr. Src protein-tyrosine kinase structure and regulation. *Biochem Biophys Res Commun* **324**, 1155-64 (2004).

287. Yeatman, T.J. A renaissance for SRC. *Nat Rev Cancer* **4**, 470-80 (2004).

288. Superti-Furga, G. & Courtneidge, S.A. Structure-function relationships in Src family and related protein tyrosine kinases. *Bioessays* **17**, 321-30 (1995).

289. Kurochkina, N. & Guha, U. SH3 domains: modules of protein-protein interactions. *Biophys Rev* **5**, 29-39 (2013). PMC5418429

290. Waksman, G., Kumaran, S. & Lubman, O. SH2 domains: role, structure and implications for molecular medicine. *Expert Rev Mol Med* **6**, 1-18 (2004).

291. Songyang, Z., Margolis, B., Chaudhuri, M., Shoelson, S.E. & Cantley, L.C. The phosphotyrosine interaction domain of SHC recognizes tyrosine-phosphorylated NPXY motif. *J Biol Chem* **270**, 14863-6 (1995).

292. Songyang, Z., Shoelson, S.E., Chaudhuri, M., Gish, G., Pawson, T., Haser, W.G., King, F., Roberts, T., Ratnofsky, S., Lechleider, R.J. & et al. SH2 domains recognize specific phosphopeptide sequences. *Cell* **72**, 767-78 (1993).

293. Sefton, B.M., Hunter, T. & Beemon, K. Product of in vitro translation of the Rous sarcoma virus src gene has protein kinase activity. *J Virol* **30**, 311-8 (1979). PMC353324

294. Musacchio, A., Wilmanns, M. & Saraste, M. Structure and function of the SH3 domain. *Prog Biophys Mol Biol* **61**, 283-97 (1994).

295. Weng, Z., Rickles, R.J., Feng, S., Richard, S., Shaw, A.S., Schreiber, S.L. & Brugge, J.S. Structure-function analysis of SH3 domains: SH3 binding specificity altered by single amino acid substitutions. *Mol Cell Biol* **15**, 5627-34 (1995). PMC230813

296. Abrams, C.S. & Zhao, W. SH3 domains specifically regulate kinase activity of expressed Src family proteins. *J Biol Chem* **270**, 333-9 (1995).

297. Mayer, B.J. & Baltimore, D. Mutagenic analysis of the roles of SH2 and SH3 domains in regulation of the Abl tyrosine kinase. *Mol Cell Biol* **14**, 2883-94 (1994). PMC358656

298. Pluk, H., Dorey, K. & Superti-Furga, G. Autoinhibition of c-Abl. *Cell* **108**, 247-59 (2002).

299. Nagar, B., Hantschel, O., Young, M.A., Scheffzek, K., Veach, D., Bornmann, W., Clarkson, B., Superti-Furga, G. & Kuriyan, J. Structural basis for the autoinhibition of c-Abl tyrosine kinase. *Cell* **112**, 859-71 (2003).

300. Hantschel, O., Grebien, F. & Superti-Furga, G. The growing arsenal of ATP-competitive and allosteric inhibitors of BCR-ABL. *Cancer Res* **72**, 4890-5 (2012). PMC3517953

301. Lorenz, S., Deng, P., Hantschel, O., Superti-Furga, G. & Kuriyan, J. Crystal structure of an SH2-kinase construct of c-Abl and effect of the SH2 domain on kinase activity. *Biochem J* **468**, 283-91 (2015). PMC5936049

302. Kemp, B.E. & Pearson, R.B. Intrasteric regulation of protein kinases and phosphatases. *Biochim Biophys Acta* **1094**, 67-76 (1991).

303. Malumbres, M. Cyclin-dependent kinases. *Genome Biol* **15**, 122 (2014). PMC4097832

304. Bourne, Y., Watson, M.H., Hickey, M.J., Holmes, W., Rocque, W., Reed, S.I. & Tainer, J.A. Crystal structure and mutational analysis of the human CDK2 kinase complex with cell cycle-regulatory protein CksHs1. *Cell* **84**, 863-74 (1996).

305. Ahn, J., Urist, M. & Prives, C. The Chk2 protein kinase. *DNA Repair (Amst)* **3**, 1039-47 (2004).

306. Cai, Z., Chehab, N.H. & Pavletich, N.P. Structure and activation mechanism of the CHK2 DNA damage checkpoint kinase. *Mol Cell* **35**, 818-29 (2009).

307. Edwards, D.C. & Gill, G.N. Structural features of LIM kinase that control effects on the actin cytoskeleton. *J Biol Chem* **274**, 11352-61 (1999).

308. Sala, S. & Ampe, C. An emerging link between LIM domain proteins and nuclear receptors. *Cell Mol Life Sci* **75**, 1959-1971 (2018).

309. UniProt, C. UniProt: the Universal Protein Knowledgebase in 2023. *Nucleic Acids Res* (2022).

310. Sievers, F., Wilm, A., Dineen, D., Gibson, T.J., Karplus, K., Li, W., Lopez, R., McWilliam, H., Remmert, M., Soding, J., Thompson, J.D. & Higgins, D.G. Fast, scalable generation of high-quality protein multiple sequence alignments using Clustal Omega. *Mol Syst Biol* **7**, 539 (2011). PMC3261699

311. Waterhouse, A.M., Procter, J.B., Martin, D.M., Clamp, M. & Barton, G.J. Jalview Version 2--a multiple sequence alignment editor and analysis workbench. *Bioinformatics* **25**, 1189-91 (2009). PMC2672624

312. Boggon, T.J. & Eck, M.J. Structure and regulation of Src family kinases. *Oncogene* **23**, 7918-27 (2004).

313. Kimple, M.E., Siderovski, D.P. & Sondek, J. Functional relevance of the disulfide-linked complex of the N-terminal PDZ domain of InaD with NorpA. *EMBO J* **20**, 4414-22 (2001). PMC125561

314. Birrane, G., Chung, J. & Ladias, J.A. Novel mode of ligand recognition by the Erbin PDZ domain. *J Biol Chem* **278**, 1399-402 (2003).

315. Gogl, G., Zambo, B., Kostmann, C., Cousido-Siah, A., Morlet, B., Durbesson, F., Negroni, L., Eberling, P., Jane, P., Nomine, Y., Zeke, A., Ostergaard, S., Monsellier, E., Vincentelli, R. & Trave, G. Author Correction: Quantitative fragmentomics allow affinity mapping of interactomes. *Nat Commun* **13**, 7555 (2022). PMC9729566

316. Ernst, A., Appleton, B.A., Ivarsson, Y., Zhang, Y., Gfeller, D., Wiesmann, C. & Sidhu, S.S. A structural portrait of the PDZ domain family. *J Mol Biol* **426**, 3509-19 (2014).

317. Ivarsson, Y., Arnold, R., McLaughlin, M., Nim, S., Joshi, R., Ray, D., Liu, B., Teyra, J., Pawson, T., Moffat, J., Li, S.S., Sidhu, S.S. & Kim, P.M. Large-scale interaction profiling of PDZ domains through proteomic peptide-phage display using human and viral phage peptidomes. *Proc Natl Acad Sci U S A* **111**, 2542-7 (2014). PMC3932933

318. Kabsch, W. Xds. *Acta Crystallogr D Biol Crystallogr* **66**, 125-32 (2010). PMC2815665

319. Evans, P. Scaling and assessment of data quality. *Acta Crystallogr D Biol Crystallogr* **62**, 72-82 (2006).

320. McCoy, A.J., Grosse-Kunstleve, R.W., Adams, P.D., Winn, M.D., Storoni, L.C. & Read, R.J. Phaser crystallographic software. *J Appl Crystallogr* **40**, 658-674 (2007). PMC2483472

321. Terwilliger, T.C., Grosse-Kunstleve, R.W., Afonine, P.V., Moriarty, N.W., Zwart, P.H., Hung, L.W., Read, R.J. & Adams, P.D. Iterative model building, structure refinement and density modification with the PHENIX AutoBuild wizard. *Acta Crystallographica Section D-Biological Crystallography* **64**, 61-69 (2008).

322. Emsley, P., Lohkamp, B., Scott, W.G. & Cowtan, K. Features and development of Coot. *Acta Crystallographica Section D-Biological Crystallography* **66**, 486-501 (2010).

323. Liebschner, D., Afonine, P.V., Moriarty, N.W., Poon, B.K., Chen, V.B. & Adams, P.D. CERES: a cryo-EM re-refinement system for continuous improvement of deposited models. *Acta Crystallogr D Struct Biol* **77**, 48-61 (2021). PMC7787109

324. Altschul, S.F., Madden, T.L., Schäffer, A.A., Zhang, J., Zhang, Z., Miller, W. & Lipman, D.J. Gapped BLAST and PSI-BLAST: a new generation of protein database search programs. *Nucleic acids research* **25**, 3389-3402 (1997).

325. Kang, H., Bradley, M.J., Cao, W., Zhou, K., Grintsevich, E.E., Michelot, A., Sindelar, C.V., Hochstrasser, M. & De La Cruz, E.M. Site-specific cation release drives actin filament severing by vertebrate cofilin. *Proc Natl Acad Sci U S A* **111**, 17821-6 (2014). PMC4273407

326. Cox, J.S., Chapman, R.E. & Walter, P. The unfolded protein response coordinates the production of endoplasmic reticulum protein and endoplasmic reticulum membrane. *Mol Biol Cell* **8**, 1805-14 (1997). PMC305738

327. Ragusa, M.J., Dancheck, B., Critton, D.A., Nairn, A.C., Page, R. & Peti, W. Spinophilin directs protein phosphatase 1 specificity by blocking substrate binding sites. *Nat Struct Mol Biol* **17**, 459-64 (2010). PMC2924587

328. Choi, Y., Yun, J.H., Yoo, J., Lee, I., Kim, H., Son, H.N., Kim, I.S., Yoon, H.S., Zimmermann, P., Couchman, J.R., Cho, H.S., Oh, E.S. & Lee, W. New structural

insight of C-terminal region of Syntenin-1, enhancing the molecular dimerization and inhibitory function related on Syndecan-4 signaling. *Sci Rep* **6**, 36818 (2016). PMC5103296

329. Raman, A.S., White, K.I. & Ranganathan, R. Origins of Allostery and Evolvability in Proteins: A Case Study. *Cell* **166**, 468-480 (2016).

330. Moon, A.L., Janmey, P.A., Louie, K.A. & Drubin, D.G. Cofilin is an essential component of the yeast cortical cytoskeleton. *J Cell Biol* **120**, 421-35 (1993). PMC2119511

331. Iida, K., Moriyama, K., Matsumoto, S., Kawasaki, H., Nishida, E. & Yahara, I. Isolation of a yeast essential gene, COF1, that encodes a homologue of mammalian cofilin, a low-M(r) actin-binding and depolymerizing protein. *Gene* **124**, 115-20 (1993).

332. Camara-Artigas, A., Murciano-Calles, J. & Martinez, J.C. Conformational changes in the third PDZ domain of the neuronal postsynaptic density protein 95. *Acta Crystallogr D Struct Biol* **75**, 381-391 (2019).

333. Feng, W., Fan, J.S., Jiang, M., Shi, Y.W. & Zhang, M. PDZ7 of glutamate receptor interacting protein binds to its target via a novel hydrophobic surface area. *J Biol Chem* **277**, 41140-6 (2002).

334. Jumper, J., Evans, R., Pritzel, A., Green, T., Figurnov, M., Ronneberger, O., Tunyasuvunakool, K., Bates, R., Zidek, A., Potapenko, A., Bridgland, A., Meyer, C., Kohl, S.A.A., Ballard, A.J., Cowie, A., Romera-Paredes, B., Nikolov, S., Jain, R., Adler, J., Back, T., Petersen, S., Reiman, D., Clancy, E., Zielinski, M., Steinegger, M., Pacholska, M., Berghammer, T., Bodenstein, S., Silver, D., Vinyals, O., Senior, A.W., Kavukcuoglu, K., Kohli, P. & Hassabis, D. Highly accurate protein structure prediction with AlphaFold. *Nature* **596**, 583-589 (2021). PMC8371605

335. Zhao, Z.S. & Manser, E. PAK and other Rho-associated kinases--effectors with surprisingly diverse mechanisms of regulation. *Biochem J* **386**, 201-14 (2005). PMC1134783

336. Pei, J. & Grishin, N.V. PROMALS: towards accurate multiple sequence alignments of distantly related proteins. *Bioinformatics* **23**, 802-8 (2007).

337. Holm, L. DALI and the persistence of protein shape. *Protein Sci* **29**, 128-140 (2020). PMC6933842

338. McNicholas, S., Potterton, E., Wilson, K.S. & Noble, M.E. Presenting your structures: the CCP4mg molecular-graphics software. *Acta Crystallogr D Biol Crystallogr* **67**, 386-94 (2011). PMC3069754

339. Sumi, T., Hashigasako, A., Matsumoto, K. & Nakamura, T. Different activity regulation and subcellular localization of LIMK1 and LIMK2 during cell cycle transition. *Exp Cell Res* **312**, 1021-30 (2006).

340. Okada, M. Regulation of the SRC family kinases by Csk. *Int J Biol Sci* **8**, 1385-97 (2012). PMC3492796

341. Neet, K. & Hunter, T. Vertebrate non-receptor protein-tyrosine kinase families. *Genes Cells* **1**, 147-69 (1996).

342. Takeuchi, S., Takayama, Y., Ogawa, A., Tamura, K. & Okada, M. Transmembrane phosphoprotein Cbp positively regulates the activity of the carboxyl-terminal Src kinase, Csk. *J Biol Chem* **275**, 29183-6 (2000).

343. Cole, P.A., Shen, K., Qiao, Y. & Wang, D. Protein tyrosine kinases Src and Csk: a tail's tale. *Curr Opin Chem Biol* **7**, 580-5 (2003).

344. Kemp, B.E., Parker, M.W., Hu, S., Tiganis, T. & House, C. Substrate and pseudosubstrate interactions with protein kinases: determinants of specificity. *Trends Biochem Sci* **19**, 440-4 (1994).

345. Ha, B.H., Morse, E.M., Turk, B.E. & Boggon, T.J. Signaling, Regulation, and Specificity of the Type II p21-activated Kinases. *J Biol Chem* **290**, 12975-83 (2015). PMC4505552

346. Velyvis, A., Vaynberg, J., Yang, Y., Vinogradova, O., Zhang, Y., Wu, C. & Qin, J. Structural and functional insights into PINCH LIM4 domain-mediated integrin signaling. *Nat Struct Biol* **10**, 558-64 (2003).

347. Schmidt, E.F., Shim, S.O. & Strittmatter, S.M. Release of MICAL autoinhibition by semaphorin-plexin signaling promotes interaction with collapsin response mediator protein. *J Neurosci* **28**, 2287-97 (2008). PMC2846290

348. Aicart-Ramos, C. & Rodriguez-Crespo, I. Binding of PDZ domains to the carboxy terminus of inducible nitric oxide synthase boosts electron transfer and NO synthesis. *FEBS Lett* **589**, 2207-12 (2015).

349. Varadi, M., Anyango, S., Deshpande, M., Nair, S., Natassia, C., Yordanova, G., Yuan, D., Stroe, O., Wood, G., Laydon, A., Zidek, A., Green, T., Tunyasuvunakool,

K., Petersen, S., Jumper, J., Clancy, E., Green, R., Vora, A., Lutfi, M., Figurnov, M., Cowie, A., Hobbs, N., Kohli, P., Kleywegt, G., Birney, E., Hassabis, D. & Velankar, S. AlphaFold Protein Structure Database: massively expanding the structural coverage of protein-sequence space with high-accuracy models. *Nucleic Acids Res* **50**, D439-D444 (2022). PMC8728224

350. Hopkins, J.B., Gillilan, R.E. & Skou, S. BioXTAS RAW: improvements to a free open-source program for small-angle X-ray scattering data reduction and analysis. *J Appl Crystallogr* **50**, 1545-1553 (2017). PMC5627684

351. Rambo, R.P. & Tainer, J.A. Accurate assessment of mass, models and resolution by small-angle scattering. *Nature* **496**, 477-81 (2013). PMC3714217

352. Piiadov, V., Ares de Araujo, E., Oliveira Neto, M., Craievich, A.F. & Polikarpov, I. SAXSMoW 2.0: Online calculator of the molecular weight of proteins in dilute solution from experimental SAXS data measured on a relative scale. *Protein Sci* **28**, 454-463 (2019). PMC6319763

353. Grant, T.D. Ab initio electron density determination directly from solution scattering data. *Nat Methods* **15**, 191-193 (2018).

354. Grant, T.D. Ab initio electron density determination directly from solution scattering data. *Nature Methods* **15**, 191-193 (2018).

355. Schneidman-Duhovny, D., Hammel, M., Tainer, J.A. & Sali, A. FoXS, FoXSDock and MultiFoXS: Single-state and multi-state structural modeling of proteins and their complexes based on SAXS profiles. *Nucleic Acids Res* **44**, W424-9 (2016). PMC4987932

356. Schneidman-Duhovny, D., Hammel, M., Tainer, J.A. & Sali, A. Accurate SAXS profile computation and its assessment by contrast variation experiments. *Biophys J* **105**, 962-74 (2013). PMC3752106

357. Svergun, D., Barberato, C. & Koch, M.H.J. CRYSOL– a Program to Evaluate X-ray Solution Scattering of Biological Macromolecules from Atomic Coordinates. *Journal of Applied Crystallography* **28**, 768-773 (1995).

358. Franke, D., Jeffries, C.M. & Svergun, D.I. Correlation Map, a goodness-of-fit test for one-dimensional X-ray scattering spectra. *Nat Methods* **12**, 419-22 (2015).

359. Svergun, D. Determination of the regularization parameter in indirect-transform methods using perceptual criteria. *Journal of applied crystallography* **25**, 495-503 (1992).

360. Mizuno, K. [Cofilin phosphorylation and regulation of actin cytoskeletal reorganization by LIM-kinase]. *Seikagaku* **71**, 345-50 (1999).

361. Lawler, S. Regulation of actin dynamics: The LIM kinase connection. *Curr Biol* **9**, R800-2 (1999).

362. Yang, J., Cron, P., Thompson, V., Good, V.M., Hess, D., Hemmings, B.A. & Barford, D. Molecular Mechanism for the Regulation of Protein Kinase B/Akt by Hydrophobic Motif Phosphorylation. *Molecular Cell* **9**, 1227-1240 (2002).

363. Huse, M. & Kuriyan, J. The conformational plasticity of protein kinases. *Cell* **109**, 275-82 (2002).